AD NUMBER
ADC028075
CLASSIFICATION CHANGES
TO: unclassified
FROM: confidential
LIMITATION CHANGES
TO: Approved for public release, distribution unlimited
FROM: Controlling DoD Organization. Naval Electronic Systems Command, Washington, DC 20360.
AUTHORITY
ONR ltr, 31 Jan 2006; ONR ltr, 31 Jan 2006

CONFIDENTIAL

NOSC

NOSC TR 680

NOSC TR 680

Technical Report 680

COHERENCE VARIABILITY OF ARRAYS DURING BEARING STAKE (U)

JA Neubert

August 1981

Research Report: July 1980 — March 1981

Prepared for
Naval Electronic Systems Command

AD C028 075

Classified by: OPNAVINST S5513.5-42
Review on: 31 August 2001

"NATIONAL SECURITY INFORMATION"

"Unauthorized Disclosure Subject to Criminal Sanctions"

DTIC FILE COPY

NAVAL OCEAN SYSTEMS CENTER
SAN DIEGO, CALIFORNIA 92152

CONFIDENTIAL

NAVAL OCEAN SYSTEMS CENTER, SAN DIEGO, CA 92152

AN ACTIVITY OF THE NAVAL MATERIAL COMMAND

SL GUILLE, CAPT, USN
Commander

HL BLOOD
Technical Director

ADMINISTRATIVE INFORMATION (U)

(U) This report was prepared under a subtask of the FY-80 NOSC Block Program in Environmental Acoustic Surveillance Technology, Program Element 62759, Subproject Task XF-59-552, sponsored by the Naval Electronic Systems Command, Code 612.

Released by
NO Booth, Head
Environmental Acoustics Division

Under authority of
JD Hightower, Head
Environmental Sciences
Department

CONFIDENTIAL

SECURITY CLASSIFICATION OF THIS PAGE *(When Data Entered)*

REPORT DOCUMENTATION PAGE

READ INSTRUCTIONS BEFORE COMPLETING FORM

1. REPORT NUMBER: NOSC Technical Report 680 (TR 680)	2. GOVT ACCESSION NO.: AD-C028075
3. RECIPIENT'S CATALOG NUMBER:	
4. TITLE *(and Subtitle)*: COHERENCE VARIABILITY OF ARRAYS DURING BEARING STAKE (U)	5. TYPE OF REPORT & PERIOD COVERED: Research Report, July 1980 – March 1981
	6. PERFORMING ORG. REPORT NUMBER:
7. AUTHOR(s): JA Neubert	8. CONTRACT OR GRANT NUMBER(s):
9. PERFORMING ORGANIZATION NAME AND ADDRESS: Naval Ocean Systems Center, San Diego, CA 92152	10. PROGRAM ELEMENT, PROJECT, TASK AREA & WORK UNIT NUMBERS: 62759, XF-59-552
11. CONTROLLING OFFICE NAME AND ADDRESS: Naval Electronic Systems Command, Washington, DC	12. REPORT DATE: August 1981
	13. NUMBER OF PAGES: 170
14. MONITORING AGENCY NAME & ADDRESS *(if different from Controlling Office)*	15. SECURITY CLASS. *(of this report)*: Confidential
	15a. DECLASSIFICATION/DOWNGRADING SCHEDULE: Review on: 31 August 2001

16. DISTRIBUTION STATEMENT *(of this Report)*

17. DISTRIBUTION STATEMENT *(of the abstract entered in Block 20, if different from Report)*

18. SUPPLEMENTARY NOTES

19. KEY WORDS *(Continue on reverse side if necessary and identify by block number)*

Sonar	Surveillance
Line array	Array configuration
Signal processing	Oceanic environment

20. ABSTRACT *(Continue on reverse side if necessary and identify by block number)*

(C) By the use of acoustic synoptic factors, this study investigates how the variable and random sound field structure influences the performance of wide-aperture, horizontal line array systems for low-frequency, narrowband sources in the northwestern Indian Ocean using data from the Bearing Stake exercise. Several acoustic synoptic factors are defined and illustrated. The patterned and coherence behavior of arrays is studied in detail. The degrading effects of an array turn are considered graphically and synoptically. The interaction of several of the acoustic synoptic factors is shown. The stability of time averages is investigated synoptically. It was found that the more stable the time average of the phase is, the better the coherence is. On the other hand, the stability of the time average of the amplitude had little impact on the coherence. Finally, it was shown that a normal mode model was suitable for representing the Bearing Stake results.

DD FORM 1 JAN 73 1473 EDITION OF 1 NOV 65 IS OBSOLETE

S/N 0102-LF-014-6601

CONFIDENTIAL

SECURITY CLASSIFICATION OF THIS PAGE *(When Data Entered)*

CONTENTS (U)

NOTATION (U)

A_j	instantaneous amplitude measured at sensor j
θ_j	instantaneous residual phase of Eq (2)
Σ_A	normalized amplitude standard deviation of Eq (4)
S+N	signal plus noise power of Eq (9)
N	noise power of Eq (10)
C_p	array phase coherence coefficient of Eq (12)
ASG	array signal gain of Eq (13)
CA_j	amplitude nonhomogeneity factor of Eq (15)
C_j^σ	percent relative amplitude standard deviation of Eq (16)
$CNA_{j\ell}$	normalized amplitude covariance of Eq (20)
$C_{j\ell}^p$	array phase coherence matrix of Eq (21)
$(\gamma_{j\ell}^c)^2$	classical coherence matrix of Eq (22)
CD1	plot notation for $CNA_{j\ell}$; see Eq (23)
CD2	plot notation for $C_{j\ell}^p$; see Eq (24)
CD3	plot notation for $(\gamma_{j\ell}^c)^2$; see Eq (25)
SD_i	plot notation for $(\sigma_i^i)^2$ of Eq (27)
SND_i	plot notation for Σ_σ^i of Eq (28)
CJ_i	plot notation for C_J^i of Eq (29)
MND_i	plot notation for μ_N^i of Eq (30)
MS_i	plot notation for μ_σ^i of Eq (31)
CF	coherence factor of Eq (32)
SF	structure factor of Eq (33)
CM4	plot notation for $CM_{j\ell}$ of Eq (37)
NAC	amount of negative amplitude correlation as defined by Eq (39)
DS_i	plot notation for Δ_i (ΔT) of Eq (40)
ADS_i	plot notation of $A\Delta_i$ of Eq (43)

I. (U) INTRODUCTION

(C) This report investigates (via acoustic synoptic factors) how the variable and random sound field structure influences the performance of wide-aperture, horizontal line array systems for low-frequency, narrowband sources in the northwestern Indian Ocean using data from the Bearing Stake exercise.

(U) When operating an array system in the ocean, a complex situation results. There are environmental and system variables that result in a variable system behavior. Environmental variables are oceanic conditions (eg, multipath), geographic location, and measurement conditions (eg, array depth and surveillance range). Examples of system variables are averaging time and processing algorithms. The variable system behavior manifests itself by its impact on array gain, sidelobe degradation, etc.

(U) Obviously these variables interact. A convenient and representative summary is given below.

A. Environmental variables:
   1. Oceanic conditions, eg, propagation loss, bathymetry, bottom interaction and losses, sea state, sound-speed channels, multipaths, internal waves, diffraction, dispersion, scattering, structure of the sound-speed profile, fronts and eddies, noise, fluctuations
   2. Geographic location
   3. Season
   4. Array deformation
   5. Measurement conditions, eg, source level and tow speed, frequency, bandwidth, surveillance range, target bearing and aspect, array depth and tilt, array aperture length and configuration, type of target signal, track of maneuvering submarine, doppler.

B. System variables:
   1. Averaging time and method
   2. Bandwidth
   3. Beamformer weighting (array shading)
   4. Degree of signal clipping
   5. Processing algorithms and criteria
   6. Array operation procedure (eg, tow speed and turns).

C. Variable system behavior can be characterized by
   1. Array gain
   2. Coherence
   3. Sidelobe degradation
   4. Quality of the main beam (eg, effective beamwidth, beam splitting, beam jumping) (Ref 1)
   5. Quality of the CMAP passive ambiguity surface (Ref 1)
   6. Target detectability
   7. False alarms

1. J. A. Neubert, "Performance Variability of Sonar Systems (U)," NOSC TR 679, April 1981 (CONF).

(U) To permit consideration of as many of these factors as feasible, extensive experiments such as Bearing Stake (discussed below) have accumulated massive data bases. In order to use these large quantities of data to systematically appraise system performance, synoptic factors have been computed and then tabulated and/or plotted versus the variables of interest. For example, the array signal gain behavior of an array system can be summarized for each data set by the coefficient ASG of Eq (13). Then ASG can be tabulated versus, say, range and integration time. Examining these tabulations gives a quantitative appraisal of such things as the importance of array deformation and the limitations of integration time and range. These tabulations can be further simplified by taking the mean and standard deviation of ASG. These statistical values can then be compared as a function of, say, array depth and tilt, target bearing, geographic location, and season to analyze array system behavior and its models.

(U) What is a synoptic factor? It is not an abstract concept, but is a computed synoptic quantity determined by the actual data themselves. Hence synoptic factors can consider the complex effects of the environmental and systems variables on the behavior of specific systems. They use actual ocean data to concisely characterize the pertinent system behavior. Each synoptic factor is specifically classified by the conditions that occur during the ocean measurement and by the method of system application. Synoptic factors quantify the impact of complex environmental and system variables on the amplitude and phase (and their interaction) across the array and relate these to the behavior of array systems. Actually it is easier to think in terms of two types of synoptic factors: acoustic synoptic factors and system synoptic factors. Acoustic synoptic factors are coefficients that summarize quantitatively the acoustic behavior across arrays as a function of the environmental variables. System synoptic factors are coefficients that summarize quantitatively the impact of the environmental and system variables on array system behavior. This report is primarily interested in the application of acoustic synoptic factors to array systems. However, C_{ai} of Ref 1 is an example of an effective system synoptic factor for some cases (see Fig 6 and 8 of Ref 1).

(U) By themselves synoptic factors cannot predict array system behavior if the underlying pertinent conditions change. They merely synopsize this behavior in a useful form that is sensitive to the changes in the underlying pertinent conditions. Therefore, they are useful for quantitatively comparing changing oceanic situations and often for discerning which changing conditions affect the system behavior and by how much. Examples of this are found in Sections III and IV. However, synoptic factors can be used with deterministic theoretical models such as normal modes (Ref 2) and Raywave (Ref 3). Deterministic models can consider or approximate some of the wide range of interacting oceanic variables and then be input into the synoptic factor algorithms. The theoretical results produced thereby can then be compared with the synoptic factor algorithms using real oceanic data inputs. The results can be used to appraise the suitability of the theoretical models for the situation under consideration. By iterative use of this approach, the theoretical models can be improved and the pertinent oceanic conditions can be better understood (Ref 4). In short, synoptic factors can succinctly evaluate the accuracy and variability of deterministic theoretical approaches as a function of environmental and system variables in order to suggest improvements in these theoretical models.

2. M. A. Pedersen and G. S. Yee, "Propagation Loss Assessment of the Bearing Stake Exercise (U)," NOSC TR 467, 28 September 1979, CONF.

3. W. H. Watson and R. W. McGirr, "Raywave II: A Propagation Loss Model for the Analysis of Complex Ocean Environments," NUC TN 1516, 1975.

4. D. F. Gordon, "Array Simulation at the Bearing Stake Sites (U)," NOSC TR 664, April 1981, CONF.

(U) The synoptic factor technique discussed below is universal (ie, it is not site specific), while the data from any site may be unique. Once developed for a sufficiently complex region (like the northwestern Indian Ocean), the synoptic factors can be applied with equal validity to other ocean regions (such as the Mediterranean Sea, the Norwegian Sea and the Sea of Japan) as the data are made available. By comparing archival data and using appropriate models, projections of array systems behavior to other regions, where data are not yet available, can be made from regions for which data presently exist. This makes synoptic factors useful for planning experiments and for projecting present and future array system performance to other regions.

(C) Figure 1 shows the northwestern Indian Ocean surveyed during Bearing Stake. It has been shown (Ref 5 through 10) that the sound field was highly structured and variable in this strategically important ocean region and that the sound field structure changed from site to site. For wide-aperture, horizontal line arrays in this multipath environment, the sound field structure can be described by

1. the amplitude nonhomogeneity across the array,
2. the wavefront corrugation across the array,
3. the fluctuations,

and

4. the interaction of these as discussed below.

(U) Three arrays were employed for several projector tows for five sites shown in Fig 1 during Bearing Stake. These three arrays were:

1. Ocean Acoustic Measurement System (OAMS) array,
2. Long Acoustic Towed Array (LATA) (formally called Lambda I), and
3. Bottom-Mounted Array (BMA).

(U) In Section II several acoustic synoptic factors are given and explained. Section III extends the sound field structure study of Ref 7 by introducing several new acoustic synoptic factors. It also illustrates the impact of an array turn on the performance of an array. It concludes by showing some interactions between acoustic synoptic parameters. Section IV discusses the stability of time averages for the purposes of appraising array performance and introduces an appropriate class of acoustic synoptic factors. Section V discusses the merits of a normal mode array performance model using Bearing Stake data.

(U) In this report the first 11 signal array arrivals for projector tow 2P3A and the first 12 signal array arrivals for projector 4P1 are considered as representative of the Bearing Stake data. These data are shown in Fig 2 through 24 and pertain to the relations in Sections II and IV. Acoustic synoptic factors from Sections II through IV for all of projectors tows 2P3A and 4P1 are found in Tables 1 and 2.

---

5. J. A. Neubert, "Bearing Stake Coherence Data Analysis: Part I. The OAMS Array (U)," NOSC TN 380, 6 February 1978, CONF.
6. J. A. Neubert, "Bearing Stake Coherence Data Analysis: Bottom-Mounted Array (U)," NOSC TN 452, 31 May 1978, CONF.
7. A. G. Fabula and J. A. Neubert, "Bearing Stake Data Analysis: LATA (U)," NOSC TN 589, November 1978, CONF.
8. J. A. Neubert, "Bearing Stake Array Signal Gain Analysis (U)," NOSC TN 624, December 1978, CONF.
9. J. A. Neubert, "Bearing Stake Coherence and Array Signal Gain Area Assessment Report (U)," NOSC TR 383, December 1978, CONF.
10. J. A. Neubert, "Coherence and Its Sound Field Structure in the Northwestern Indian Ocean (U)," J. Underwater Acoustics, November 1980, CONF.

II. (U) ACOUSTIC SYNOPTIC FACTORS

(U) Represent a narrowband signal arriving at the j^{th} sensor along a wide-aperture, horizontal line array at time t by

$$F_j = A_j \exp\left[i(\phi_j - \omega t)\right] \tag{1}$$

where A_j is the amplitude, ϕ_j is the phase and ω is the angular frequency. Given the target bearing Φ_o (defined as zero for a forward endfire arrival), define the residual phase as

$$\theta_j \equiv \phi_j - k_o d_j \cos \Phi_o \ , \tag{2}$$

where k_o is the wavenumber and d_j is the distance from the first sensor to the j^{th} sensor ($d_1 = 0$). The amplitude fluctuations are given by

$$\delta A_j = A_j - \langle A_j \rangle \ . \tag{3}$$

The total number of array sensors is denoted by J.

(U) For an array of J sensors, $\theta_j = \theta_\ell$ for all $j \neq \ell$ represents a plane arrival for a linear horizontal array. Likewise, $A_j = A_\ell$ for all $j \neq \ell$ represents a homogeneous amplitude arrival along the array. Wavefront corrugation occurs when $\theta_j \neq \theta_\ell$ for any $j \neq \ell$, ie, it represents a nonlinear phase variation along the array. Amplitude nonhomogeneity (ie, amplitude variation along the array) occurs when $A_j \neq A_\ell$ for any $j \neq \ell$. Amplitude nonhomogeneity and wavefront corrugation represent the sound field structure as experienced by the array in a multipath ocean.

(U) In order to quantify, analyze, and model the sound field structure across the array, the following acoustic synoptic factors were devised. Two classes of acoustic synoptic factors will be considered below: total array synoptic factors and intra-array synoptic factors.

TOTAL ARRAY SYNOPTIC FACTORS (U)

Σ_A Factor (U)

(U) The signal plus noise amplitude fluctuation behavior is given by the normalized standard deviation

$$\Sigma_A \equiv \sigma_A / \bar{A}_a \geq 0 \ . \tag{4}$$

where

$$\bar{A}_a \equiv \frac{1}{J} \sum_{j=1}^{J} \langle A_j \rangle \ . \tag{5}$$

$$\sigma_A^2 \equiv \frac{1}{J} \sum_{j=1}^{J} \sigma_j^2 \ . \tag{6}$$

and

$$\sigma_j^2 \equiv \langle (A_j - \langle A_j \rangle)^2 \rangle = \langle (\delta A_j)^2 \rangle \tag{7}$$

with the operator $\langle \cdot \rangle$ representing a time average. Normalizing by $\bar{A}_a$ avoids changes in the propagation conditions from biasing the measure Σ_A.

(U) Σ_A has been tabulated on a site-by-site basis and gives the following overview of the Bearing Stake exercise (Ref 9, 10):

1. Σ_A is sensitive to the propagation conditions.
   a. It discerned the bottom-limited propagation for Sites 3 and 1 from the non-bottom-limited propagation for Site 4.
   b. It sensed the propagation interference due to the presence of a seamount, ie, it discerned the difference between projector tows 5P1 (no seamount) and 2P3A (seamount between source and OAMS array).
2. Σ_A is sensitive to array behavior (eg, array tilt and/or tow depth).
   a. It discerned that the LATA (towed at 300 ft) was not sensitive to the propagation condition differences between Site 4 (not bottom-limited) and Sites 5 and 2 (bottom-limited) while the OAMS array (towed at 200 ft) was.
   b. It showed that the BMA and the OAMS array performed essentially the same at Sites 3 and 1B. [This was confirmed by the C_p and ASG analyses (Ref 9, 10).]
3. Σ_A is sensitive to array sensor calibration and/or damage [eg, it discerned the OAMS array "crush event" during Site 4 projector tows (Ref 5)].

SNR Factor (U)

(U) The signal plus noise-to-noise ratio in dB is given by

$$\mathrm{SNR} \equiv (S+N) - N \ , \tag{8}$$

where

$$(S+N) \equiv 10 \log_{10} \overline{A^2} \quad \text{(for signal plus noise)} \ , \tag{9}$$

$$N \equiv 10 \log_{10} \overline{A^2} \quad \text{(for noise only)} \ , \tag{10}$$

and

$$\overline{A^2} \equiv \frac{1}{J} \sum_{j=1}^{J} \langle A_j^2 \rangle \ . \tag{11}$$

C_p Factor (U)

(U) The wavefront coherence is measured by the array phase coherence coefficient

$$C_p \equiv \frac{1}{J^2} \sum_{j=1}^{J} \sum_{\ell=1}^{J} \langle \cos(\theta_j - \theta_\ell) \rangle \leq 1 \ , \tag{12}$$

where $\langle \cos(\theta_j - \theta_\ell) \rangle$ measures the phase incoherence due to wavefront corrugation and array deformation.

(U) Plots of C_p versus range R measure the phase incoherence due to wavefront corrugation and array deformation, ie, high C_p values occurring intermittently at all ranges show that the array deformation is effectively negligible for a radial projector tow. Then the existence of intermittent low values of C_p rangewise shows the occurrence of beam jumping during this projector tow due to variable wavefront corrugation. C_p is also used to evaluate the array modeling ability and limitations of normal mode theory (see Section V).

ASG Factor (U)

(U) By conveniently normalizing (to compensate for the use of various array shading schemes) the beam array signal gain [see Eq (26) of Ref 1], the array signal gain can be given by (Ref 8)

$$\mathrm{ASG} = 10 \log_{10} \mathrm{asg} \leq 0 \ , \tag{13}$$

where

$$\mathrm{asg} \equiv \frac{\sum_{j=1}^{J} \sum_{\ell=1}^{J} W_j W_\ell \langle A_j A_\ell \cos(\theta_j - \theta_\ell) \rangle}{\sum_{j=1}^{J} W_j \sum_{\ell=1}^{J} W_\ell \quad \bar{A}^2} \tag{14}$$

and the weighting factors are $0 \leq W_j, W_\ell \leq 1$. The mean and standard deviation of ASG are usually of the most interest.

INTRA-ARRAY SYNOPTIC FACTORS (U)

(U) Two types of intra-array synoptic factors will be considered below: one-point structure factors and two-point structure factors.

One-Point Structure Factors Versus Sensor Number j (U)

(U) **CA_j FACTOR.** The amplitude nonhomogeneity factor

$$CA_j \equiv 10 \log_{10} \langle A_j \rangle \tag{15}$$

measures the amplitude nonhomogeneity that impacts the degree of beam splitting and sidelobe suppression (Ref 1). In situ CA_j can check for sensor calibration and damage as was shown in Ref 7

(U) C_j^a FACTOR. The percent relative amplitude standard deviation

$$C_j^a \equiv 100\,\sigma_j/\langle A_j\rangle \tag{16}$$

is very sensitive to signal multipaths but not to noise multipaths and amplitude nonhomogeneity. See Ref 7.

Two-Point Structure Factors Versus Sensor Separation (U)

(U) $CNA_{j\ell}$ FACTOR. The normalized amplitude covariance

$$CNA_{j\ell} \equiv \frac{\langle A_j\,A_\ell\rangle/\langle A_j\rangle\langle A_\ell\rangle}{\max\left(\langle A_j\,A_\ell\rangle/\langle A_j\rangle\langle A_\ell\rangle\right)} \tag{20}$$

gives the structure of the amplitude field across an array in a multipath ocean. Note that $CNA_{j\ell}$ varies about its value for zero covariance, which is $1/\max\left(\langle A_j\,A_\ell\rangle/\langle A_j\rangle\langle A_\ell\rangle\right)$. This zero covariance level is indicated in the $CNA_{j\ell}$ plots of Fig 2 through 24 by the solid horizontal line with arrows on either end.

(U) $C_{j\ell}^p$ FACTOR. The array phase coherence matrix

$$C_{j\ell}^p \equiv \langle\cos(\theta_j - \theta_\ell)\rangle \tag{21}$$

gives the structure of the nonlinear phase field across an array in a multipath ocean.

(U) $(\gamma_{j\ell}^c)^2$ FACTOR. The classical coherence matrix

$$(\gamma_{j\ell}^c)^2 = \frac{\langle A_j\,A_\ell\cos(\theta_j - \theta_\ell)\rangle^2 + \langle A_j\,A_\ell\sin(\theta_j - \theta_\ell)\rangle^2}{\langle A_j^2\rangle\langle A_\ell^2\rangle} \tag{22}$$

gives the interaction of the structure of the amplitude field and the nonlinear residual phase field across an array in a multipath ocean.

III. (U) SOUND FIELD STRUCTURE STUDY

(U) The plots of $CNA_{j\ell}$, $C_{j\ell}^{p}$ and $(\gamma_{j\ell}^{c})$ (see Fig 2 through 24) show the nature of sound field structure at Sites 2 and 4 for Bearing Stake. These figures are somewhat difficult to follow and understand. In this section we introduce some additional synoptic factors that clarify the interpretation of these figures; they are included with each figure. Table 3 then aids the reader in prioritizing the figures in order of their coherence via the coherence factor CF of Eq(32). In addition, Table 3 shows that the impact of off-broadside incidence $\Delta\Phi_o$ of the received signal has no real influence on the coherence. Also it is seen that C_p is a poor prioritizing factor compared to CF. Table 3 also shows that the phase time stability, as synopsized by ADS3 of Eq(43), is closely related to the quality of coherence, while the amplitude time stability, as synopsized by ADS1 of Eq(43), is not. On page 12 a narrative guide through Fig 2 through 24 is given in terms of the coherence structure. As a further aid to understanding Fig 2 through 24, Eq (34) through (36) relate some of the pertinent stochastic factors that appear on the figures.

(U) The sound field structure of Fig 2 through 24 is synopsized as follows. $C_{j\ell}^{i}$ is plotted as a function of sensor separation $d = |d_j - d_\ell|$; that is, $C_d^i = C_{j\ell}^i$, $i = 1, 2, 3$, where

$$C_d^1 = C_{j\ell}^1 = CNA_{j\ell} = CD1\,, \tag{23}$$

$$C_d^2 = C_{j\ell}^2 = C_{j\ell}^p = CD2\,, \tag{24}$$

and

$$C_d^3 = C_{j\ell}^3 = (\gamma_{j\ell}^c)^2 = CD3\,. \tag{25}$$

At each separation d there exists a number n_d of values for $C_d^i = C_d^i(k)$, $1 \leqslant k \leqslant n_d$. That is, n_d is a function of d. There is a total $N = J$ sensor separations. The first separation d is $d_1 = 0$ and the maximum separation d is $d_J \equiv D$. With each separation d there is an associated set of n_d values $C_d^i(k)$. This can be represented by relating the vector

$$(d) = (d_1, ..., d_N \equiv D)$$

to the vector

$$(n_d) = (n_1, ..., n_D = 1).$$

(U) At each value of d, compute

$$\mu_d^i \equiv \frac{1}{n_d} \sum_{k=1}^{n_d} C_d^i(k) \tag{26}$$

and

$$(\sigma_d^i)^2 \equiv \frac{1}{n_d} \sum_{k=1}^{n_d} \left[C_d^i(k) - \mu_d^i \right]^2 \geq 0, \quad \sigma_d^i = \text{SDi}. \tag{27}$$

μ_d^i and σ_d^i represent the two essential properties of the behavior of the sound field structure as manifested in Fig 2 through 24. The mean structure μ_d^i represents the structured behavior of C_d^i versus d. The standard deviation σ_d^i represents the vertical spread about the mean structure μ_d^i versus d. Both μ_d^i and σ_d^i come from normalized functions, and it has been found that the behavior of μ_d^i and σ_d^i versus d have largely independent structure. The appropriate acoustic synoptic factors are

$$\Sigma_\sigma^i \equiv \frac{1}{N} \sum_{d=d_1}^{N} \sigma_d^i = \text{SNDi}, \tag{28}$$

$$C_J^i \equiv \frac{1}{J^2} \sum_{j=1}^{J} \sum_{\ell=1}^{J} C_{j\ell}^i = \text{CJi}, \tag{29}$$

where $C_J^2 = C_p$ of Eq (12),

$$\mu_N^i \equiv \frac{1}{N} \sum_{d=d_1}^{N} \mu_d^i = \text{MNDI}, \tag{30}$$

and

$$(\mu_\sigma^i)^2 \equiv \frac{1}{N} \sum_{d=d_1}^{N} (\mu_d^i - \mu_N^i)^2 \geq 0, \quad \mu_\sigma^i = \text{MSi}. \tag{31}$$

Note that in general μ_d^i will not equal C_J^i. μ_σ^i is of special interest since it becomes smaller as the vertical variation of μ_d^i versus d decreases in vertical extent. μ_d^i is drawn as a solid curve through the plots of CDi in Fig 2 through 24; CJi, MNDi, SNDi, and MSi are also given on each of these plots.

(U) Several characteristics of the sound field structure are evident in Fig 2 through 24. The quality of the classical coherence $(\gamma_{12}^c)^2$ is better the higher μ_d^3 remains and the smaller σ_d^i is. Thence, the Coherence Factor is defined by the convenient measure

$$\text{CF} \equiv 1 - \frac{\Sigma_\sigma^3}{C_J^3} \leq 1. \tag{32}$$

The closer this factor is to unity, the higher the quality of the coherence observed. In terms of CF, Table 1 shows the plots of $(\gamma^c_\ell)^2$ rated in order of decreasing coherence. The amount of structure in $(\gamma^c_{12})^2$ is determined μ^3_σ and σ^3_d. To synopsize this, define the Structure Factor by

$$SF = \Sigma^3_\sigma \cdot \mu^3_\sigma \,. \tag{33}$$

The smaller SF is, the less structure that is occurring in $(\gamma^c_{j\ell})^2$. SF is shown in the plots (Fig 2 through 24) of $(\gamma^c_{j\ell})^2$, where it is seen that SF correlates well with CF. However, visual inspection of the plots of $(\gamma^c_{j\ell})^2$ shows that CF is the better coherence prioritizing factor. Table 3 shows that CF is also a far better prioritizing factor than C_p.

(U) The amplitude, phase, and coherence behavior for the first 12 signal periods for projector tows 2P3A and 4P1 is shown in Fig 2 through 24. The Tow 4P1 behavior is discussed first. Tow 4P1 has one turn at about time 1111 ZULU. Comparing Fig 16c (at the time of the turn) with Fig 14c (24 min before the turn) shows that during the turn, the coherence fluctuation increases greatly and the coherence becomes structured. This is also evident in the relative amplitude behavior (see Fig 14a and 16a) and in the relative phase behavior (cf. Fig 14b and 16b). In Fig 17 (7 min after the turn) the patterned amplitude and phase behavior persists but is not as well correlated. In Fig 18 (20 min after the turn) the coherence fluctuation has decreased while it has become much more patterned, and the amplitude and phase are patterned and in correlation. In Fig 19c (36 min after the turn) and in Fig 20c (50 min after the turn), the coherence shows its greatest pattern magnitudes. In Fig 21c (1 hr 45 min after the turn), the coherence pattern magnitude has decreased significantly (but shows more cycles of pattern). In Fig 22c (1 hr, 50 min after the turn) the coherence pattern magnitude has decreased greatly and again shows fewer cycles of pattern.

(U) Tow 2P3A has no turns. Figure 2c shows only fair coherence, but Fig 3c (24 min later) shows excellent coherence, and Fig 4c (5 min later) shows good coherence. Seventeen minutes later (Fig 5c) the coherence is again only fair, but the coherence is again excellent seventeen minutes later in Fig 6c. The coherence is good 29 min later (Fig 7c) and remains good in Fig 8c (9 min later), and in Fig 9c (45 min later). Sixty-one minutes later (Fig 10c) the coherence declines somewhat but remains good. However, in Fig 11c (16 min later) the coherence is only moderate and continues to be moderate in Fig 12c (11 min later). Thus, the coherence varied considerably during the straight-line tow 2P3A. (Table 3 also indicates this behavior.)

(U) Some observations can be made about Fig 2 through 24 using the synoptic factors that appear above each figure. In general, the mean vertical structure of $CNA_{j\ell}$ times the mean structure of $C^p_{j\ell}$ nearly equals the mean structure of $(\gamma^c_{j\ell})^2$, ie,

$$\frac{\mu^1_d \cdot \mu^2_d}{\mu^3_d} \cong 1 \,. \tag{34}$$

(The only case in which this does not occur closely is for Fig 12, where the value is 0.764.) This relation between the mean structure is to be expected because of the definitions of $CNA_{j\ell}$, $C^p_{j\ell}$ and $(\gamma^c_{j\ell})^2$ in Eq (20, (21) and (22), respectively.

(U) The quantity $(\gamma^c_{j\ell})^2$ is a measure of the correlation of the amplitude and phase structure. The smaller Σ^3_σ is relative to the sum of Σ^1_σ and Σ^2_σ, the better the phase-amplitude correlation. This is measured by

$$\Sigma_r \equiv \frac{\Sigma^1_\sigma + \Sigma^2_\sigma}{\Sigma^3_\sigma} \quad . \tag{35}$$

In general, Σ_r is greater than unity (the only exceptions are Fig 24, 21 and 17, where Σ_r equals 0.744, 0.9744 and 0.875, respectively). In general, Σ_r decreases as CF decreases. The relation of Σ^2_σ to Σ^1_σ is also of interest. In all cases, the phase coherence fluctuations exceed the amplitude fluctuations, ie,

$$\frac{\Sigma^2_\sigma}{\Sigma^1_\sigma} > 1 \, , \tag{36}$$

and this ratio roughly declines as CF declines.

(U) For signals (but less so for noise), σ^1_j generally declines with d as the number of sample sets decreases. This effect is less pronounced when the structure of $C^p_{j\ell}$ is more patterned, but it is very definite when the patterned structure of $C^p_{j\ell}$ abates. For signals (but less so for noise), σ^2_d tends to peak in mid-range for d. This represents a compensating trend between the occurrence of many samples for small separations d and reduced phase coherence for greater separations d.

(U) The behavior of

$$CM_{j\ell} \equiv \frac{\langle A_j A_\ell \rangle}{\langle A_j \rangle \langle A_\ell \rangle} = CM_4 \tag{37}$$

plotted in Fig 2 through 24 is interesting. It correlates with the observation that the higher CF is and the less structured $CNA_{j\ell}$ is, the more likely $CNA_{j\ell}$ is to remain above its zero correlation line given by $1/\max(\langle A_j A_\ell \rangle / \langle A_j \rangle \langle A_\ell \rangle)$. Thence, the relation of $CNA_{j\ell}$ to its zero correlation line and the amount of $CNA_{j\ell}$ with negative correlation will be determined as follows. $CNA_{j\ell}$ has a negative correlation when $\langle A_j A_\ell \rangle / \langle A_j \rangle \langle A_\ell \rangle < 1$. Therefore, define

$$CA^3_d \equiv \frac{\langle A_j A_\ell \rangle}{\langle A_j \rangle \langle A_\ell \rangle} \tag{38}$$

when $\langle A_j A_\ell \rangle < \langle A_j \rangle \langle A_\ell \rangle$ and set it to zero otherwise. CA^3_d can be treated in the same manner that C^3_d was. Briefly, at each separation d there may exist a number $n_{\bar{d}}$ of values for $CA^3_d = C^3_d(k) < 1$, $1 \leq k \leq n_{\bar{d}}$, with $n_{\bar{d}}$ a nonempty subset of n_d. Denote the total

number of separations when n_d^- is nonempty by N^-, which makes N^- a nonempty subset of N. Therefore, analogously to μ_N^i, define the amount of Negative Amplitude Correlation by

$$NAC \equiv \frac{1}{N^-} \sum_{d=d_1}^{N^-} \frac{1}{n_d^-} \sum_{k=1}^{n_d^-} \left| CA_d^3(k) \right| . \tag{39}$$

IV. (U) STABILITY OF THE TIME AVERAGES

(U) The question arises as to the stability of the synoptic factors as the averaging time ΔT is changed. This issue is addressed by considering the stability of some representative quantities [denoted by $S_i(\Delta T)$] of the sound field structure as ΔT is increased. In Ref 5 through 10, an averaging time of about 4 min was employed. (This was chosen after a preliminary study of CA_j and C_p for various values of ΔT.) To see how sensitive the quantities $S_i(\Delta T)$ are to changes in ΔT, assume a reference averaging time ΔT_r of about 4 min and consider how those quantities $S_i(\Delta T)$ vary relative to their values $S_i(\Delta T_r)$ at ΔT_r as a function of ΔT. In particular, consider

$$\Delta_i(\Delta T) \equiv \frac{S_i(\Delta T)}{S_i(\Delta T_r)} = DS_i . \tag{40}$$

(U) A suitable set of representative sound field structure quantities $S_i(\Delta T)$ was chosen for the acoustic synoptic factors of Section II. From these it was determined that the behavior of the quantities

$$S_1 = \bar{A}_a \equiv \frac{1}{J} \sum_{j=1}^{J} \langle A_j \rangle \tag{41}$$

and

$$S_3 = C_P \equiv \frac{1}{J^2} \sum_{j=1}^{J} \sum_{\ell=1}^{J} \langle \cos(\theta_j - \theta_\ell) \rangle \tag{42}$$

were adequate for the purpose of this study.

(U) Let the samples s(m) be indexed by m and summed to M, which corresponds to ΔT. Then

$$S_i(\Delta T) = S_i(M) = \frac{1}{M} \sum_{m=1}^{M} s_i(m) , \quad i = 1, 3.$$

Since we are dealing with indexed samples, say $s_{j\ell}(m)$, the above result is obtained as follows (note that the function index i has been suppressed):

$$S(\Delta T) = S(M) = \frac{1}{J^2} \sum_{j=1}^{J} \sum_{\ell=1}^{J} \frac{1}{M} \sum_{m=1}^{M} s_{j\ell}(m)$$

$$= \frac{1}{M} \sum_{m=1}^{M} \left(\frac{1}{J^2} \sum_{j=1}^{J} \sum_{\ell=1}^{J} s_{j\ell}(m) \right)$$

$$\equiv \frac{1}{M} \sum_{m=1}^{M} s(m)$$

$$= \frac{s(1) + \ldots + s(M)}{M}$$

$$\equiv \frac{s(1, \ldots, M)}{M}$$

where $s(1, \ldots, M)$ replaces $s(1) + \ldots + s(M)$ for brevity. Therefore,

$$\Delta_i(\Delta T) = \Delta_i(M) = \frac{\frac{s_i(1, \ldots, M)}{M}}{\frac{s_i(1, \ldots, M_r)}{M_r}} = \frac{s_i(1, \ldots, M)}{s_i(1, \ldots, M_r)} \frac{M_r}{M} ,$$

where M_r corresponds to ΔT_r.

(U) To quantify the total area between the curve $\Delta_i(\Delta T)$ and the line $\Delta_i = 1$, the synoptic factor

$$A\Delta_i \equiv \sum_{M=1}^{M_r} \left| \Delta_i(M) - 1 \right| = ADS_i \qquad (43)$$

is utilized and appears in Table 3 and Fig 2 through 24.

(U) The behavior of five functions $\Delta_i(\Delta T)$ for the first 12 signal periods for projector tows 2P3A and 4P1 was plotted. It was found that $\Delta_1(\Delta T)$ and $\Delta_3(\Delta T)$ were related to the other three functions in a logical manner, so only these two functions are included in this report for each of the 23 signal periods (Fig 2 through 24). The synoptic factors $A\Delta_1$ and $A\Delta_3$ are shown at the top of each of these figures and in Table 3. Table 3 shows that $A\Delta_3$ is related to CF (except for those corresponding to Fig 10, 19 and 23) in that $A\Delta_3$ generally increases as CF decreases. On the other hand, Table 1 shows that there is no correlation between $A\Delta_1$ and CF. Therefore, it is concluded that the more stable the time average of C_p is, the better the coherence $(\gamma^c_{j\ell})^2$ is. On the other hand, the stability of the time average of the amplitude has little impact on the coherence $(\gamma^c_{j\ell})^2$ for the cases investigated in Fig 2 through 24.

V. (U) NORMAL MODE MODEL FOR BEARING STAKE

(U) A normal mode model has been applied to Bearing Stake. This section discusses the suitability of this model for representing Bearing Stake results (Ref 4, 9, 11). The model found in Ref 9 that the Bearing Stake sound field structure is at least three times as complex as that of the open Atlantic and Pacific Oceans. In its Pacific and Atlantic results, Ref 11 found that, with respect to sound field complexity across arrays, vertical projections are about 15 times as important as radial projections. With regard to wavefront corrugations, both vertical and radial (ie, rangewise or endfire) projections should be more important than transverse (ie, broadside) projections. (Being essentially two-dimensional, the model cannot treat behavior transverse to the plane of sound projection.) Wavefront corrugations (a sound field propagation effect) and array deformations are indiscernible near broadside. Wavefront corrugation near endfire is mainly caused by the radial field along the array, which is averaged over 4 min of mainly relative radial motion of the array (the aspect angle determines the relative amount of radial and transverse source motion).

(U) The normal mode model can treat radial and vertical projections of the sound field structure but not the transverse sound field structure. Therefore the model was employed to examine the 50-ft difference in vertical projections between the OAMS array (925.4 m or 3036 ft long times 1 deg of tilt equals 53 ft vertical projection) and the LATA (1200 m or 3936 ft long times 1 deg of tilt equals 103 ft vertical projection). For Site 4, the OAMS array subset of the LATA (Ref 8) reduced the LATA vertical projection by about 1/4 to 79.48 ft (ie, 3036 ft long times sin 1½ deg) due to the approximately 1/4 length reduction of the LATA. This reduces the residual phase variability by about 1/3 near broadside as shown in Fig 25. Therefore, reducing the vertical projection does reduce the wavefront corrugation significantly. It may even be true that the transverse wavefront corrugation is essentially negligible. This is important for modeling purposes when one considers how difficult it is to remove all array tilt.

(U) The broadside OAMS array behavior with respect to C_p is observed (see Fig 26) to be about the same as the OAMS array subset of the LATA (Fig 25a). Thus, it appears that the LATA and the OAMS array are comparable at broadside with respect to C_p. For the LATA for Site 2 and for the OAMS array for Site 5, the LATA tilt was probably no worse (if not better) due to "array trimming" (Ref 8) than the OAMS array tilt. The OAMS array on Tow 5P1 (Fig 27) was comparable to the LATA on Tow 2P3A (Fig 29) and on Tow 4P1 (Fig 31) near broadside with respect to C_p. However, the OAMS array on Tow 5P1 (Fig 27) was much better than the LATA on Tow 2P3 (Fig 33) near broadside with respect to C_p. Note that although Fig 27 shows C_p behavior that is superior to Fig 28 and 30, when only the broadside values of Fig 29 and 31 are compared to Fig 27, it appears that the OAMS array and LATA performed similarly near broadside.

(U) Figure 34 illustrates a plausible explanation of how the angle-variable behavior for the LATA agrees with the normal mode model. The solid line in Fig 34 represents the mean of C_p, and the dashed line represents the standard deviation about this mean. The normal mode model assumes that there is no transverse variation and assumes that the offset below unity of the mean C_p at broadside is due solely to the remaining vertical projection of the LATA array. The normal mode model generally agrees with the behavior shown in Fig 34 in that in moving from broadside toward endfire, the radial projection of the sound field increases, causing the mean of C_p to decrease and the standard deviation about this mean to increase.

11. Personal Communication from M. A. Pedersen of the Naval Ocean Systems Center.

VI. (U) CONCLUSIONS

(U) In Section I an overview of synoptic factors was given. The usefulness of synoptic factors for improving the utilization of theoretical models was emphasized, and Ref 4 gives examples of this. Section II defined several types of acoustic synoptic factors. Some of these are shown in Tables 1 and 2 for the Bearing Stake data addressed in this report. Two types of acoustic synoptic factors are given. These are total array acoustic synoptic factors and intra-array acoustic synoptic factors. The latter class consists of one-point structure factors and two-point structure factors. The latter type is plotted in Fig 2 through 24, and its structure received much attention in Sections III and IV.

(U) A detailed sound field structure study was developed in Section III. This consisted of developing some further acoustic synoptic factors for the structure of the sound field and finding meaningful relations between these factors. It was shown that the coherence factor CF, as determined by the structured behavior of the classical coherence $(\gamma^c_{j\ell})^2$, is very useful for categorizing array coherence behavior. In fact, Table 3 shows that CF is a more reliable parameter than the usual coherence measure C_p, the array phase coherence coefficient. In a discussion of projector Tow 4P1, it was shown that an array turn can introduce a patterned disturbance into $(\gamma^c_{j\ell})^2$ and that this behavior can persist for at least 1.75 hr after the turn event. Examining Tow 2P3A showed that even a straight radial tow can produce significant changes in the coherence behavior.

(U) The stability of the time averages used in this coherence study is given in Section IV. The results are shown in Fig 2 through 24 and in Table 3. It is concluded that the more stable the time average of the phase coherence is, the better the classical coherence is, while the stability of time average of the amplitude has far less significance.

(U) Section V discussed normal mode modeling for Bearing Stake. It can model the impact of array tilt and bearing angle. The OAMS array and LATA differences discussed in Ref 7 were resolved, and it was shown that the LATA behavior shown in Fig 34 can be explained by the normal mode model.

(U) The question arises as to how the acoustic synoptic factors are used in practice. Reference 4 gives excellent examples as to the use of some of the acoustic synoptic factors discussed in this report. In Ref 4 the array configuration and tilt are modeled in their software along with the appropriate propagation conditions. This produces the appropriate values for the amplitude and phase. These latter values are then fed into software models of the acoustic synoptic factors (for example, ASG of Eq (13) and $(\gamma^c_{j\ell})^2$ of Eq (22)) and then compared with the results obtained when actual Bearing Stake data are applied. These results were instructive, and the phenomenological ambiguities of Ref 7 were resolved. This procedure is the one recommended for predicting the behavior of the acoustic synoptic factors in other environments and/or for arrays other than those used in Bearing Stake. With the understanding gained from such an analysis, insight is gained into the sound field structure for the other environments and/or for the other arrays. With this insight, system relations such as appear in Ref 12 can be applied with confidence.

12. J. A. Neubert, "The effect of the sound field structure on array signal gain in a multipath environment," J. Acoust. Soc. Am., October 1981.

REFERENCES (U)

1. J. A. Neubert, "Performance Variability of Sonar Systems (U)," NOSC TR 679, April 1981 (CONF).

2. M. A. Pedersen and G. S. Yee, "Propagation Loss Assessment of the Bearing Stake Exercise (U)," NOSC TR 467, 28 September 1979 (CONF).

3. W. H. Watson and R. W. McGirr, "Raywave II: A Propagation Loss Model for the Analysis of Complex Ocean Environments," NUC TN 1516, 1975.

4. D. F. Gordon, "Array Simulation at the Bearing Stake Sites (U)," NOSC TR 664, April 1981, (CONF).

5. J. A. Neubert, "Bearing Stake Coherence Data Analysis: Part I. The OAMS Array (U)," NOSC TN 380, 6 February 1978 (CONF).

6. J. A. Neubert, "Bearing Stake Coherence Data Analysis: Bottom-Mounted Array (U)," NOSC TN 452, 31 May 1978 (CONF).

7. A. G. Fabula and J. A. Neubert, "Bearing Stake Data Analysis: LATA (U)," NOSC TN 589, November 1978 (CONF).

8. J. A. Neubert, "Bearing Stake Array Signal Gain Analysis (U)," NOSC TN 624, December 1978 (CONF).

9. J. A. Neubert, "Bearing Stake Coherence and Array Signal Gain Area Assessment Report (U)," NOSC TR 383, December 1978 (CONF).

10. J. A. Neubert, "Coherence and Its Sound Field Structure in the Northwestern Indian Ocean (U)," J. Underwater Acoustics, November 1980, CONF.

11. Personal Communication from M. A. Pedersen of the Naval Ocean Systems Center.

12. J. A. Neubert, "The effect of the sound field structure on array signal gain in a multipath environment," J. Acoust. Soc. Am., October 1981

TIME	ΔT (SEC)	S or N	FREQ (HZ)	BEARNG (DEG)	RANGE (KM)	S+N (DB)	N (DB)	CF	ADS3	ADS1	$\Delta\Phi_o$ (DEG)	C_p	Σ_A	ASG (DB)	NAC	SF
1855:15	240	SIGNAL	25.10	102.70	400.00	-2.7	-----	.8901	1.6	8.6	12.70	.8420	.532	-1.57	.28+00	.0184
1900:06	240	NOISE	25.10	162.70	396.58	-----	-20.7	.5368	14.0	7.0	72.70	.0736	.578	-10.49	.20+00	.0035
1900:07	240	SIGNAL	20.08	101.65	391.51	-3.8	-----	.9924	.6	8.1	11.45	.9389	.233	-.48	.30-02	.0001
1900:07	240	NOISE	25.10	58.25	391.51	-----	-20.3	.5271	11.3	3.3	-31.75	.0818	.589	-9.29	.33+00	.0045
1905:18	240	SIGNAL	25.10	101.65	389.83	-2.5	-----	.9876	.4	4.7	11.65	.9367	.429	-.17	.00	.0006
1922:36	240	SIGNAL	25.10	101.85	384.52	-7.0	-----	.8897	5.5	3.5	11.85	.7209	.480	-1.58	.37+00	.0194
1940:16	240	SIGNAL	25.10	102.50	377.26	-.8	-----	.9913	.5	14.0	12.50	.9490	.381	-.40	.00	.0003
2008:22	240	SIGNAL	25.10	102.70	366.41	.7	-----	.9843	.4	8.1	12.70	.8518	.292	-.72	.00	.0015
2018:58	240	SIGNAL	25.10	101.10	362.91	-1.4	-----	.9721	7.8	16.4	11.10	.8187	.547	-.30	.00	.0027
2104:37	228	SIGNAL	25.10	103.45	347.97	.2	-----	.9874	.2	7.1	13.45	.9331	.345	-.43	.00	.0009
2209:20	240	SIGNAL	25.10	101.25	328.09	-2.2	-----	.9626	.6	2.0	11.25	.8450	.357	-1.32	.48+00	.0039
2221:40	240	SIGNAL	25.10	98.70	321.02	-3.0	-----	.9052	3.0	13.7	8.70	.8133	.525	-.58	.00	.0109
2335:49	236	SIGNAL	25.12	13.65	292.59	3.1	-----	.9447	23.7	10.1	-76.35	.7081	.412	-.71	.41+00	.0084
2349:03	240	SIGNAL	25.12	19.55	286.27	-3.6	-----	.8756	16.6	8.8	-70.45	.5739	.578	-1.96	.29+00	.0146
0003:52	240	SIGNAL	25.12	18.10	282.05	-3.0	-----	.8852	11.6	7.2	-71.90	.6877	.433	-1.48	.34+00	.0142
0018:01	192	SIGNAL	20.10	24.35	275.73	-13.3	-----	.8588	8.9	2.2	-65.65	.3422	.533	-4.59	.58+00	.0083
0018:01	192	NOISE	25.12	22.40	275.73	-----	-20.6	.5326	19.0	1.6	-67.60	.0699	.591	-9.16	.43+00	.0040
0021:27	240	SIGNAL	25.12	17.90	273.63	-2.7	-----	.9298	6.2	2.8	-72.10	.6208	.393	-1.20	.63+00	.0119
0028:32	240	SIGNAL	20.10	18.85	269.44	-5.5	-----	.8991	3.9	5.1	-75.15	.7614	.411	-1.33	.46+00	.0118
0028:32	240	NOISE	25.12	48.20	269.44	-----	-20.8	.5792	18.9	2.3	-21.80	.0755	.567	-10.03	.42+00	.0037
0035:25	240	SIGNAL	25.10	18.50	267.34	-.1	-----	.9243	13.1	9.1	-75.50	.5487	.519	-2.54	.36+00	.0085
0104:35	240	SIGNAL	25.12	18.65	255.19	-1.9	-----	.9429	3.7	3.5	-71.35	.6929	.378	-1.35	.60+00	.0096
0121:03	240	SIGNAL	25.12	17.15	249.12	-1.5	-----	.9241	25.7	11.8	-72.90	.5376	.579	-1.42	.56+00	.0110
0138:51	232	SIGNAL	25.12	18.45	241.12	-3.3	-----	.8059	2.2	8.0	-71.55	.7554	.542	-1.67	.49+00	.0179
0156:36	236	SIGNAL	25.12	15.00	237.04	1.3	-----	.9801	8.6	7.1	-75.00	.8697	.307	-1.10	.24+00	.0062
0206:46	240	SIGNAL	25.12	12.80	230.86	2.5	-----	.9517	3.0	6.0	-77.60	.7957	.462	-.91	.46+00	.0085
0213:20	240	NOISE	25.10	18.85	226.76	-----	-21.0	.5466	6.1	1.4	-71.15	.0738	.541	-9.76	.40+00	.0037
0213:20	240	SIGNAL	20.08	23.70	226.76	-8.6	-----	.7610	10.6	10.9	-66.30	.5287	.528	-3.13	.56+00	.0251
0221:52	240	SIGNAL	25.10	10.75	224.71	-2.3	-----	.8998	6.2	8.6	-79.25	.7878	.422	-1.38	.50+00	.0133
0333:17	240	SIGNAL	25.07	113.50	200.70	2.0	-----	.9551	2.2	3.6	23.50	.8617	.356	-.55	.49+00	.0050
0350:16	240	SIGNAL	25.07	117.50	196.48	1.7	-----	.9331	11.8	6.0	27.50	.5667	.401	-1.11	.23+00	.0112
0409:16	240	SIGNAL	25.07	119.70	192.36	2.9	-----	.9345	11.7	8.8	25.70	.7778	.307	-.94	.19+00	.0078
0427:01	240	SIGNAL	25.07	118.55	188.33	-8.8	-----	.8420	18.1	6.0	24.55	.5123	.544	-2.53	.39+00	.0424
0438:08	240	SIGNAL	25.07	117.85	186.39	2.4	-----	.8797	21.2	10.3	27.85	.6228	.422	-1.04	.28+00	.0164
0455:05	240	SIGNAL	25.07	117.80	180.52	1.2	-----	.8727	19.1	5.8	27.80	.5035	.466	-1.72	.37+00	.0239
0503:09	240	SIGNAL	25.07	120.45	176.79	1.9	-----	.9105	18.2	18.4	30.45	.6065	.536	-.97	.00	.0127
0512:51	240	SIGNAL	20.06	125.15	174.39	-1.0	-----	.9588	.6	1.9	33.15	.8692	.252	-.61	.39+00	.0053
0512:51	240	NOISE	25.07	160.85	174.39	-----	-19.9	.5690	9.6	3.5	70.85	.1351	.547	-7.33	.31+00	.0045
0526:39	240	SIGNAL	25.07	125.05	173.21	1.2	-----	.8890	1.7	7.2	35.05	.7119	.448	-1.78	.44+00	.0113
0527:15	240	SIGNAL	20.06	127.60	170.89	-1.9	-----	.9712	2.0	6.0	37.60	.8201	.388	-.73	.4 +00	.0037

(CONFIDENTIAL)

(U) Table 1. Acoustic Synoptic Factors for Tow 2P3A.

CONFIDENTIAL

TIME	ΔT (SEC)	S or N	FREQ (HZ)	BEARNG (DEG)	RANGE (KM)	S+N (DB)	N (DB)	CF	ADS3	ADS1	$\Delta\Phi_o$ (DEG)	C_p	Σ_A	ASG (DB)	NAC	SF
0927:15	240	NOISE	25.07	168.65	170.89	-----	-20.2	.5049	7.3	3.6	78.65	.0898	.544	-9.06	.40+00	.0042
0935:33	240	SIGNAL	25.07	130.70	169.78	2.8	-----	.9476	1.5	11.9	40.70	.8222	.412	-1.28	.26+00	.0352
0948:32	240	SIGNAL	25.07	126.50	146.38	2.5	-----	.8860	7.8	5.4	36.50	.6248	.412	-1.35	.15+00	.0106
0402:49	240	SIGNAL	25.07	127.10	164.20	3.3	-----	.8833	11.6	6.3	37.10	.5628	.499	-2.18	.33+00	.0147
0422:15	240	SIGNAL	25.06	129.55	158.75	-3.1	-----	.6983	6.5	2.5	39.55	.3985	.533	-3.56	.48+00	.0366
0442:12	240	NOISE	25.07	29.65	158.75	-----	-19.7	.5486	21.8	4.3	-60.35	.1045	.545	-8.13	.37+00	.0048
0441:35	240	SIGNAL	25.07	176.95	152.40	-.9	-----	.7833	12.1	10.5	36.90	.6632	.492	-1.69	.41+00	.0317
0701:35	240	SIGNAL	25.07	129.80	188.99	1.0	-----	.8836	31.6	14.9	35.80	.4799	.674	-2.44	.49+00	.0156
0718:45	240	SIGNAL	25.05	126.90	166.16	5.5	-----	.9478	2.9	1.0	36.90	.8710	.324	-1.38	.42+00	.0054
0733:32	240	SIGNAL	25.05	128.75	183.52	1.8	-----	.7568	11.8	7.1	38.75	.5098	.582	-4.04	.31+00	.0263
0751:41	240	SIGNAL	25.05	129.60	161.03	-.9	-----	.7761	3.5	18.0	39.60	.4256	.607	-2.98	.18+00	.0218
0805:08	240	SIGNAL	25.05	130.35	138.60	2.9	-----	.8962	4.6	3.7	40.35	.8363	.365	-.59	.12+00	.0091
0818:31	240	SIGNAL	25.04	135.75	136.31	2.7	-----	.7883	8.2	10.5	45.75	.5549	.447	-1.86	.37+00	.0219
0832:12	240	SIGNAL	25.05	136.00	134.88	4.3	-----	.7742	5.1	.6	46.00	.7585	.419	-1.18	.56+00	.0212
0847:33	240	SIGNAL	25.04	135.60	135.53	-3.1	-----	.7103	22.7	6.9	45.60	.5327	.502	-1.80	.51+00	.0425
0901:33	240	NOISE	25.04	151.65	133.53	-----	-18.4	.6278	6.8	4.9	61.65	.1414	.562	-7.05	.35+00	.0037
0914:06	240	SIGNAL	25.02	151.35	131.05	4.9	-----	.7309	14.9	5.3	61.35	.5327	.389	-2.53	.34+00	.0283
0919:42	240	SIGNAL	25.02	140.45	128.85	-.2	-----	.6787	30.4	5.9	50.45	.4839	.563	-2.30	.50+00	.0341
0932:47	240	SIGNAL	25.02	146.60	127.88	4.9	-----	.9481	1.0	1.8	56.60	.8918	.265	-.73	.57+00	.0025
0947:38	240	SIGNAL	25.02	146.90	126.28	.9	-----	.7778	4.7	2.9	56.90	.6547	.408	-2.85	.53+00	.0186
1006:57	240	SIGNAL	25.02	151.80	125.26	6.8	-----	.9759	.3	2.9	61.80	.9559	.248	-.59	.27+00	.0003
1022:10	240	SIGNAL	25.02	150.35	124.47	1.7	-----	.7271	7.6	1.1	60.35	.7182	.583	-1.26	.48+00	.0200
1027:14	240	SIGNAL	25.02	146.30	124.41	-.9	-----	.8168	9.7	.9	56.30	.6603	.638	-5.54	.60+00	.0196
1027:14	240	NOISE	25.02	183.45	124.41	-----	-18.5	.5776	10.1	1.8	53.45	.0951	.555	-10.15	.35+00	.0036
1035:13	240	SIGNAL	25.02	150.45	124.43	2.6	-----	.9815	.9	1.5	60.95	.8192	.422	-2.86	.42+00	.0017
1107:37	240	SIGNAL	25.00	69.35	121.78	-6.2	-----	.9781	.3	.7	-47.65	.9334	.311	-.80	.43+00	.0005

(CONFIDENTIAL)

(U) Table 1. Continued

CONFIDENTIAL

TIME	ΔT (SEC)	S or N	FREQ (HZ)	BEARNG (DEGR)	RANGE (KM)	S+N (DB)	N (DB)	CF	ADS3	ADS1	$\Delta\Phi_o$ (DEG)	C_p	Σ_A	ASG (DB)	NAC	SF
1004:40	240	SIGNAL	25.05	102.35	73.37	-8.8	-----¬	.8709	13.2	5.3	12.55	.5971	.485	-1.73	.56+00	.0239
1006:29	240	SIGNAL	25.04	109.95	65.73	-6.8	-----¬	.9505	1.4	7.6	19.95	.8516	.413	-1.20	.49+00	.0058
1008:11	240	SIGNAL	25.04	109.70	63.91	-18.7	-----¬	.7944	16.5	8.6	17.70	.4767	.556	-2.60	.47+00	.0139
1008:11	240	NOISE	25.05	56.55	63.91	----→	-29.5	.5774	10.0	6.4	-33.45	.0988	.634	-9.28	.29+00	.0043
1111:16	240	SIGNAL	25.04	116.65	61.06	-8.9	-----¬	.9100	5.5	3.6	26.65	.8523	.438	-1.00	.51+00	.0128
1111:16	240	NOISE	25.05	10.65	61.06	----→	-29.3	.6168	5.2	4.2	-79.35	.1119	.620	-8.27	.32+00	.0080
1118:06	240	SIGNAL	25.05	114.55	60.11	-5.9	-----¬	.8153	15.1	7.3	28.50	.3848	.480	-4.01	.33+00	.0293
1131:30	240	SIGNAL	25.05	119.70	57.31	-5.7	-----→	.9410	2.9	12.4	29.70	.7332	.671	-2.52	.30+00	.0078
1166:57	240	SIGNAL	25.05	125.30	56.56	-5.6	-----→	.9417	5.8	7.4	32.30	.5071	.566	-3.04	.42+00	.0081
1201:07	236	SIGNAL	25.05	122.80	52.05	-5.9	-----¬	.8724	8.0	8.9	32.80	.5940	.536	-3.31	.43+00	.0193
1254:51	240	SIGNAL	25.04	104.90	46.30	-8.0	-----¬	.9381	.6	.9	56.90	.8279	.486	-1.95	.51+00	.0078
1259:51	240	NOISE	25.05	80.30	46.30	----→	-27.7	.6425	5.6	4.7	-9.70	.1608	.656	-6.91	.11+00	.0056
1301:54	240	SIGNAL	25.05	104.30	43.61	-.1	-----¬	.9775	1.5	2.9	54.30	.9249	.362	-.80	.40+00	.0018
1314:05	240	SIGNAL	25.04	101.90	41.56	-3.9	-----→	.7898	2.8	6.7	51.90	.8122	.557	-.63	.40+00	.0284
1359:51	240	SIGNAL	25.02	133.45	36.26	-6.9	-----→	.9485	.7	1.5	43.45	.9318	.380	-.74	.55+00	.0035
1359:51	240	NOISE	25.02	83.30	36.26	----→	-25.2	.6995	6.2	3.0	-46.70	.2486	.649	-5.58	.19+00	.0082
1401:10	240	SIGNAL	25.02	133.35	35.61	-2.0	-----¬	.8038	7.0	1.1	43.30	.4108	.544	-3.60	.48+00	.0220
1417:39	240	SIGNAL	25.02	131.45	33.70	-1.6	-----→	.9022	3.5	1.2	41.45	.8364	.454	-1.55	.52+00	.0137
1450:58	240	SIGNAL	25.02	130.20	31.84	-9.0	-----→	.9056	2.7	1.0	40.20	.8491	.887	-1.52	.47+00	.0098
1508:48	240	SIGNAL	25.02	131.05	30.03	-7.8	-----¬	.9278	.8	3.8	41.05	.8889	.413	-1.17	.39+00	.0037
1508:48	192	SIGNAL	25.03	130.10	29.85	-19.0	-----¬	.6798	9.0	2.3	40.10	.4878	.669	-4.31	.37+00	.0176
1555:52	192	NOISE	25.02	78.05	29.85	----→	-37.1	.5971	19.8	18.7	-13.35	.1279	.952	-12.20	.19-02	.0050
1559:59	240	SIGNAL	25.02	129.25	28.26	-13.5	-----¬	.7786	8.5	1.5	39.25	.6292	.524	-2.55	.47+00	.0141
1919:12	240	SIGNAL	25.02	126.30	26.37	-12.4	-----→	.6877	8.3	6.0	36.30	.4738	.562	-2.81	.42+00	.0218
1931:13	240	SIGNAL	25.02	119.95	25.04	-6.8	-----→	.8057	7.5	1.2	29.95	.7586	.459	-1.98	.40+00	.0205
1946:18	236	SIGNAL	25.02	116.10	23.85	-2.3	-----¬	.9620	1.0	4.3	26.10	.6504	.362	-1.69	.38+00	.0020
1710:47	240	SIGNAL	25.00	57.79	17.77	-12.0	-----¬	.9087	1.0	.7	-57.30	.9009	.937	-1.62	.30+00	.0045
1710:47	240	NOISE	25.00	109.45	17.77	----→	-28.8	.6813	5.3	1.0	59.45	.1447	.638	-7.12	.35+00	.0050
1716:12	240	SIGNAL	25.00	29.65	17.74	.3	-----¬	.9797	.2	.4	-60.35	.9462	.927	-.27	.24+00	.0002
1731:00	240	SIGNAL	24.99	34.80	18.11	2.7	-----¬	.9709	1.2	1.2	-55.60	.9170	.387	-.08	.47+00	.0029
1748:24	240	SIGNAL	24.97	82.05	18.73	-6.8	-----¬	.9593	.9	1.3	-47.95	.9177	.382	-.93	.30+00	.0048
1809:27	240	SIGNAL	24.97	69.30	20.28	-2.3	-----→	.8980	1.4	1.3	-40.70	.8646	.483	-2.10	.48+00	.0099
1811:29	240	SIGNAL	24.96	67.15	20.95	-10.2	-----→	.9348	.8	2.0	-27.85	.8719	.419	-.88	.43+00	.0016
1811:29	240	NOISE	24.99	166.15	20.95	-----	-28.6	.7153	7.7	.6	76.15	.1943	.644	-5.97	.30+00	.0062
1818:05	240	SIGNAL	24.97	51.75	21.65	-8.1	-----¬	.8785	2.5	8.3	-38.25	.8030	.515	-2.46	.38+00	.0129
1831:13	240	SIGNAL	24.98	95.30	23.93	-10.1	-----¬	.8315	2.8	8.3	-38.70	.7841	.521	-2.03	.17+00	.0131
1846:52	240	SIGNAL	24.98	60.15	26.42	-1.2	-----→	.8211	19.1	6.7	-29.85	.5681	.899	-2.65	.41+00	.0178
1905:27	240	SIGNAL	24.98	67.95	29.29	-5.8	-----→	.9151	1.7	2.7	-22.05	.8240	.552	-1.80	.43+00	.0108
1911:28	240	SIGNAL	24.98	69.80	31.29	-2.5	-----¬	.9473	1.9	2.8	-20.20	.7992	.508	-1.81	.38+00	.0087
1911:28	240	NOISE	24.99	30.90	31.29	-----	-27.6	.7145	21.9	1.3	-59.10	.1565	.631	-8.13	.25+00	.0056

(CONFIDENTIAL)

(U) Table 2. Acoustic Synoptic Factors for Tow 4P1.

TIME	ΔT (SECT)	S or N	FREQ (HZ)	BEARNG (DEGT)	RANGE (KNT)	S+N (DB)	N (DB)	CF	ABSS	ABSI	$\Delta\Phi_o$ (DEGT)	C_p	Σ_A	ASG (DB)	NAC	SF
1931:37	240	SIGNAL	24.02	68.80	33.32	-5.5	---->	.8787	9.6	3.3	-21.60	.5571	.408	-3.32	.29+00	.0170
1931:52	236	SIGNAL	24.02	68.05	35.39	-2.8	---->	.9521	.9	2.7	-25.95	.8274	.486	-.71	.47+00	.0056
1948:28	240	SIGNAL	24.02	68.30	38.55	2.6	---->	.9339	7.9	1.4	-75.50	.5953	.565	-1.86	.50+00	.0109
2106:04	236	SIGNAL	24.02	170.25	62.36	-2.9	---->	.8640	14.8	3.1	80.25	.5421	.574	-2.41	.45+00	.0157
2110:60	240	SIGNAL	24.02	165.15	65.46	-9.4	---->	.8278	14.8	5.4	75.15	.3267	.491	-5.61	.42+00	.0121
2132:17	240	SIGNAL	24.02	152.90	70.10	-8.6	---->	.8773	15.1	9.0	62.90	.4028	.591	-3.35	.41+00	.0110
2141:52	240	SIGNAL	24.02	166.15	73.20	-10.0	---->	.9501	.8	.5	76.15	.8327	.476	-1.40	.49+00	.0052
2141:32	240	NOISE	24.02	85.70	73.20	---->	-21.3	.7691	15.8	5.9	-4.30	.3245	.721	-2.75	.68-02	.0110
2146:25	240	SIGNAL	24.02	167.65	76.75	-9.0	---->	.9413	.9	3.0	57.65	.8992	.484	-1.54	.40+00	.0042
2154:28	240	SIGNAL	24.02	165.15	77.85	-8.7	---->	.9334	2.7	8.9	75.15	.8147	.486	-1.48	.53+00	.0070
2156:26	240	NOISE	24.02	87.65	77.85	---->	-27.4	.6776	16.6	19.0	7.65	.1226	.751	-8.84	.34-03	.0053
2203:04	240	SIGNAL	24.02	165.65	79.32	-8.3	---->	.8975	.9	3.3	75.65	.8276	.517	-1.32	.46+00	.0108
2305:17	240	SIGNAL	24.02	172.70	97.32	-10.5	---->	.8235	6.2	4.6	82.70	.4594	.767	-4.83	.46+00	.0172
2311:42	240	SIGNAL	24.02	162.55	100.39	-12.4	---->	.8769	6.9	8.3	72.55	.6820	.580	-1.83	.46+00	.0144
2311:42	240	NOISE	24.02	87.30	100.39	---->	-27.0	.7612	7.8	6.5	2.30	.3006	.640	-5.13	.21+00	.0079
2320:13	240	SIGNAL	24.02	152.15	101.79	-14.7	---->	.8285	8.1	3.0	62.15	.5204	.569	-2.72	.53+00	.0137
2332:39	240	SIGNAL	24.02	155.50	106.26	-16.1	---->	.8482	10.7	.7	65.50	.4676	.481	-3.42	.62+00	.0091
0049:39	240	SIGNAL	24.02	84.45	129.07	-11.6	---->	.9607	1.0	6.6	-5.55	.8837	.399	-1.03	.43-01	.0024
0049:04	240	SIGNAL	10.08	84.95	127.68	-16.1	---->	.9747	.7	7.8	-5.05	.9092	.469	-.69	.00	.0027
0057:04	240	NOISE	24.02	56.25	127.68	---->	-26.3	.7854	8.8	2.6	-33.75	.2836	.642	-8.23	.21+00	.0065
0107:06	240	SIGNAL	24.02	87.25	130.27	-13.6	---->	.9768	1.4	7.5	-2.75	.8992	.503	-.79	.00	.0012
0111:39	240	SIGNAL	10.08	87.55	131.51	-15.7	---->	.9820	5.0	9.3	-2.45	.9089	.465	-.75	.00	.0010
0111:39	240	NOISE	24.02	87.65	131.51	---->	-23.8	.7965	7.5	6.0	-27.35	.5044	.655	-2.19	.21-01	.0175
0116:57	240	SIGNAL	24.02	86.40	132.71	-11.8	---->	.9578	2.7	5.1	-3.60	.6960	.439	-1.48	.50-02	.0047
0135:56	240	SIGNAL	24.02	85.80	136.22	-9.9	---->	.9673	6.0	10.5	-4.20	.7829	.636	-.95	.00	.0020
0147:55	240	SIGNAL	24.02	82.45	139.73	-14.3	---->	.9207	4.6	9.6	-7.55	.6651	.542	-1.12	.25+00	.0110

(CONFIDENTIAL)

(U) Table 2. Continued

CONFIDENTIAL

Fig No	CF	ADS3	ADS1	$\Delta\Phi_o$	C_p
3	0.9924	0.6	4.1	11.45	0.9389
6	0.9913	0.5	14.0	12.50	0.9490
4	0.9876	0.4	4.7	11.65	0.9367
9	0.9874	0.2	7.1	13.45	0.9331
7	0.9843	0.4	8.1	12.70	0.8518
22	0.9775	1.5	2.9	54.30	0.9249
8	0.9721	7.8	16.4	11.10	0.8187
10	0.9626	0.6	2.0	11.25	0.8450
14	0.9505	1.4	7.6	19.95	0.8516
24	0.9485	0.7	1.5	43.45	0.9318
12	0.9477	23.7	10.1	−76.35	0.7081
19	0.9417	5.8	2.4	32.30	0.5071
18	0.9410	2.9	12.4	29.70	0.7332
21	0.9381	0.6	0.9	54.90	0.8279
16	0.9100	5.5	3.6	26.65	0.8523
11	0.9052	3.0	13.7	8.70	0.8133
2	0.8901	1.6	8.6	12.70	0.8420
5	0.8897	5.5	3.5	11.85	0.7209
20	0.8724	8.0	4.9	32.80	0.5940
13	0.8709	13.0	3.3	12.55	0.5971
17	0.8153	15.1	7.3	24.50	0.3844
15	0.7944	16.5	8.6	17.70	0.4767
23	0.7898	2.5	6.7	51.90	0.8122

$\Delta\Phi_o$ gives the off-broadside angle.

(UNCLASSIFIED)

(U) Table 3. Study of CF.

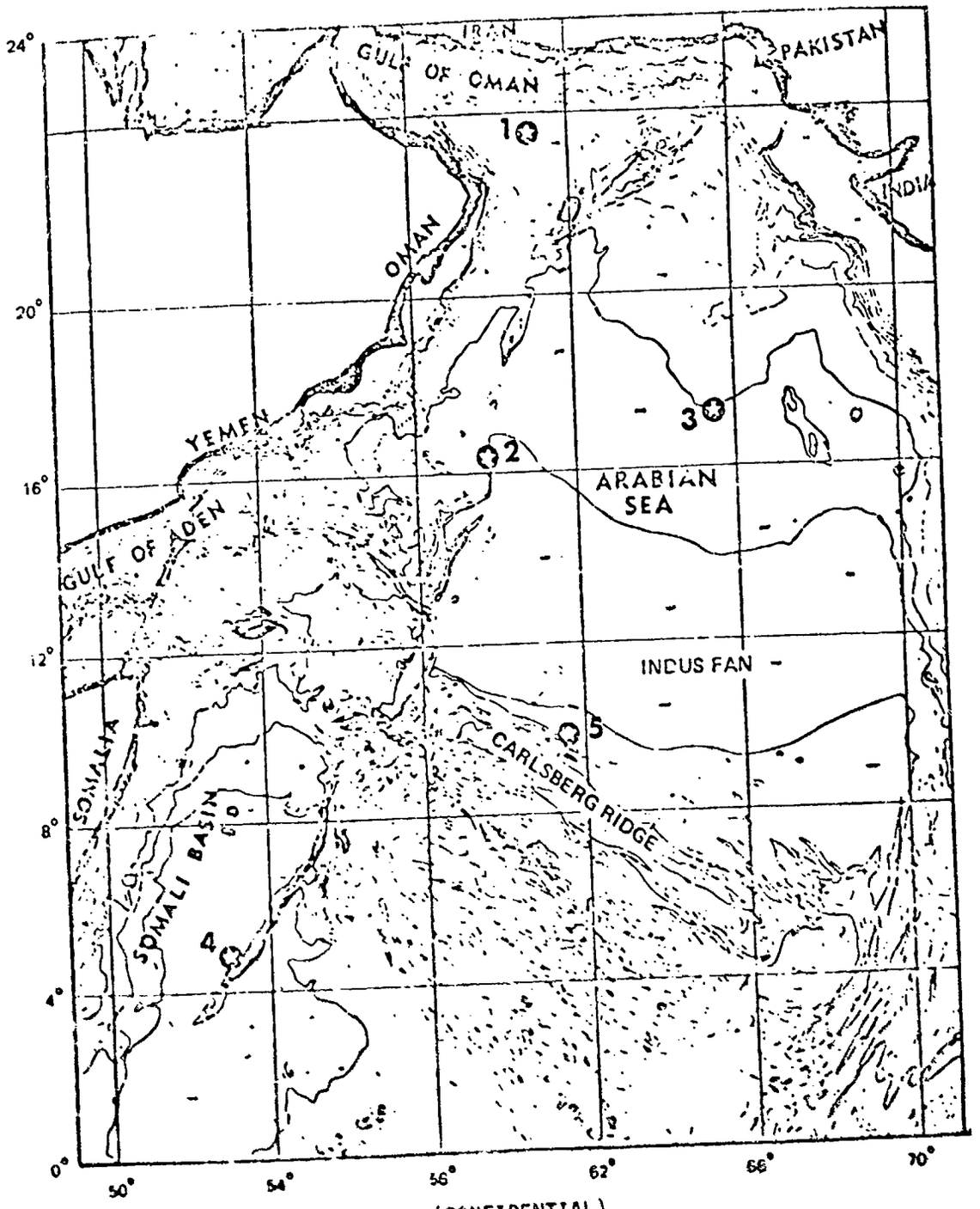

(CONFIDENTIAL)

(U) Figure 1. Bearing Stake Site Locations.

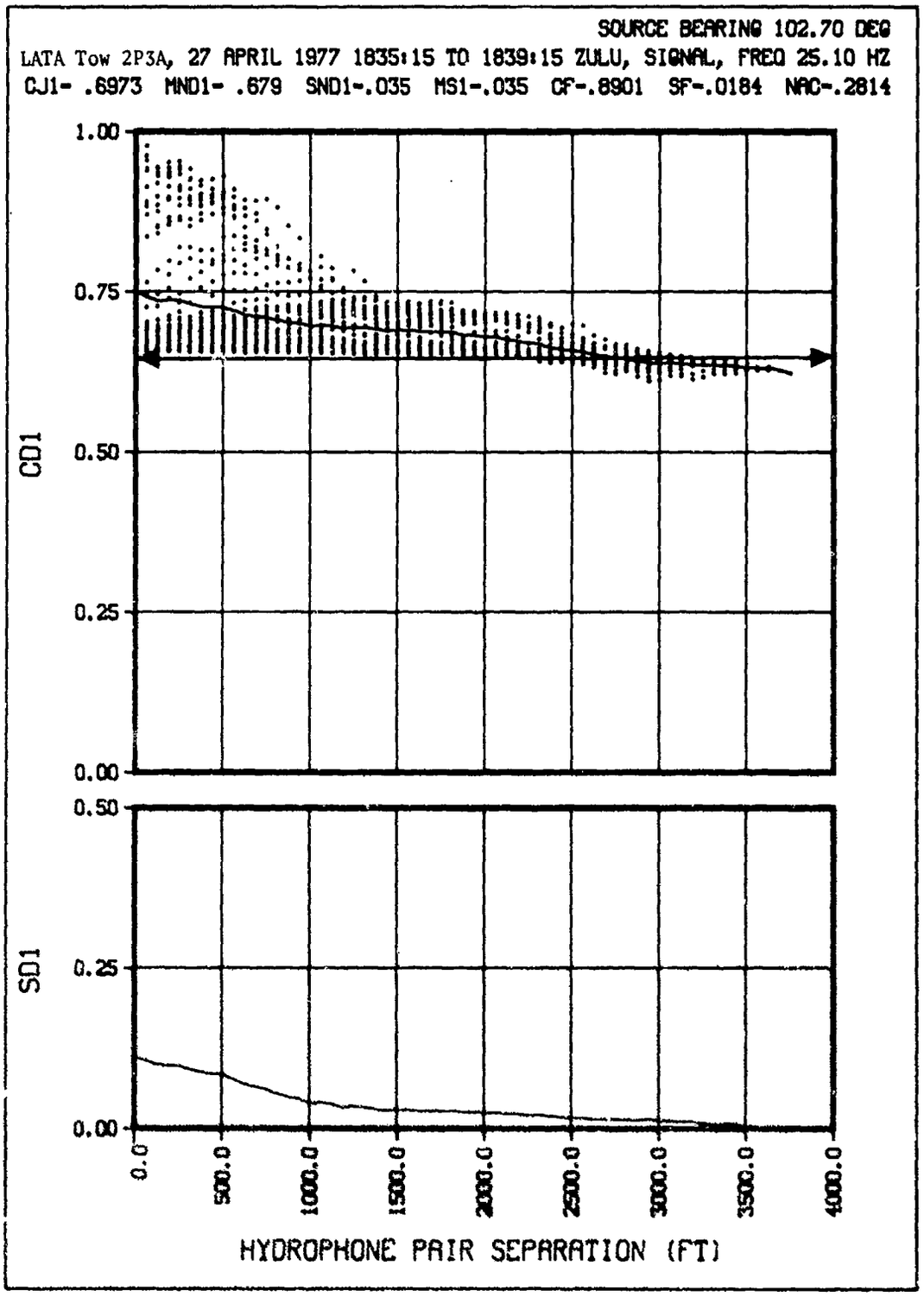

(CONFIDENTIAL)

(U) Figure 2a. Normalized amplitude covariance.

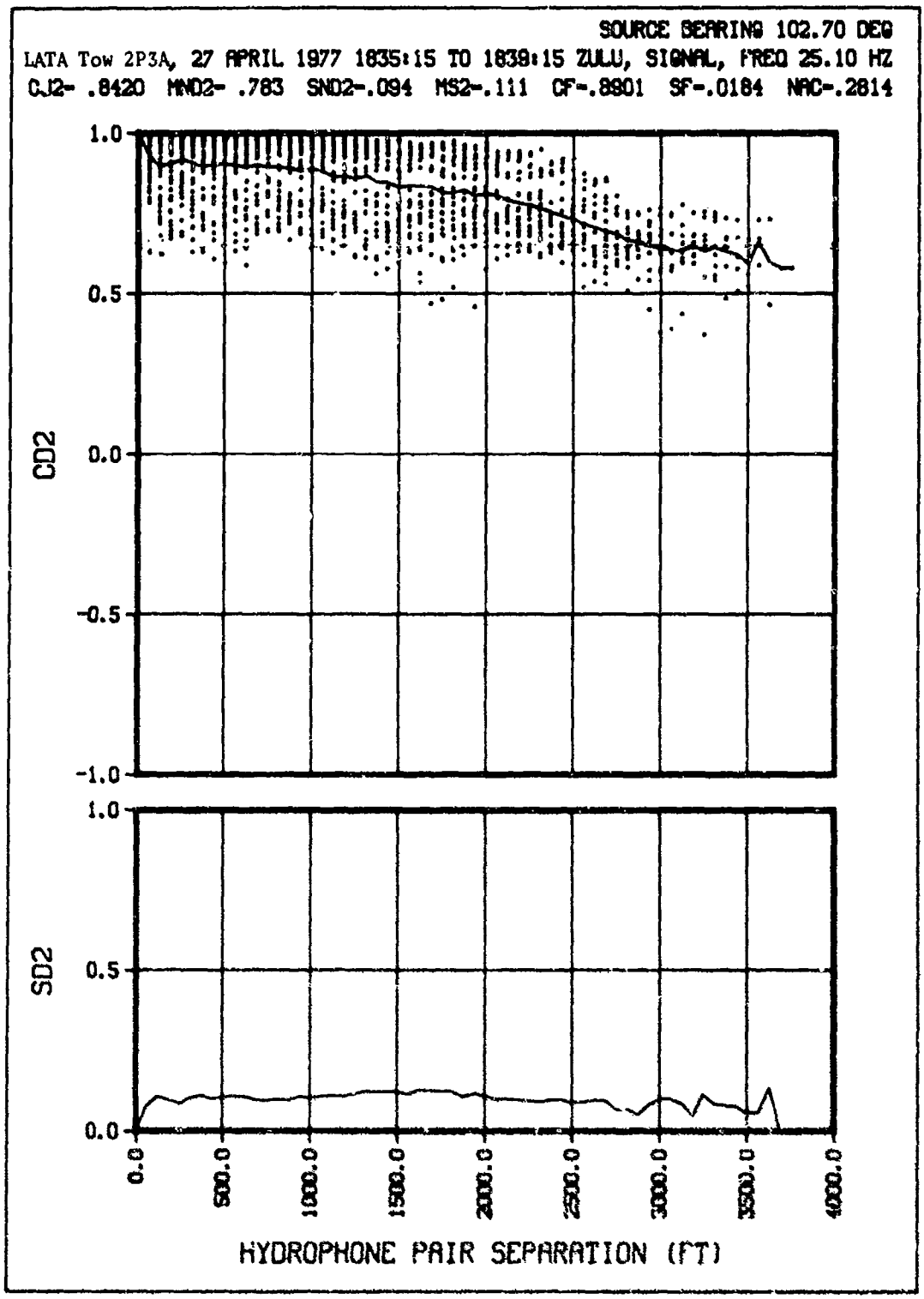

(CONFIDENTIAL)

(U) Figure 25. Array phase coherence.

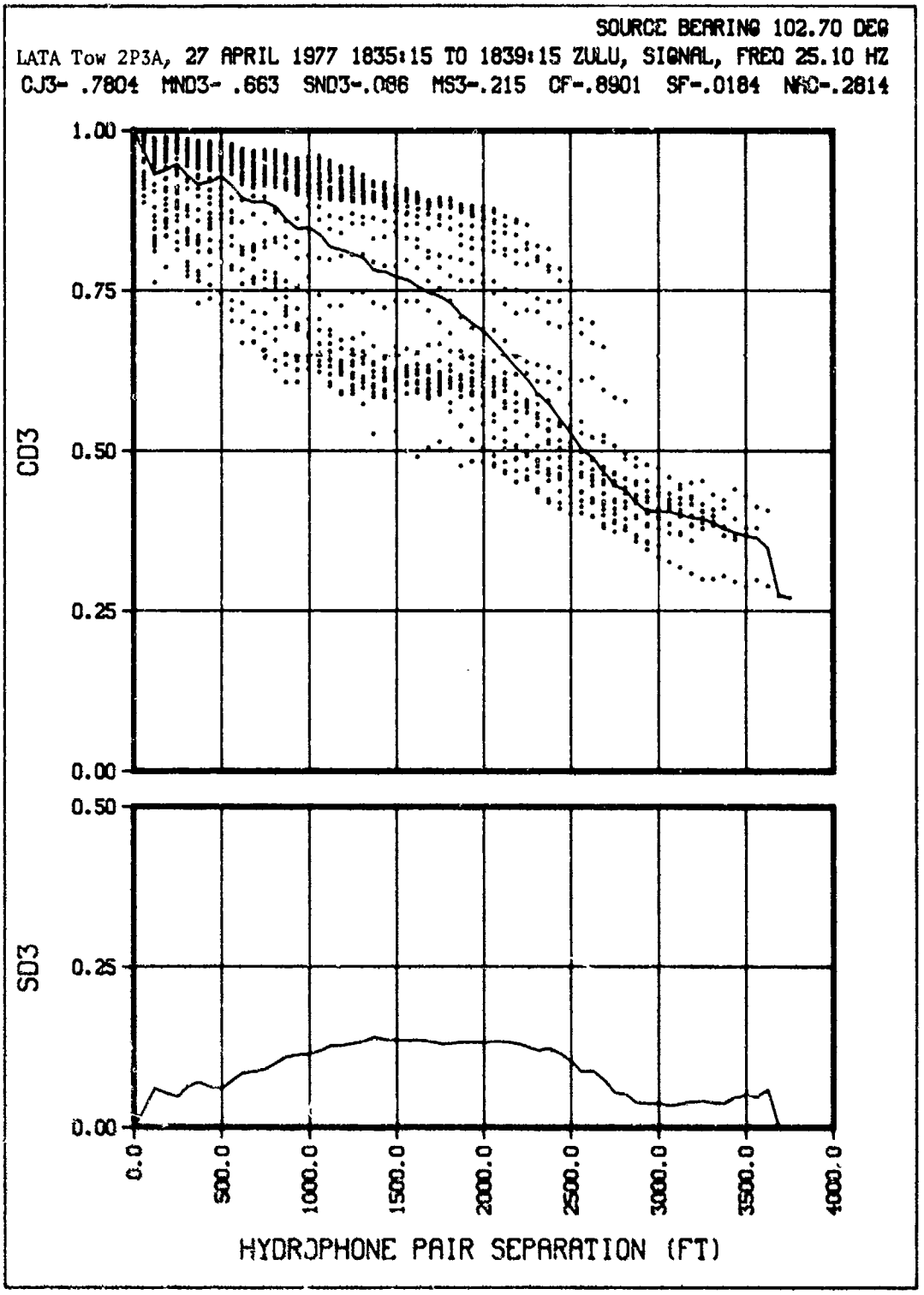

(CONFIDENTIAL)

(U) Figure 2c. Classical coherence.

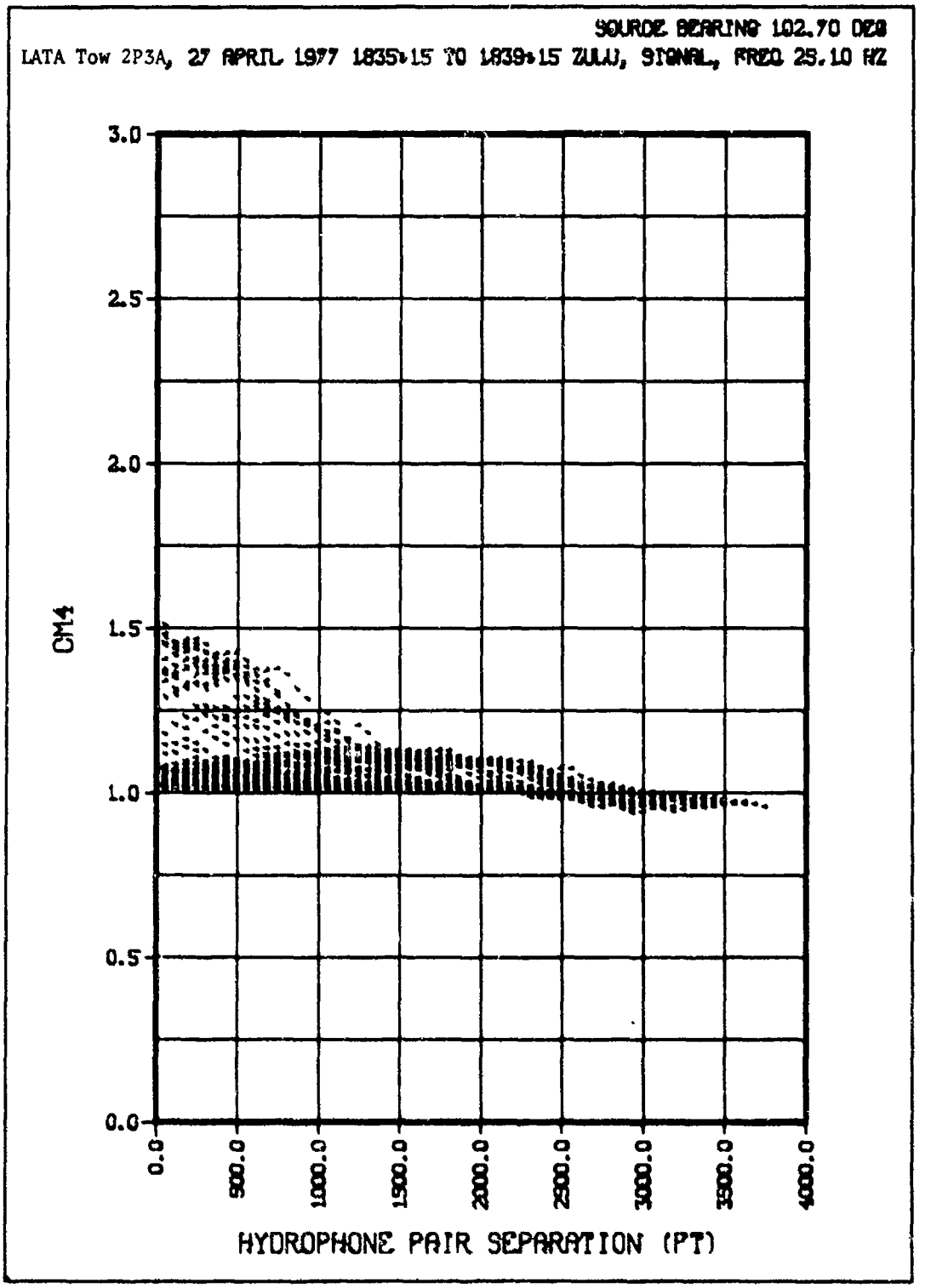

(CONFIDENTIAL)

(U) Figure 2d. Array amplitude covariance.

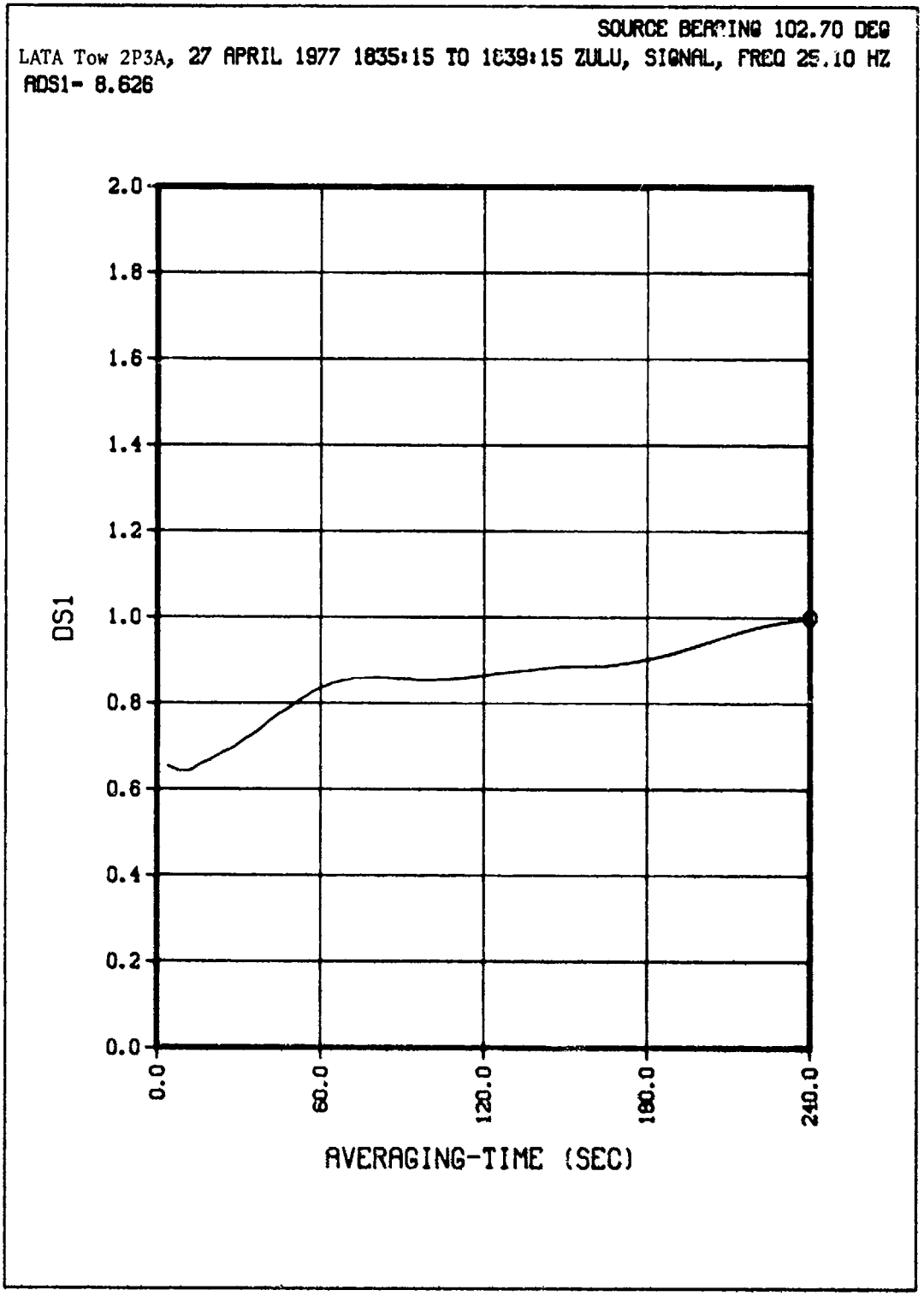

(CONFIDENTIAL)

(U) Figure 2e. Amplitude time stability.

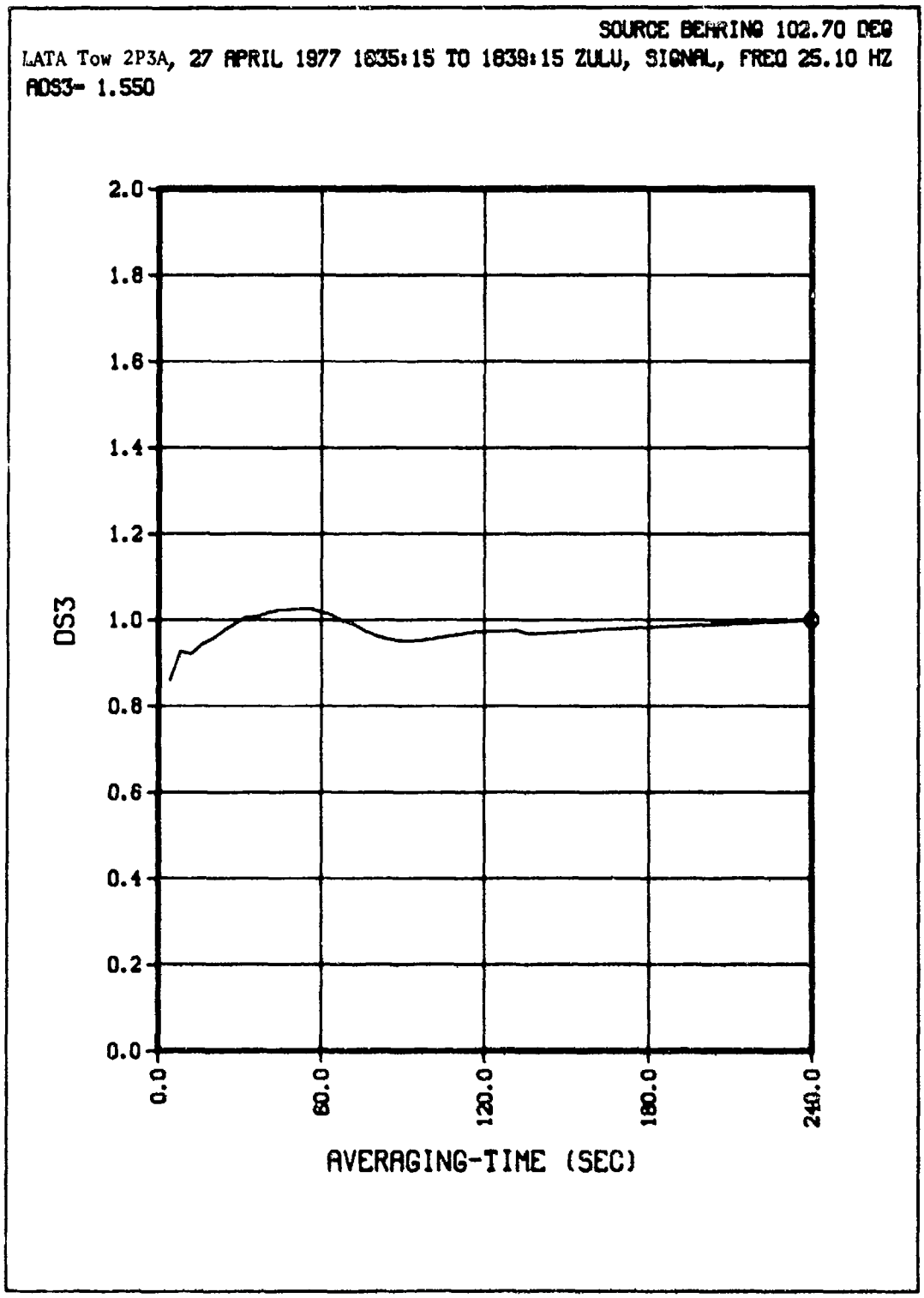

(CONFIDENTIAL)

(U) Figure 2f. Phase time stability.

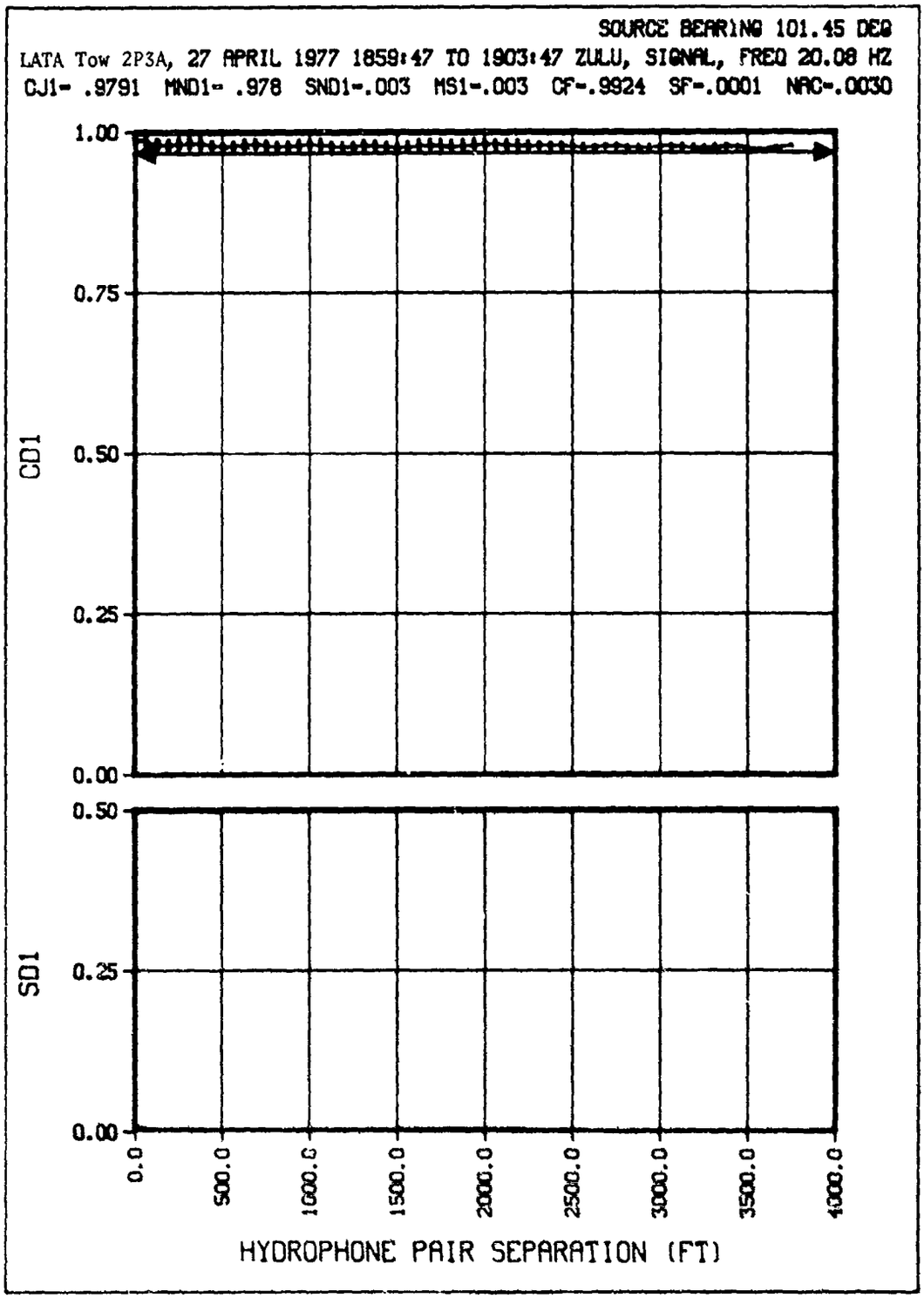

(CONFIDENTIAL)

(U) Figure 3a. Normalized amplitude covariance.

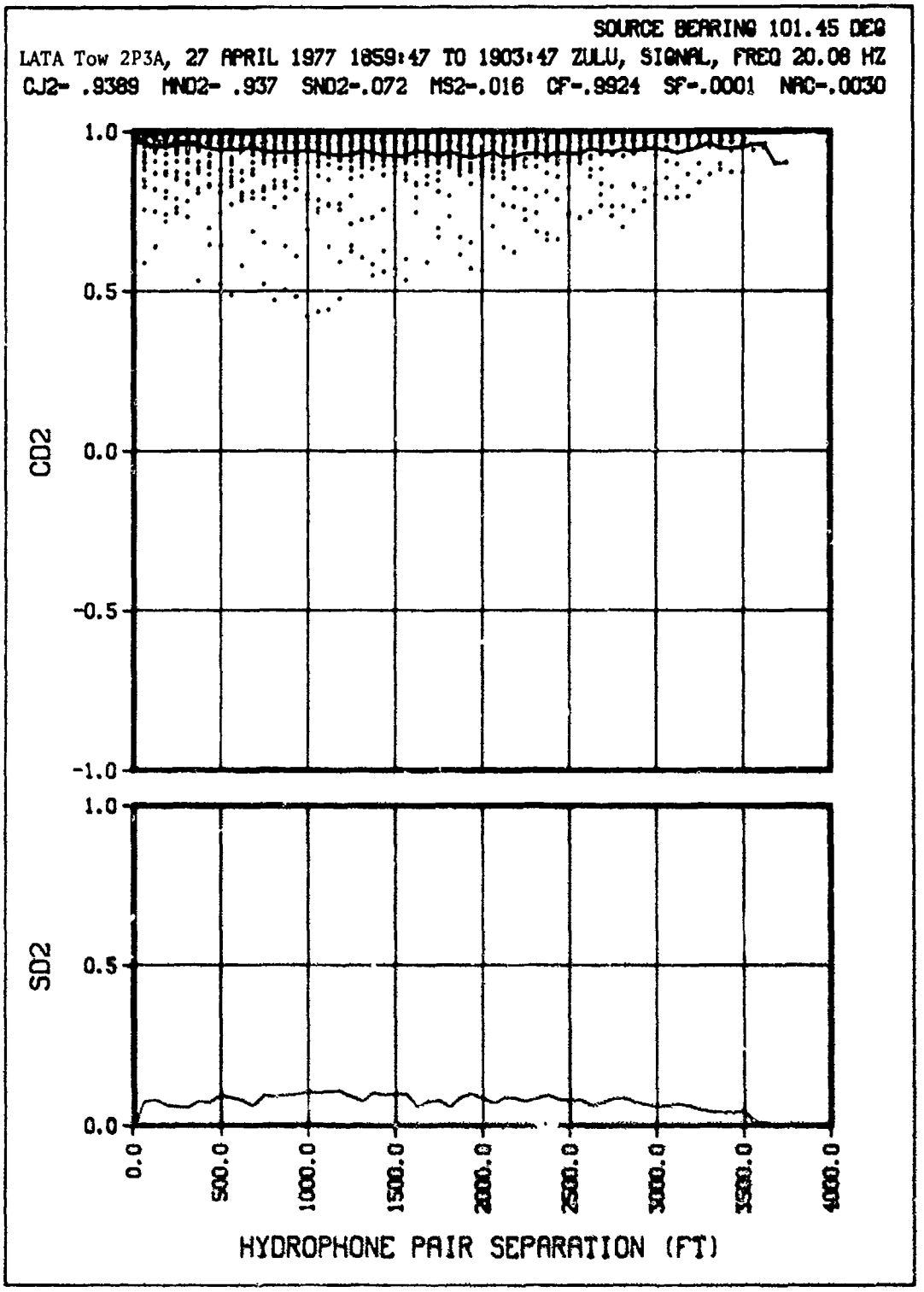

(CONFIDENTIAL)

(U) Figure 3b. Array phase coherence.

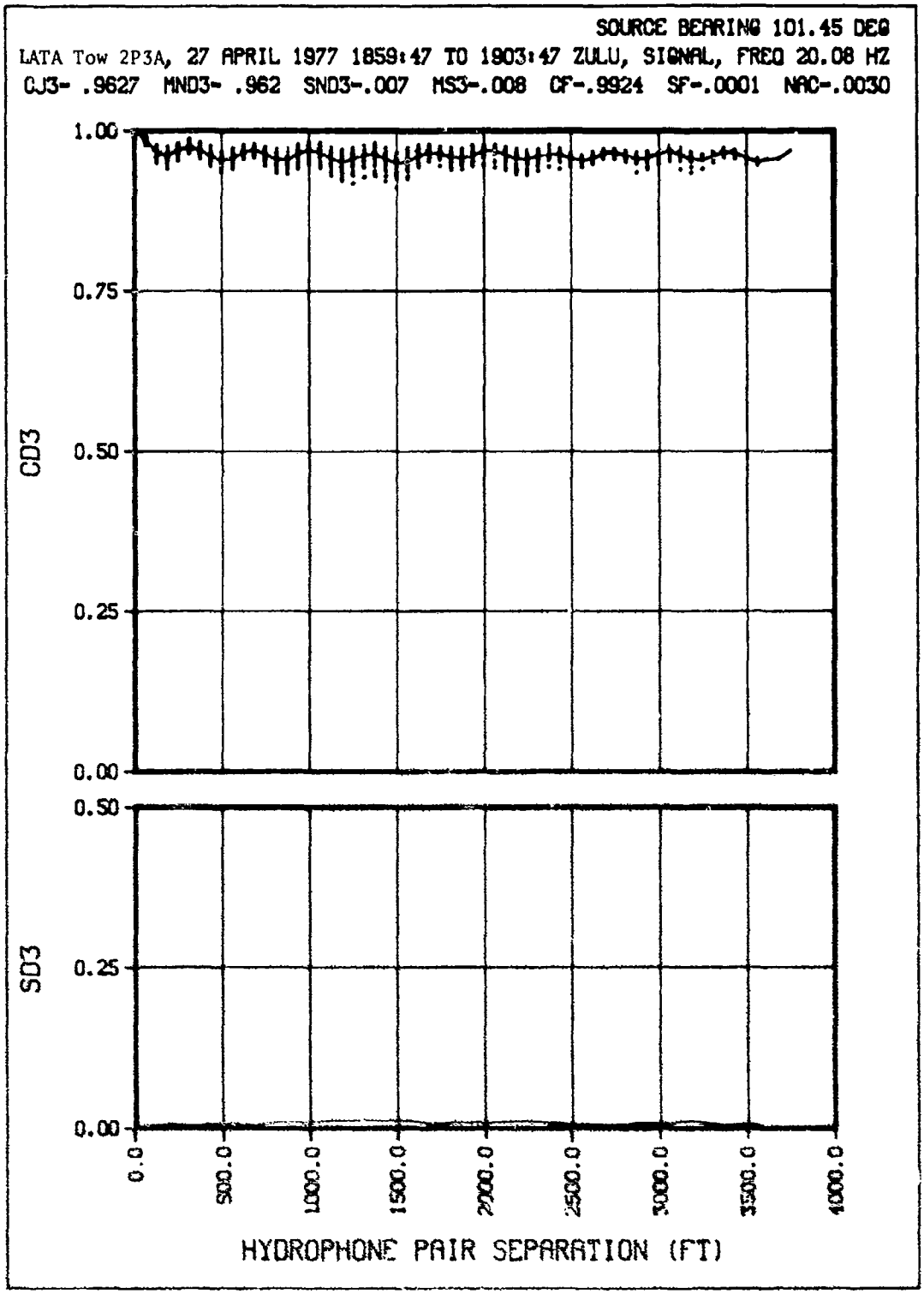

(CONFIDENTIAL)

(U) Figure 3c. Classical coherence.

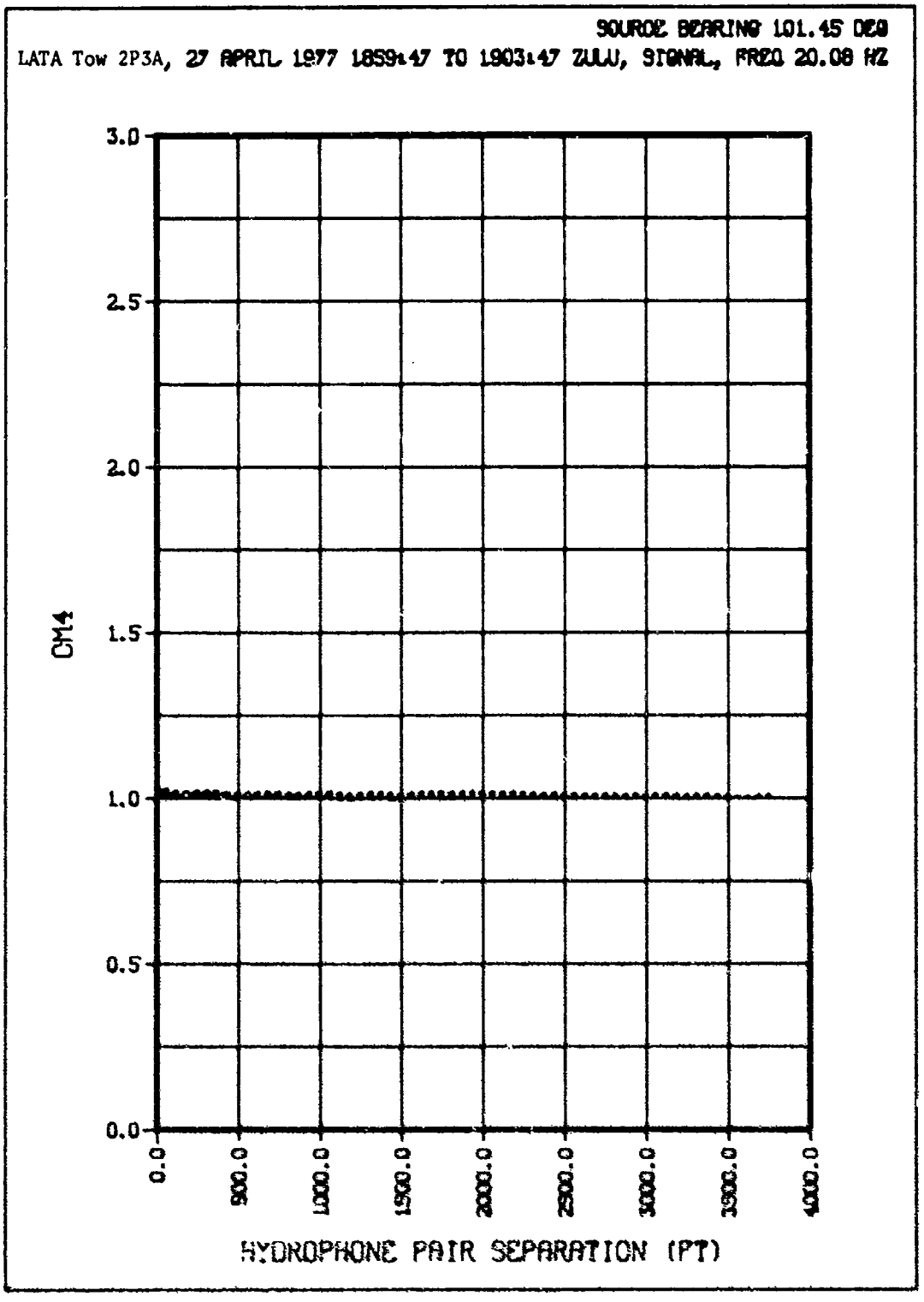

(CONFIDENTIAL)

(U) Figure 3d. Array amplitude covariance.

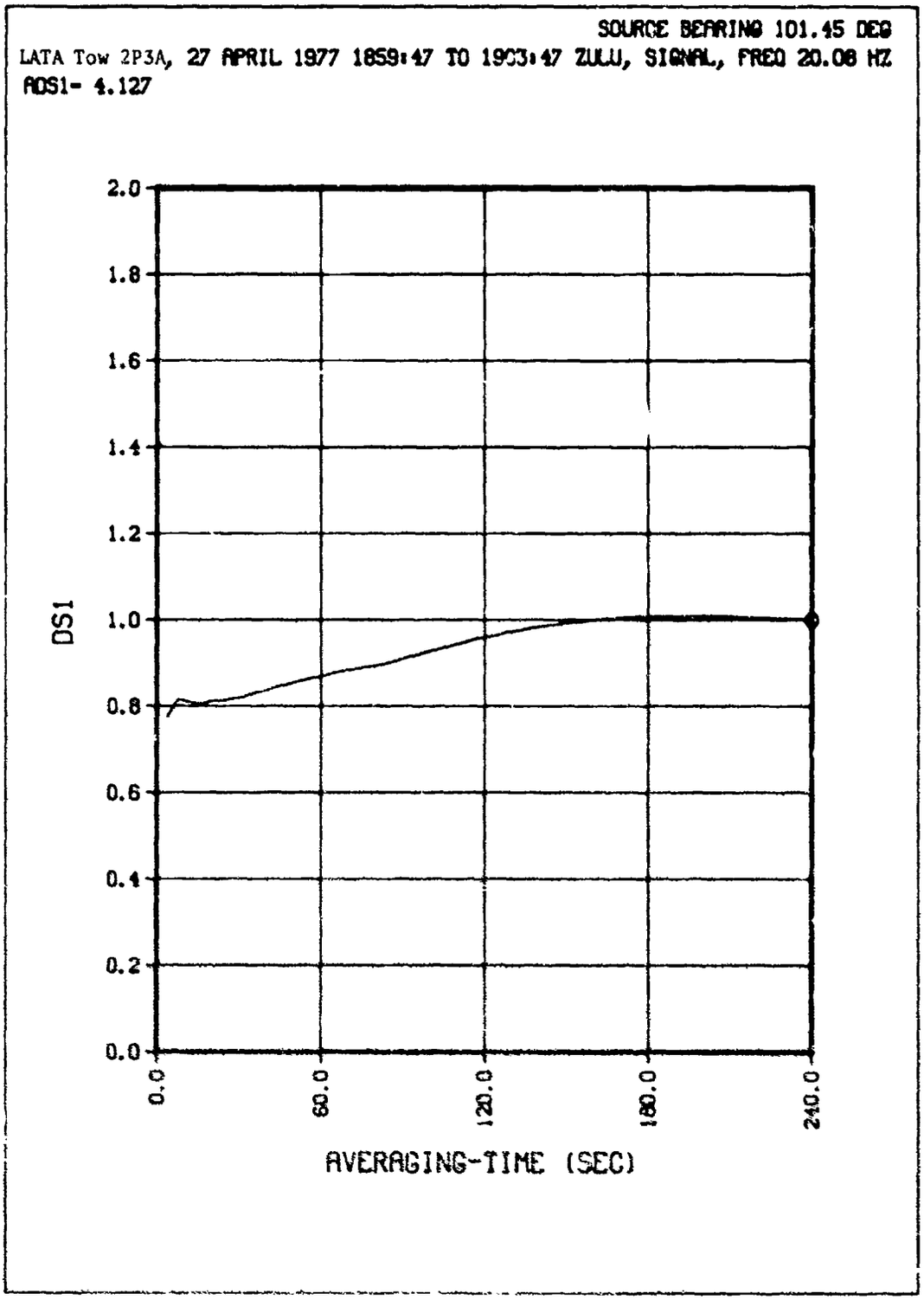

(CONFIDENTIAL)

(U) Figure 3e. Amplitude time stability.

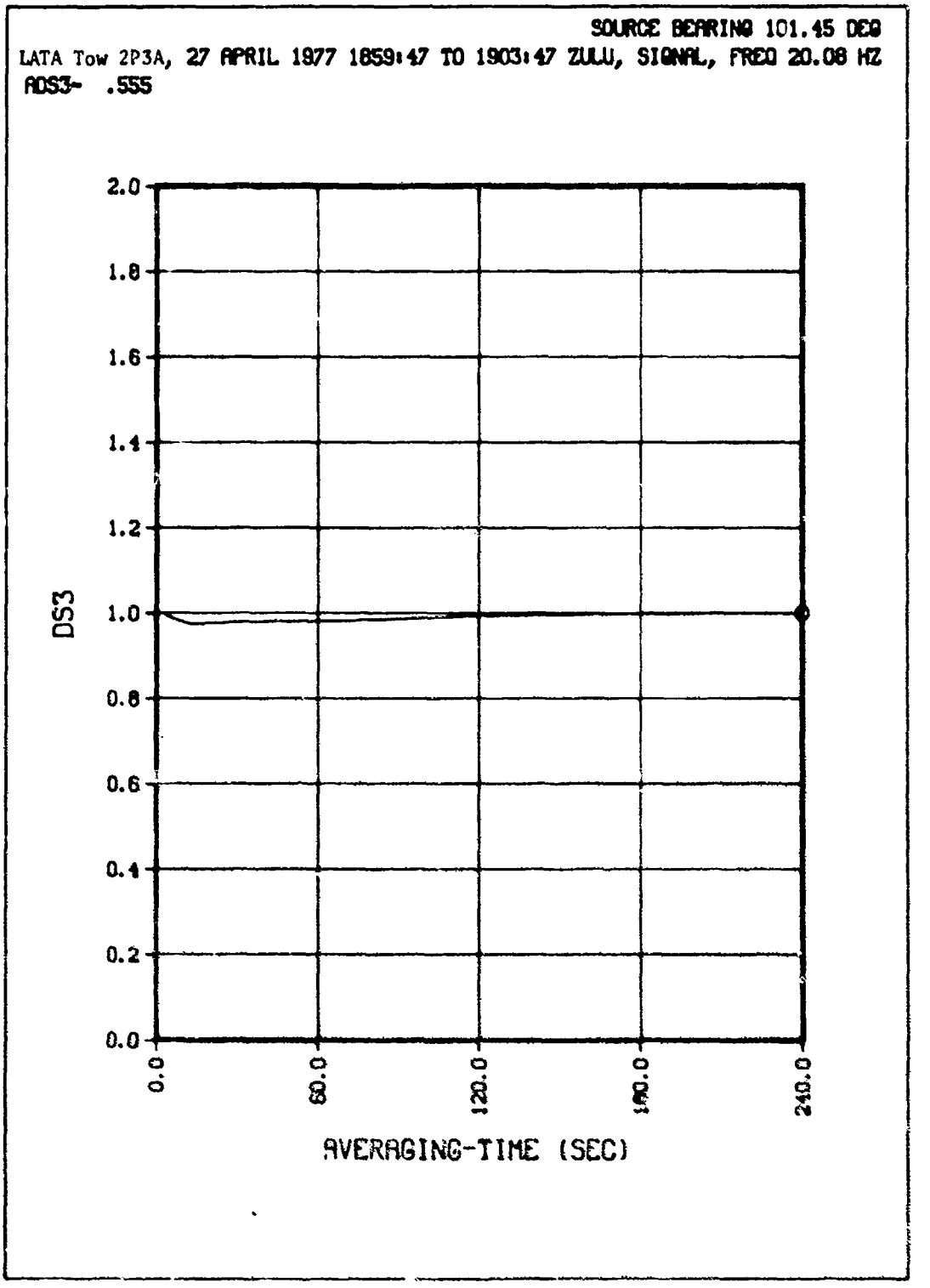

(CONFIDENTIAL)

(U) Figure 3f. Phase time stability.

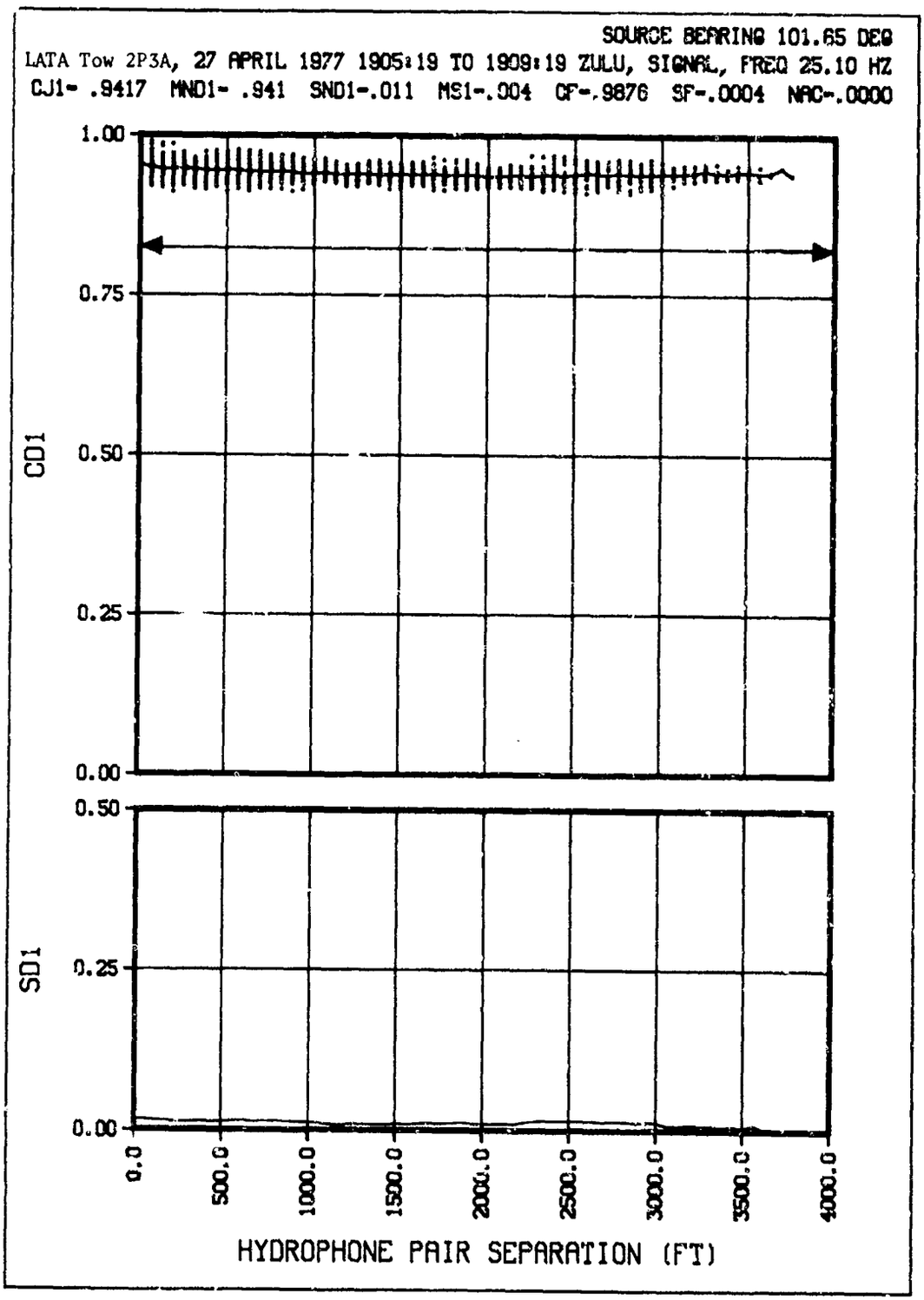

(CONFIDENTIAL)

(U) Figure 4a. Normalized amplitude covariance.

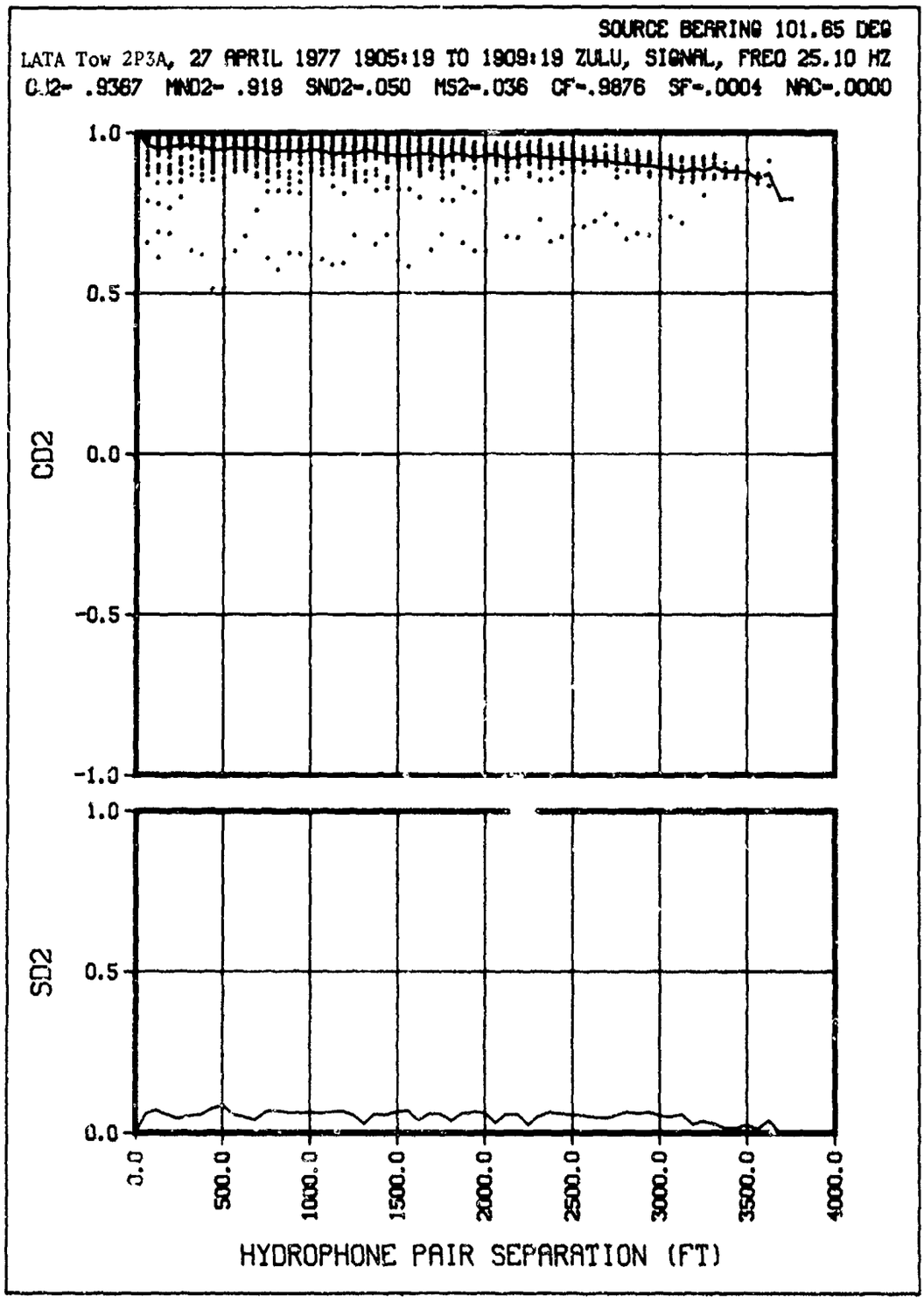

(CONFIDENTIAL)

(U) Figure 4b. Array phase coherence.

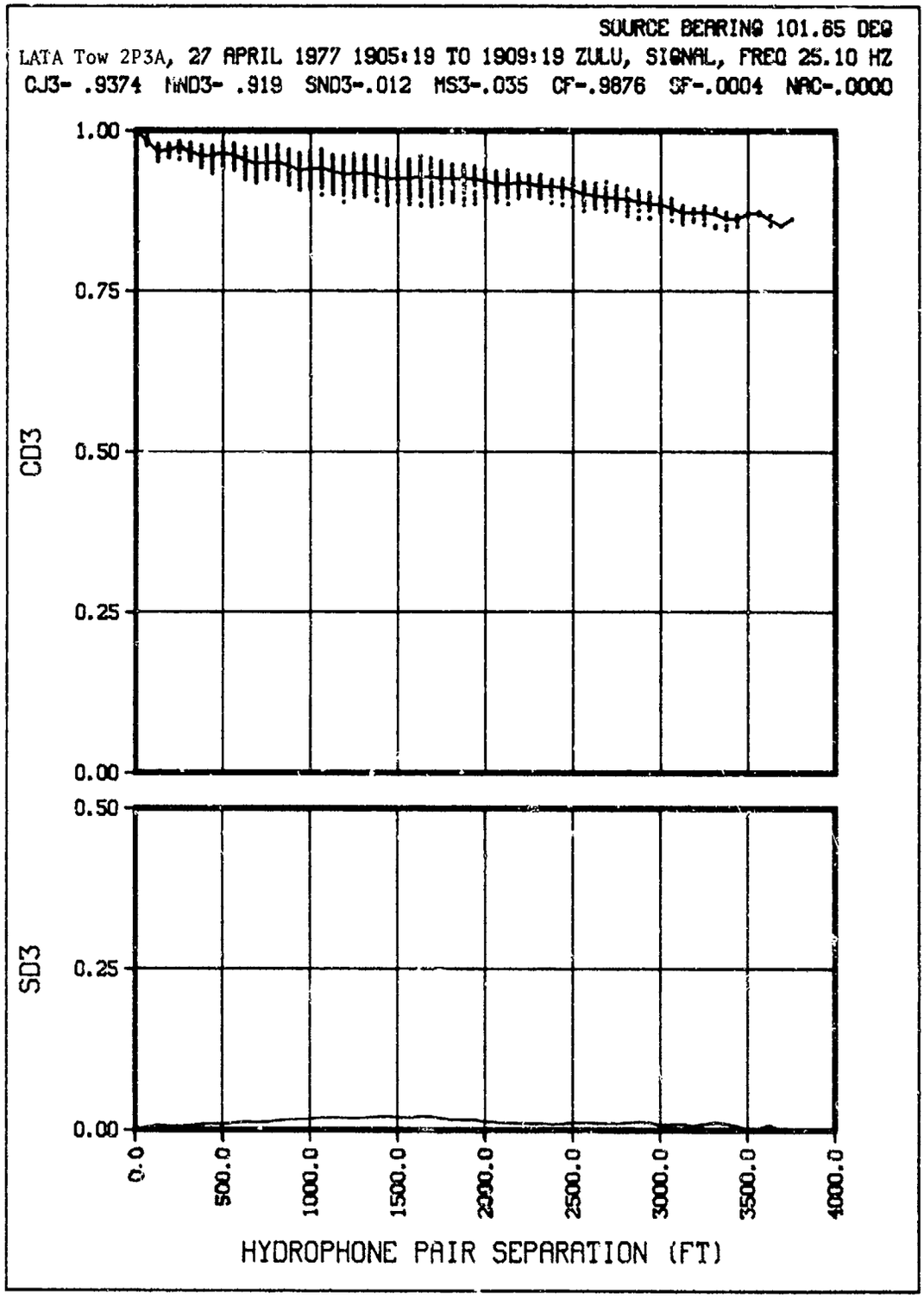

(CONFIDENTIAL)

(U) Figure 4c. Classical coherence.

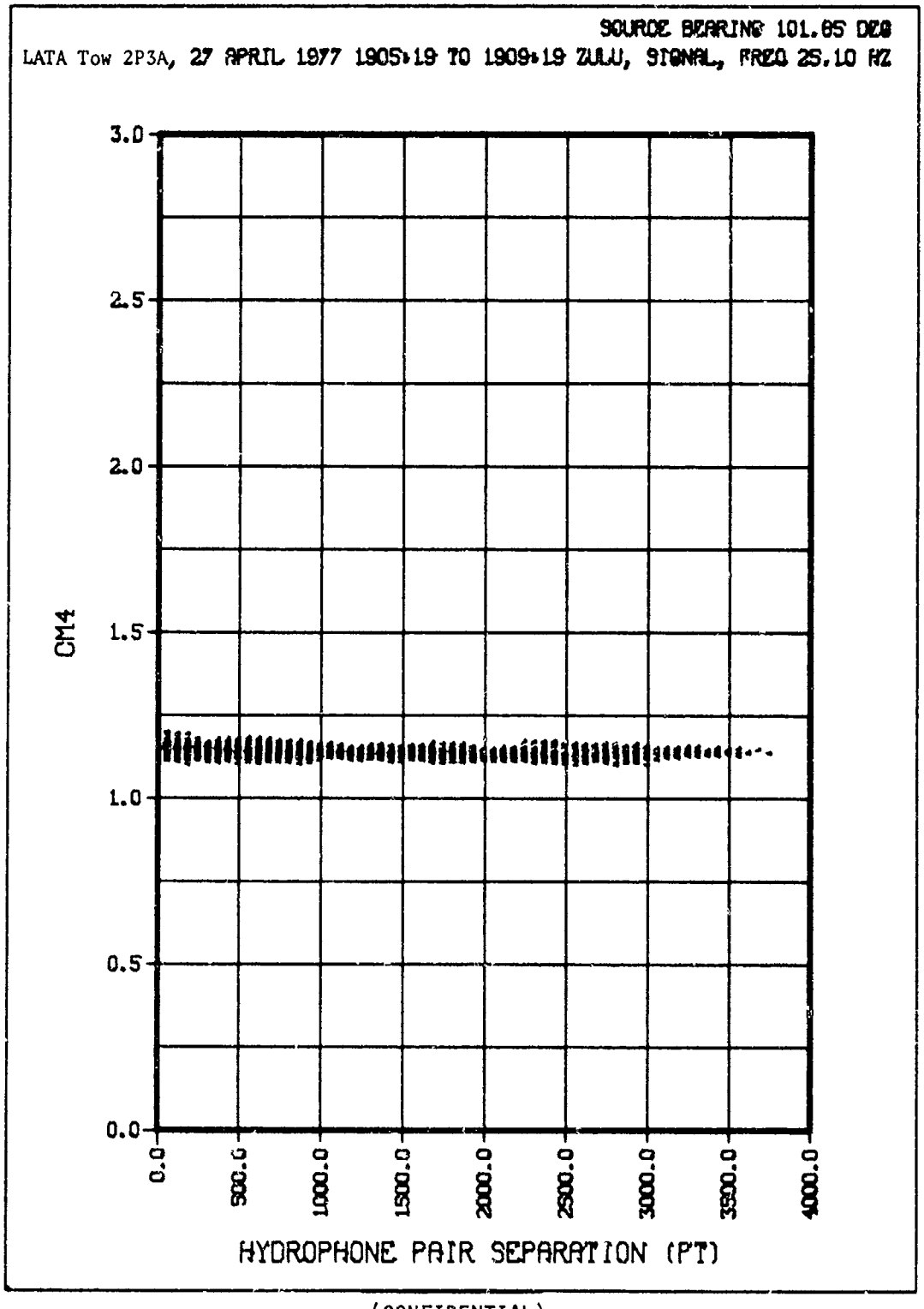

(CONFIDENTIAL)

(U) Figure 4d. Array amplitude covariance.

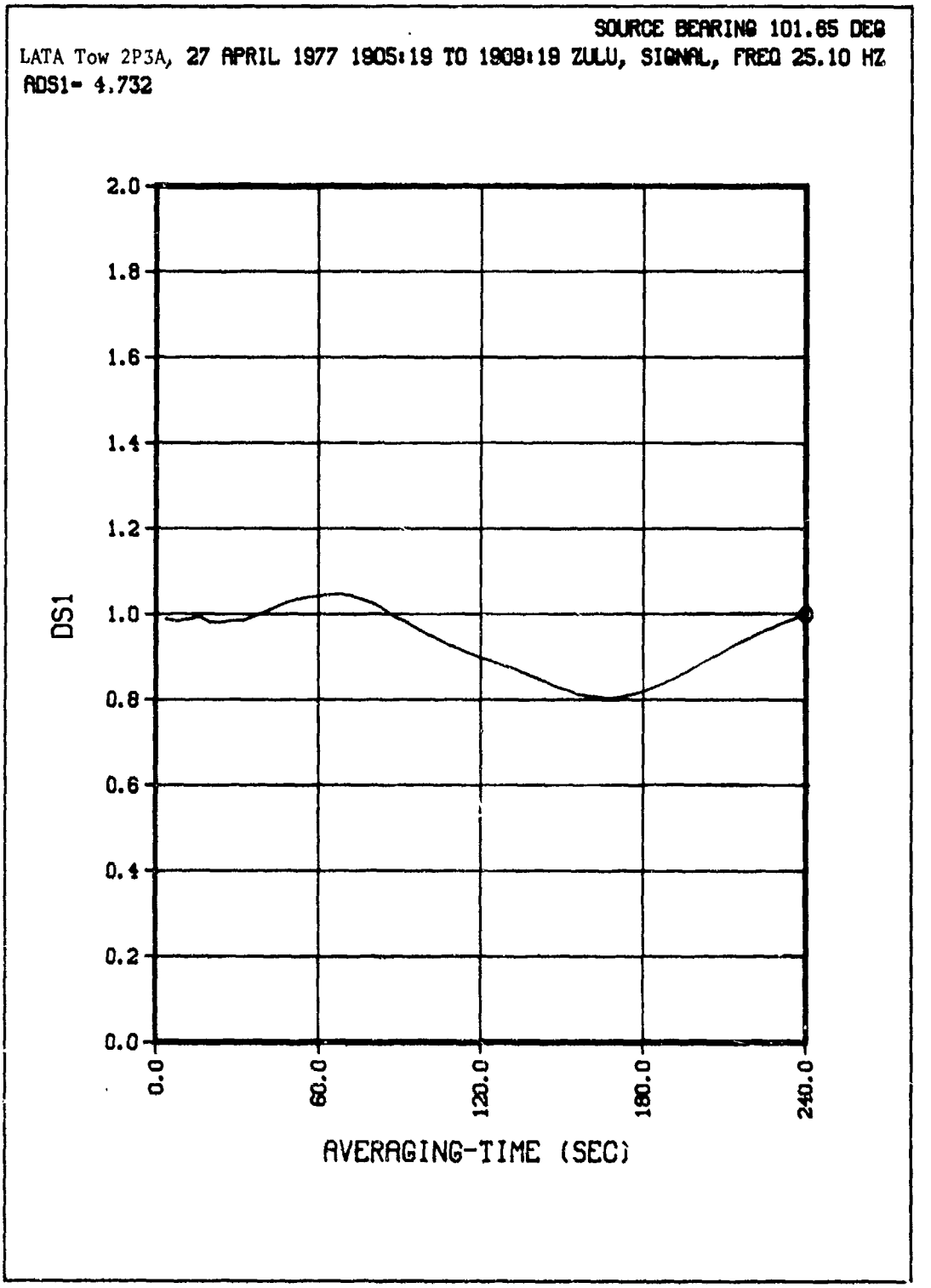

(CONFIDENTIAL)

(U) Figure 4e. Amplitude time stability.

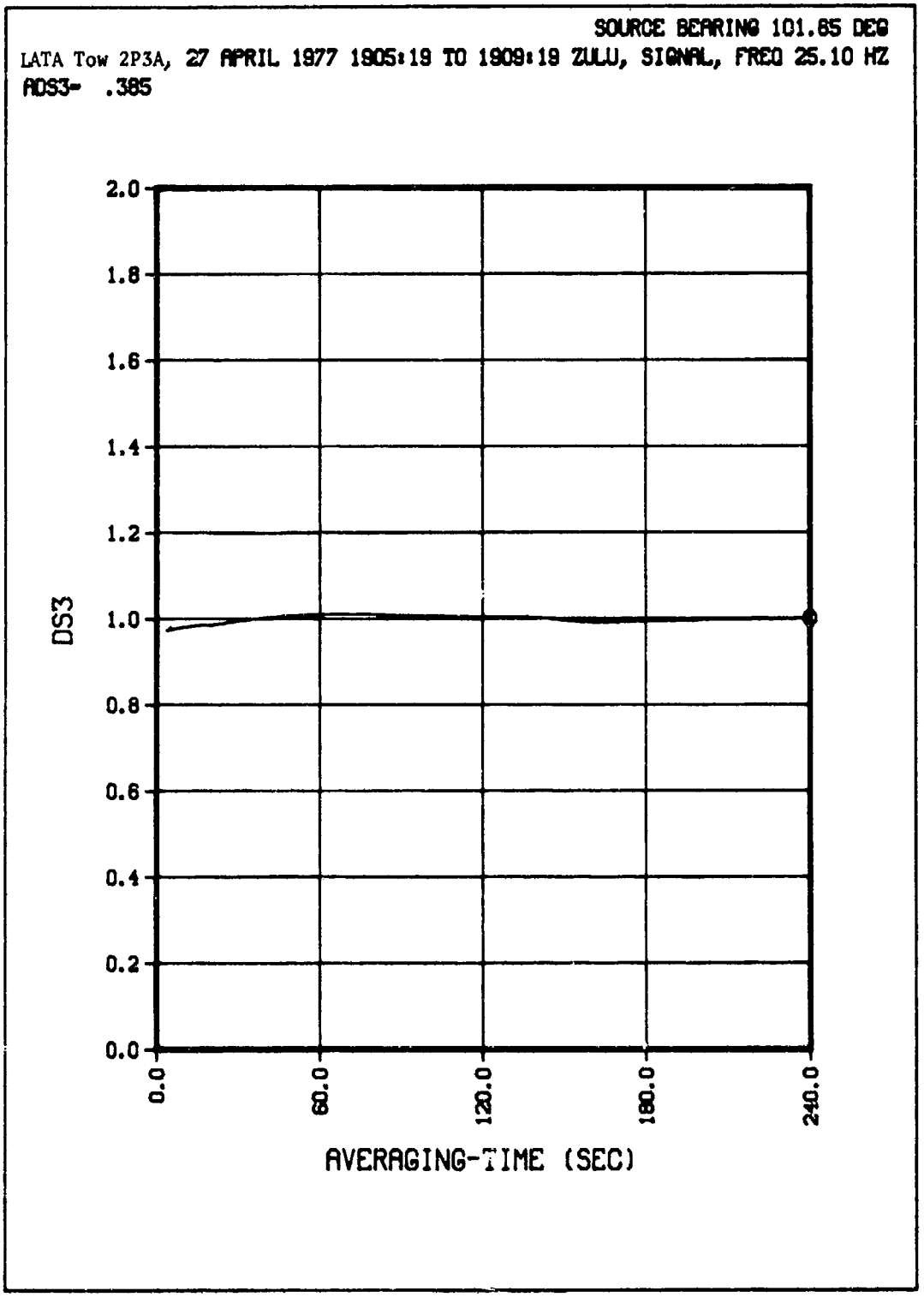

(CONFIDENTIAL)

(U) Figure 4f. Phase time stability.

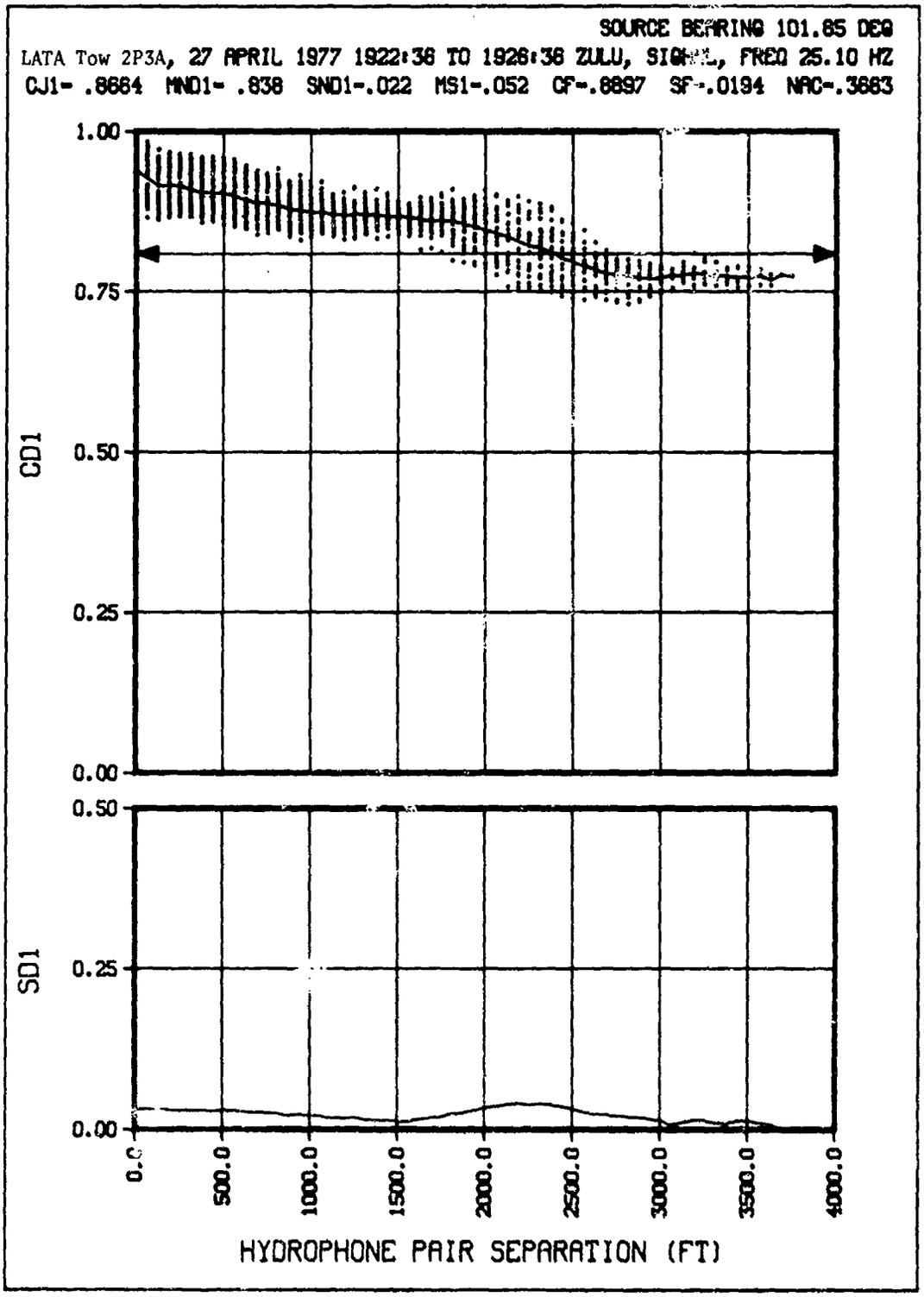

(CONFIDENTIAL)

(U) Figure 5a. Normalized amplitude covariance.

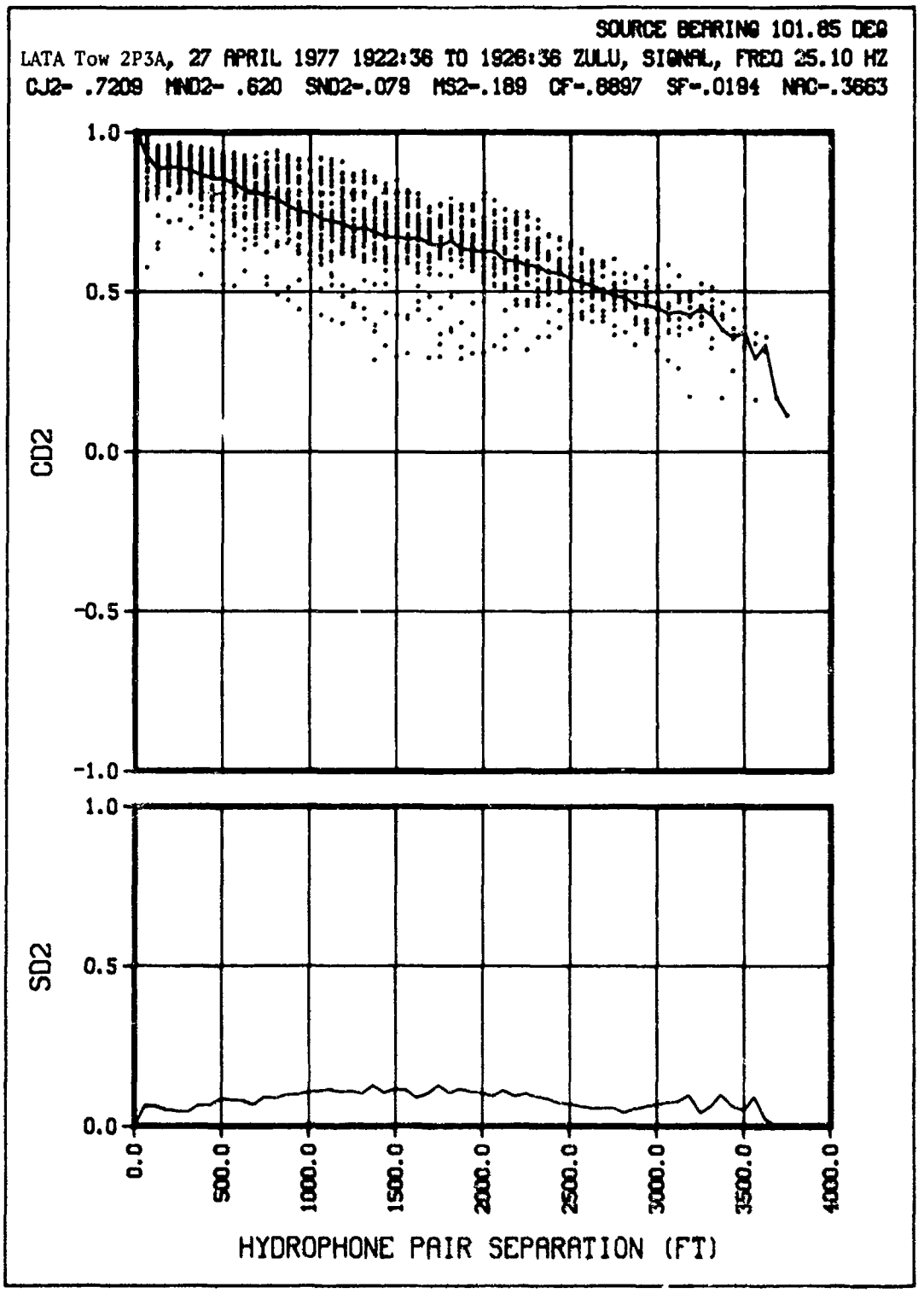

(CONFIDENTIAL)

(U) Figure 5b. Array phase coherence.

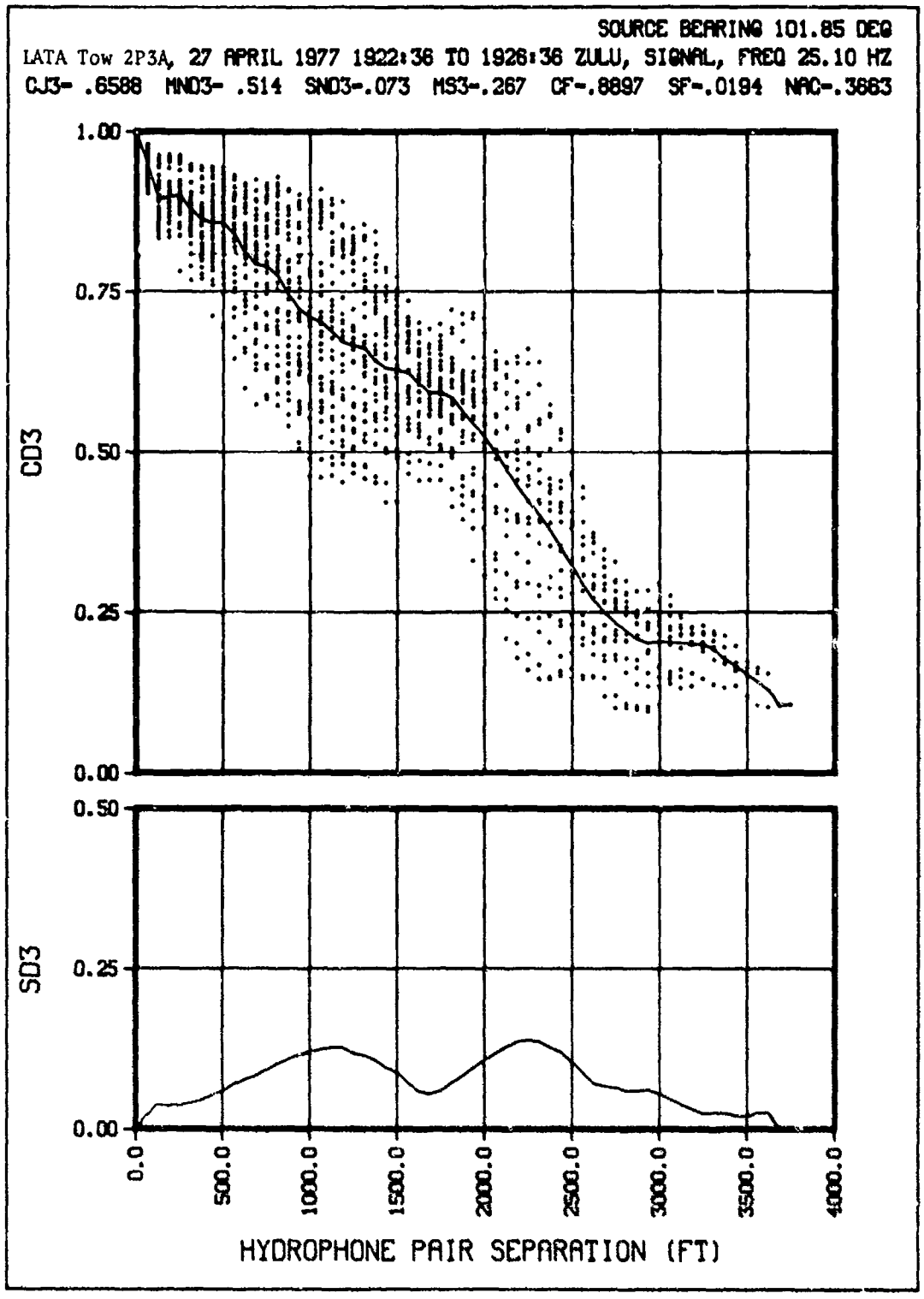

(CONFIDENTIAL)

(U) Figure 5c. Classical coherence.

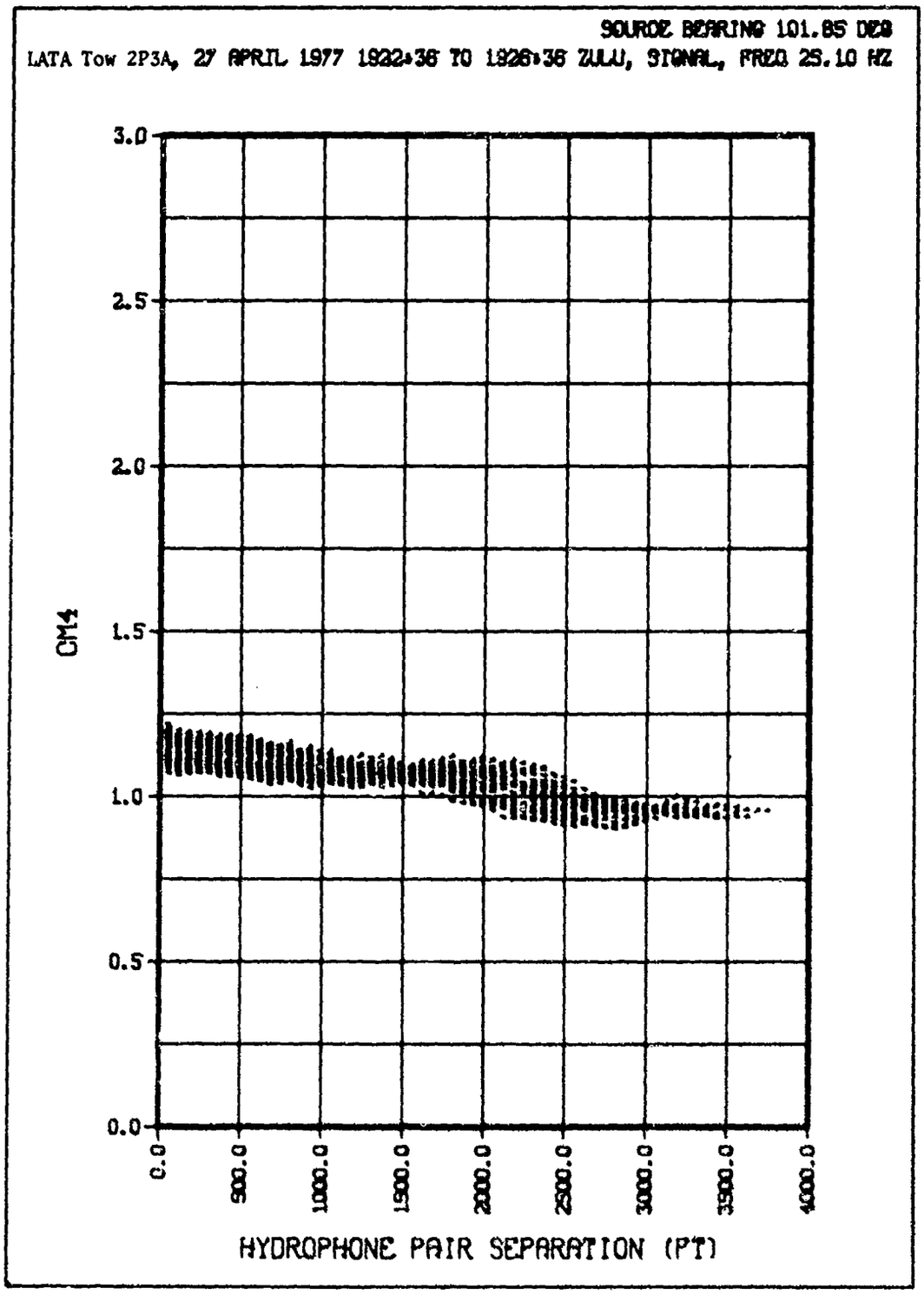

(CONFIDENTIAL)

(U) Figure 5d. Array amplitude covariance.

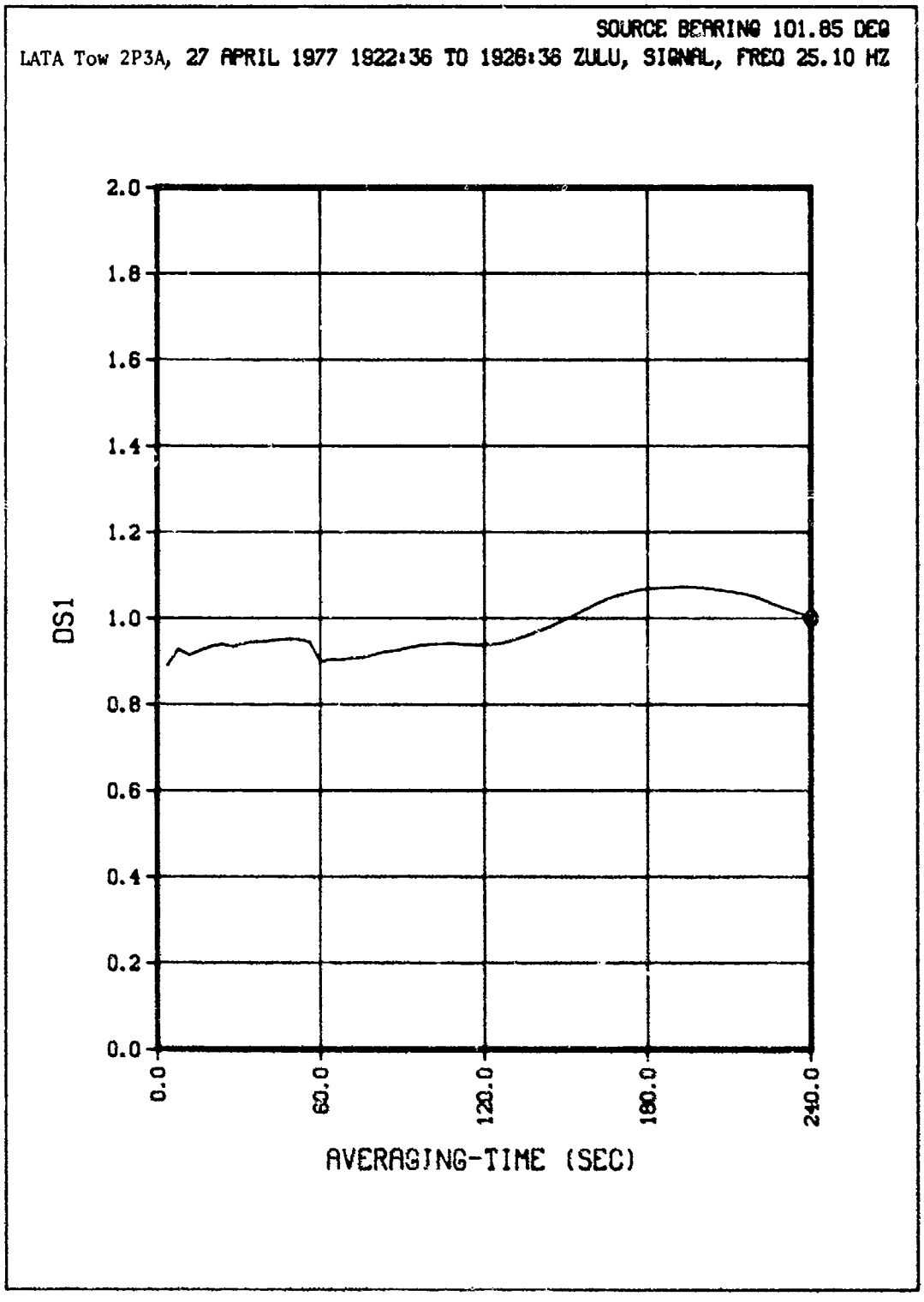

(CONFIDENTIAL)

(U) Figure 5e. Amplitude time stability.

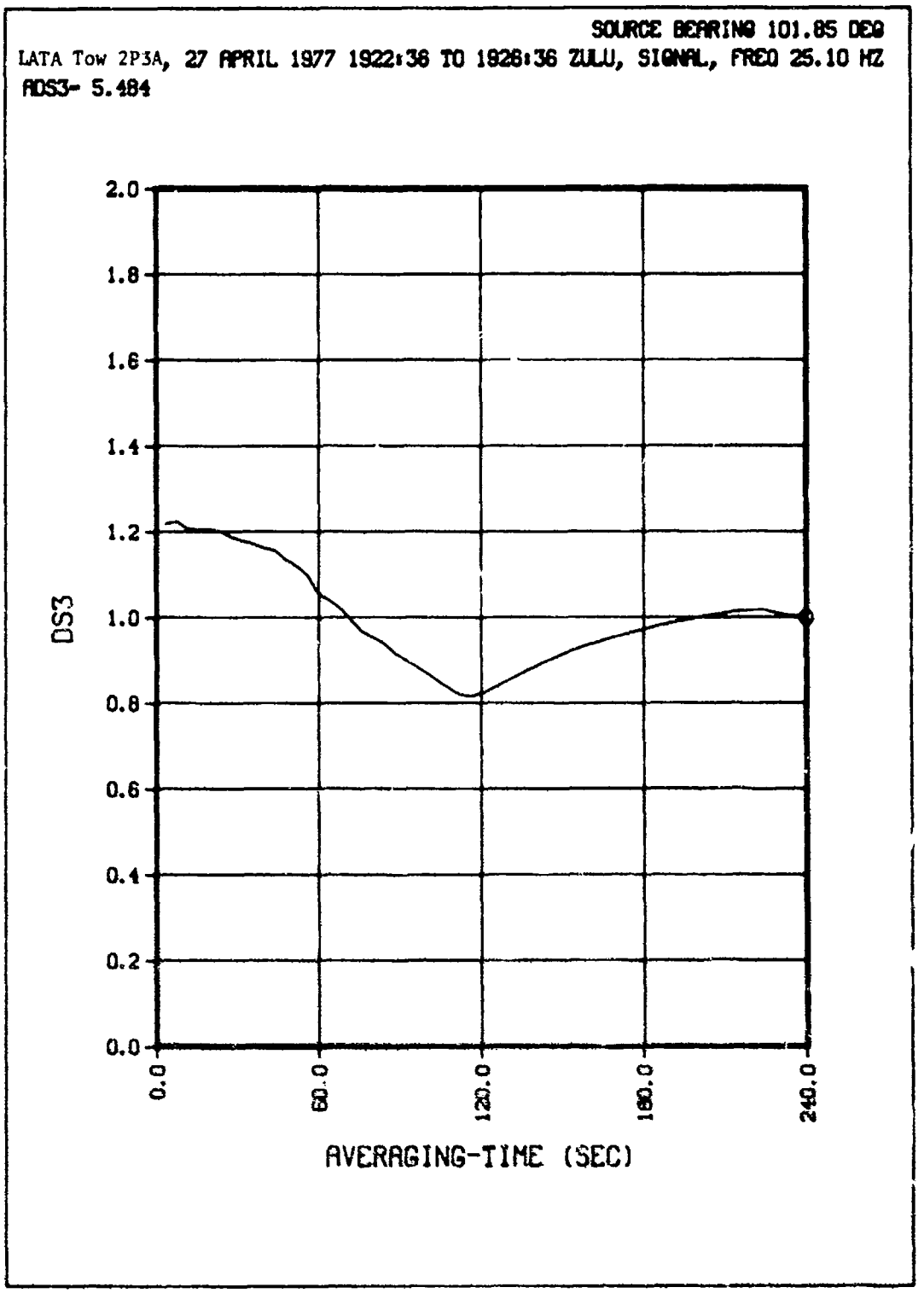

(CONFIDENTIAL)

(U) Figure 5f. Phase time stability.

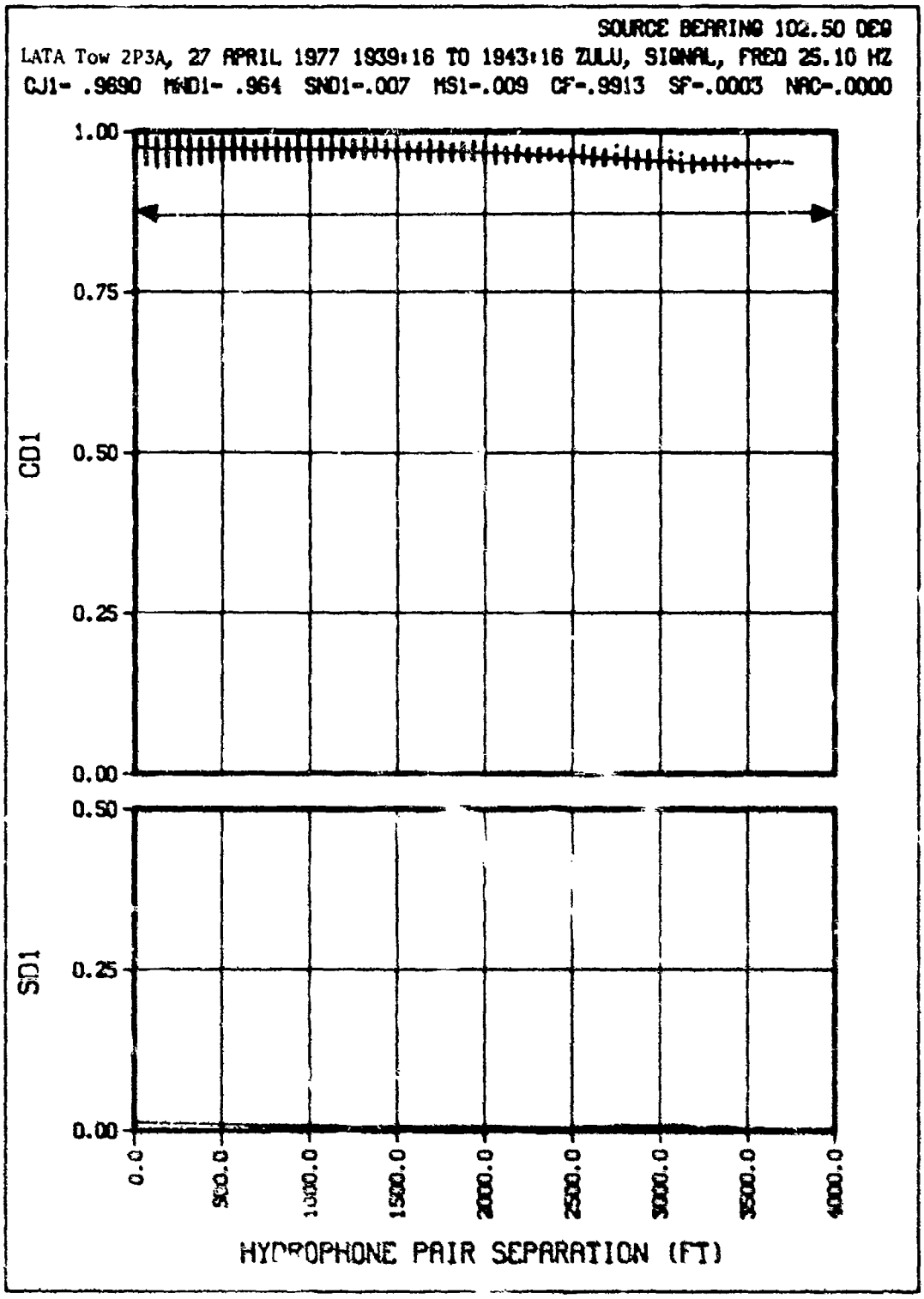

(CONFIDENTIAL)

(U) Figure 6a. Normalized amplitude covariance.

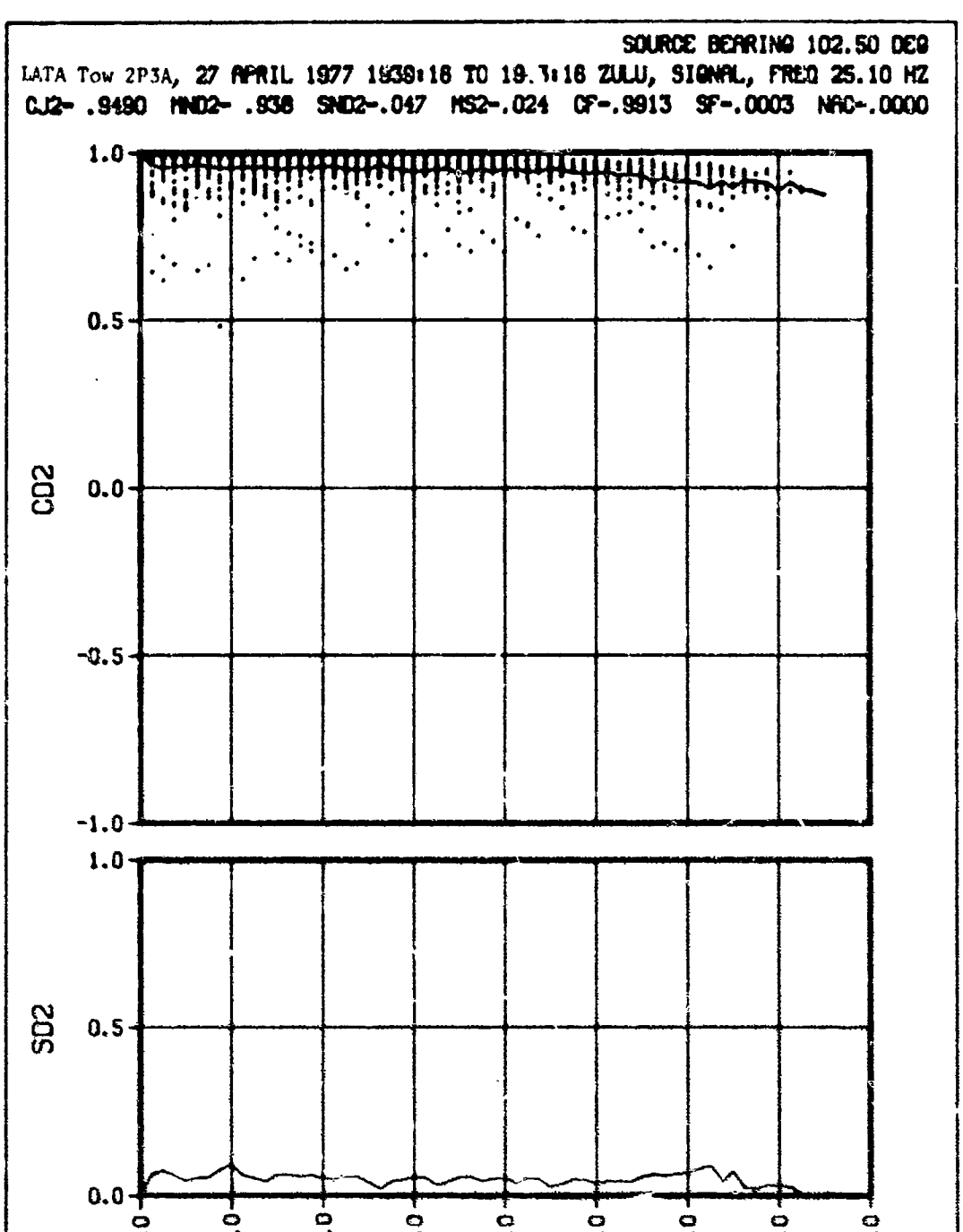

(CONFIDENTIAL)

(U) Figure 6b. Array phase coherence.

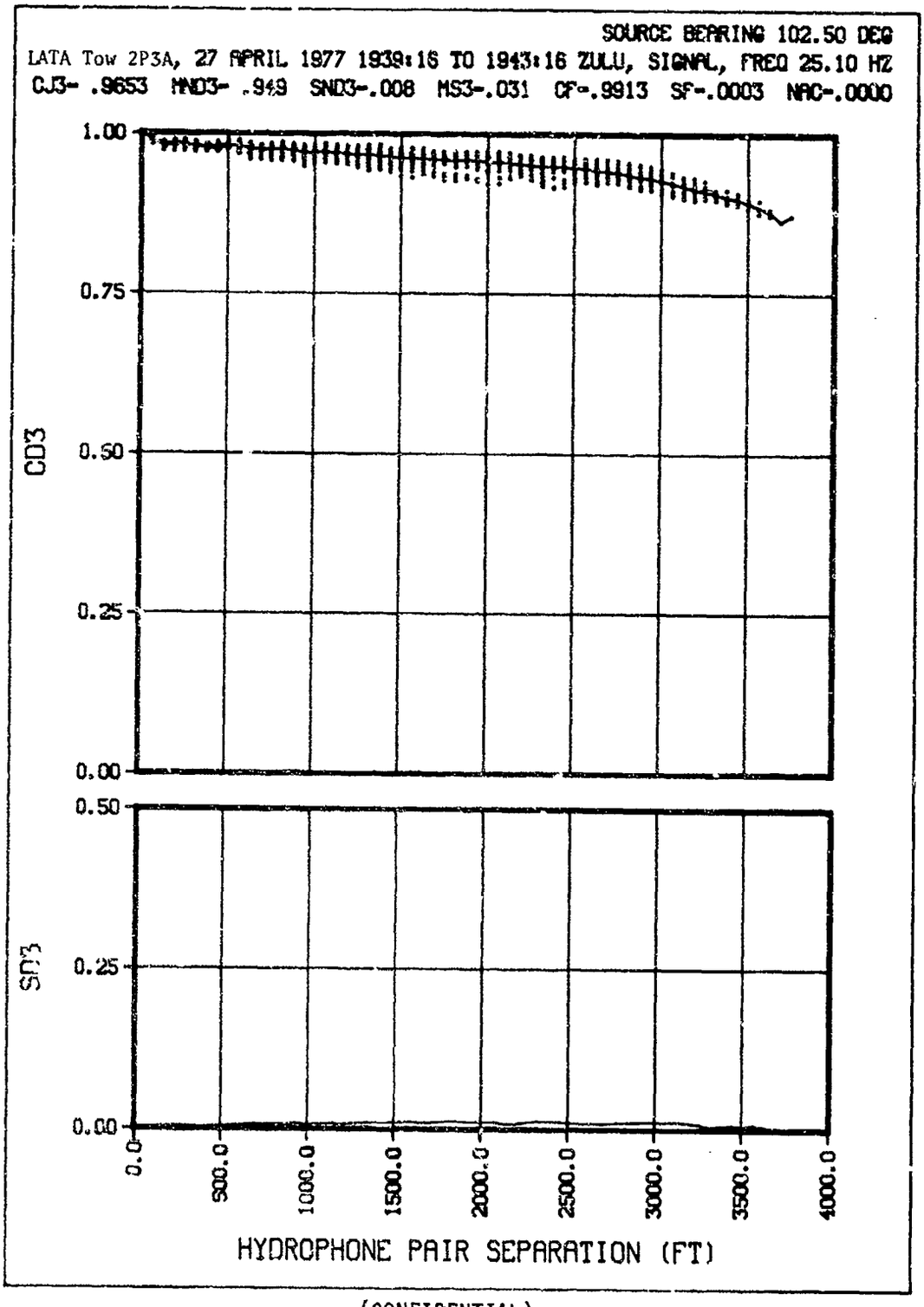

(CONFIDENTIAL)

(U) Figure 6c. Classical coherence.

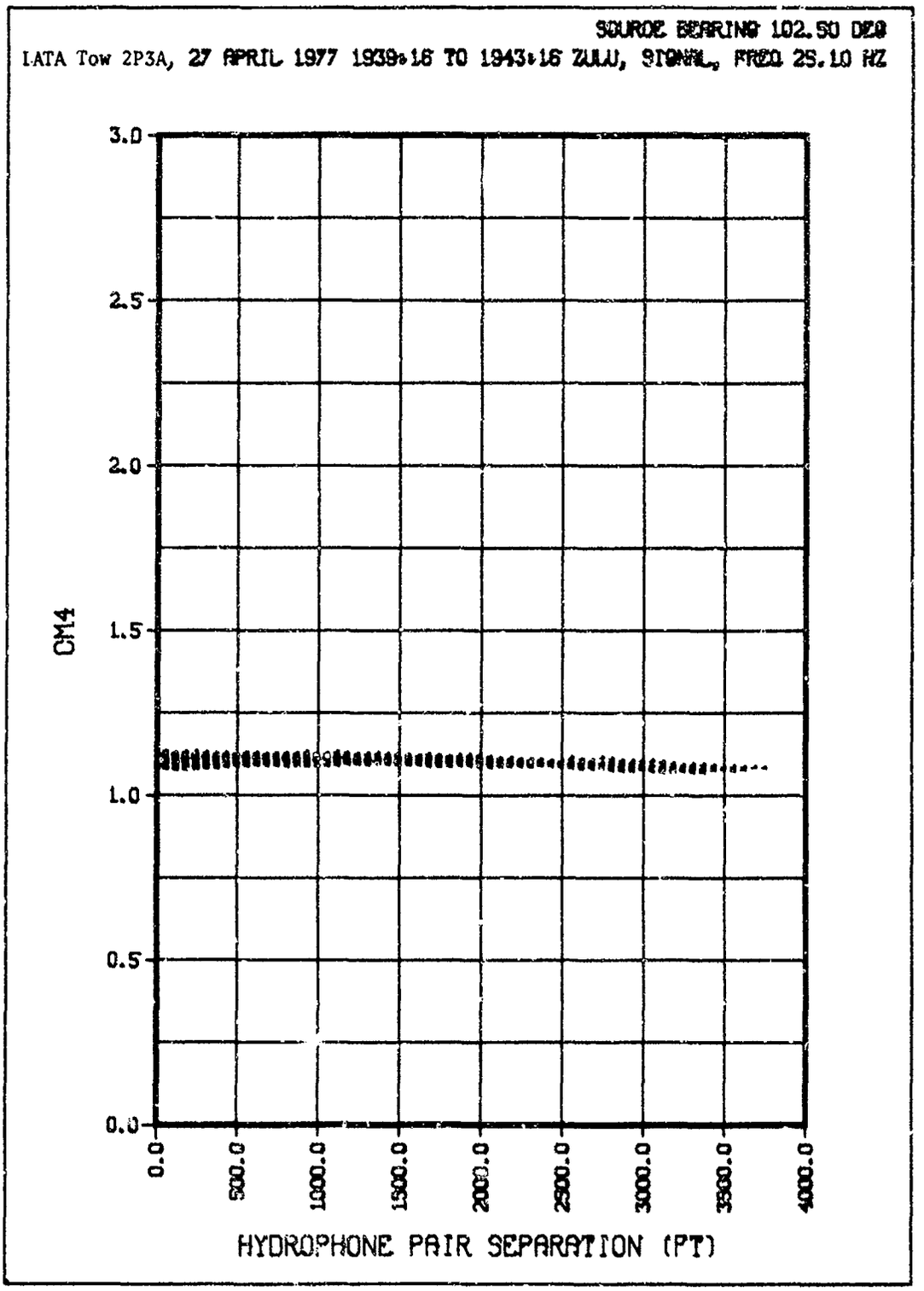

(CONFIDENTIAL)

(U) Figure 6d. Array amplitude covariance.

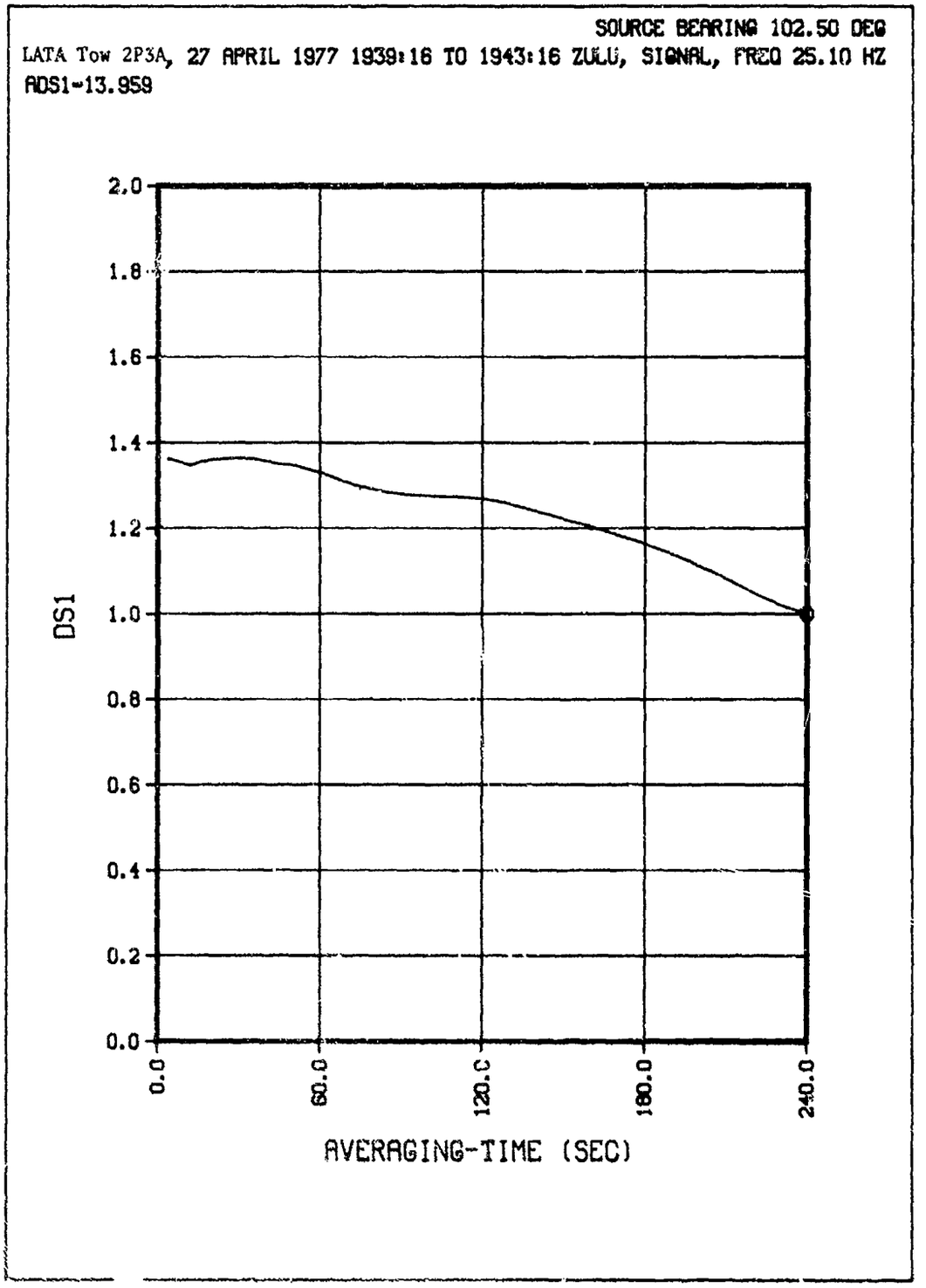

(CONFIDENTIAL)

(U) Figure 6e. Amplitude time stability.

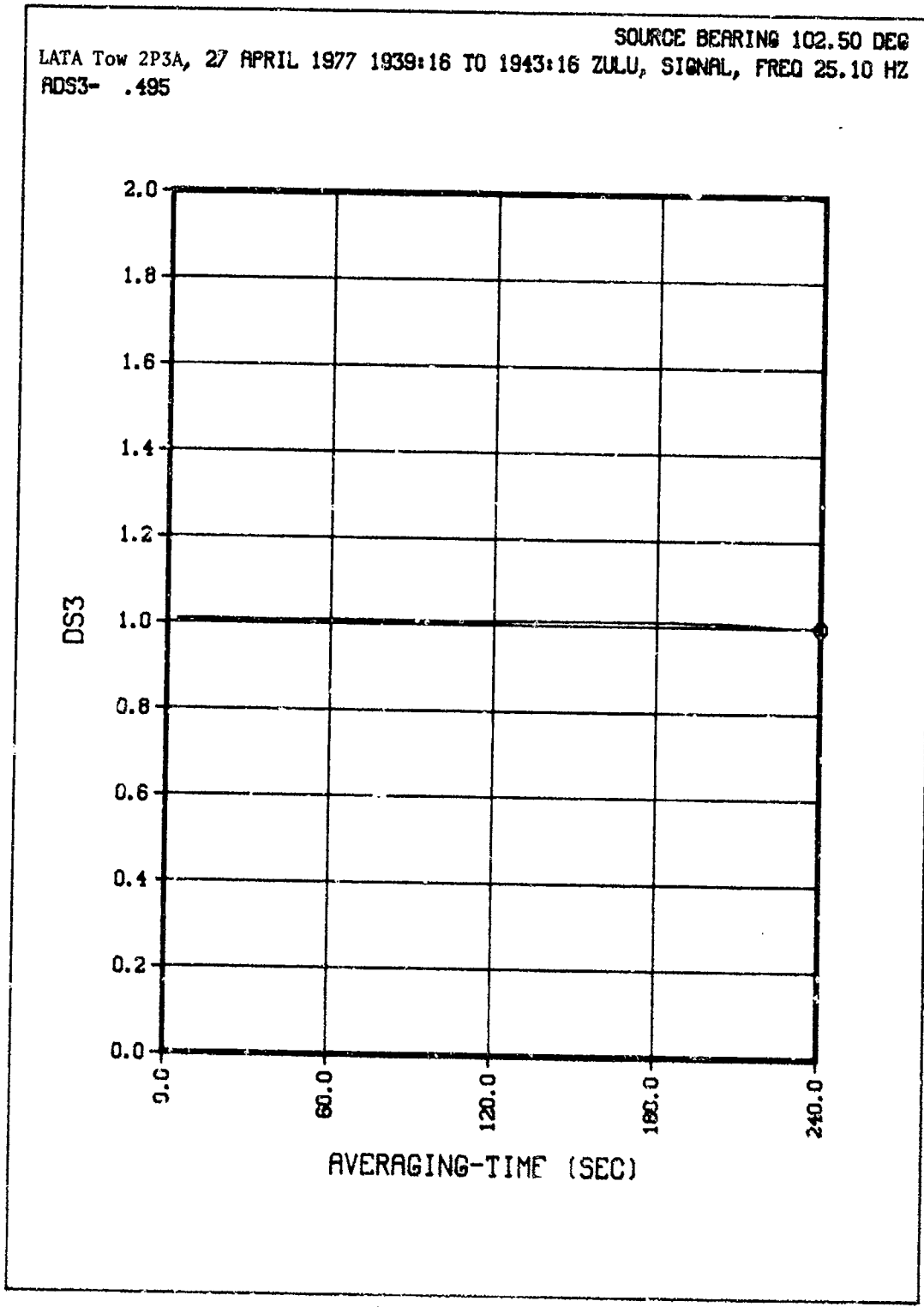

(CONFIDENTIAL)

(U) Figure 6f. Phase time stability.

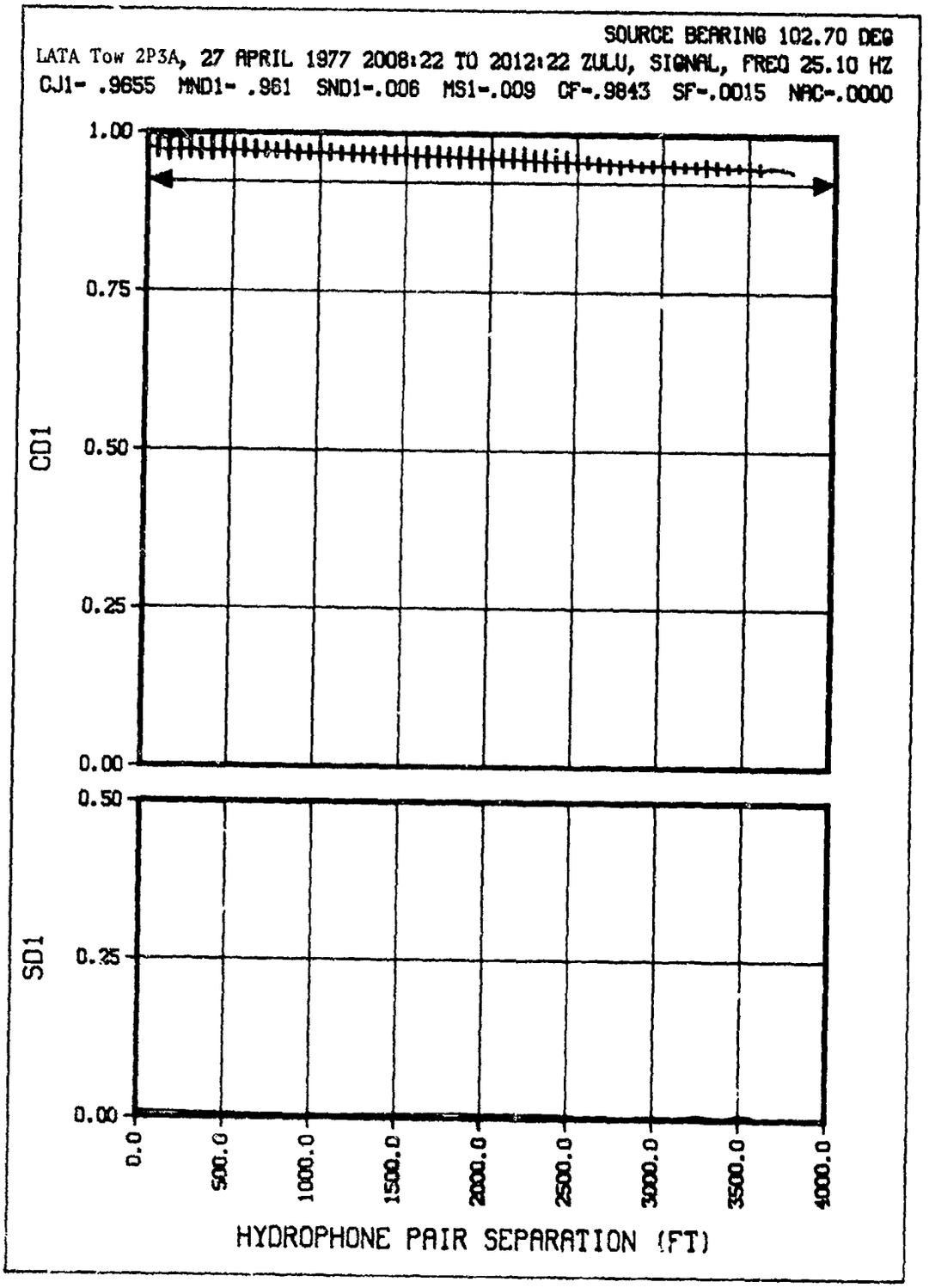

(CONFIDENTIAL)

(U) Figure 7a. Normalized amplitude covariance.

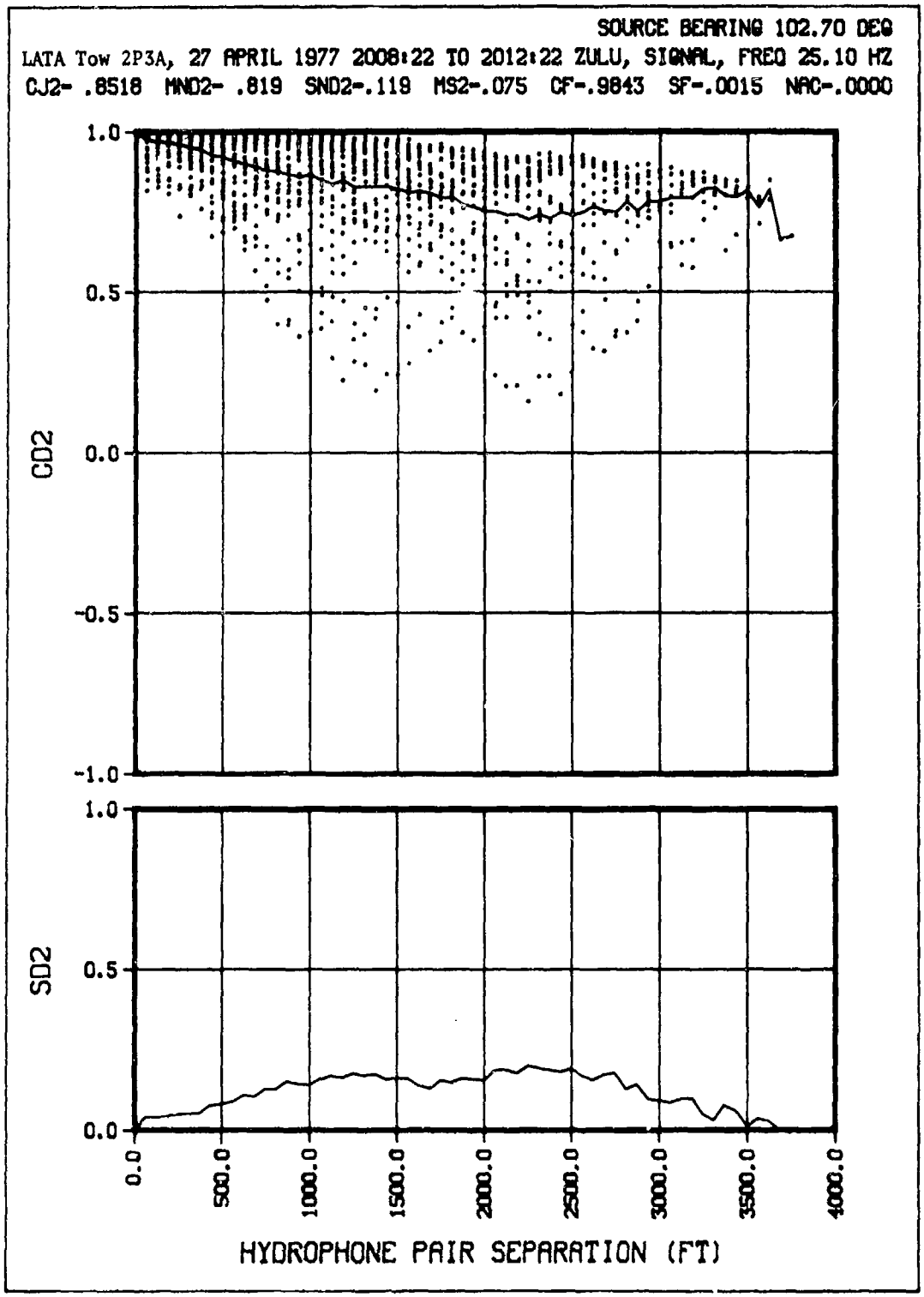

(CONFIDENTIAL)

(U) Figure 7b. Array phase coherence.

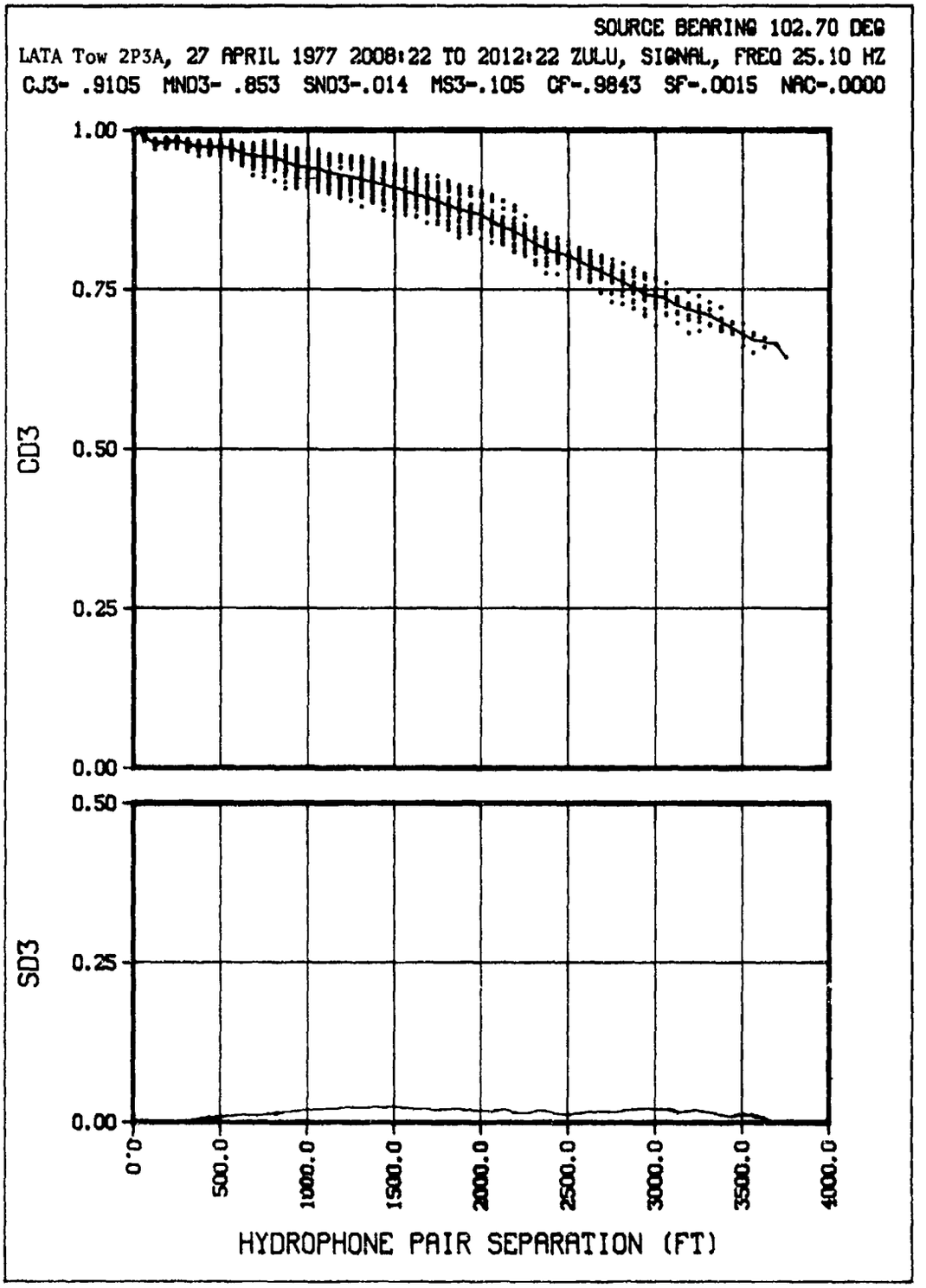

(CONFIDENTIAL)

(U) Figure 7c. Classical coherence.

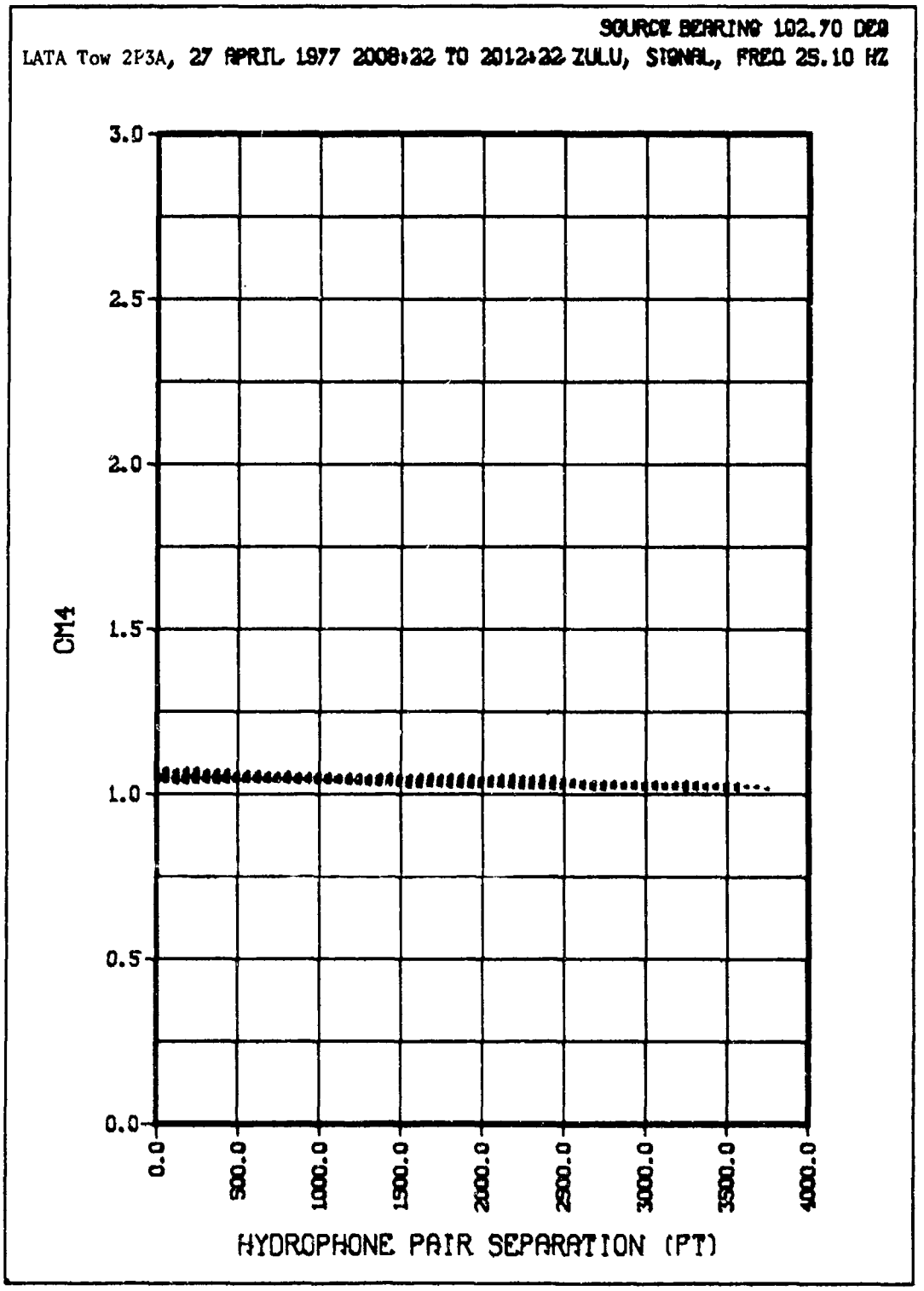

(CONFIDENTIAL)

(U) Figure 7d. Array amplitude covariance.

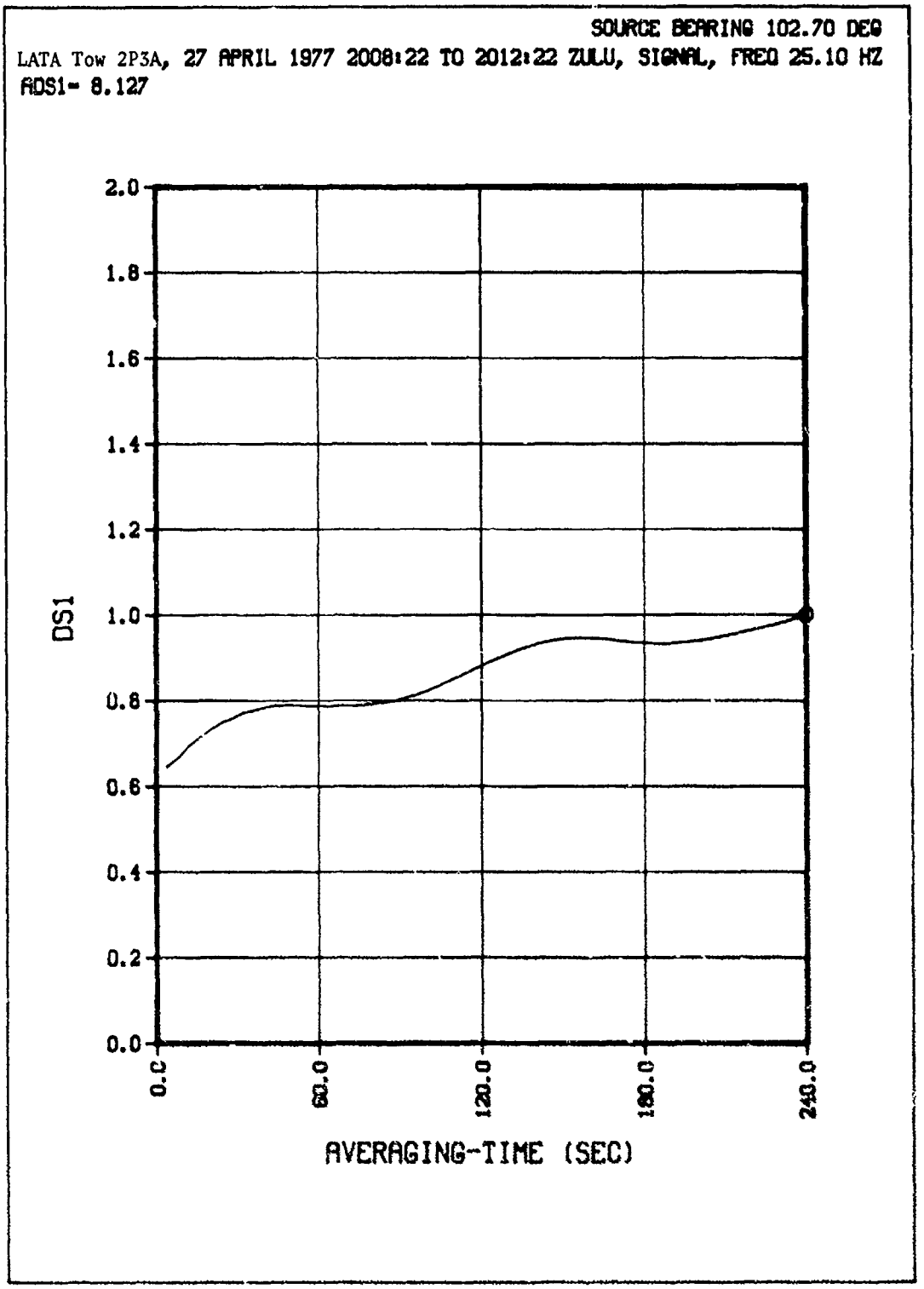

(CONFIDENTIAL)

(U) Figure 7e. Amplitude time stability.

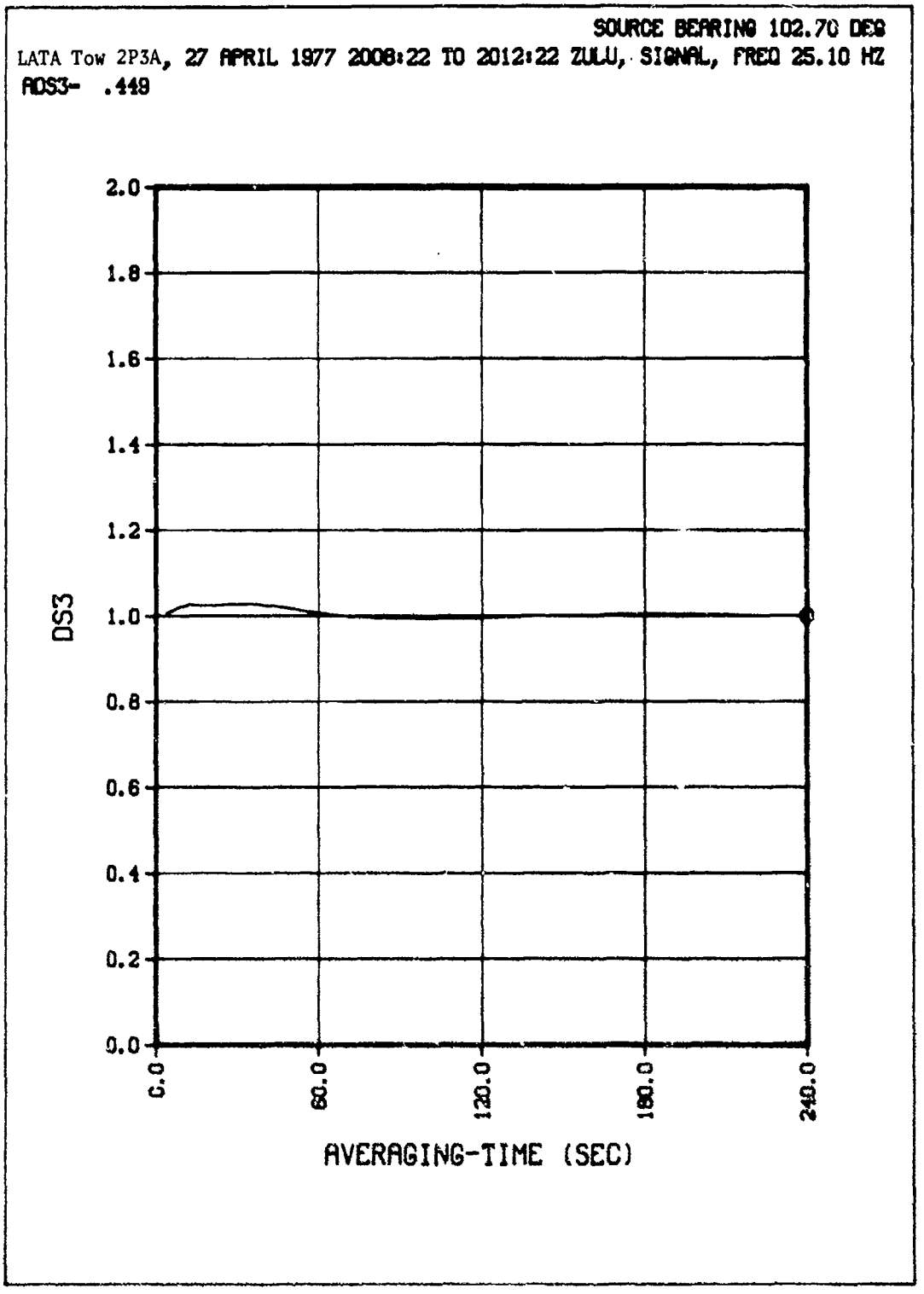

(CONFIDENTIAL)

(U) Figure 7f. Phase time stability.

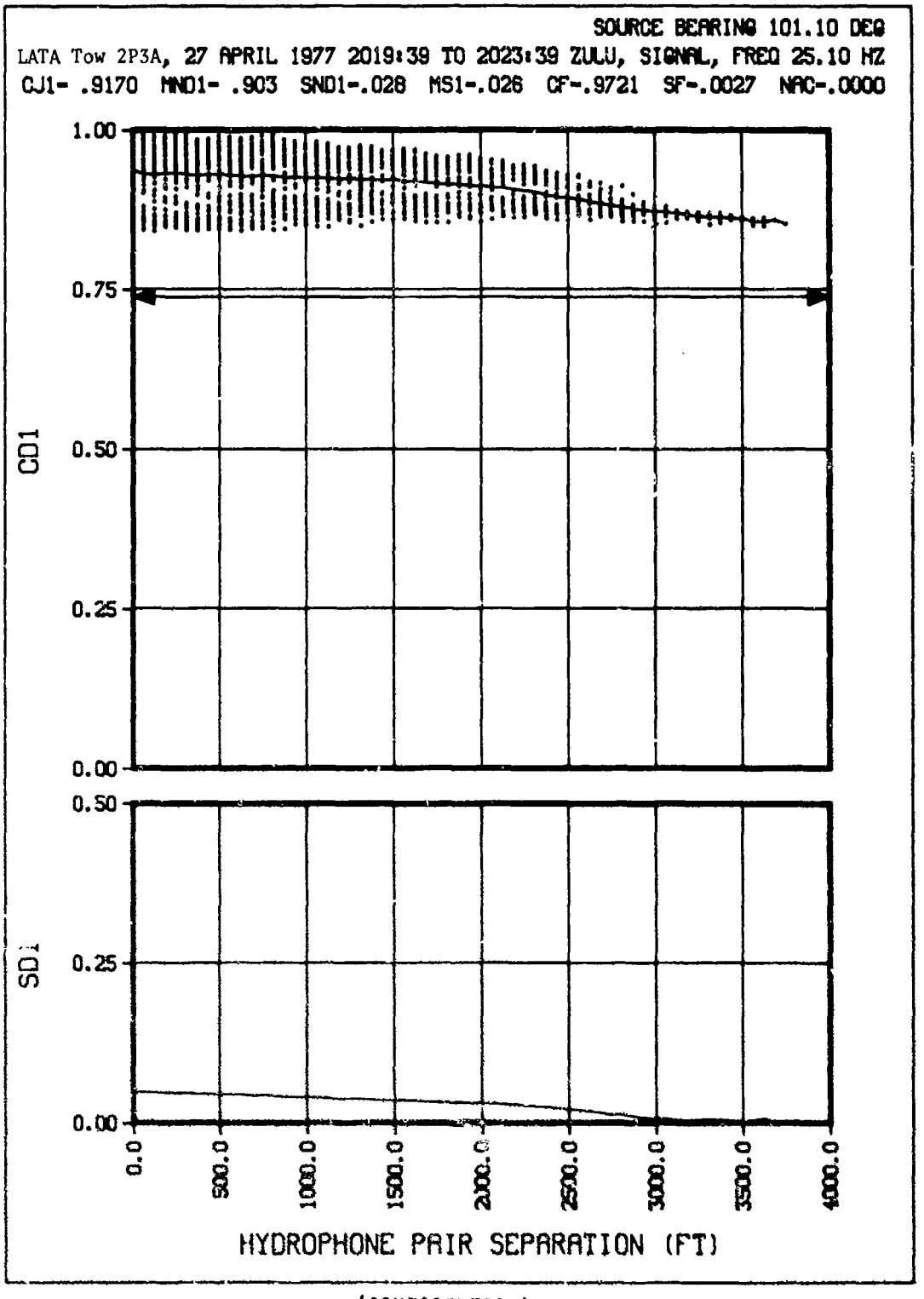

(CONFIDENTIAL)

(U) Figure 8a. Normalized amplitude covariance.

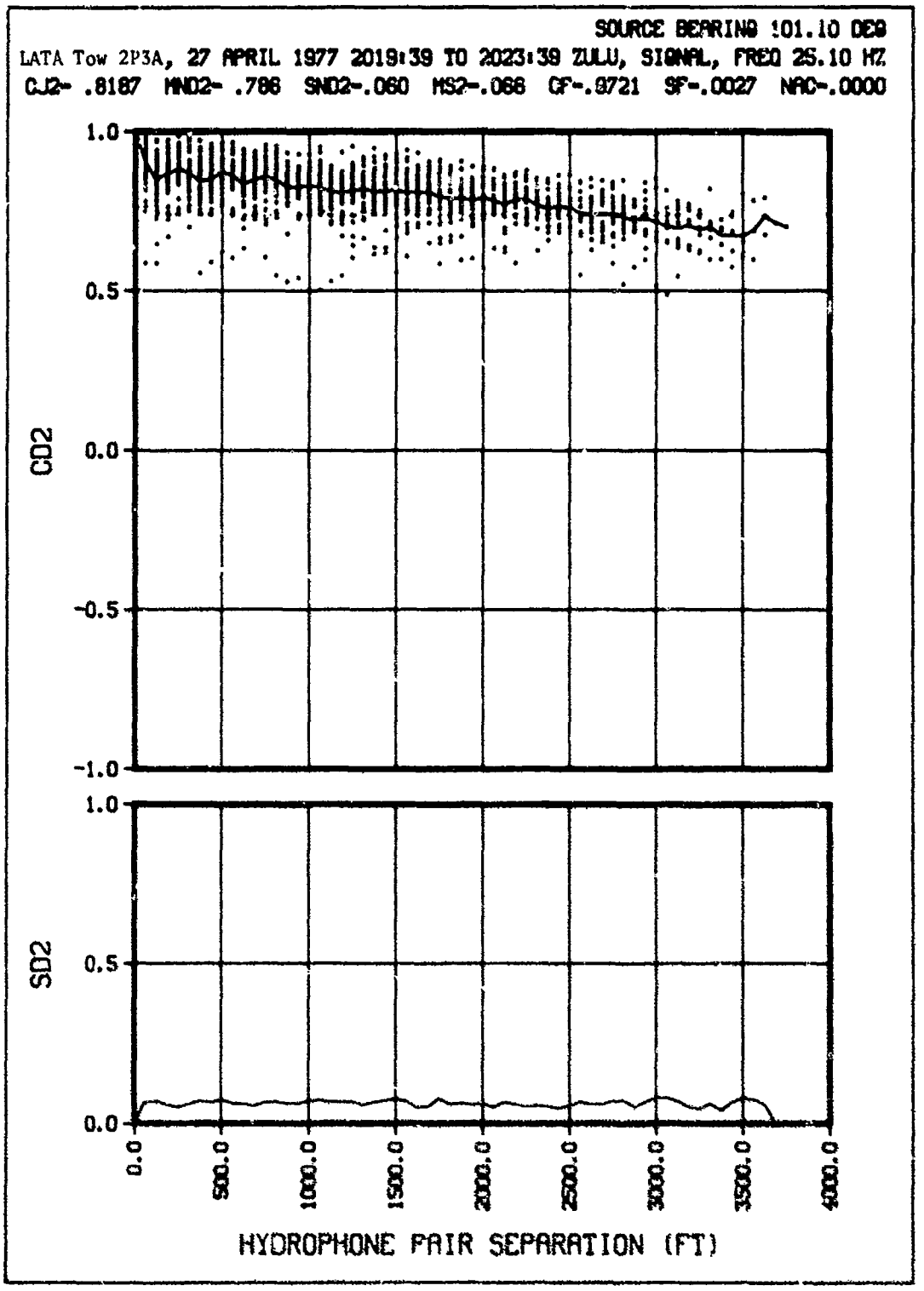

(CONFIDENTIAL)

(U) Figure 8b. Array phase coherence.

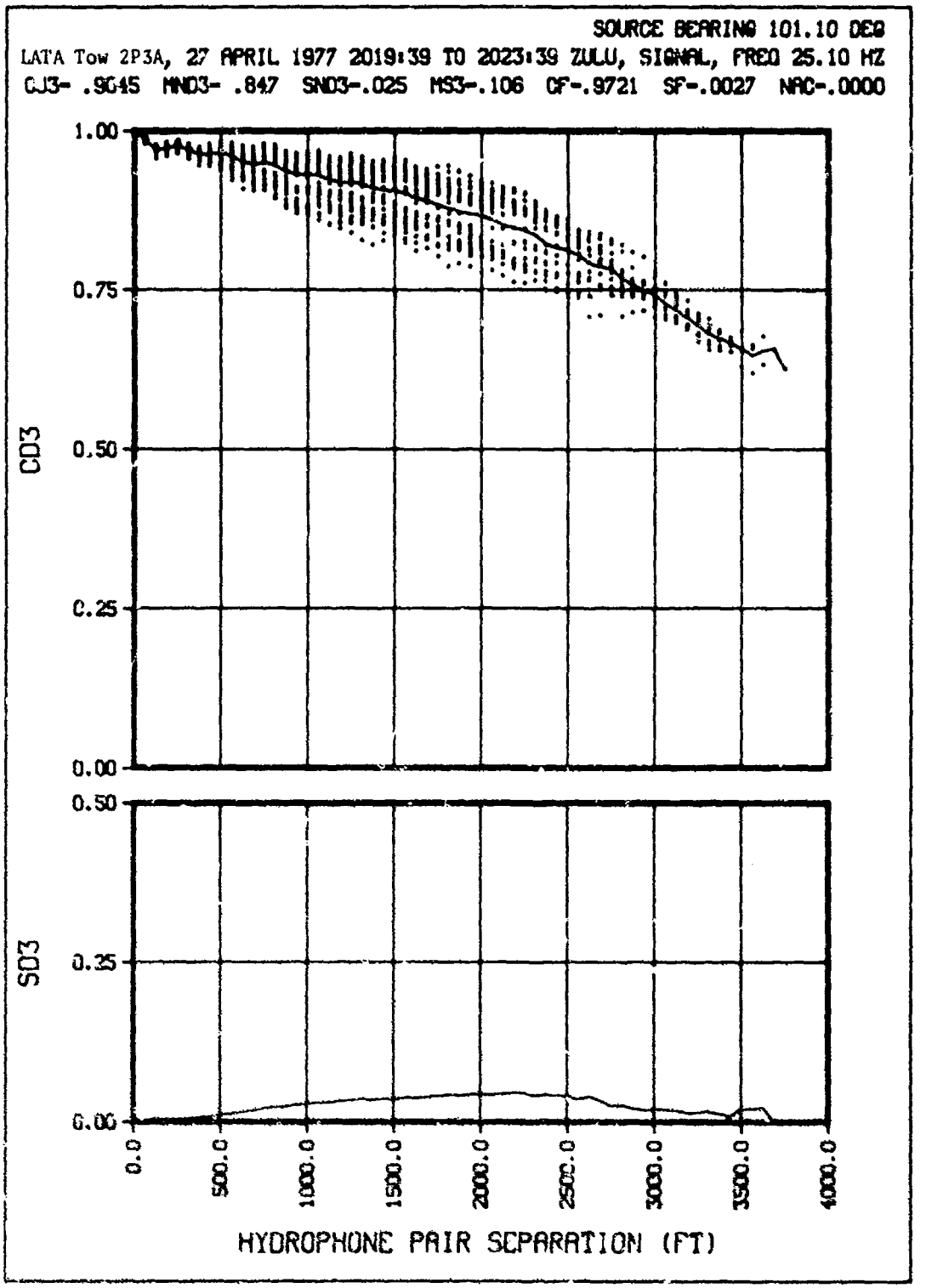

(CONFIDENTIAL)

(U) Figure 8c. Classical coherence.

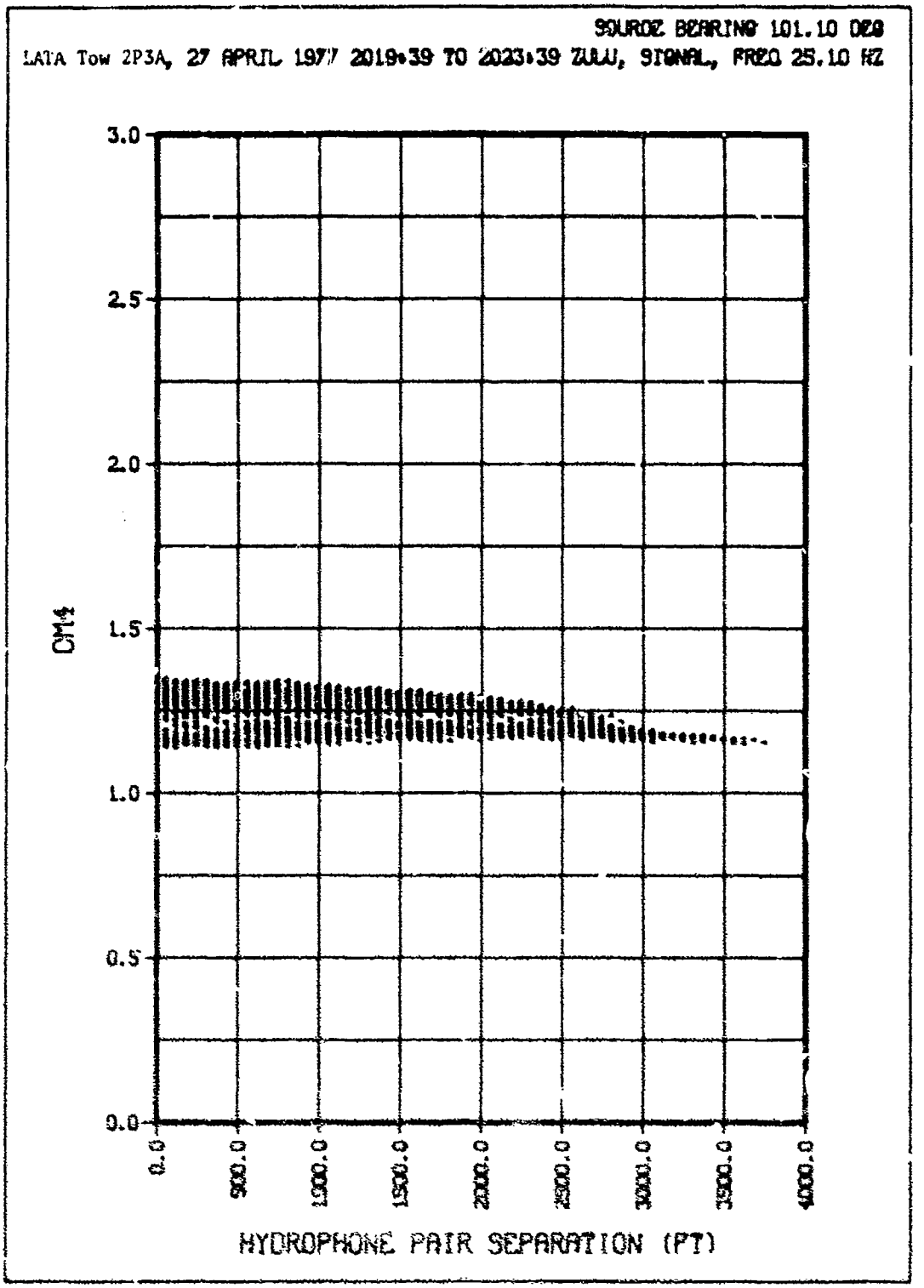

(CONFIDENTIAL)

(U) Figure 8d. Array amplitude covariance.

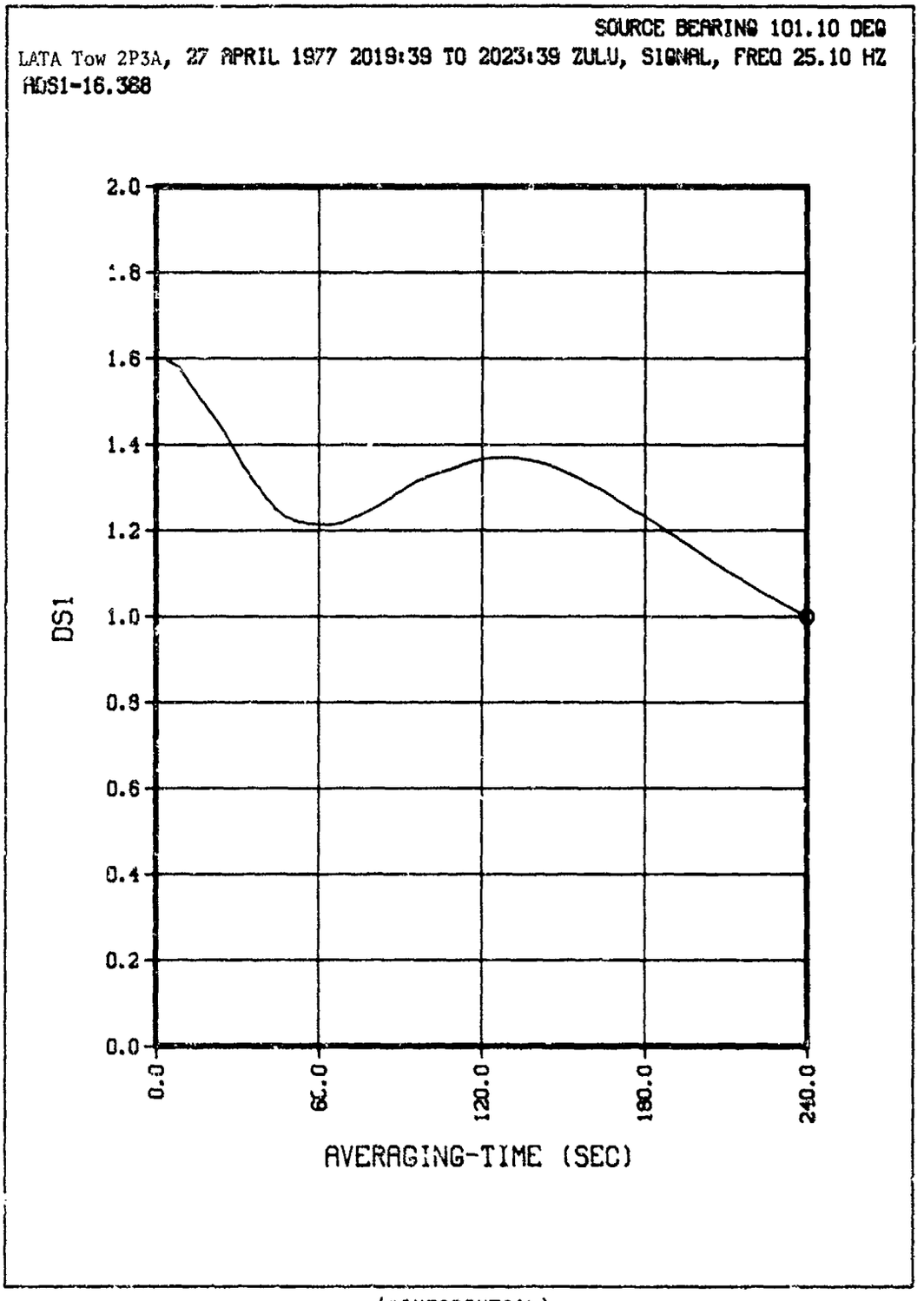

(CONFIDENTIAL)

(U) Figure 8e. Amplitude time stability.

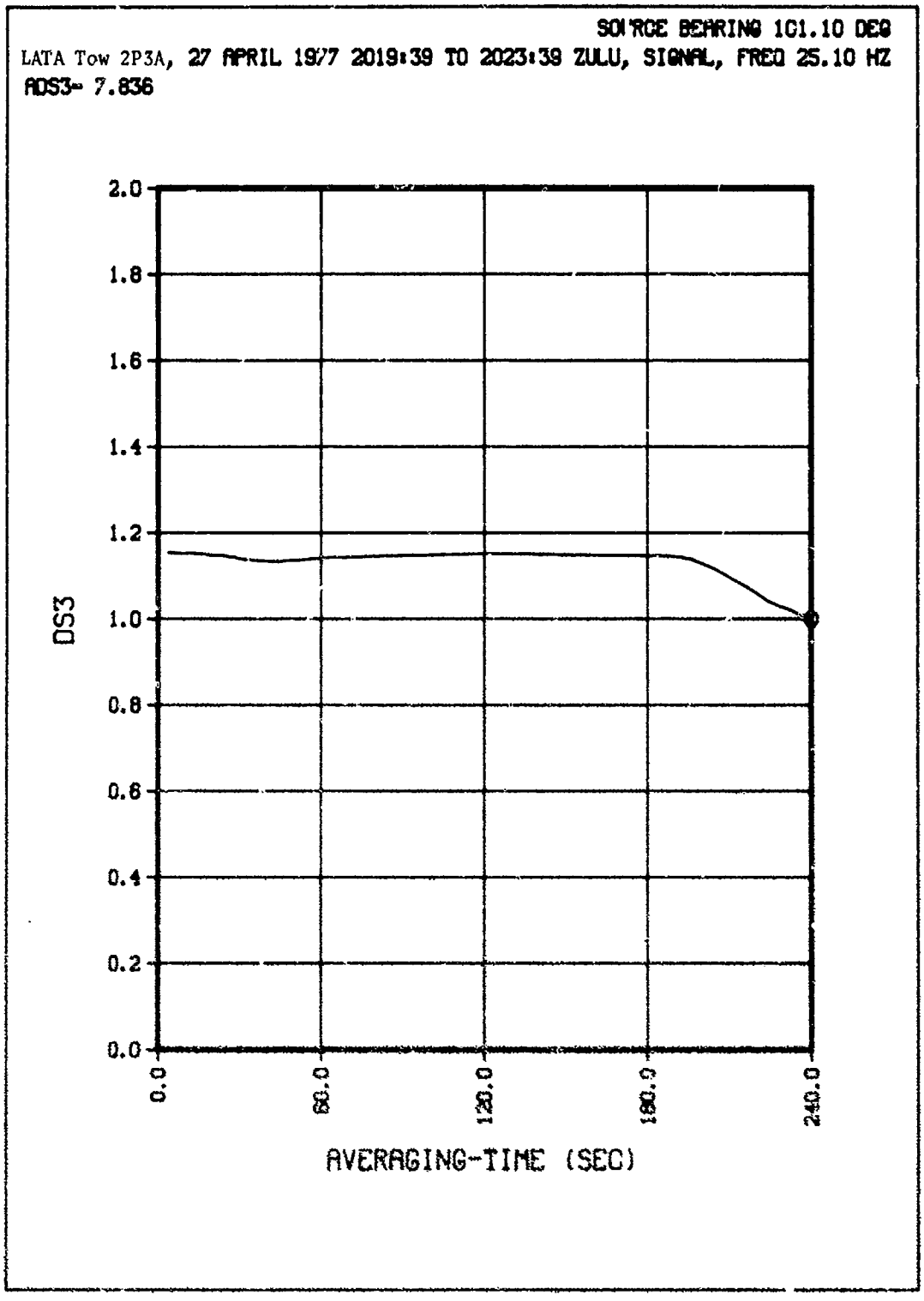

(CONFIDENTIAL)

(U) Figure 8f. Phase time stability.

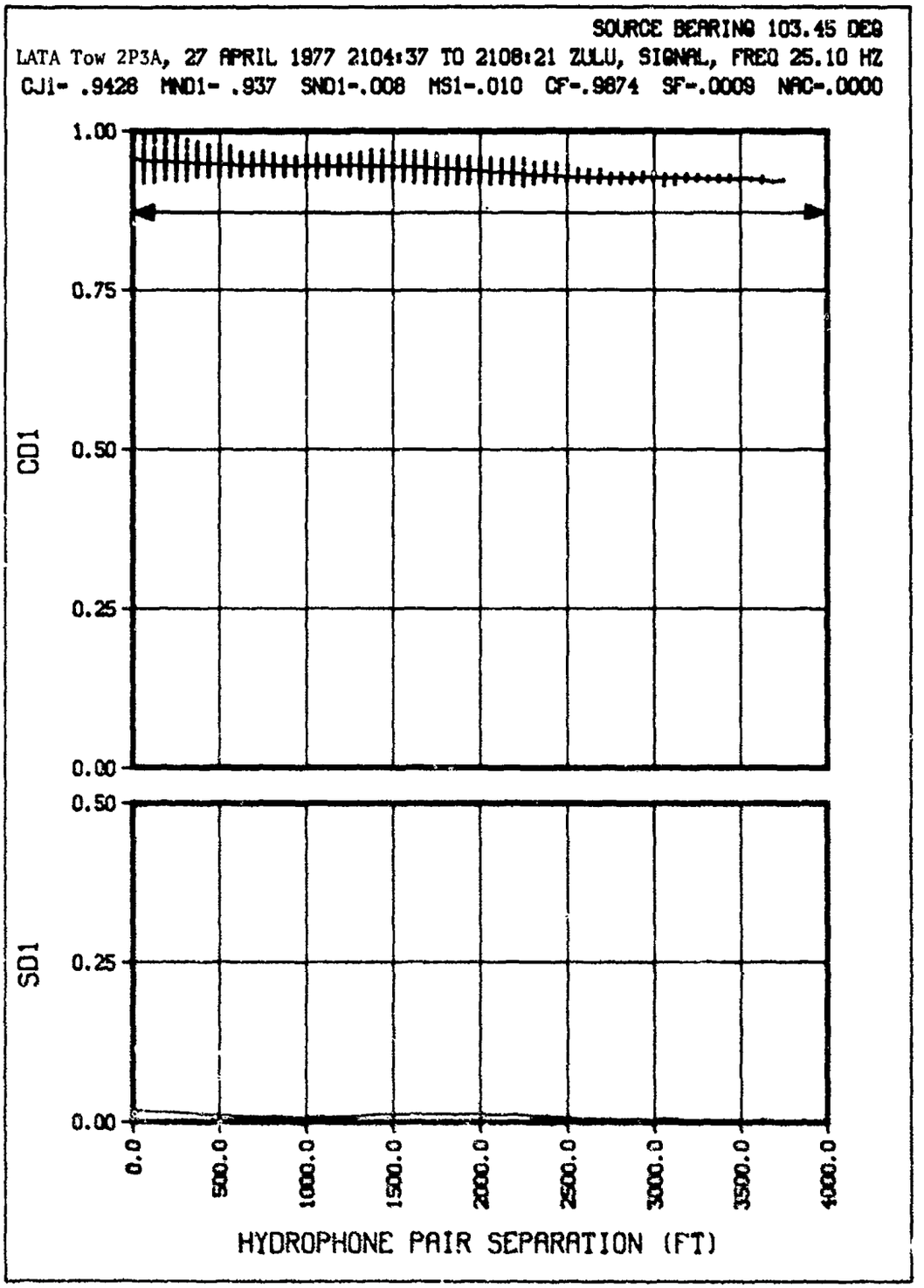

(CONFIDENTIAL)

(U) Figure 9a. Normalized amplitude covariance.

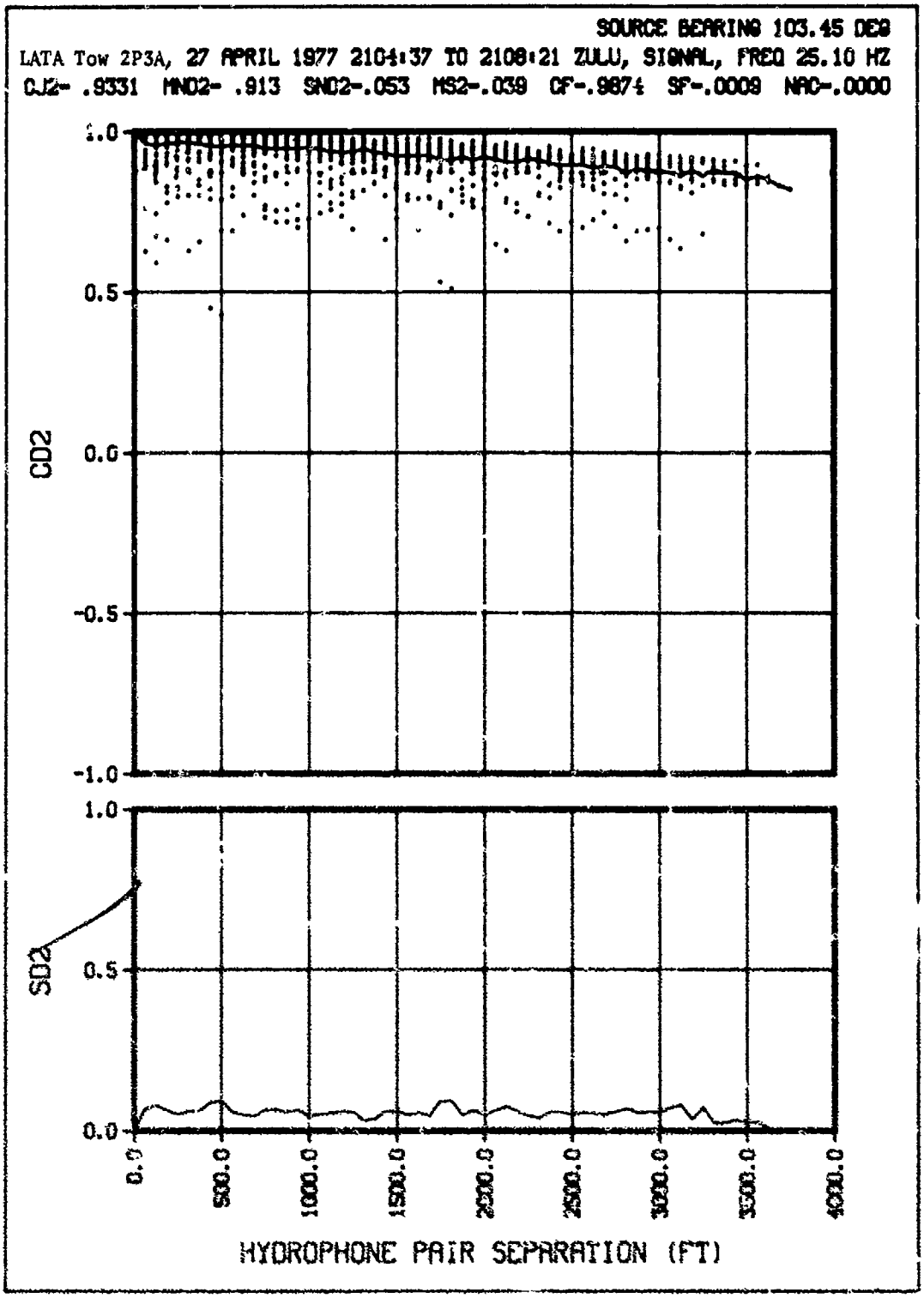

(CONFIDENTIAL)

(U) Figure 9b. Array phase coherence.

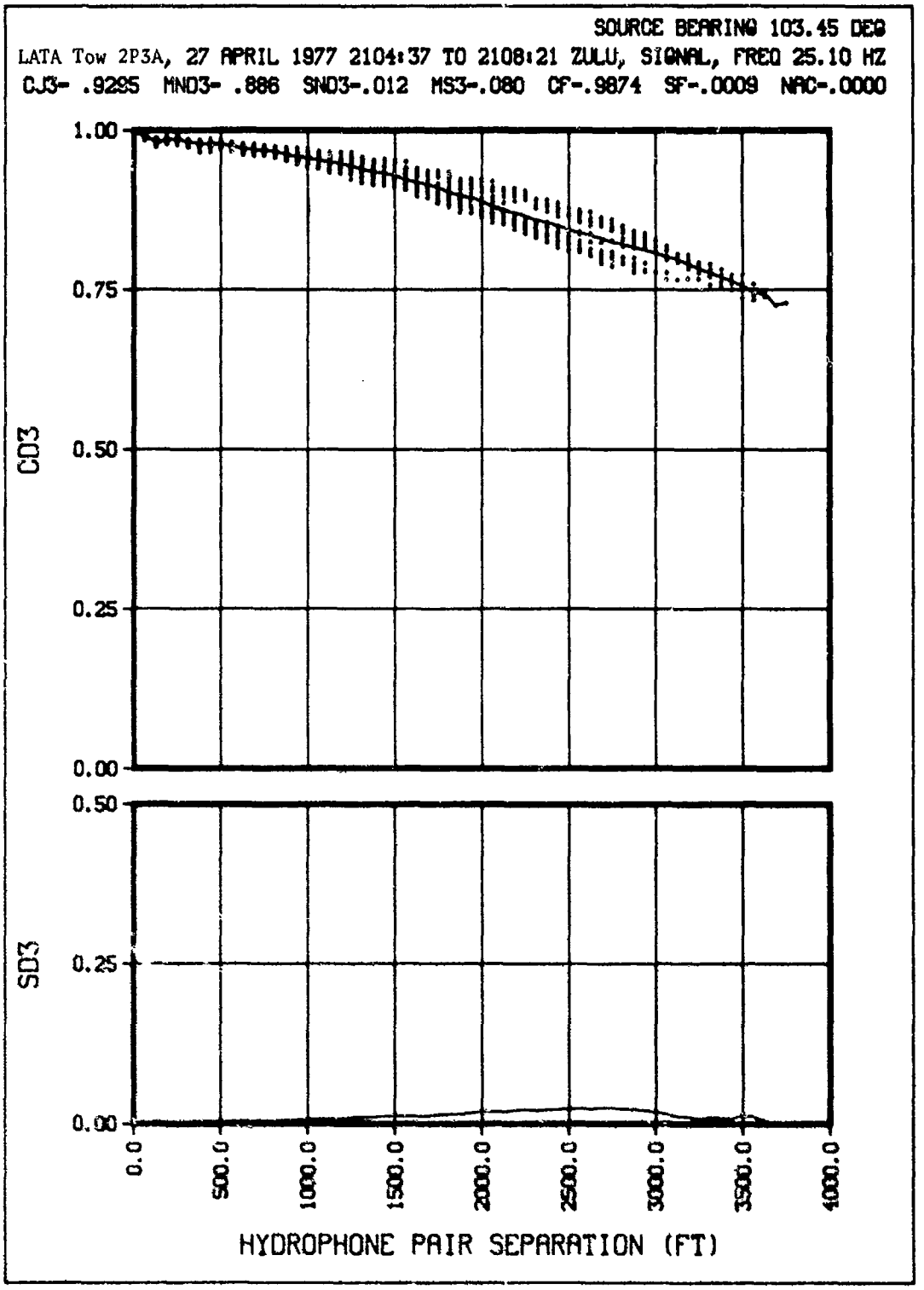

(CONFIDENTIAL)

(U) Figure 9c. Classical coherence.

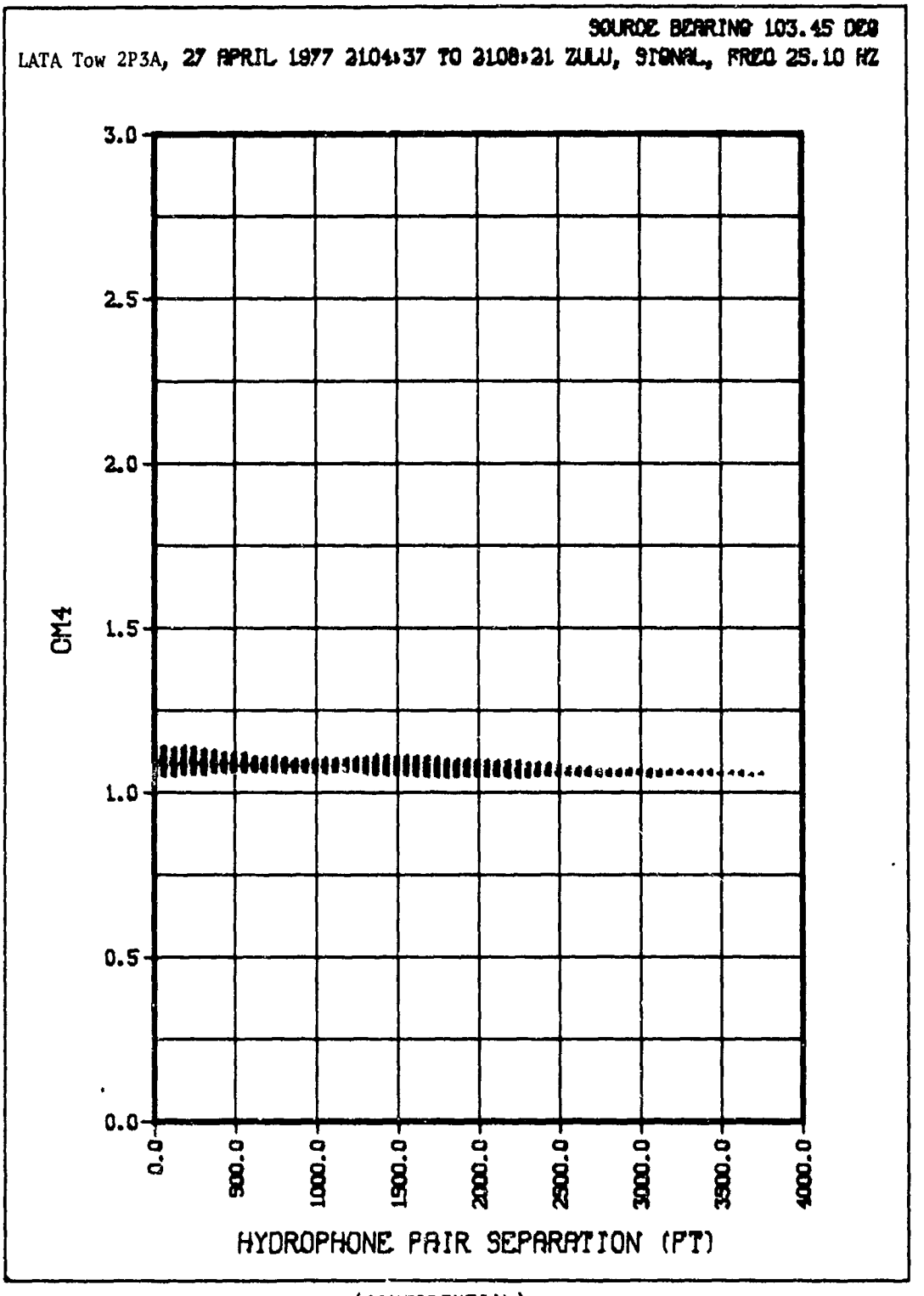

(CONFIDENTIAL)

(U) Figure 9d. Array amplitude covariance.

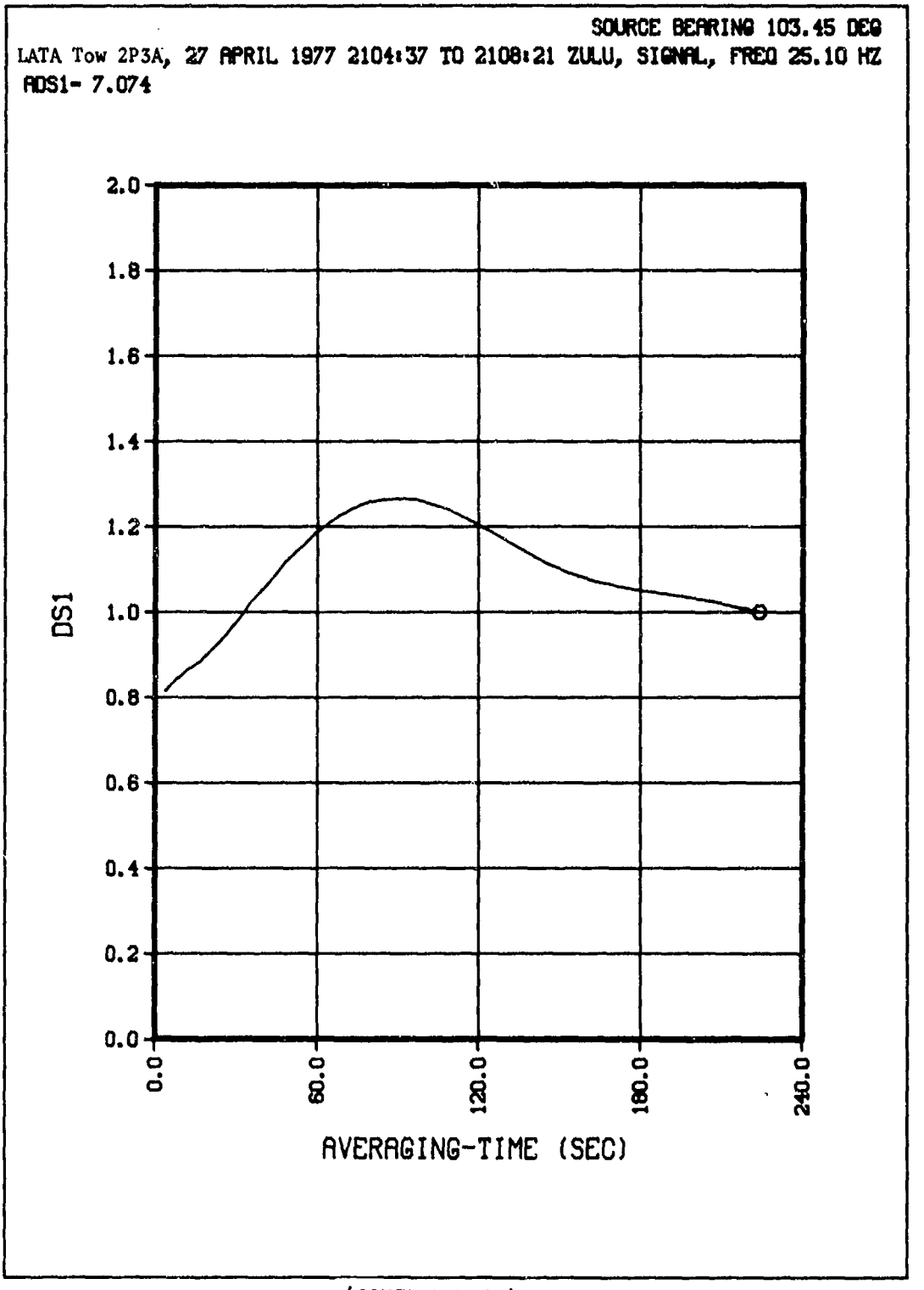

(CONFIDENTIAL)

(U) Figure 9e. Amplitude time stability.

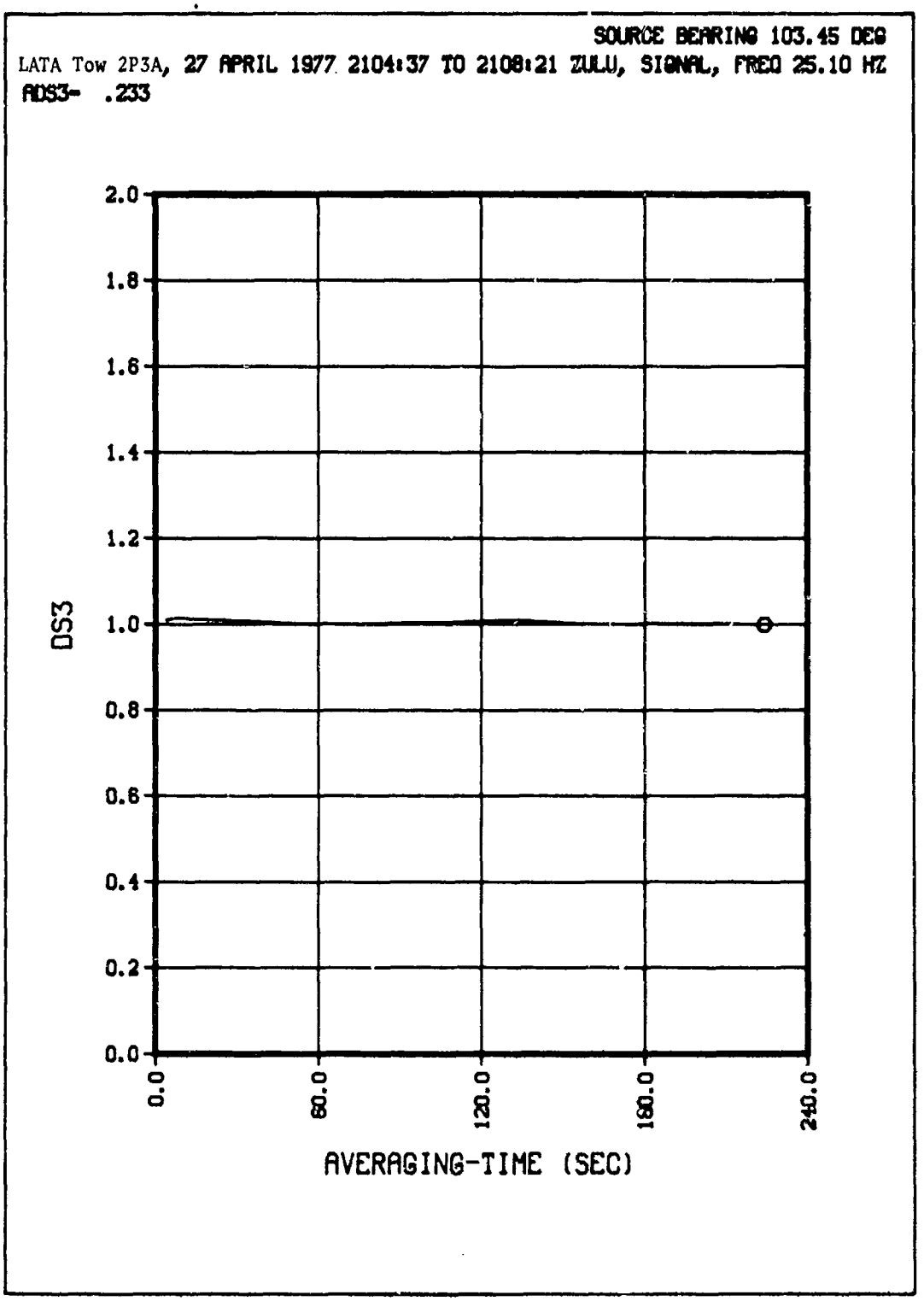

(CONFIDENTIAL)

(U) Figure 9f. Phase time stability.

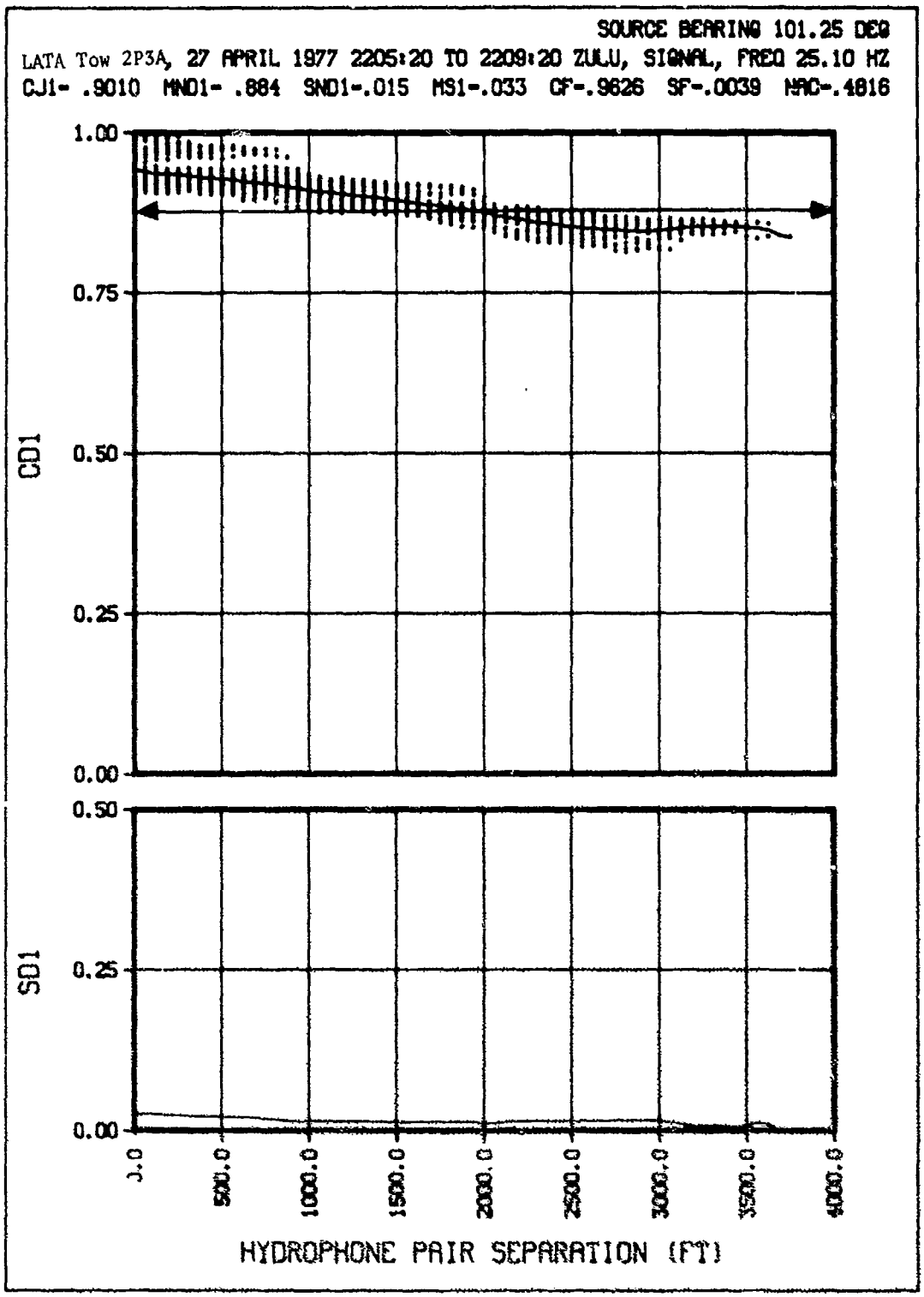

(CONFIDENTIAL)

(U) Figure 10a. Normalized amplitude covariance.

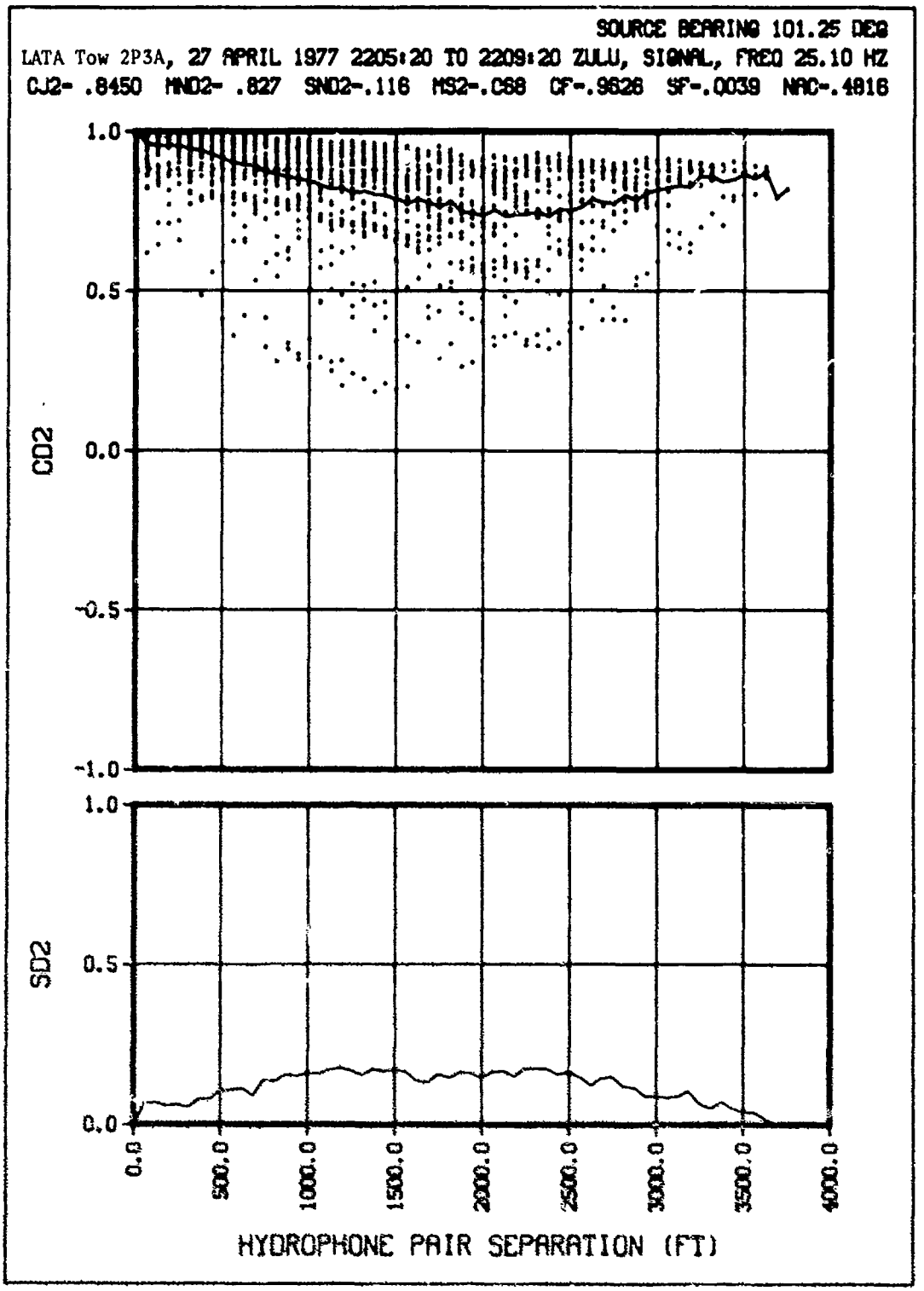

(CONFIDENTIAL)

(U) Figure 10b. Array phase coherence.

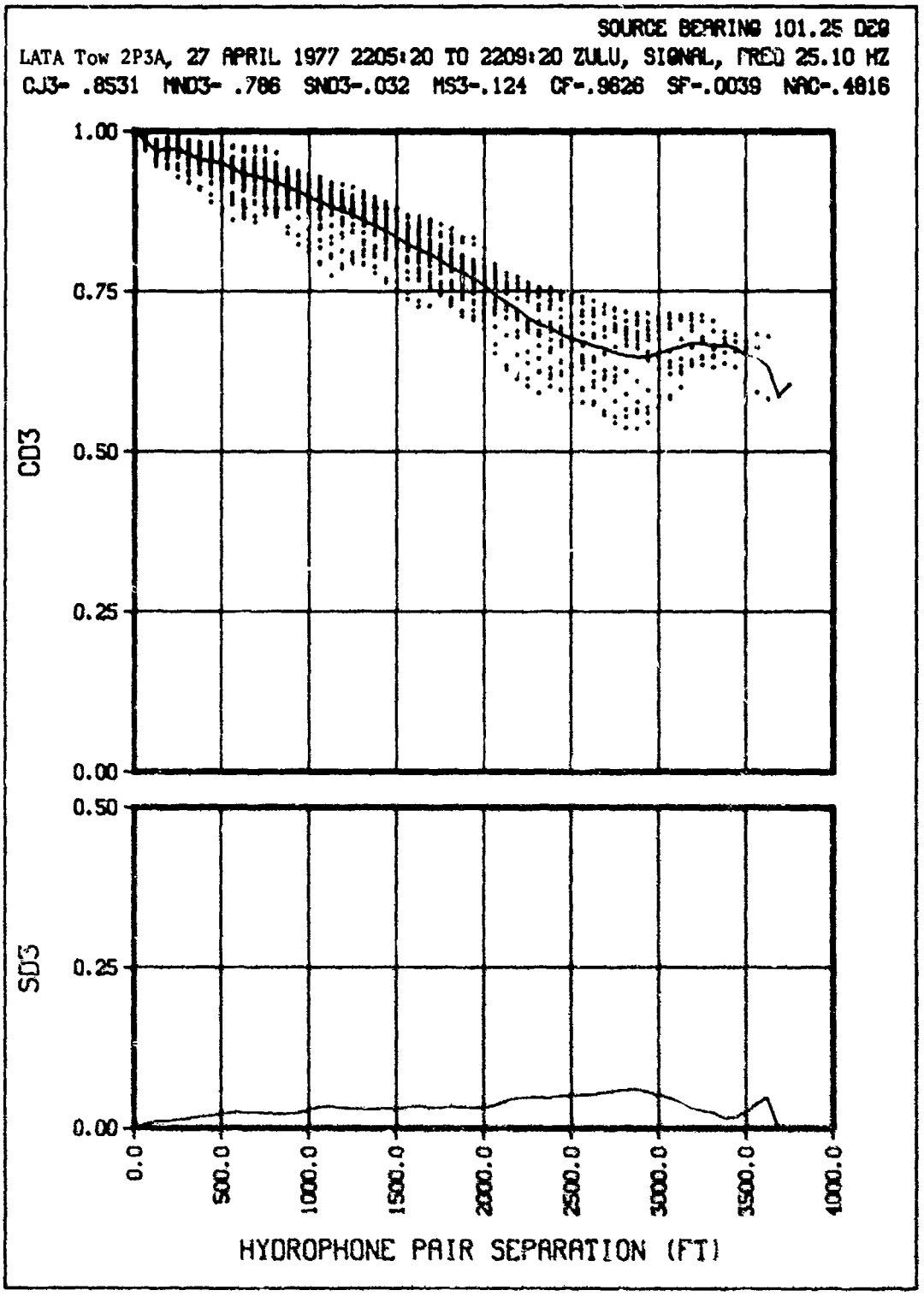

(CONFIDENTIAL)

(U) Figure 10c. Classical coherence.

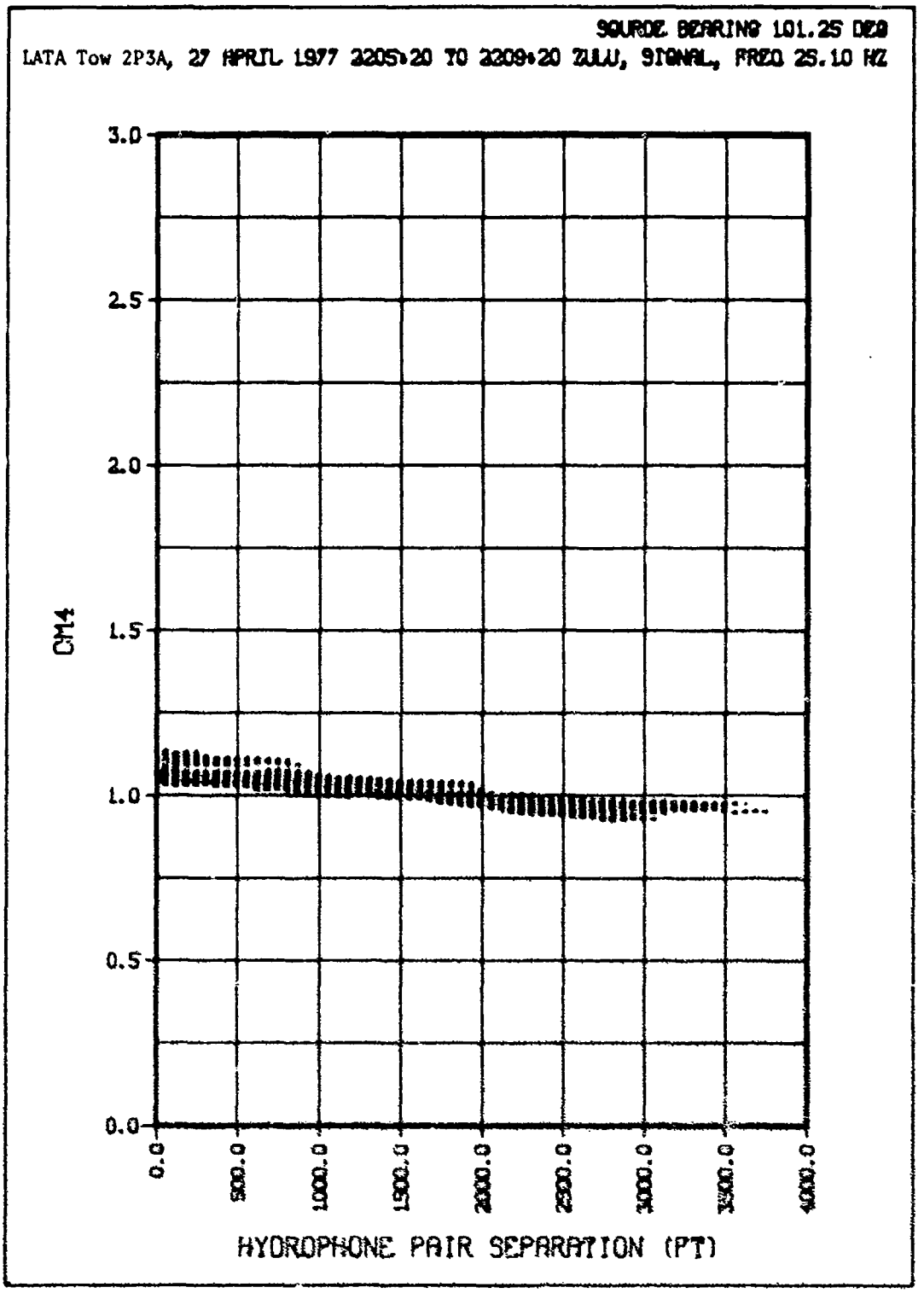

(CONFIDENTIAL)

(U) Figure 10d. Array amplitude covariance.

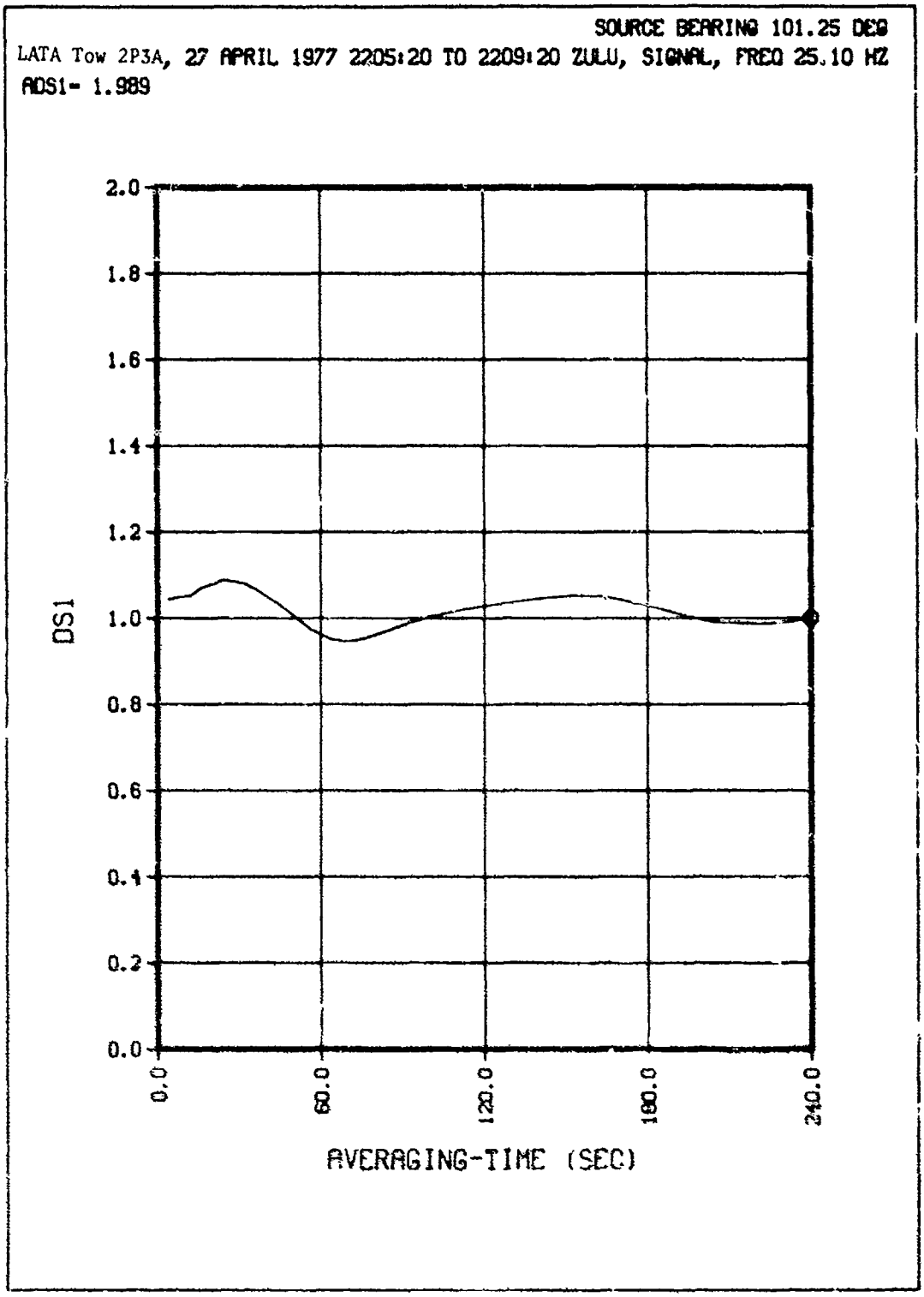

(CONFIDENTIAL)

(U) Figure 10e. Amplitude time stability.

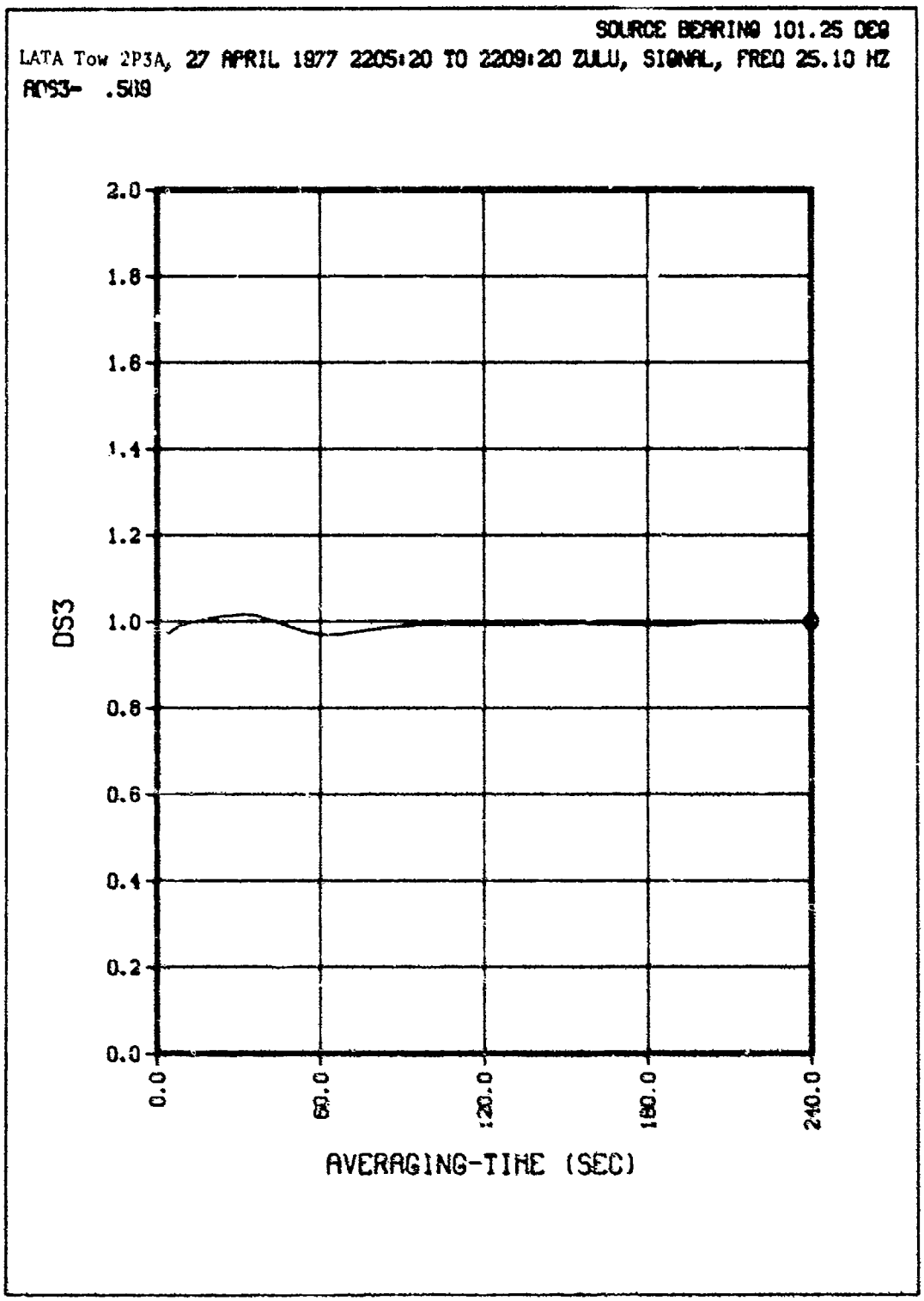

(CONFIDENTIAL)

(U) Figure 10f. Phase time stability.

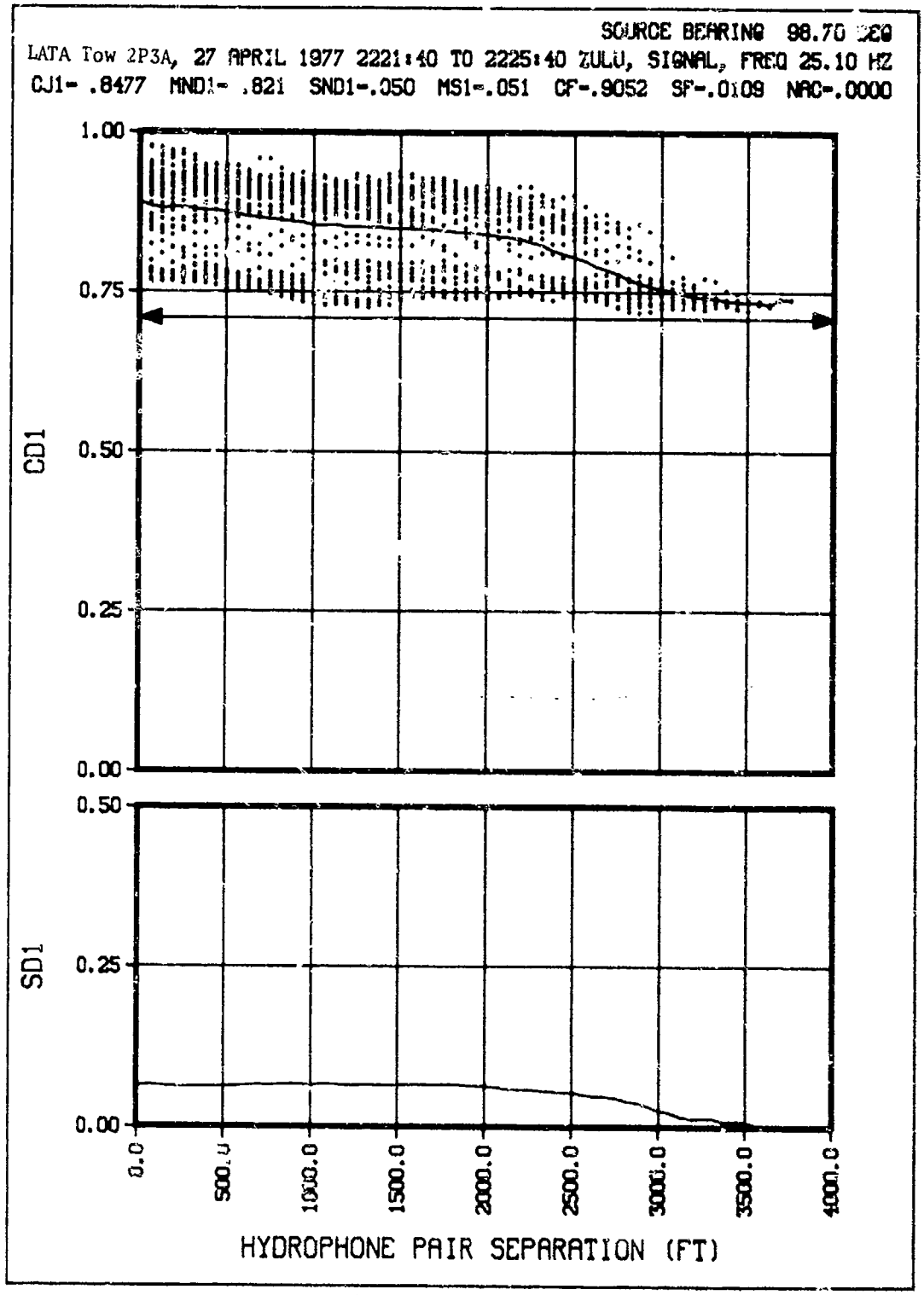

(CONFIDENTIAL)

(U) Figure 11a. Normalized amplitude covariance.

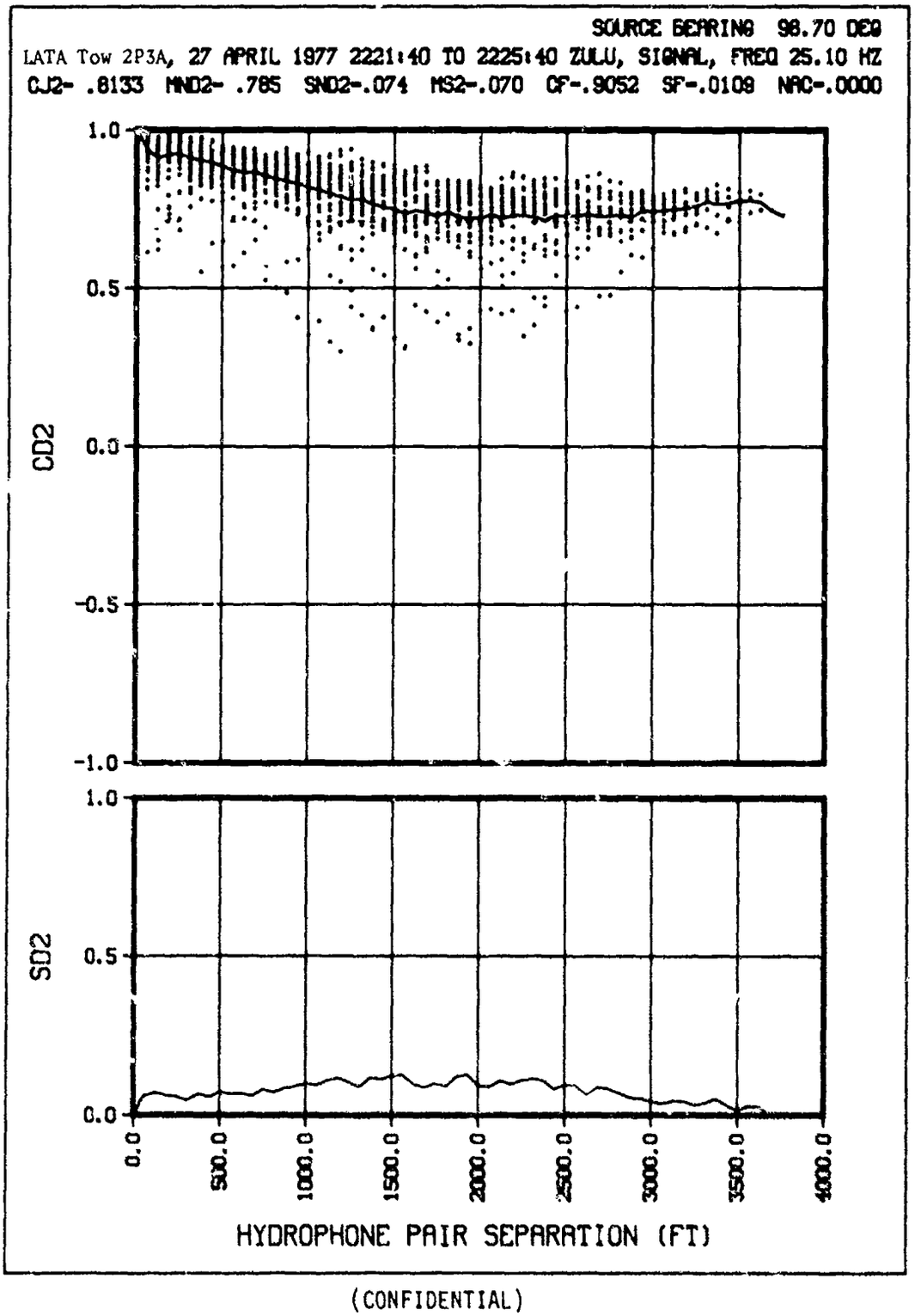

(CONFIDENTIAL)

(U) Figure 11b. Array phase coherence.

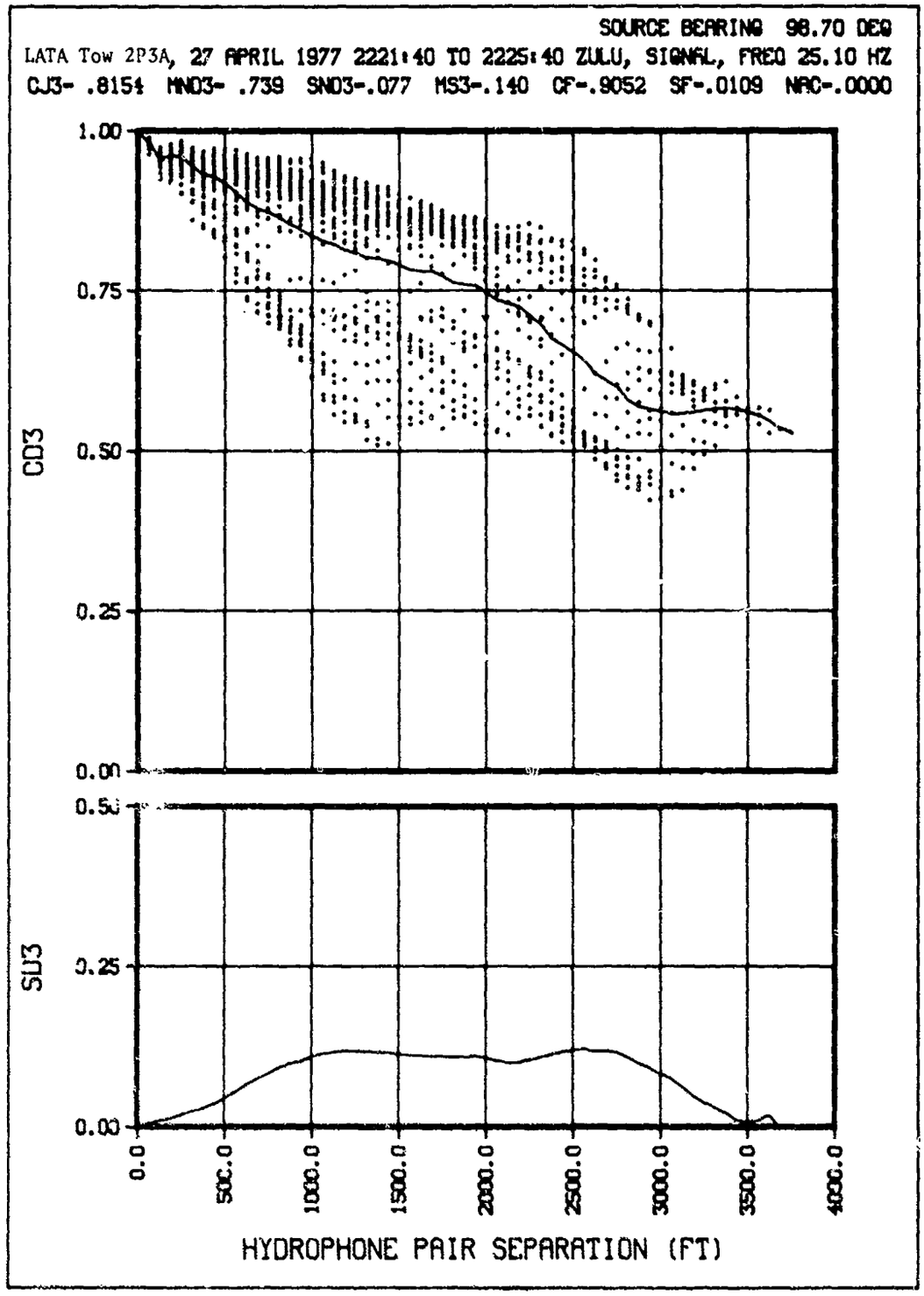

(CONFIDENTIAL)

(U) Figure 11c. Classical coherence.

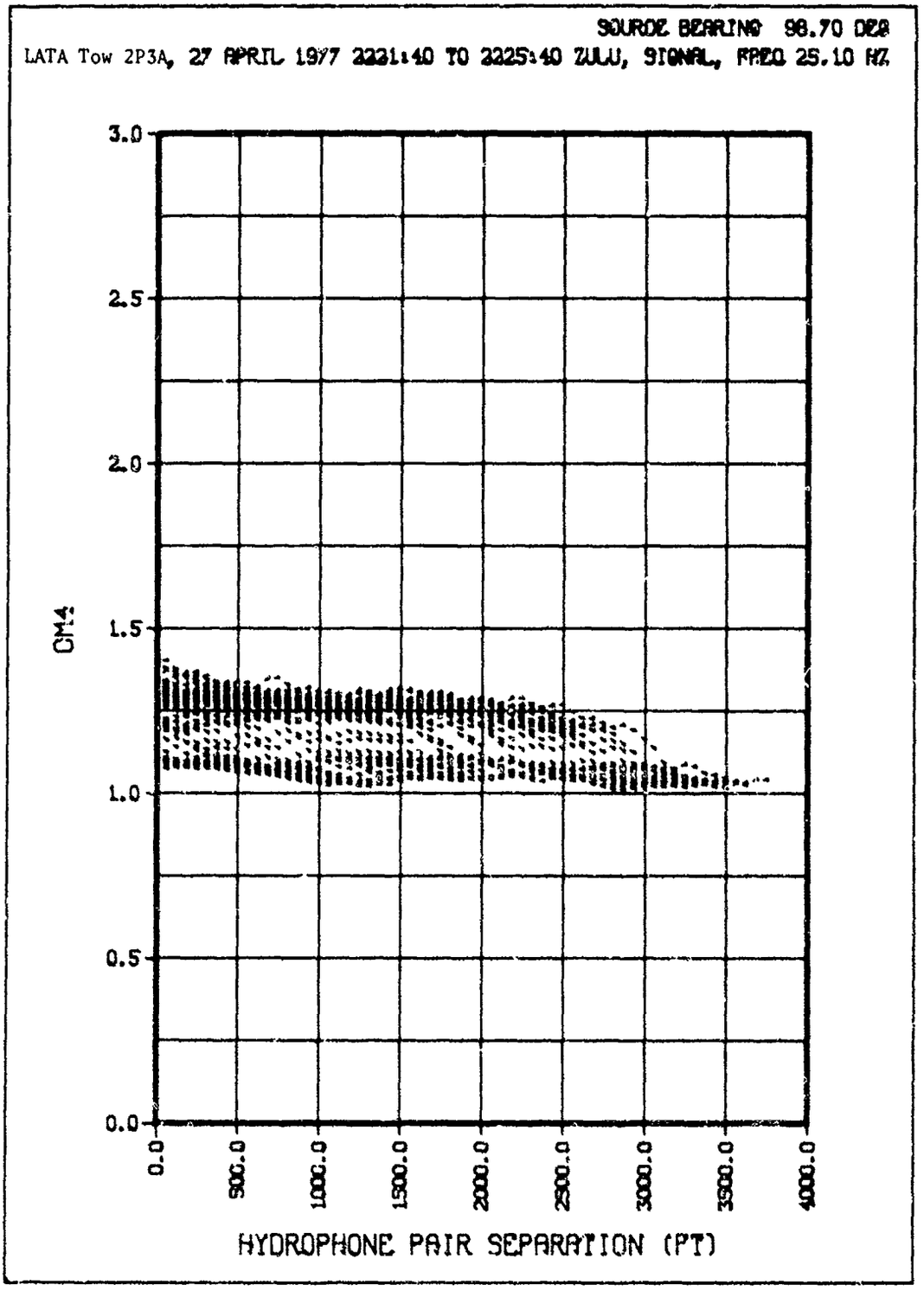

(CONFIDENTIAL)

(U) Figure 11d. Array amplitude covariance.

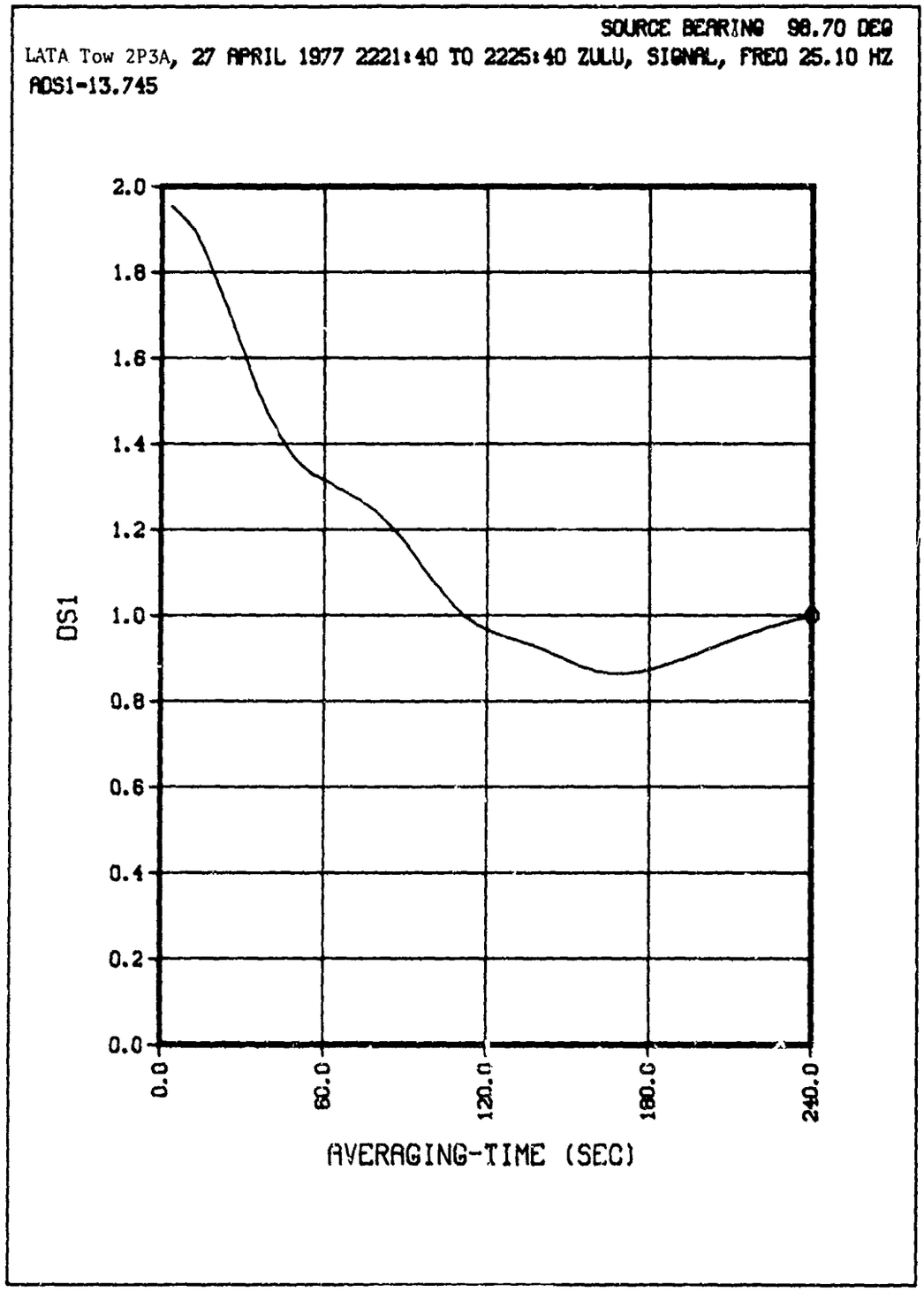

(CONFIDENTIAL)

(U) Figure 11e. Amplitude time stability.

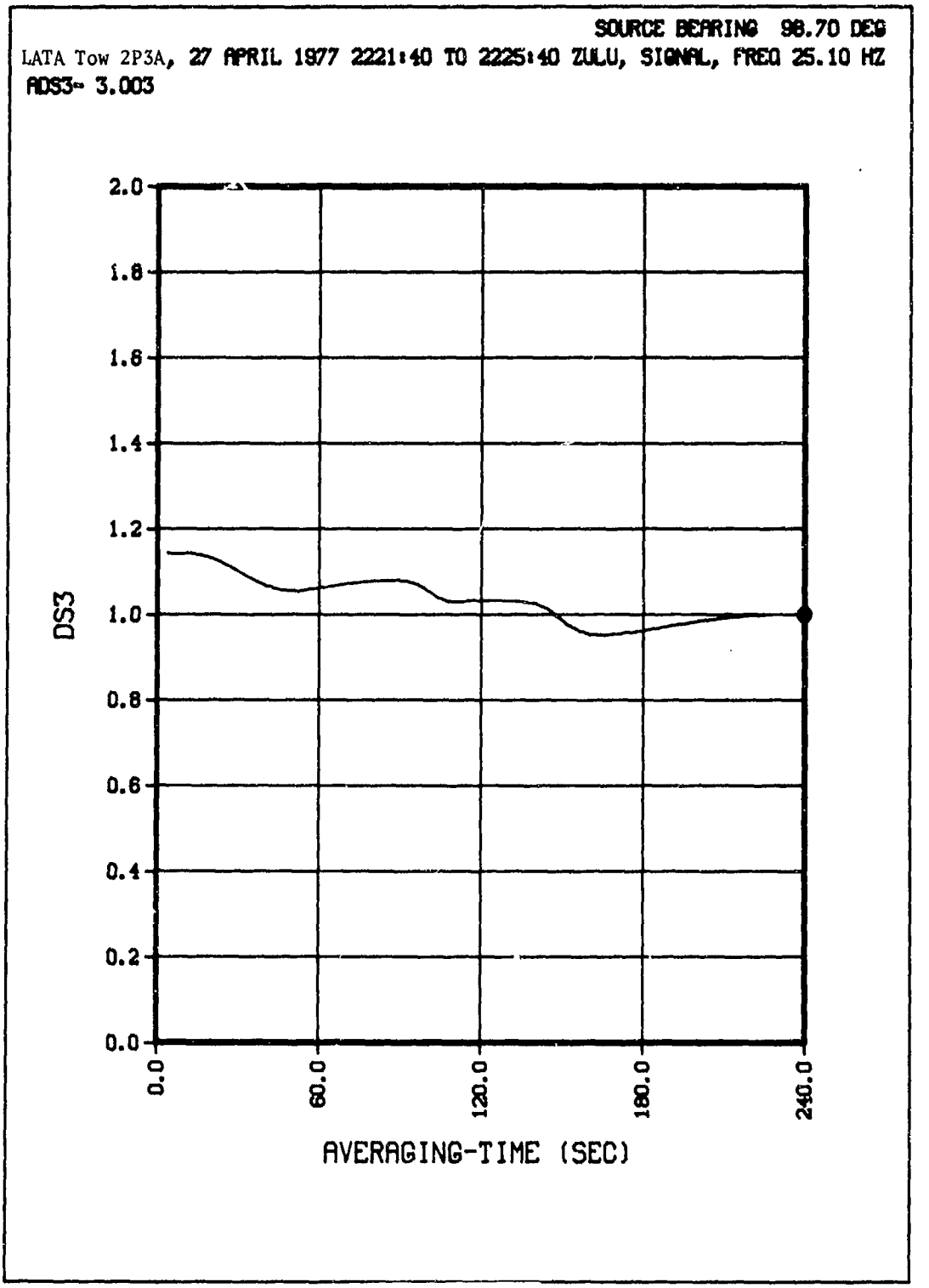

(CONFIDENTIAL)

(U) Figure 11f. Phase time stability.

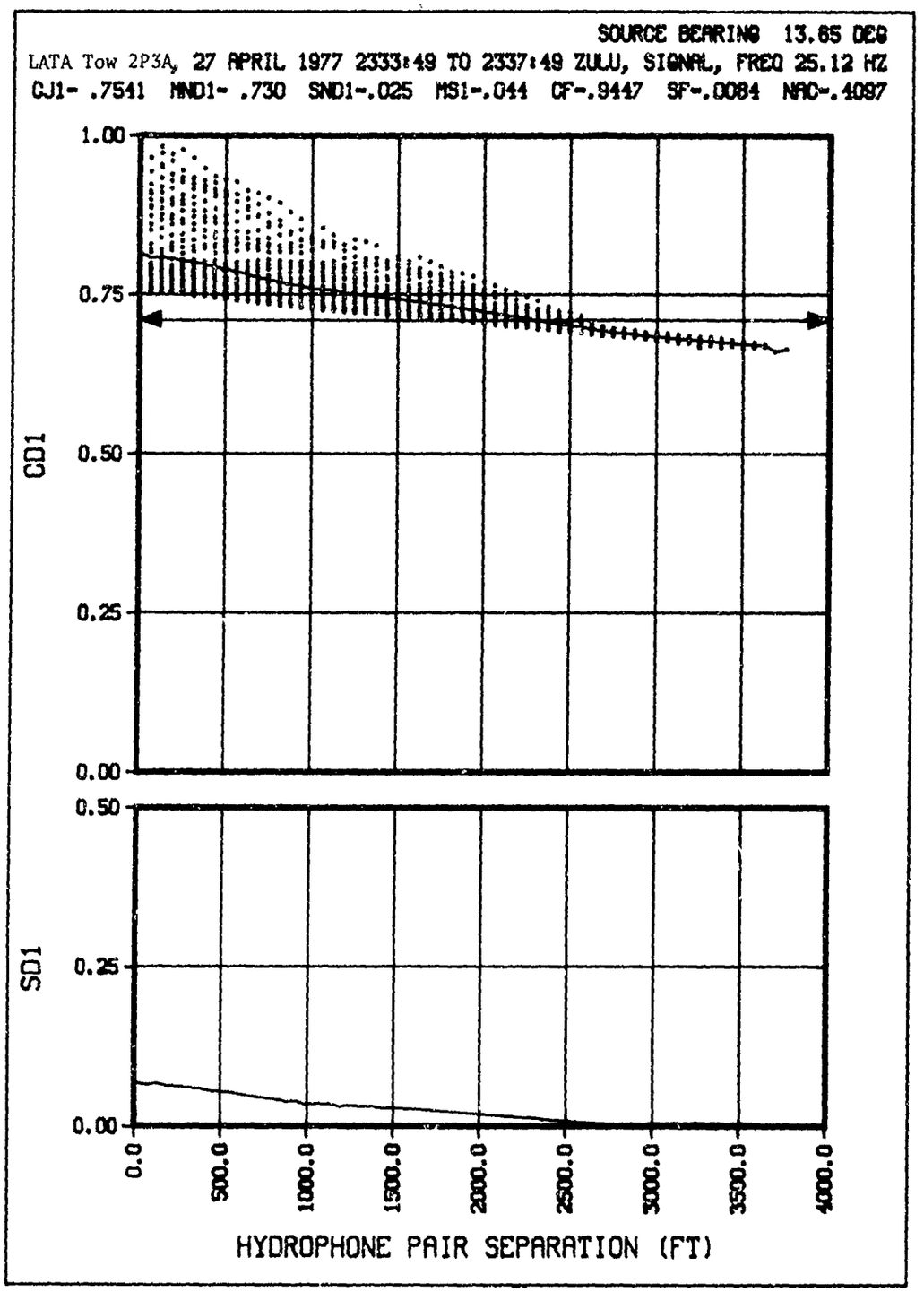

(CONFIDENTIAL)

(U) Figure 12a. Normalized amplitude covariance.

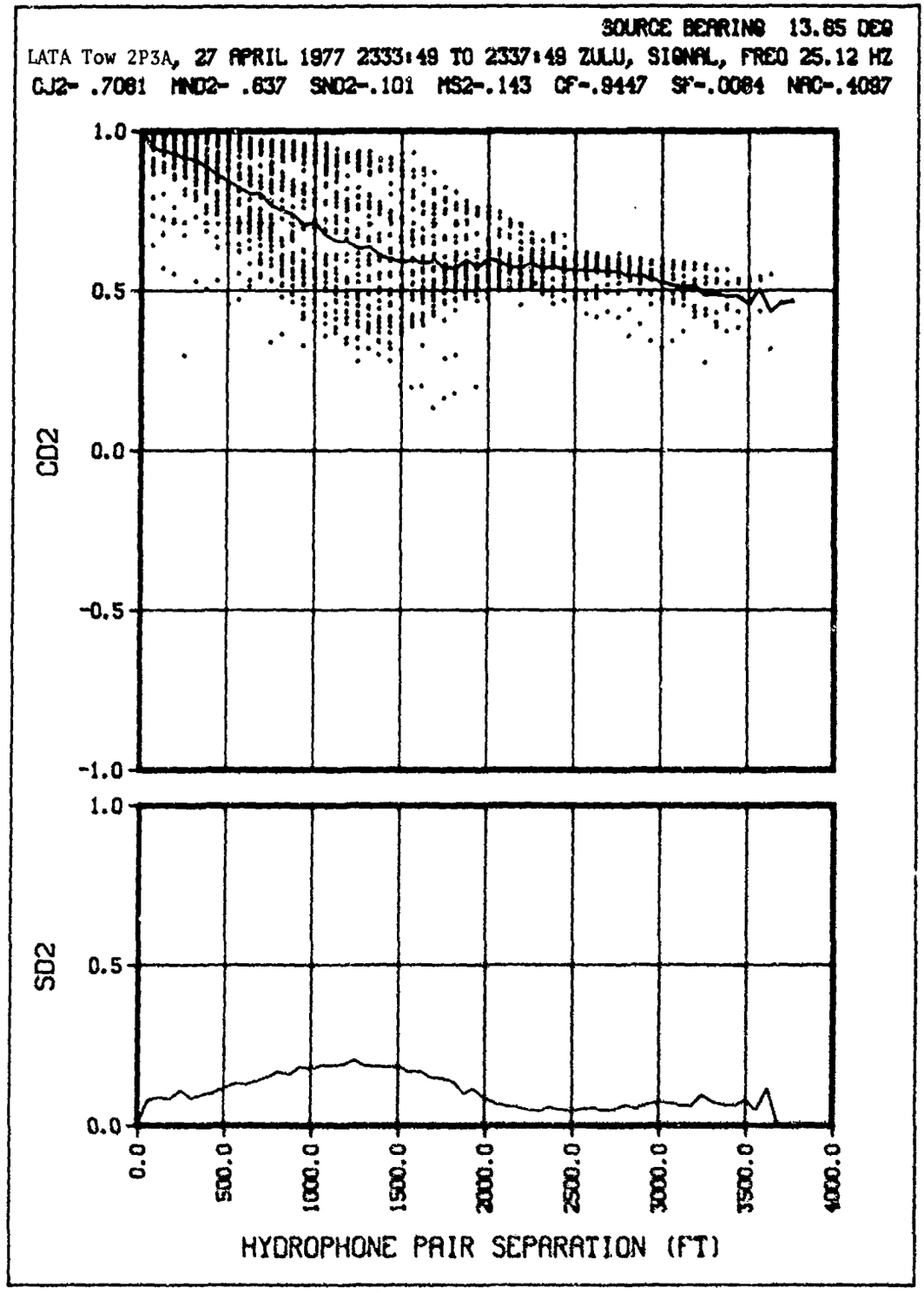

(CONFIDENTIAL)

(U) Figure 12b. Array phase coherence.

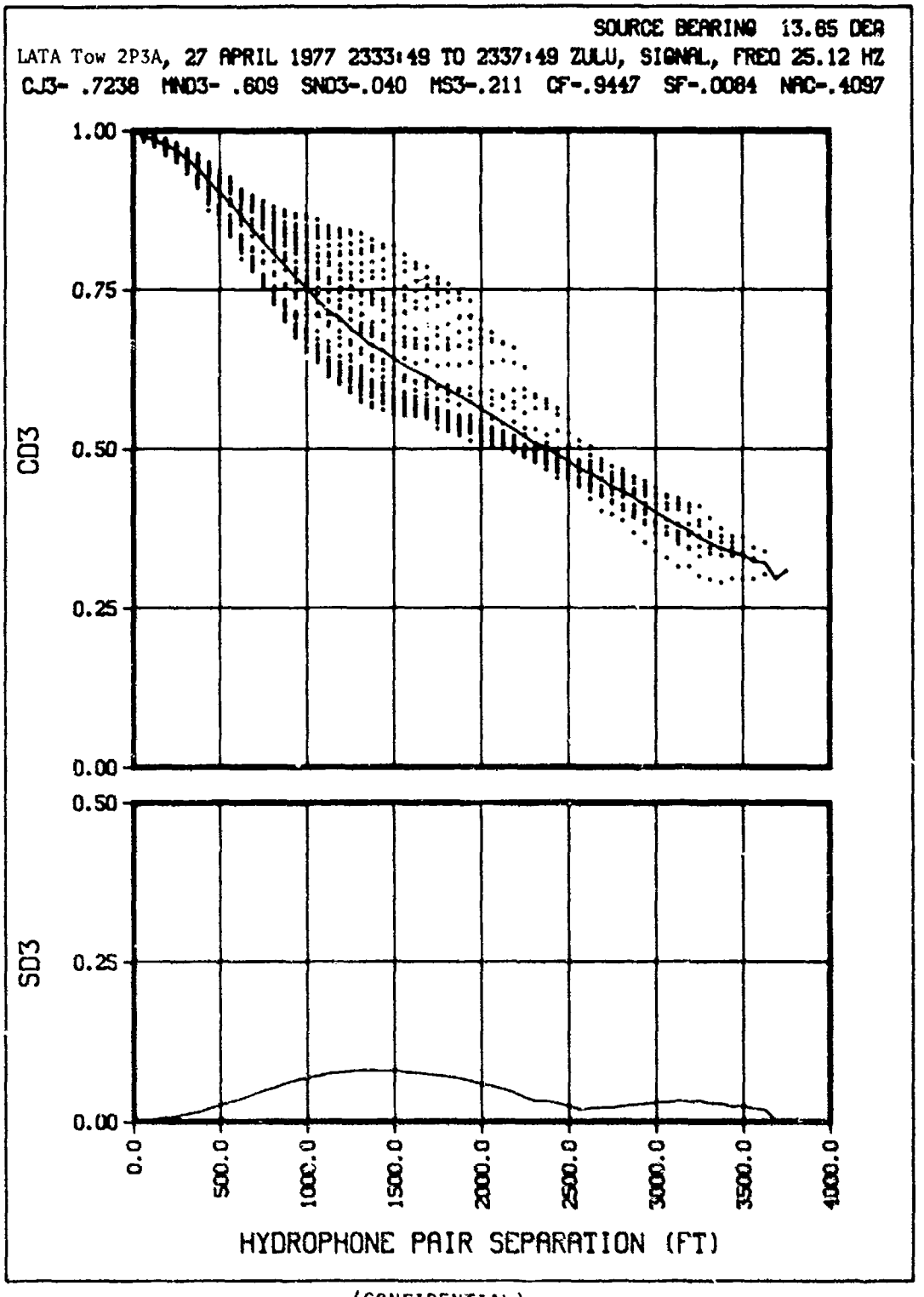

(CONFIDENTIAL)

(U) Figure 12c. Classical coherence.

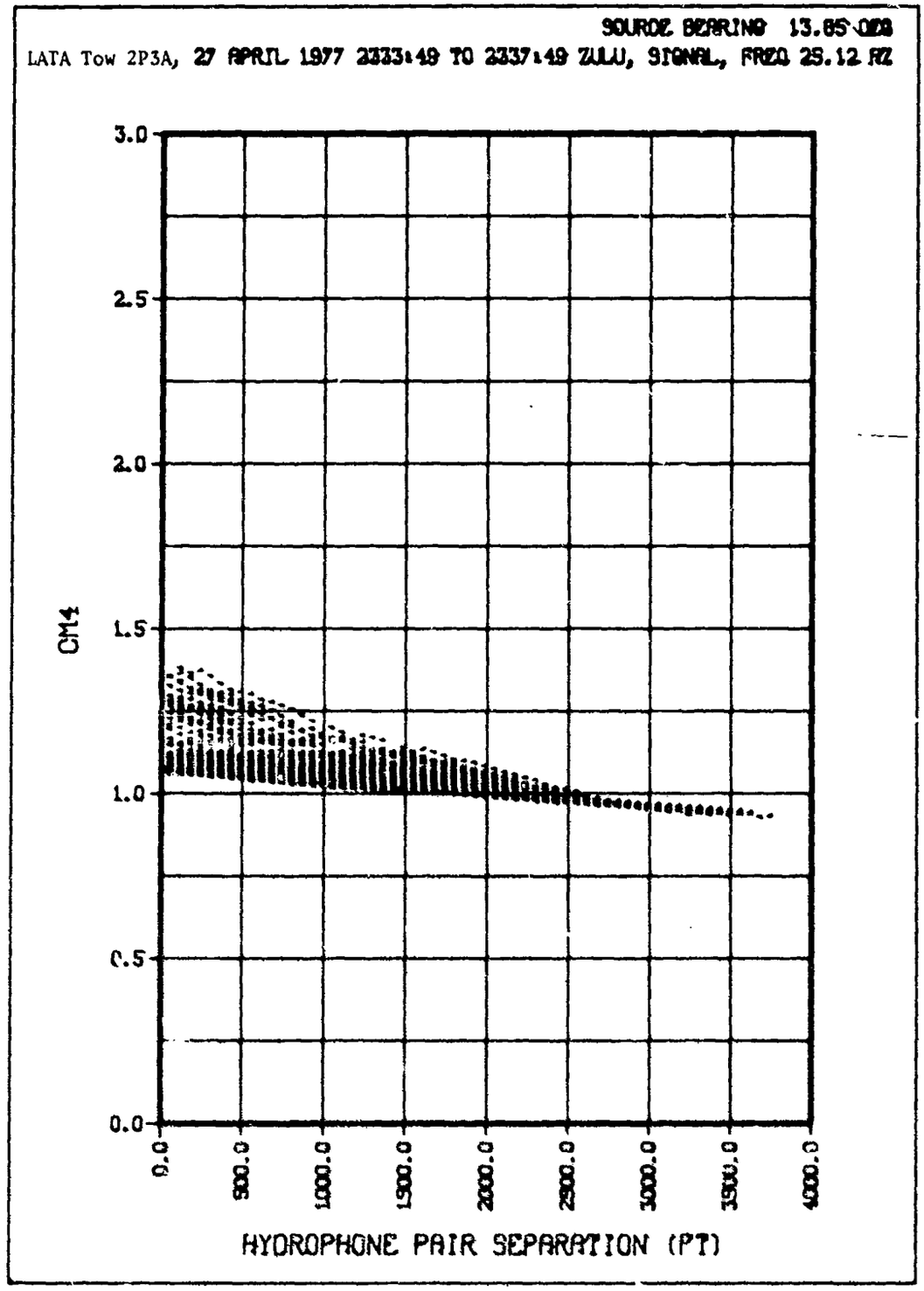

(CONFIDENTIAL)

(U) Figure 12d. Array amplitude covariance.

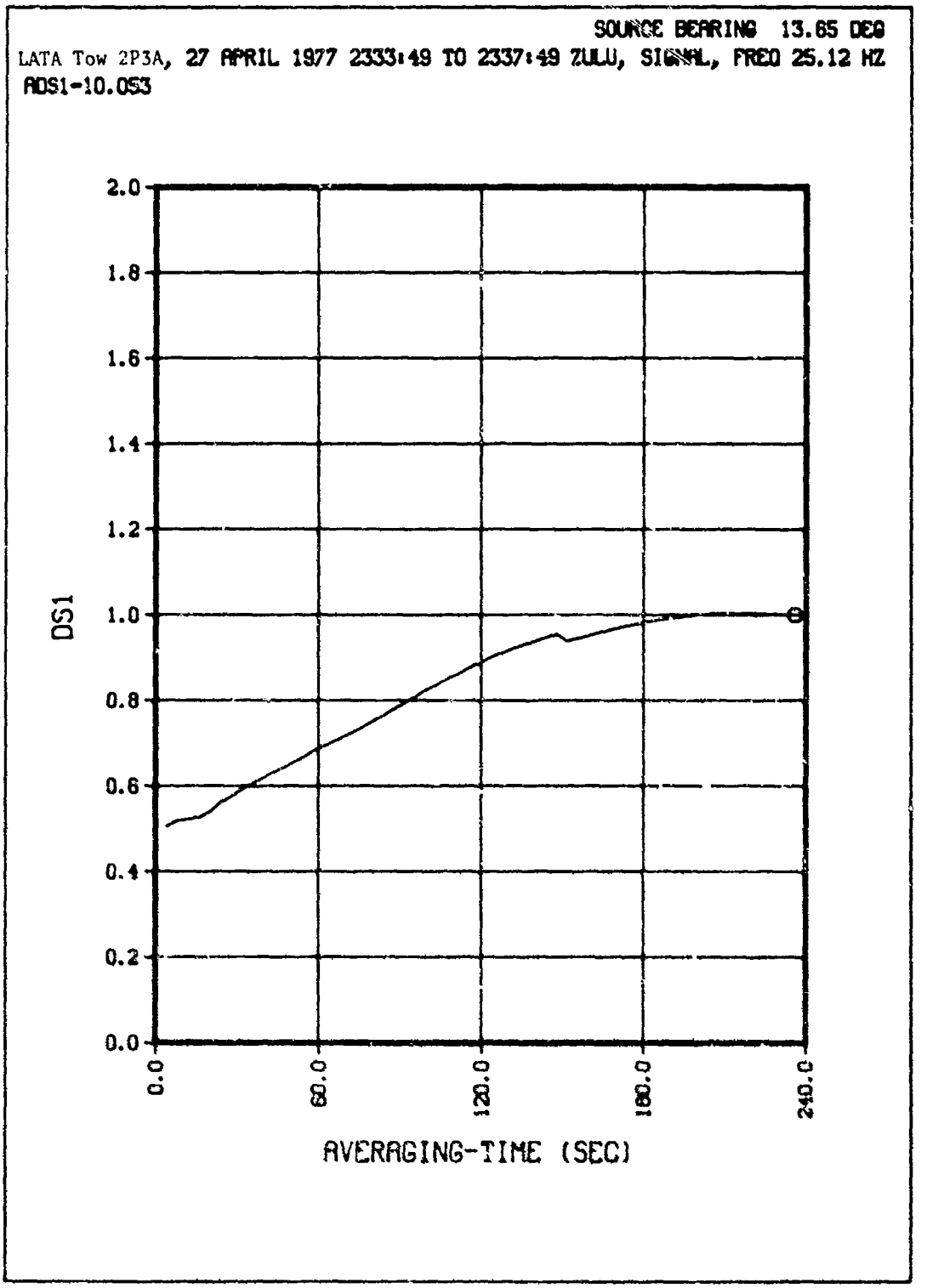

(CONFIDENTIAL)

(U) Figure 12e. Amplitude time stability.

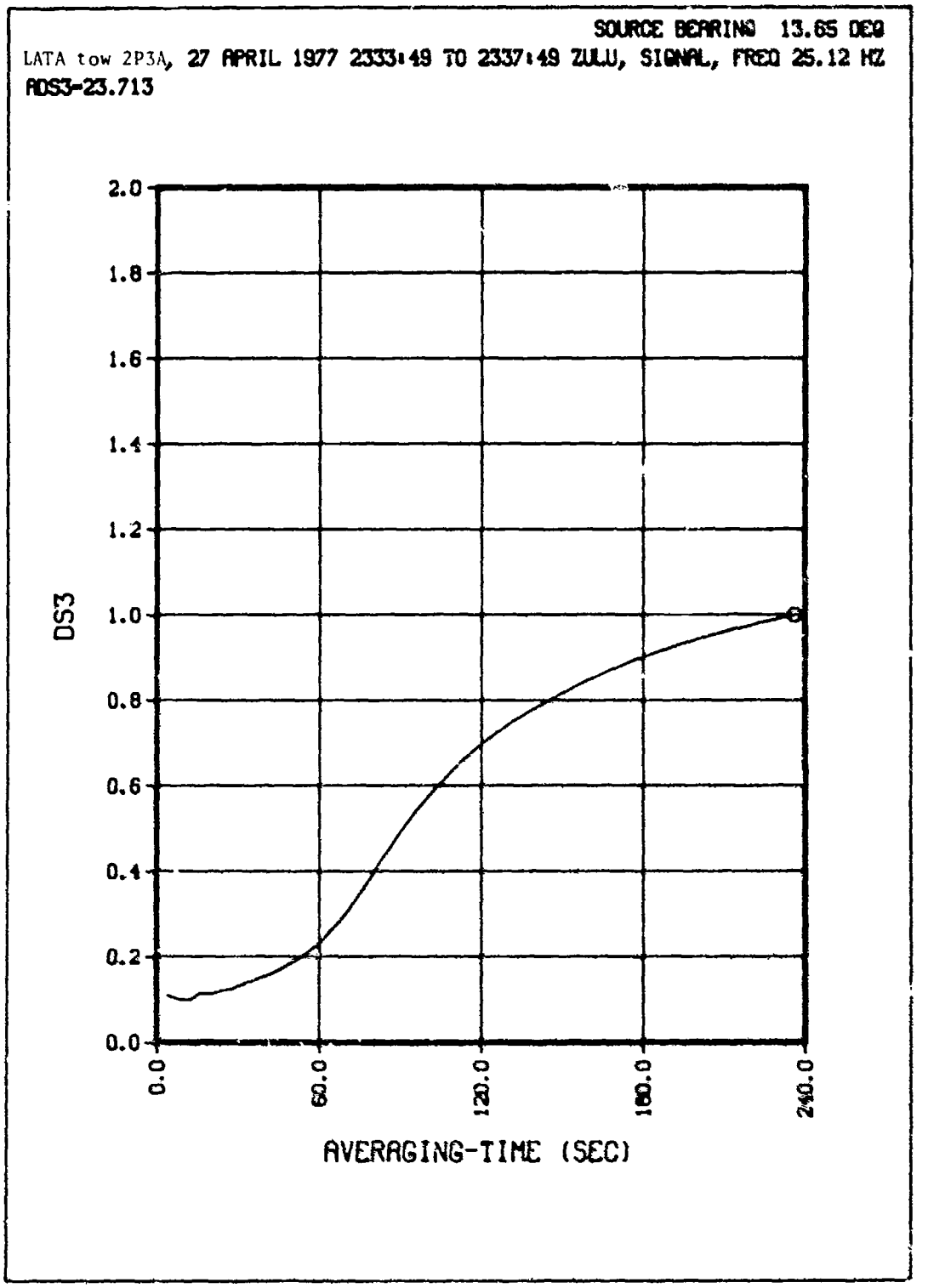

(CONFIDENTIAL)

(U) Figure 12f. Phase time stability.

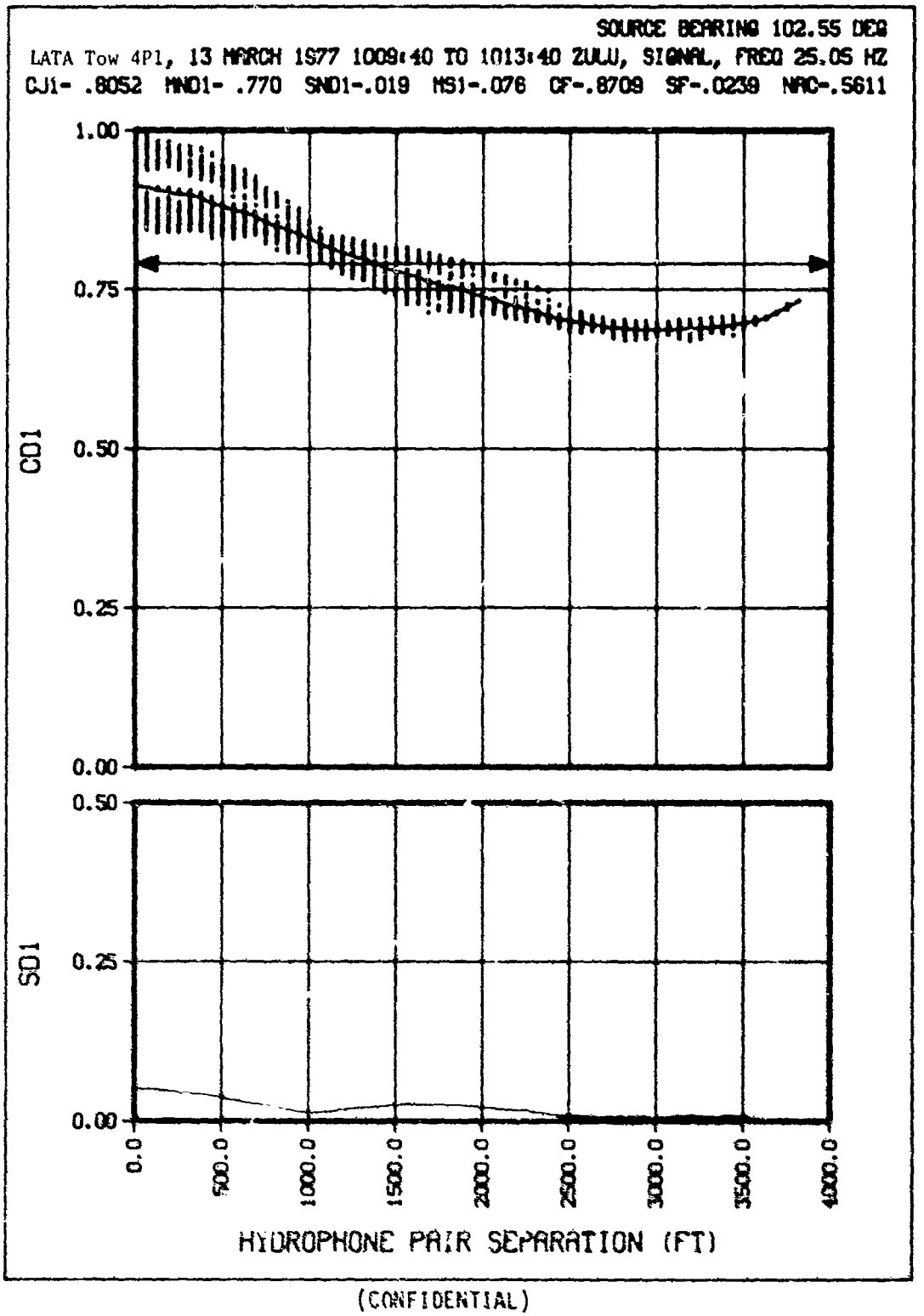

(CONFIDENTIAL)

(U) Figure 13a. Normalized amplitude covariance.

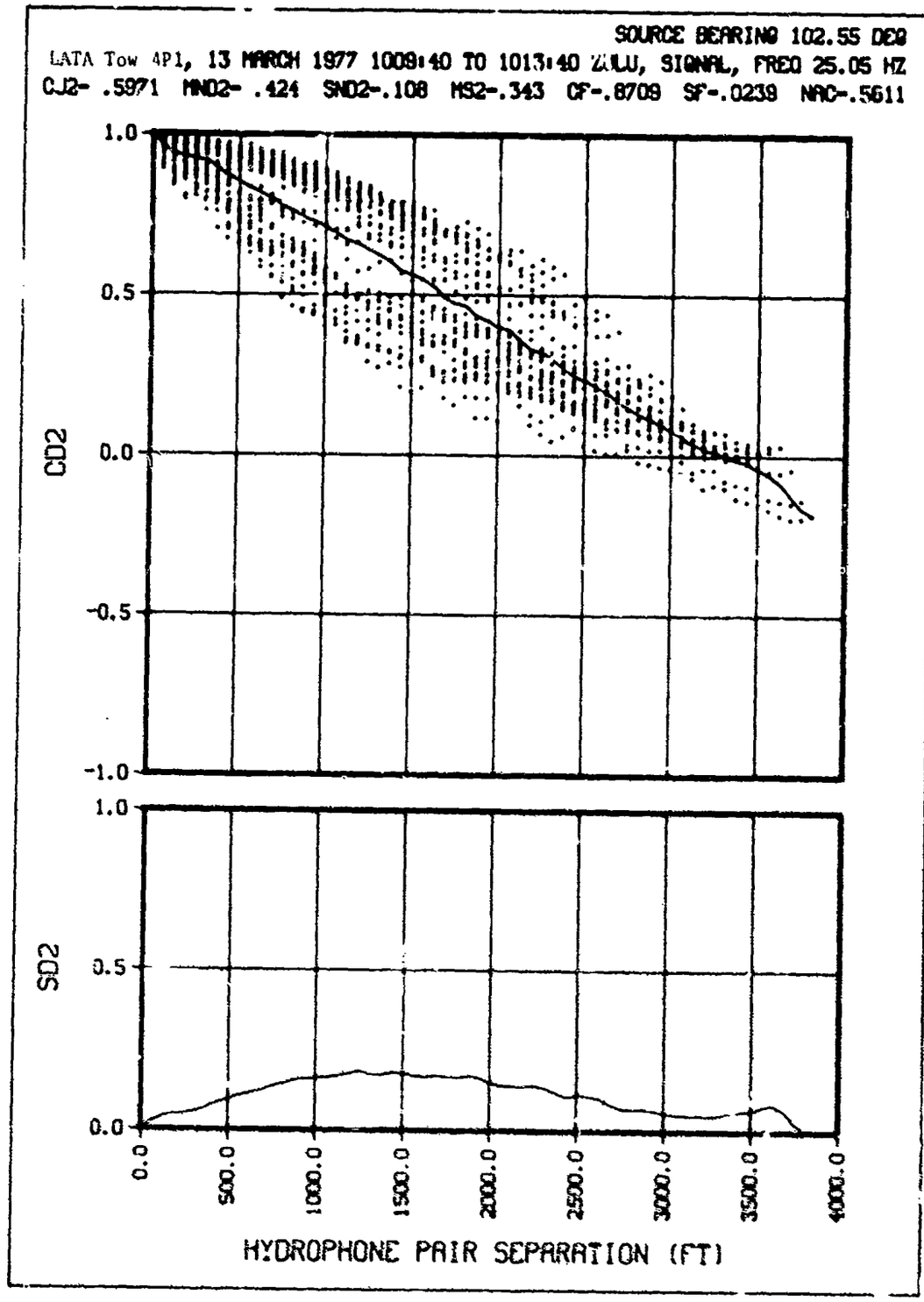

(CONFIDENTIAL)

(U) Figure 13b. Array phase coherence.

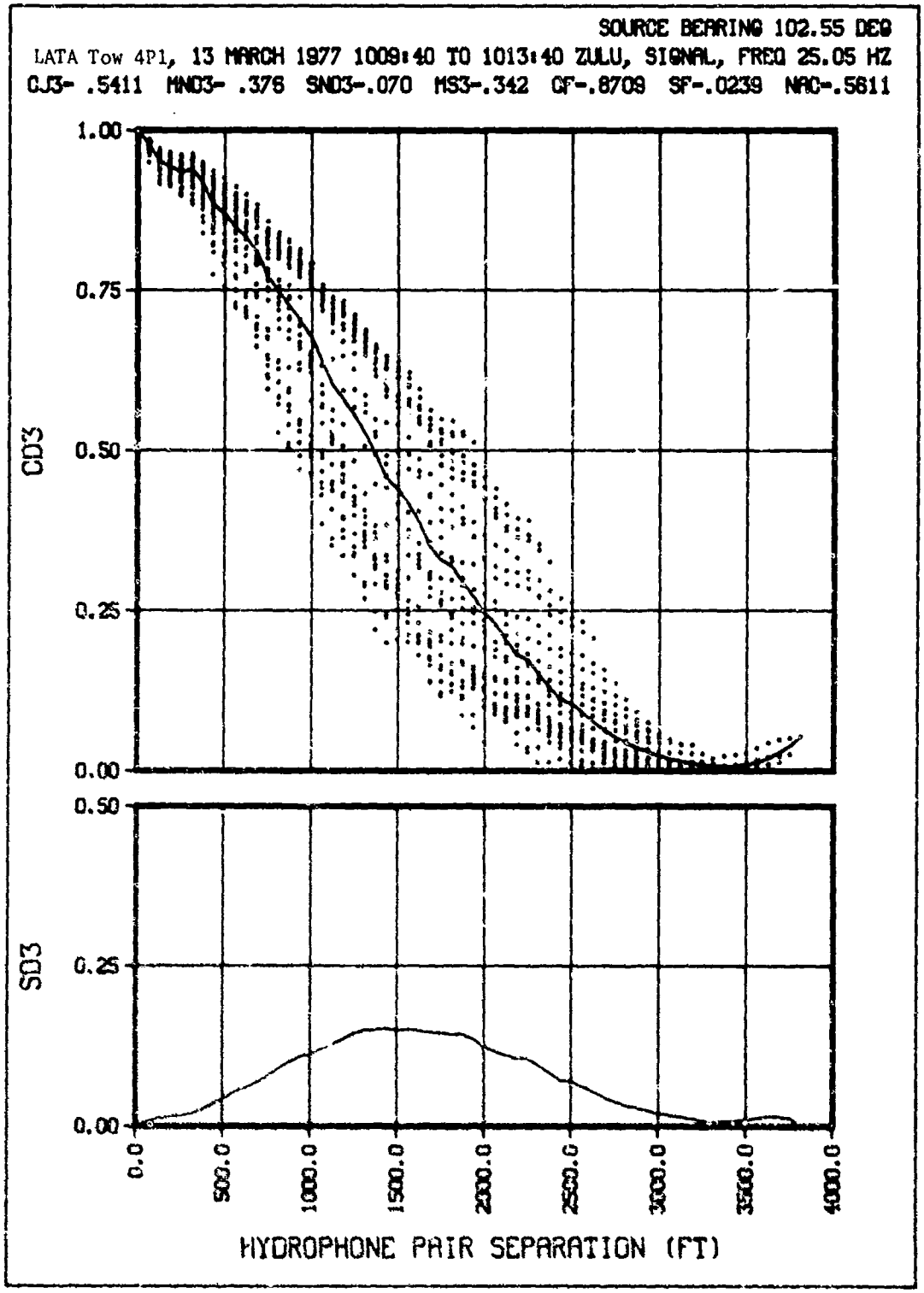

(CONFIDENTIAL)

(U) Figure 13c. Classical coherence.

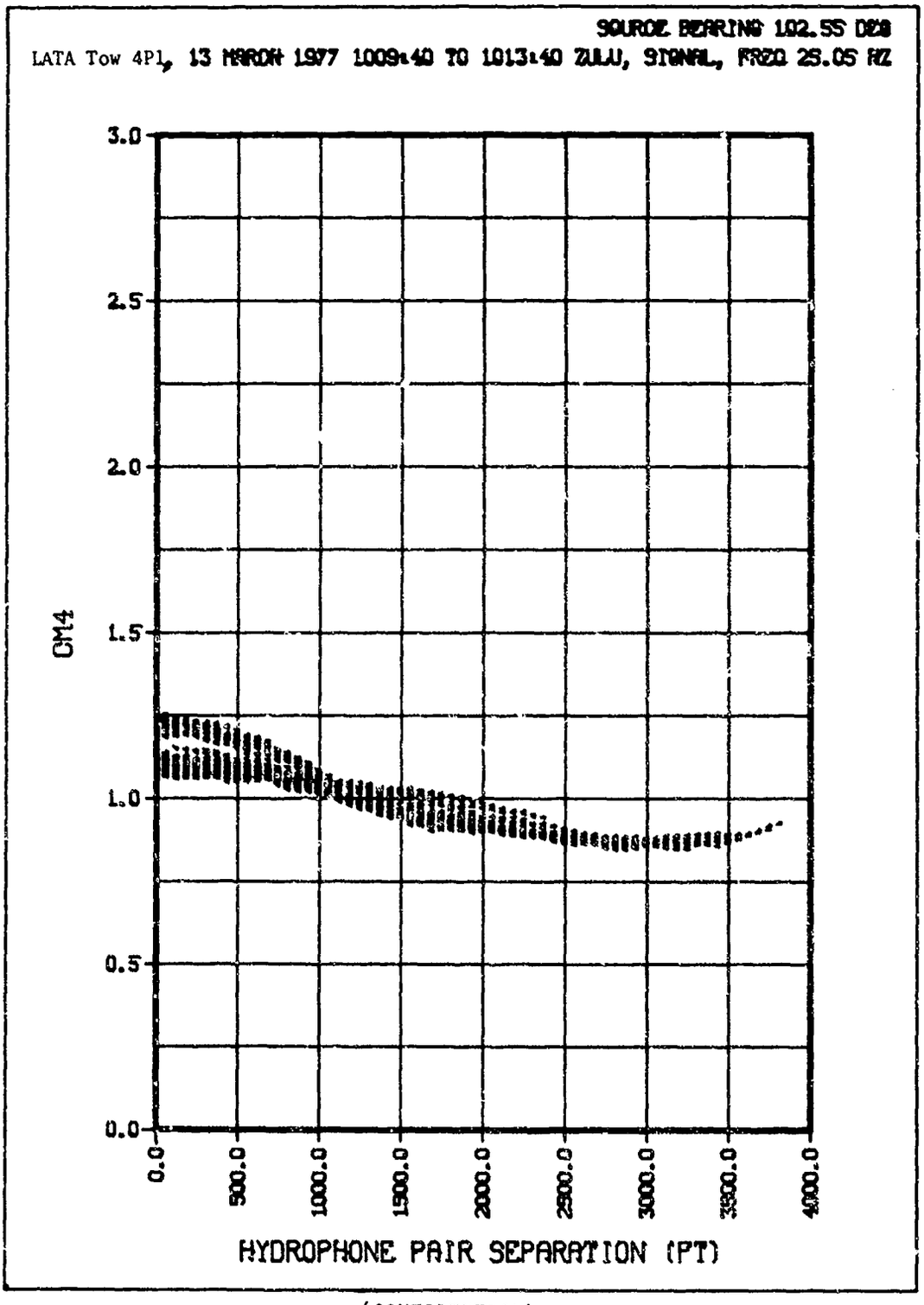

(CONFIDENTIAL)

(U) Figure 13d. Array amplitude covariance.

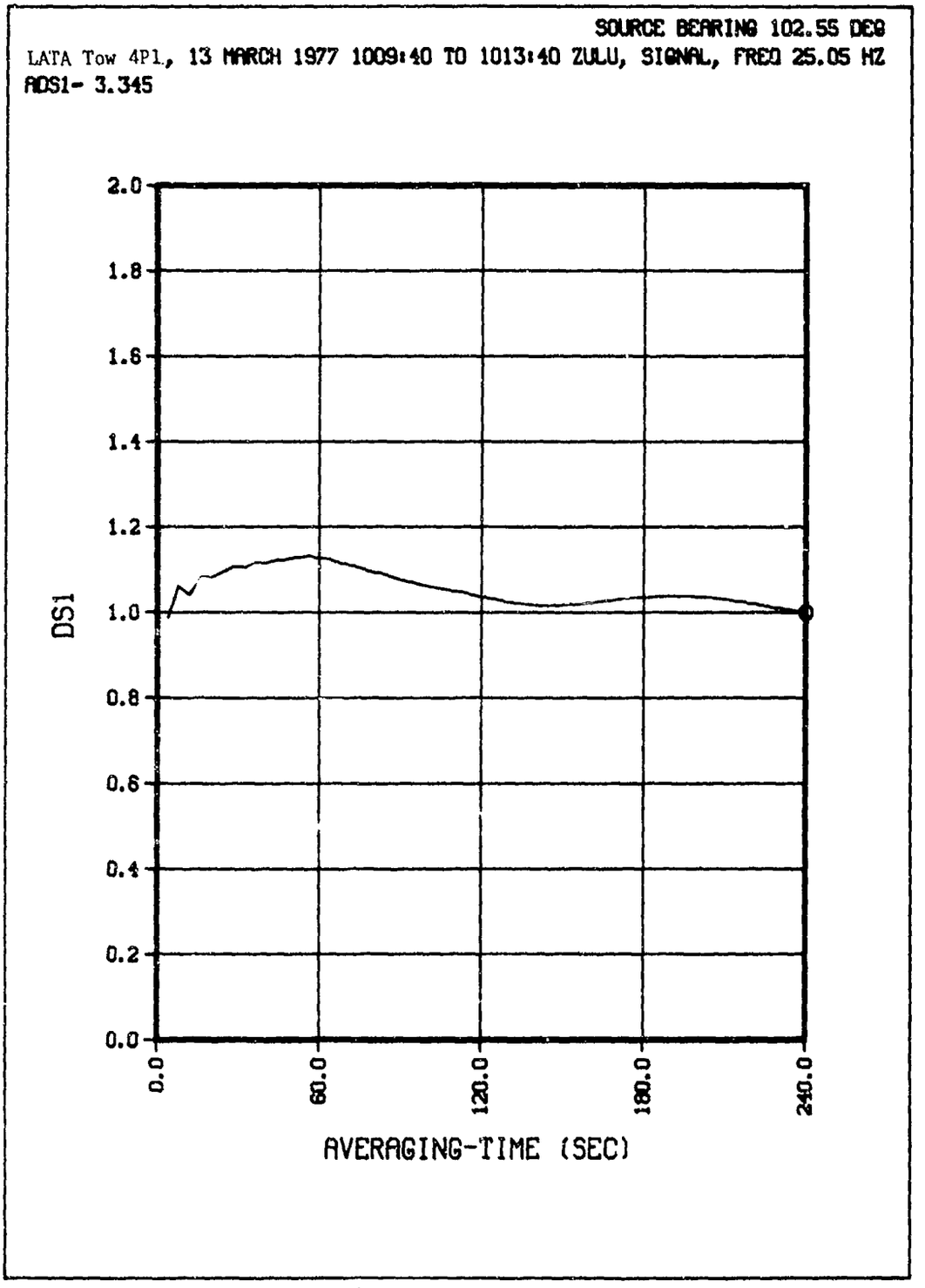

(CONFIDENTIAL)

(U) Figure 13e. Amplitude time stability.

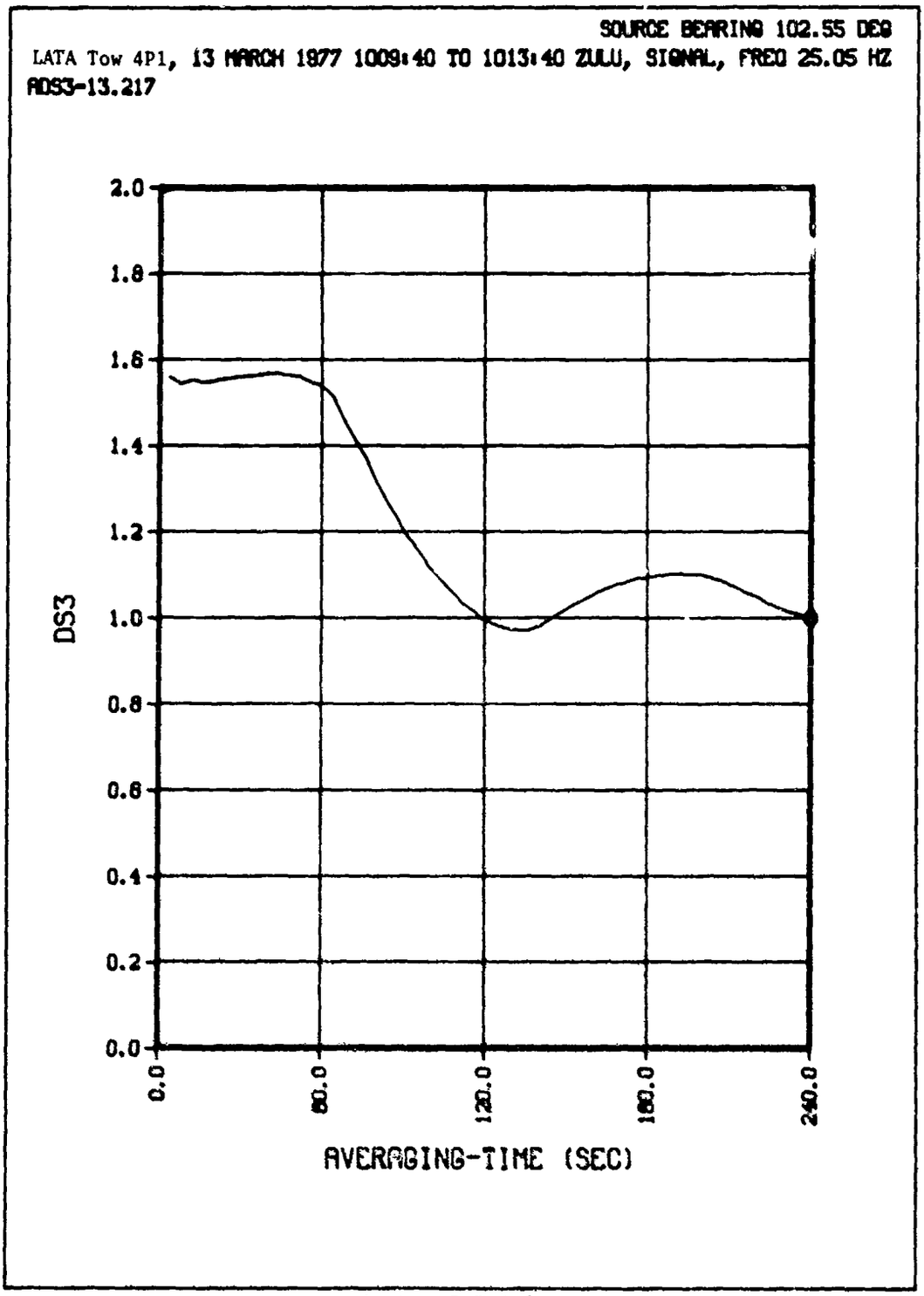

(CONFIDENTIAL)

(U) Figure 13f. Phase time stability.

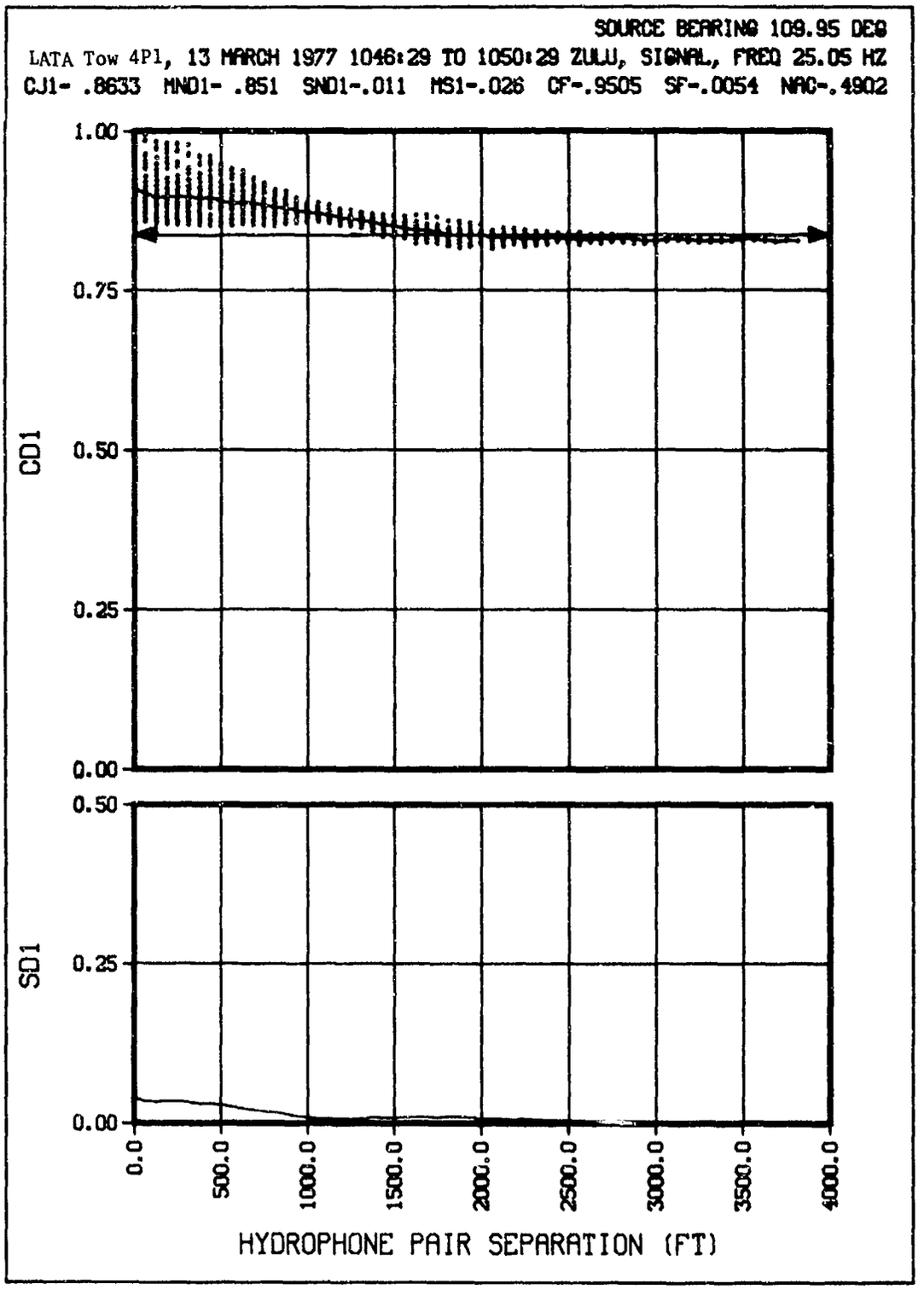

(CONFIDENTIAL)

(U) Figure 14a. Normalized amplitude covariance.

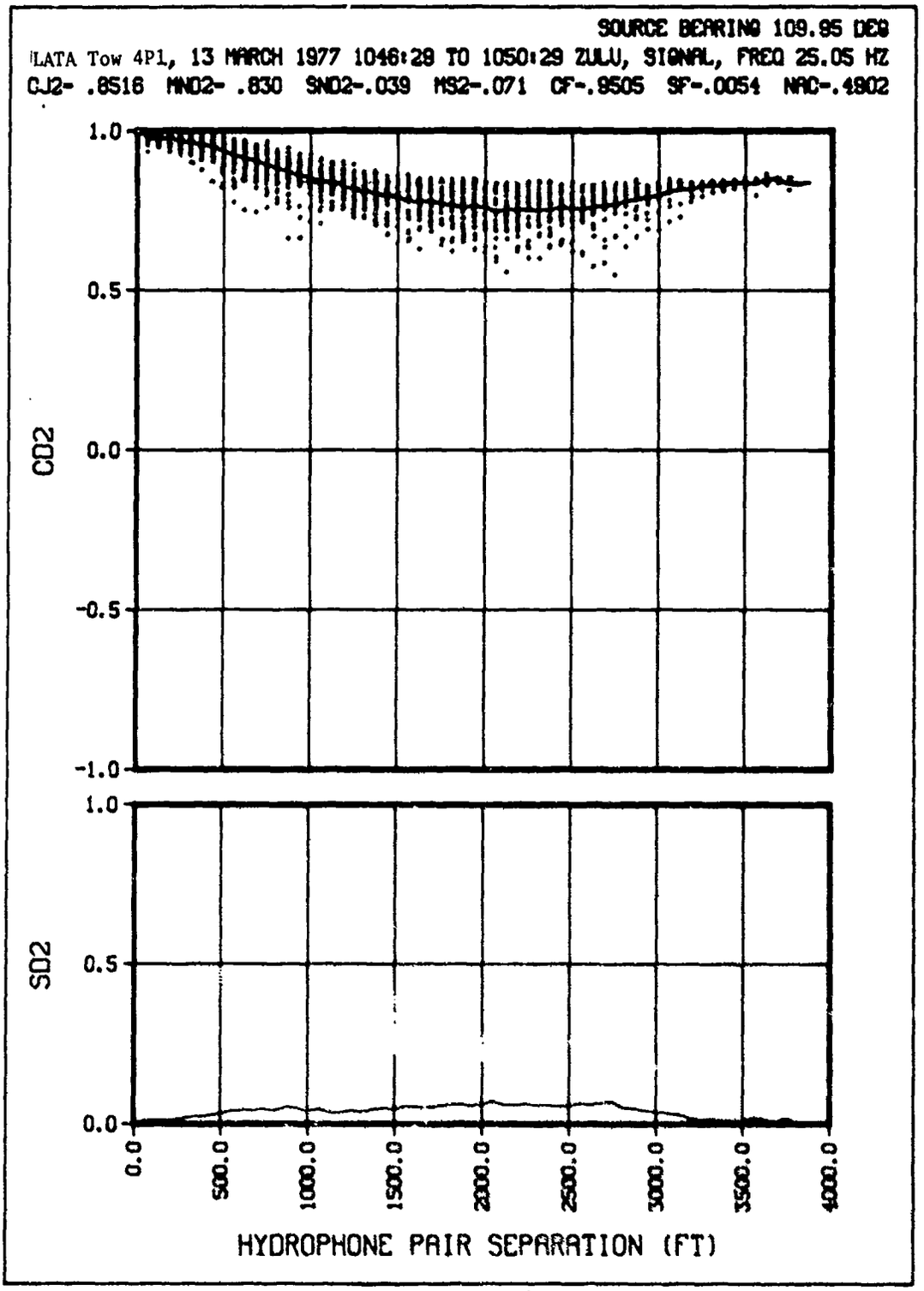

(CONFIDENTIAL)

(U) Figure 14b. Array phase coherence.

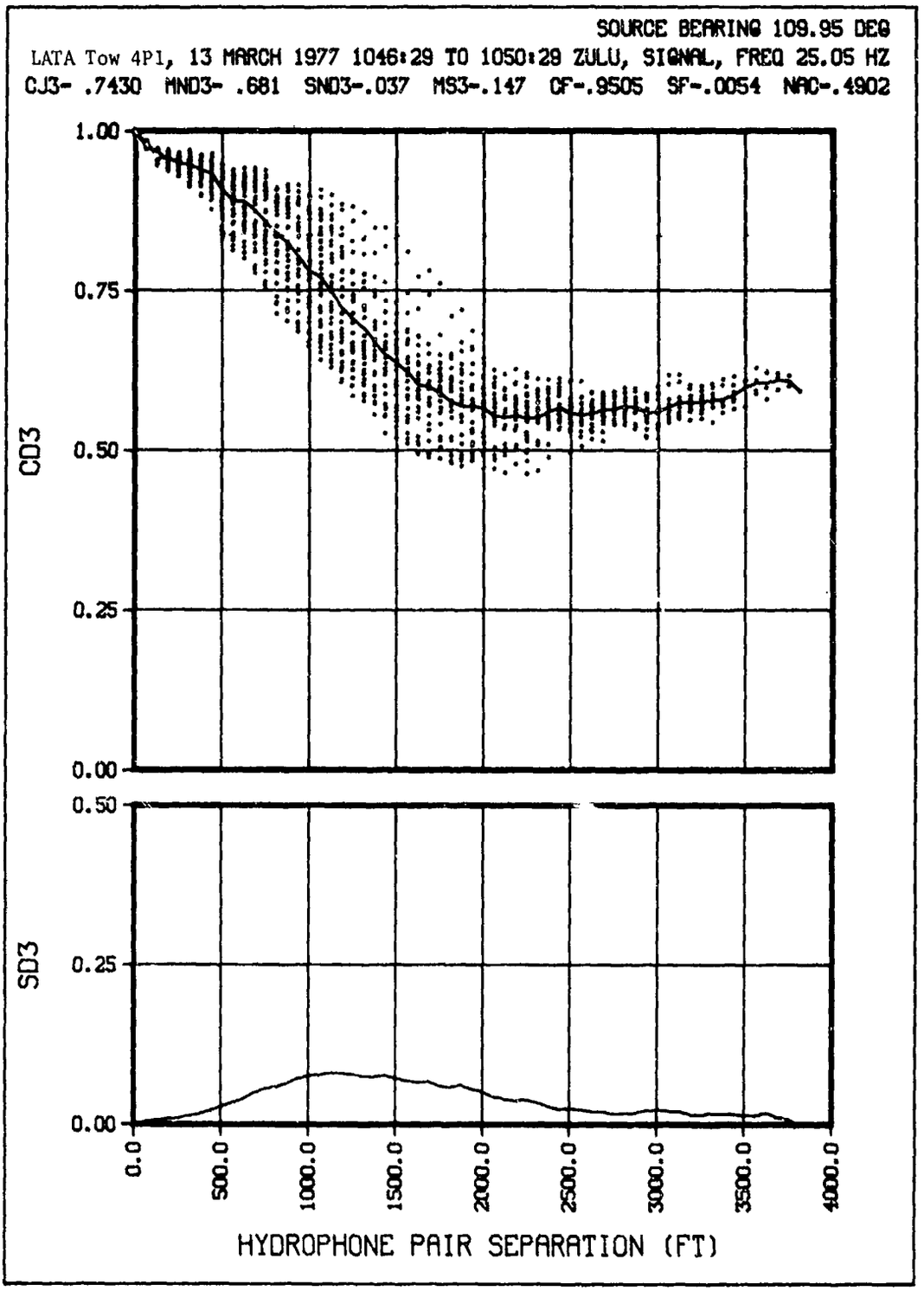

(CONFIDENTIAL)

(U) Figure 14c. Classical coherence.

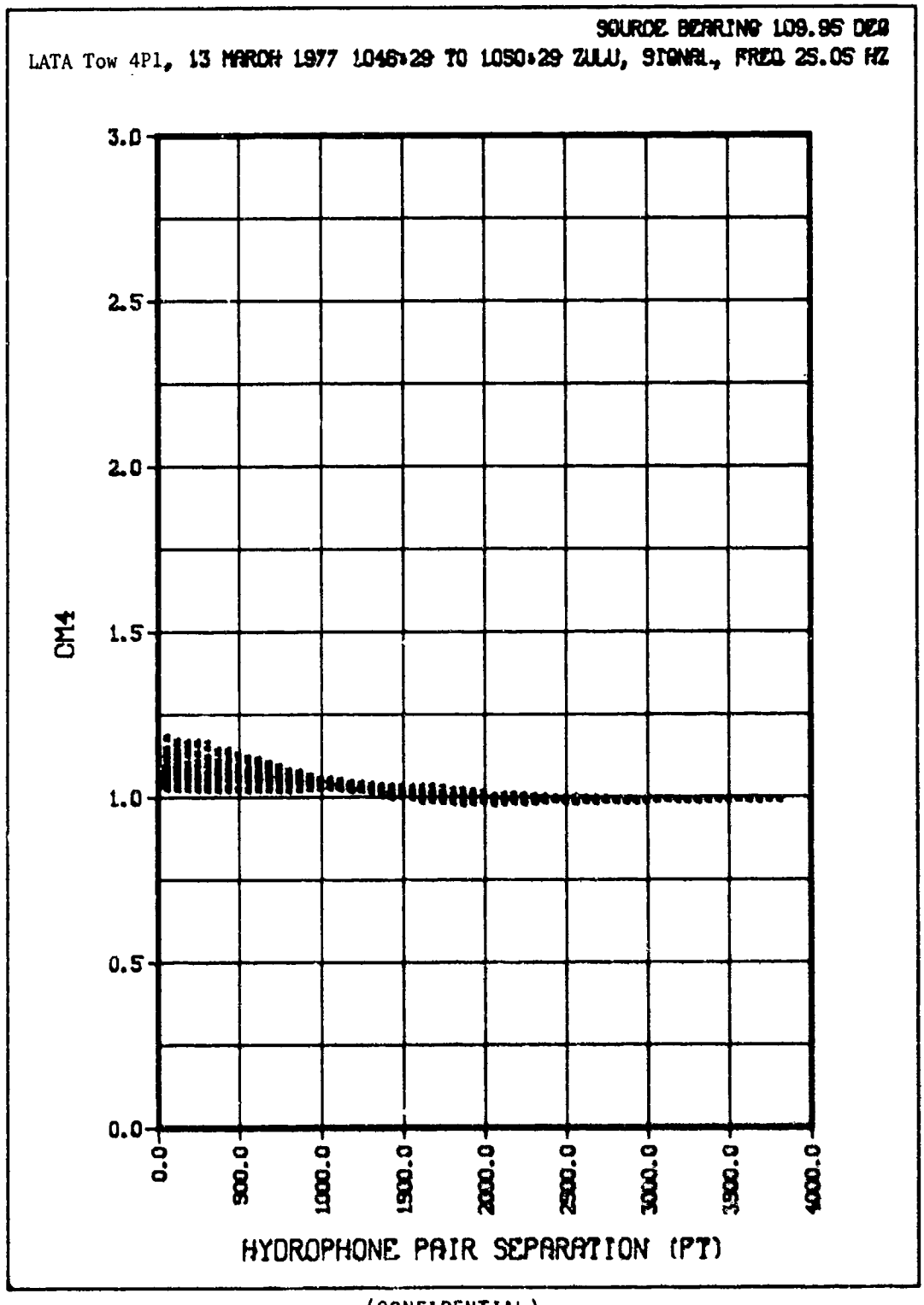

(CONFIDENTIAL)

(U) Figure 14d. Array amplitude covariance.

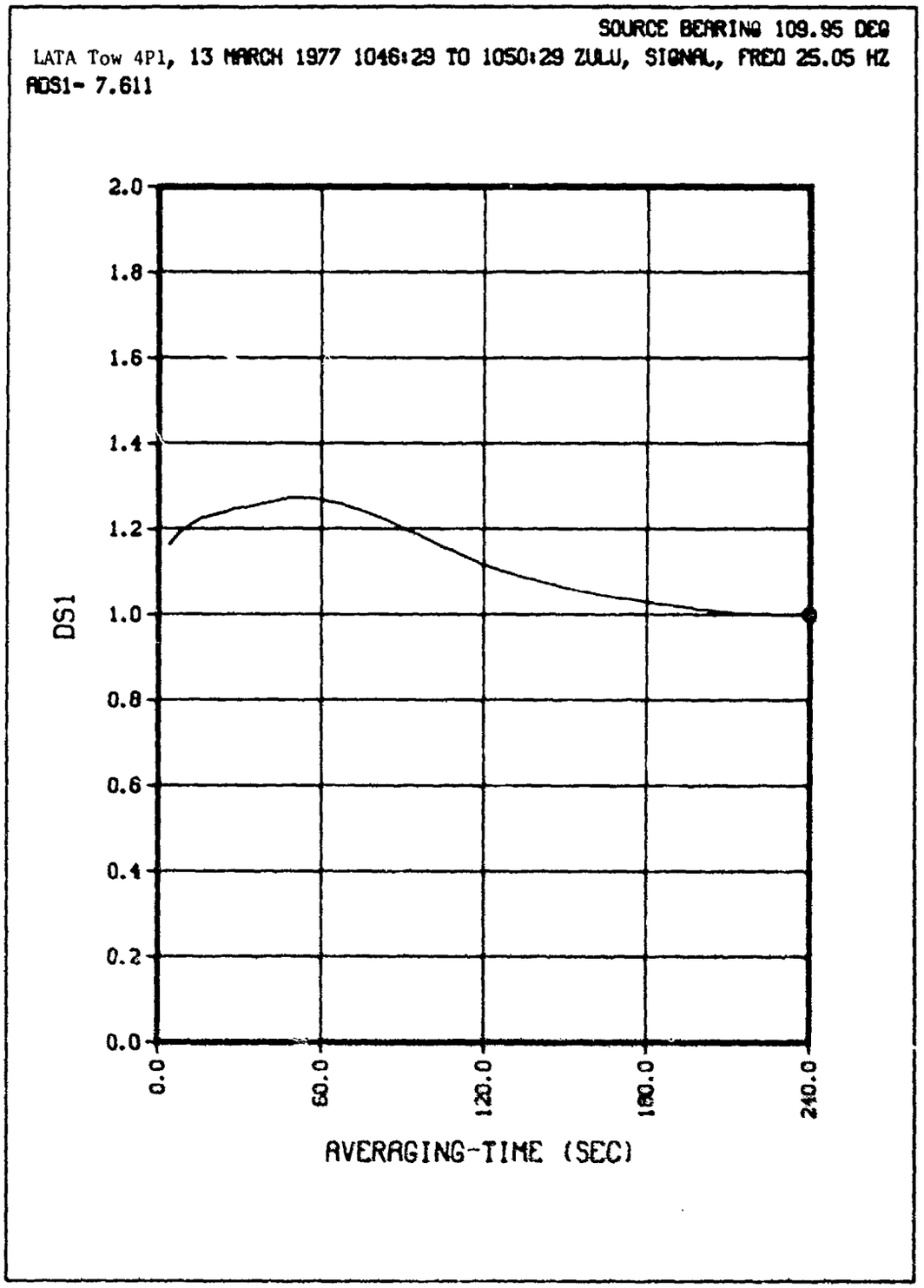

(CONFIDENTIAL)

(U) Figure 14e. Amplitude time stability.

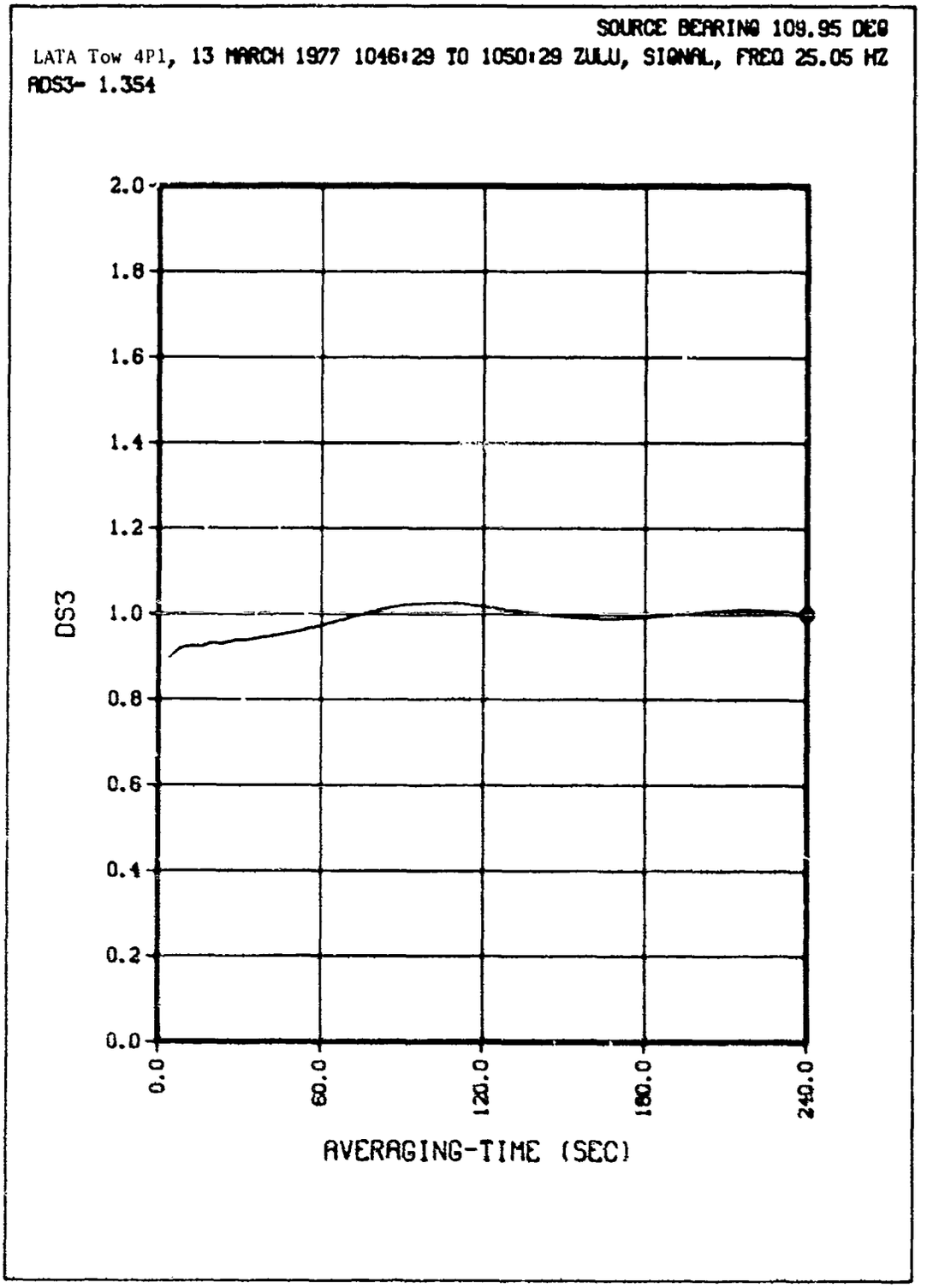

(CONFIDENTIAL)

(U) Figure 14f. Phase time stability.

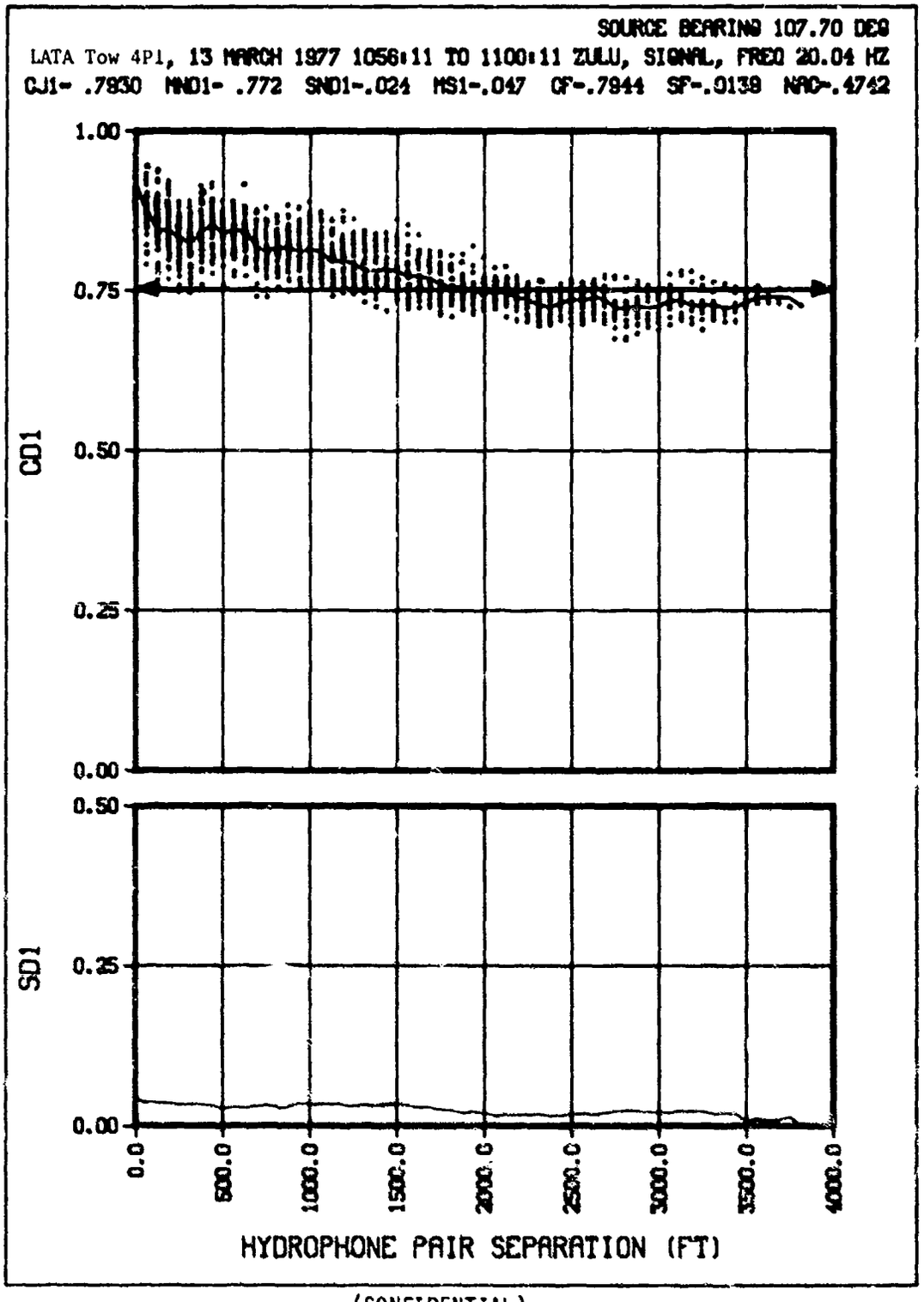

(CONFIDENTIAL)

(U) Figure 15a. Normalized amplitude covariance.

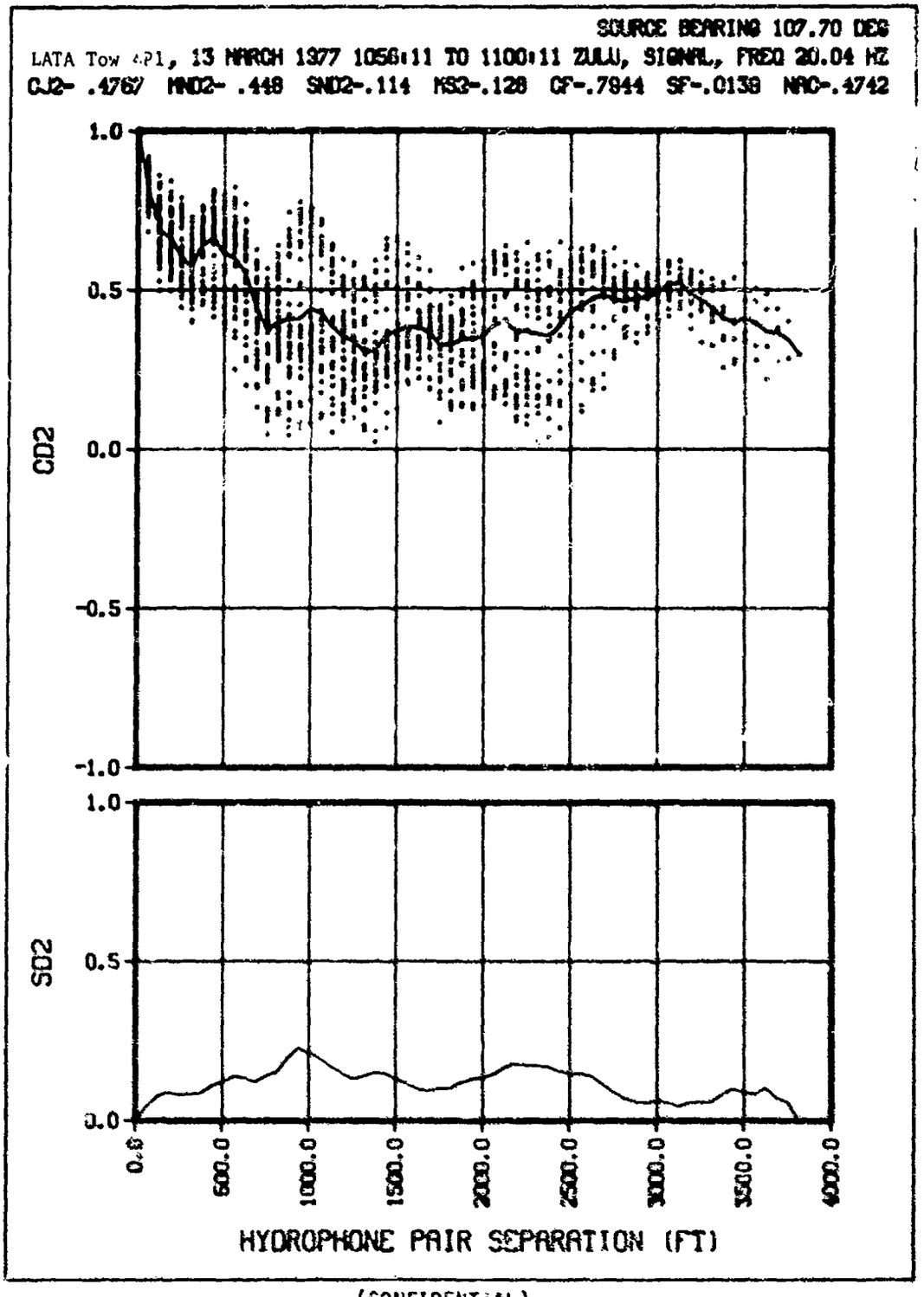

(CONFIDENTIAL)

(U) Figure 15b. Array phase coherence.

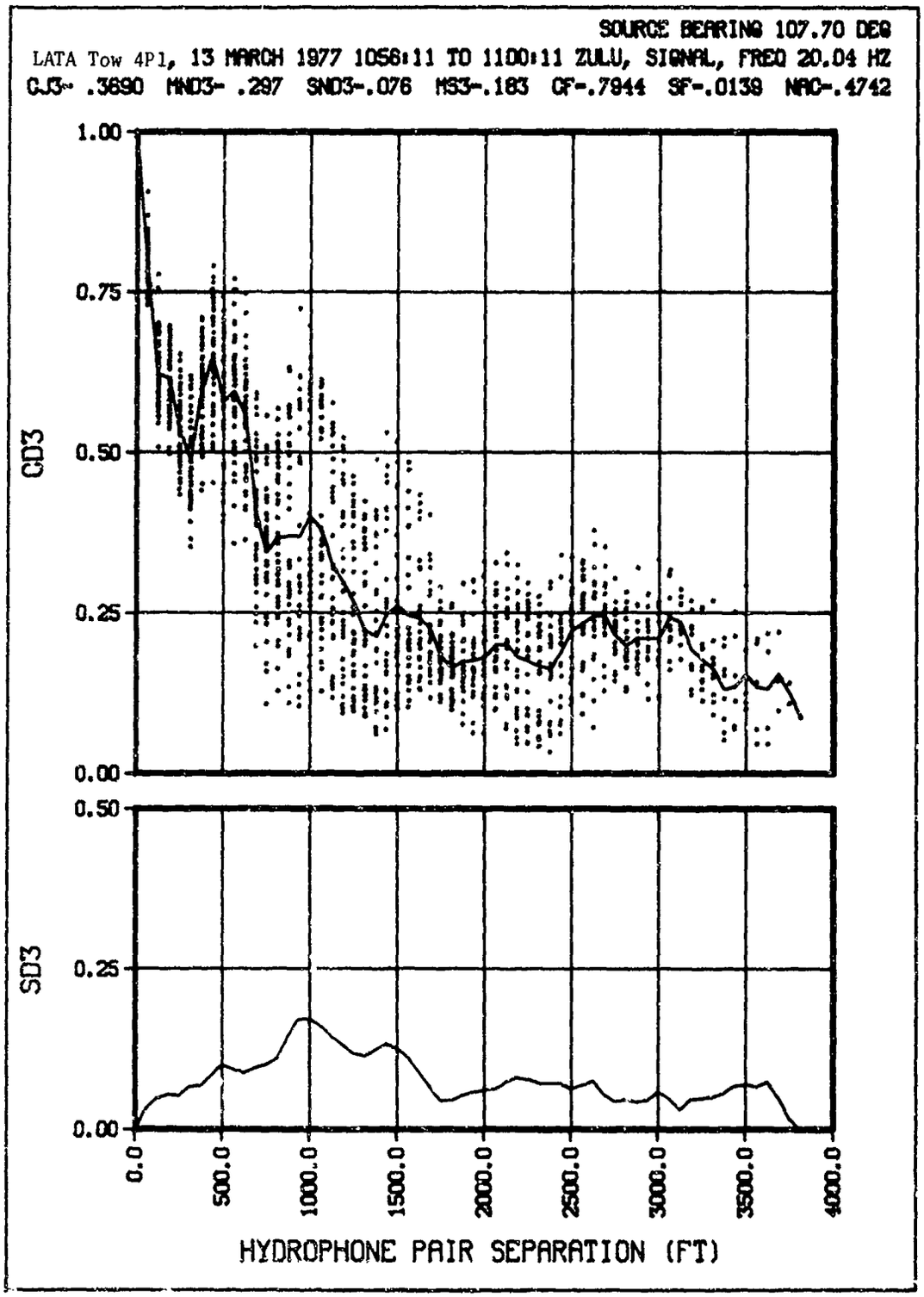

(CONFIDENTIAL)

(U) Figure 15c. Classical coherence.

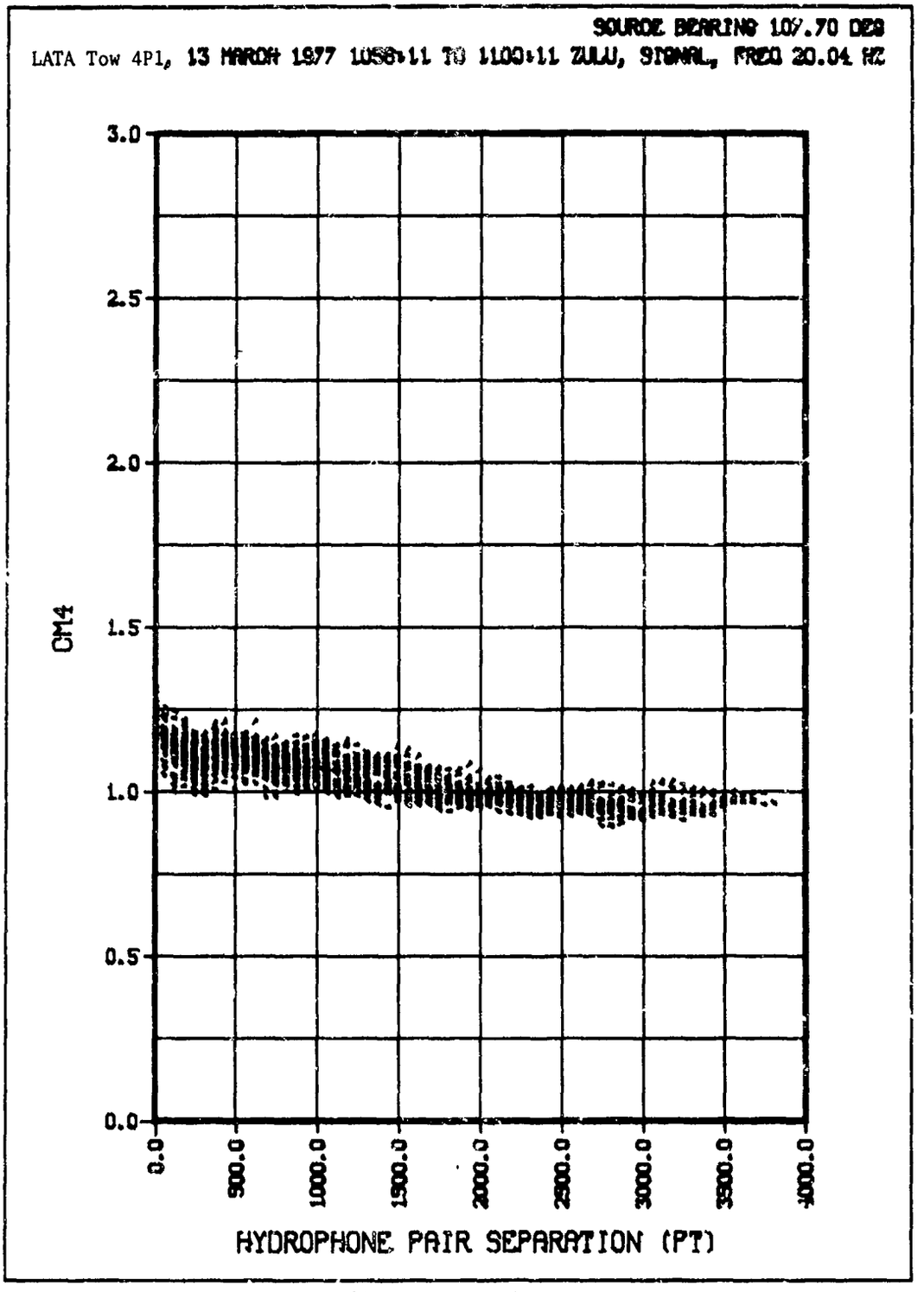

(CONFIDENTIAL)

(U) Figure 15d. Array amplitude covariance.

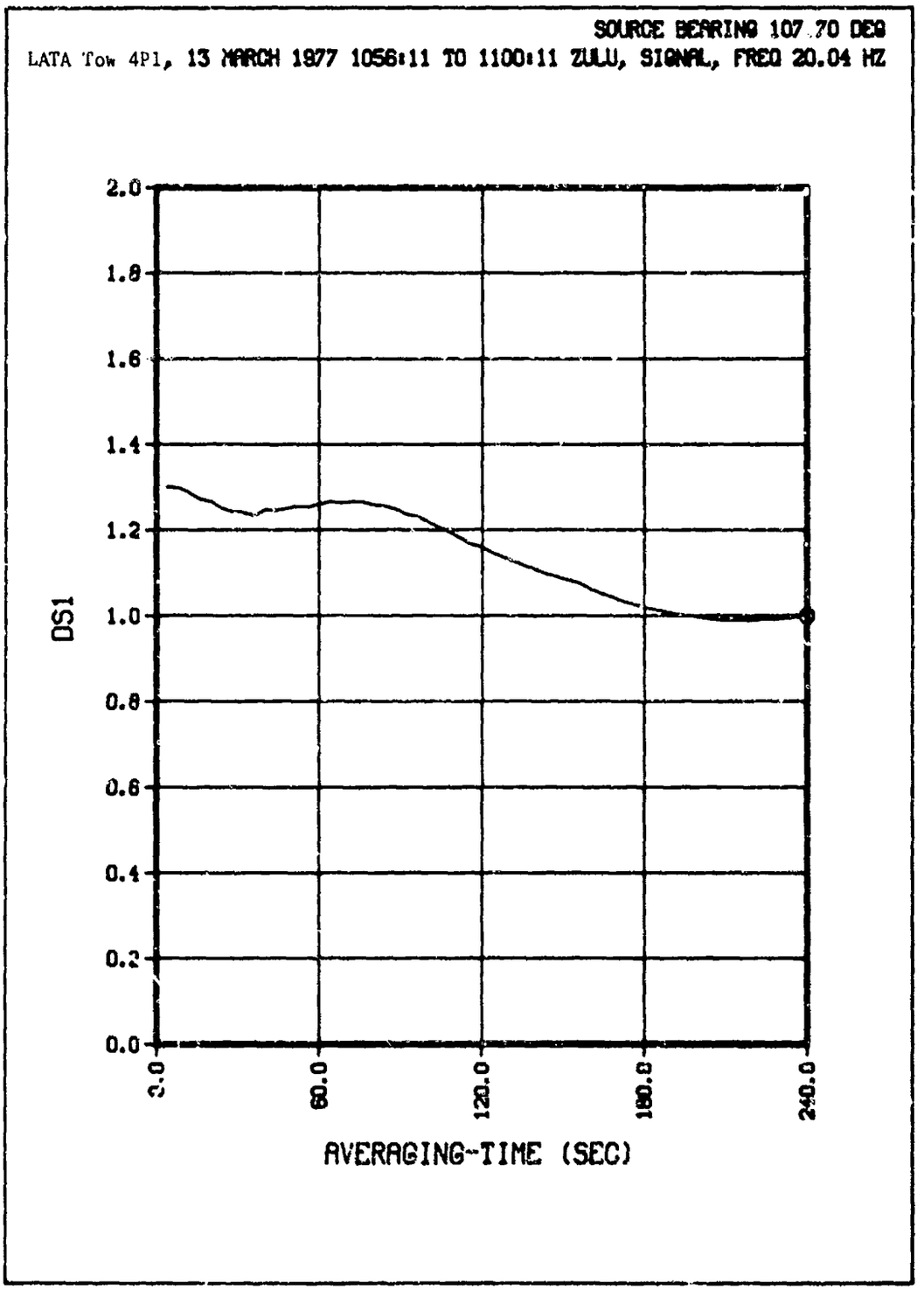

(CONFIDENTIAL)

(U) Figure 15e. Amplitude time stability.

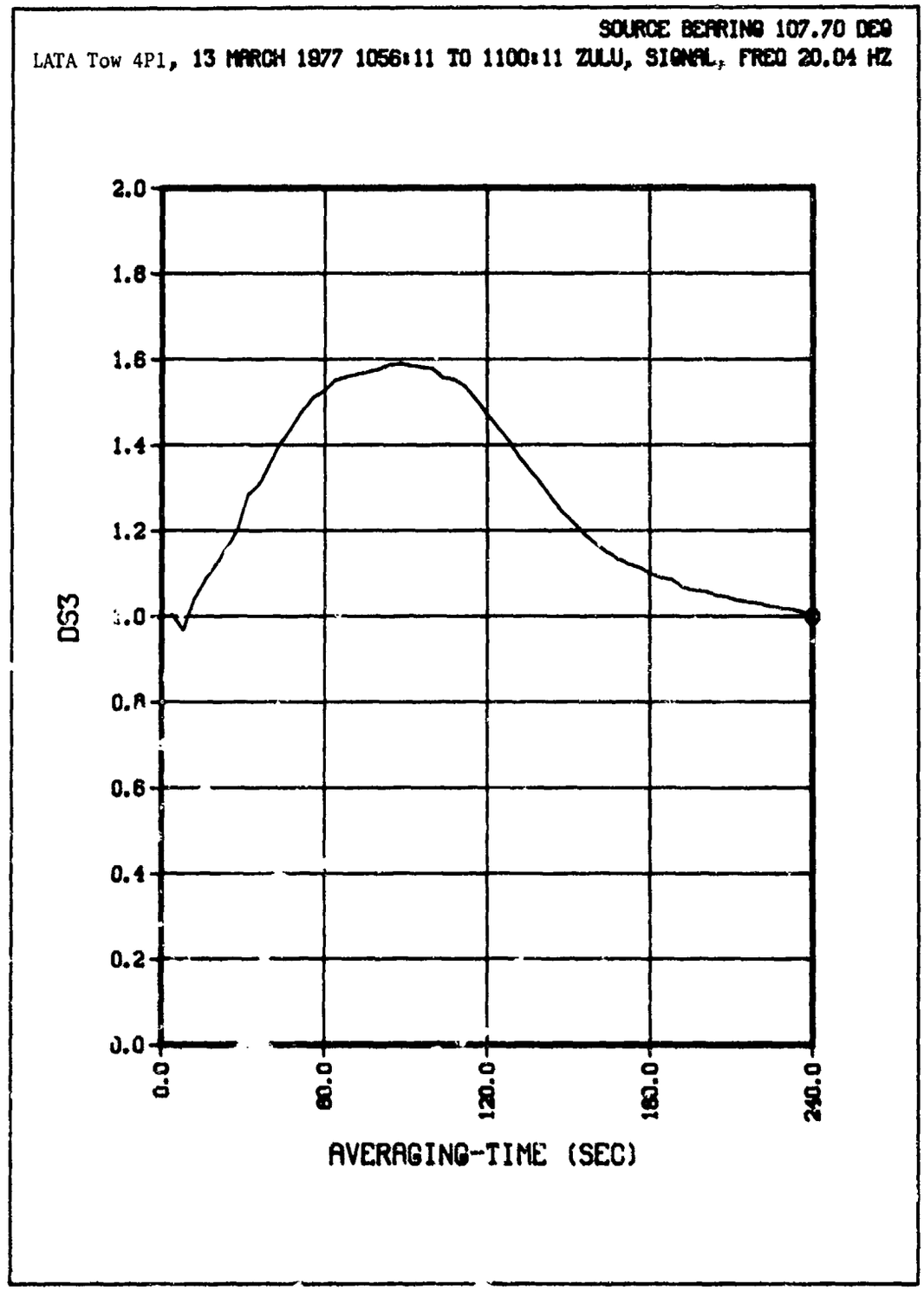

(CONFIDENTIAL)

(U) Figure 15f. Phase time stability.

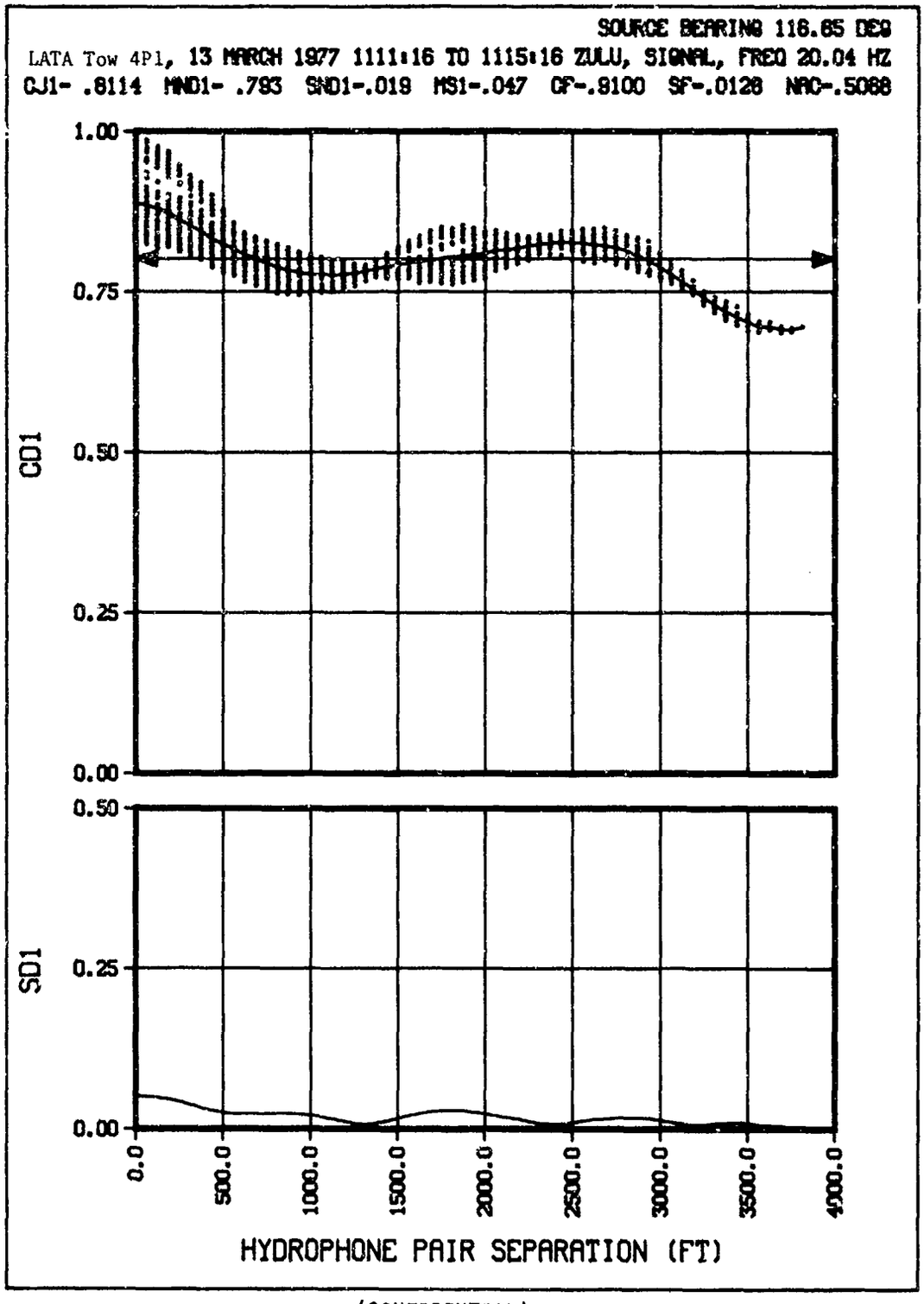

(CONFIDENTIAL)

(U) Figure 16a. Normalized amplitude covariance.

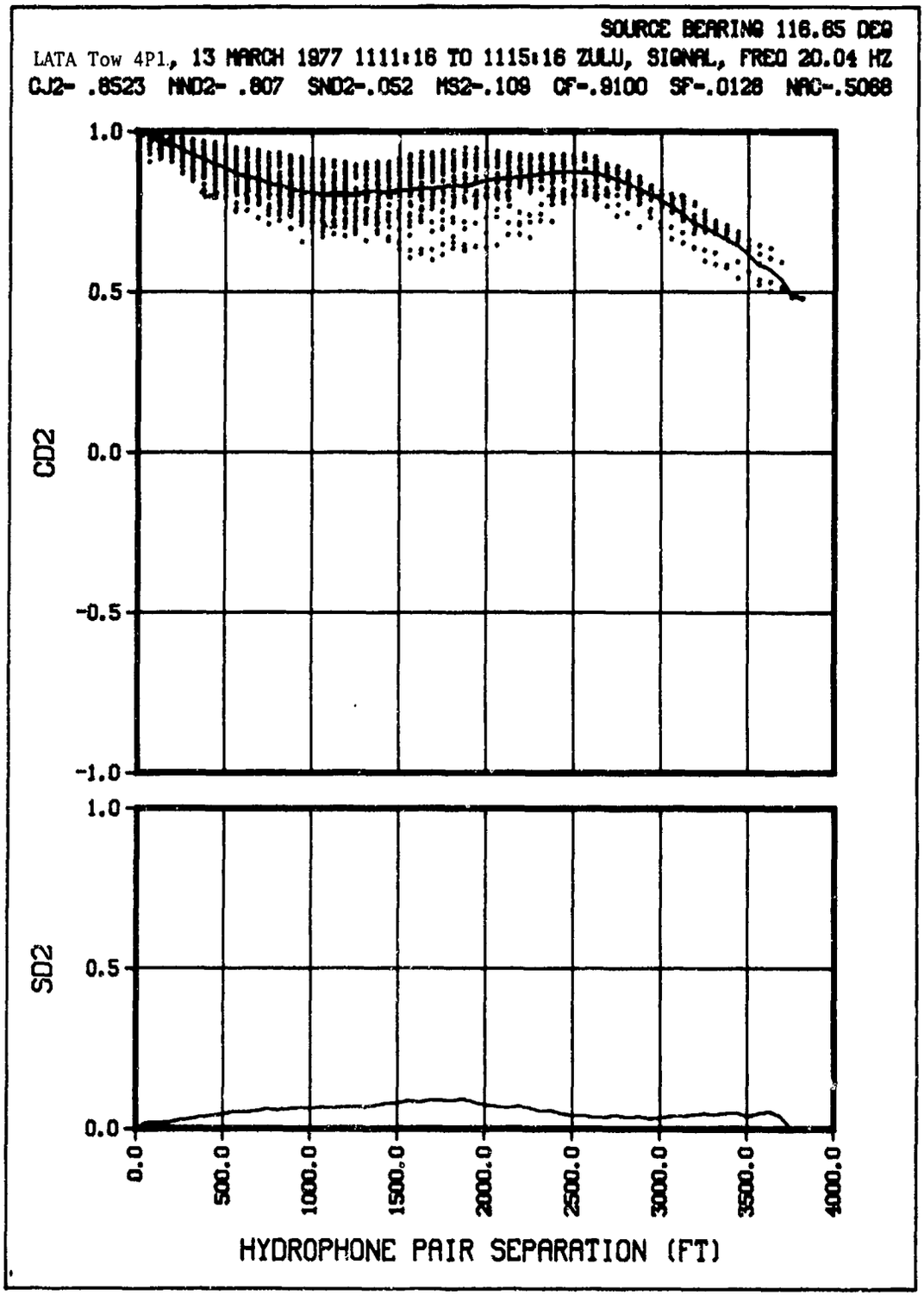

(CONFIDENTIAL)

(U) Figure 16b. Array phase coherence.

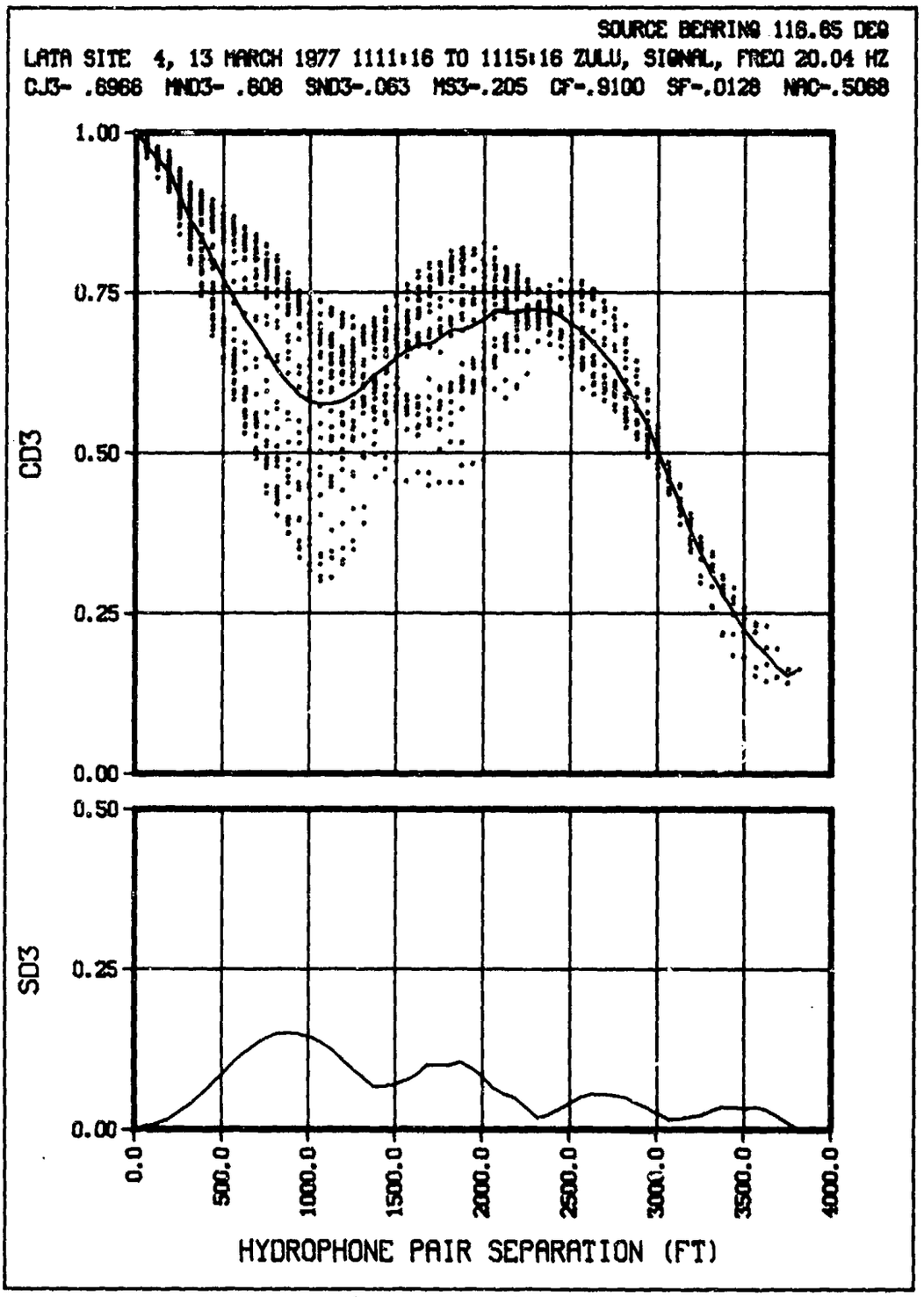

(CONFIDENTIAL)

(U) Figure 16c. Classical coherence.

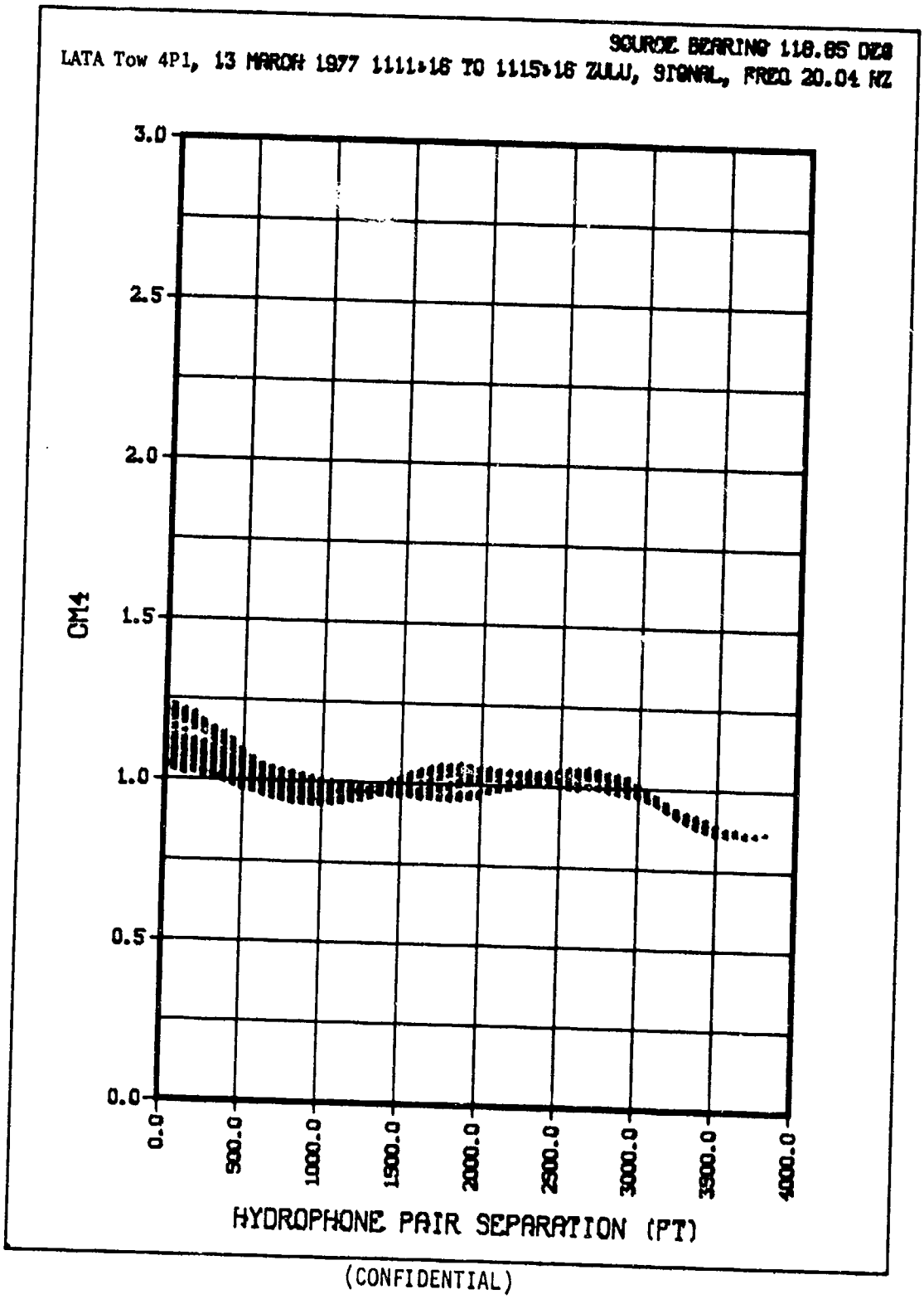

(CONFIDENTIAL)

(U) Figure 16d. Array amplitude covariance.

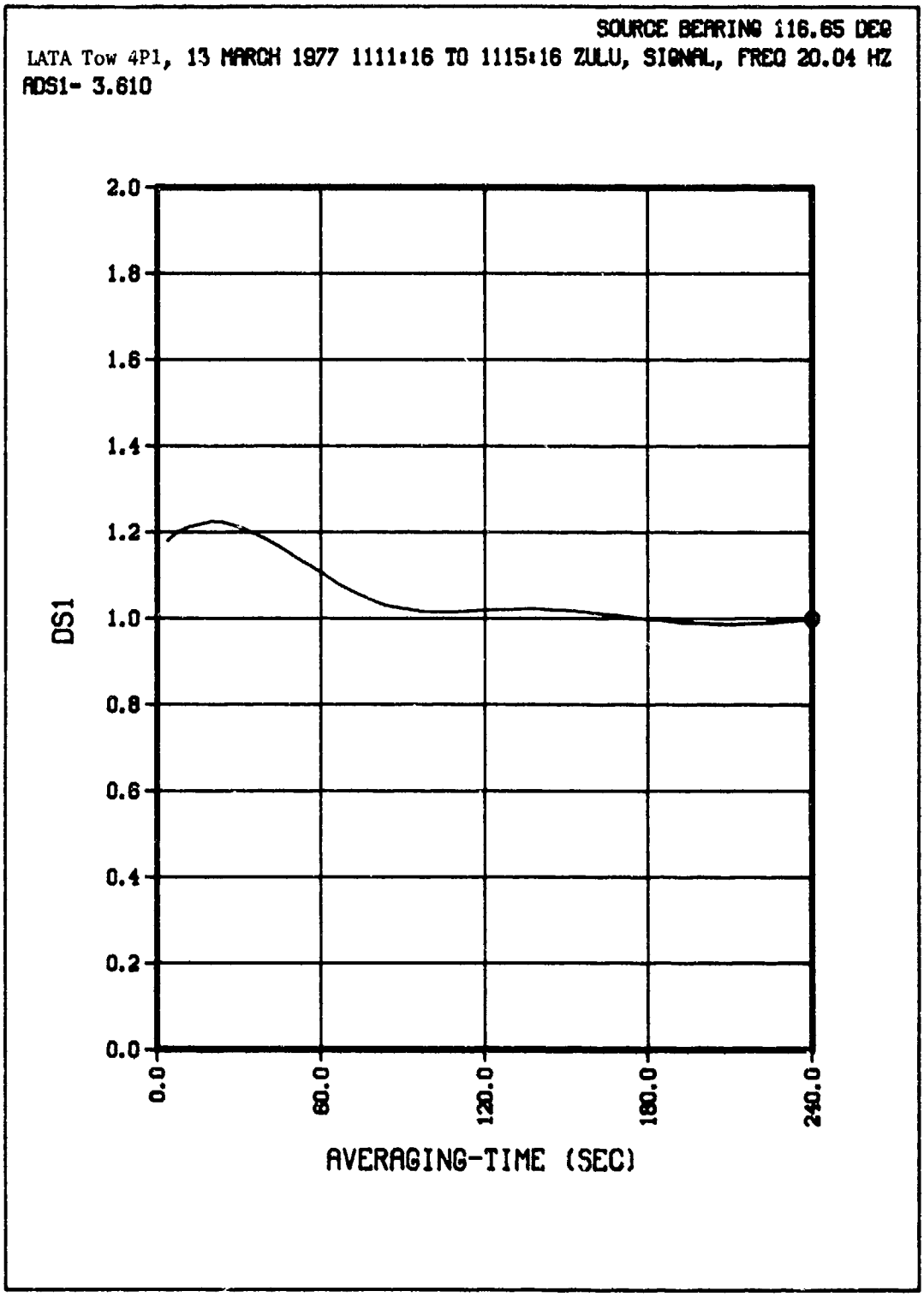

(CONFIDENTIAL)

(U) Figure 16e. Amplitude time stability.

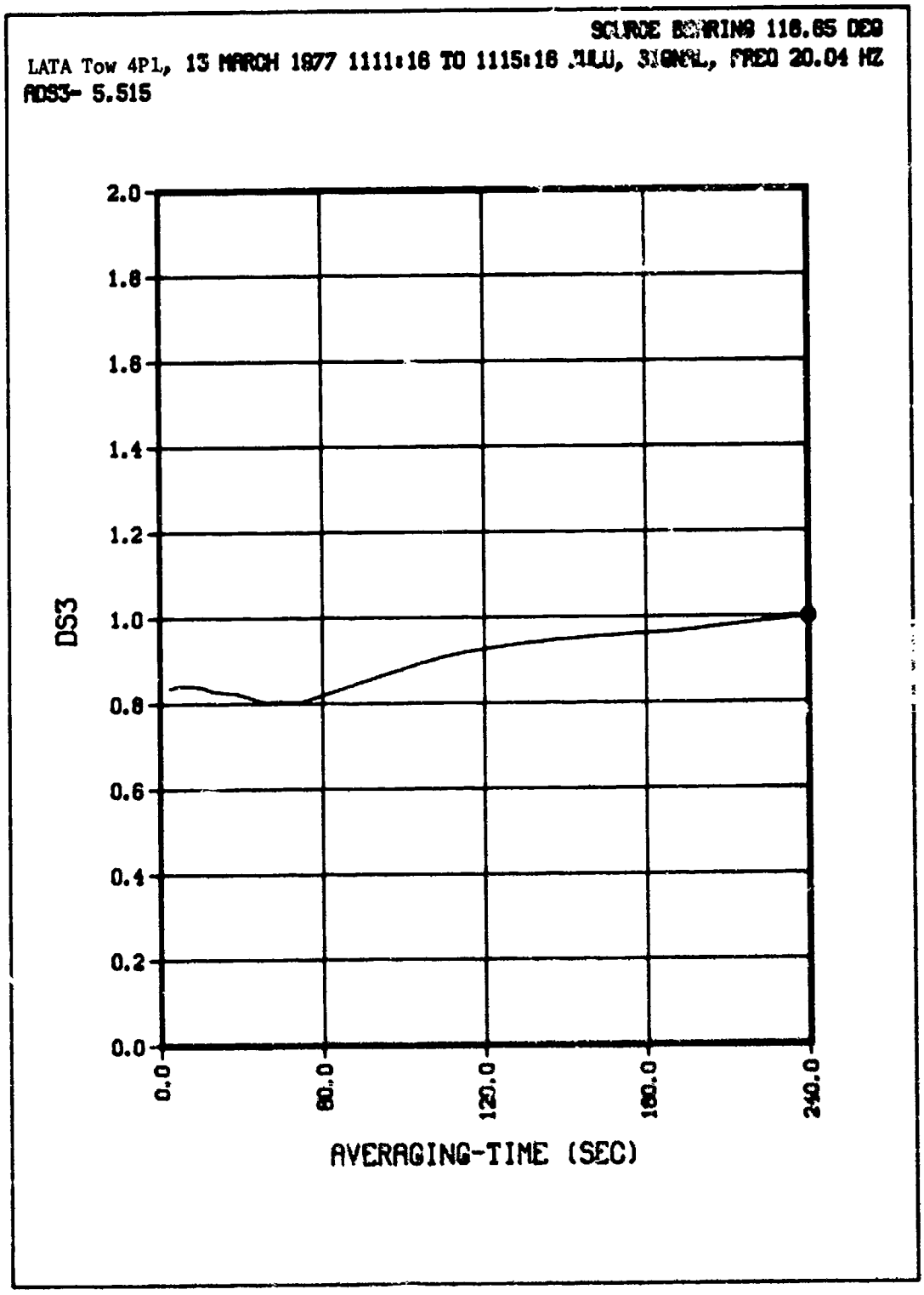

(CONFIDENTIAL)

(U) Figure 16f. Phase time stability.

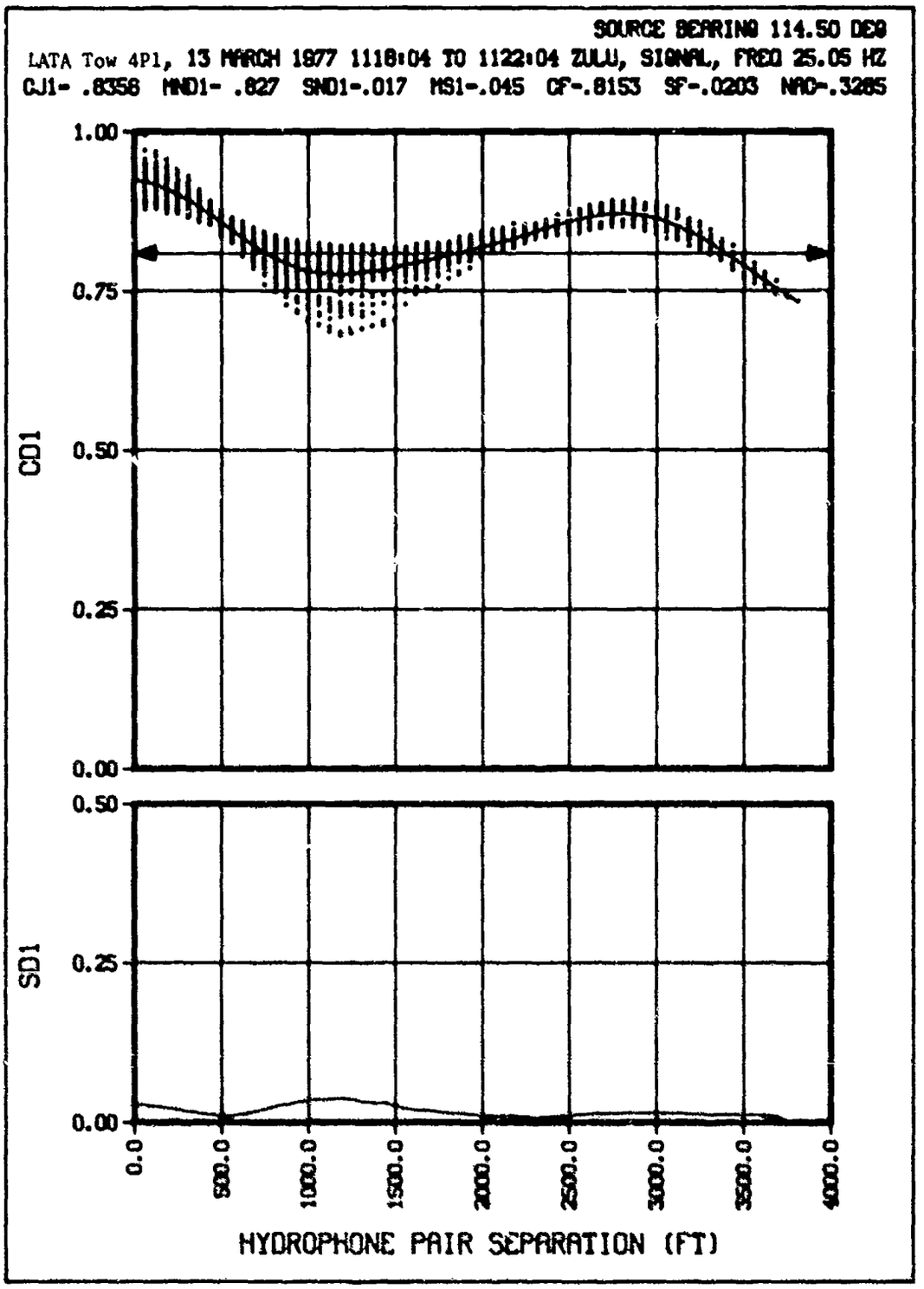

(CONFIDENTIAL)

(U) Figure 17a. Normalized amplitude covariance.

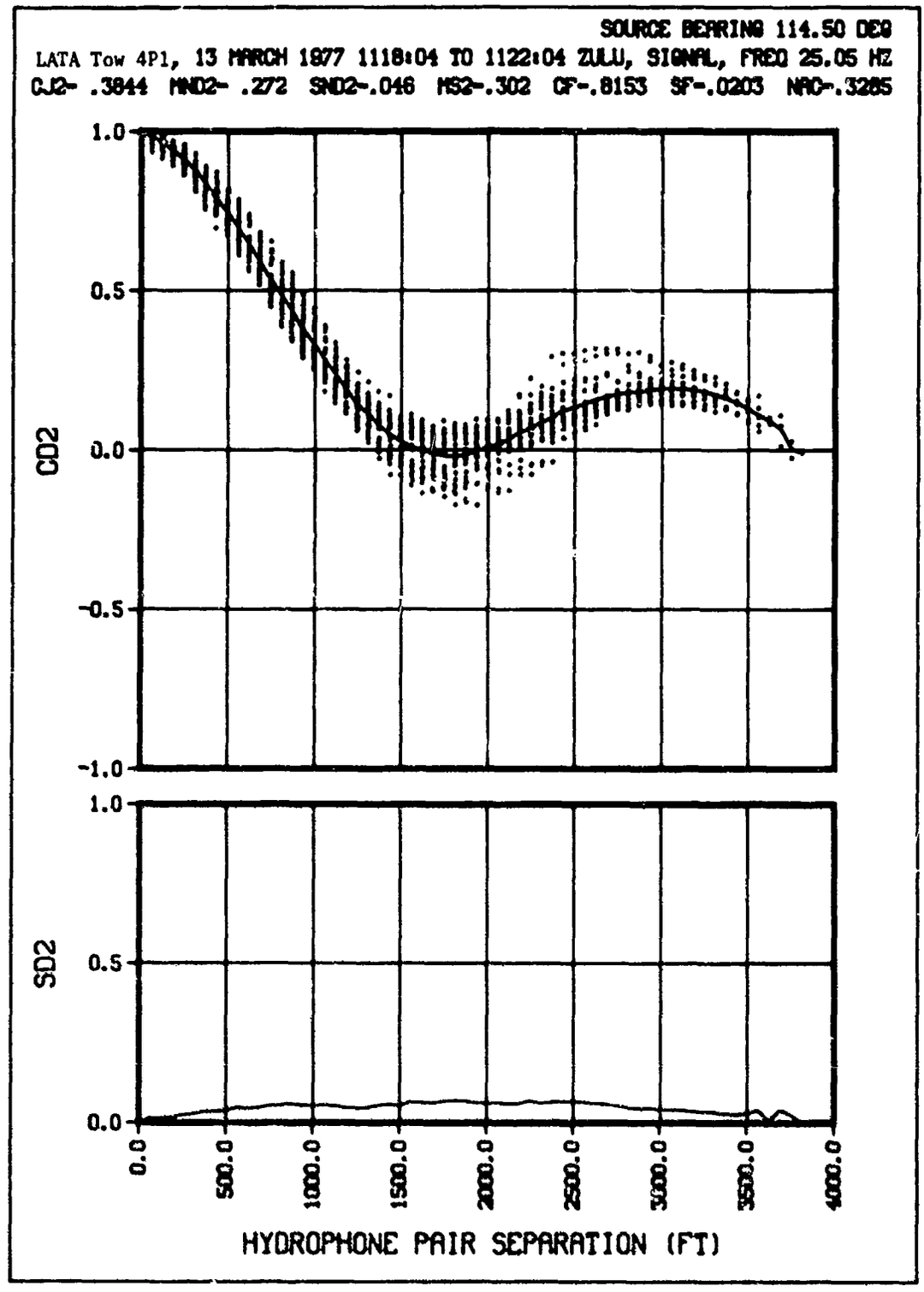

(CONFIDENTIAL)

(U) Figure 17b. Array phase coherence.

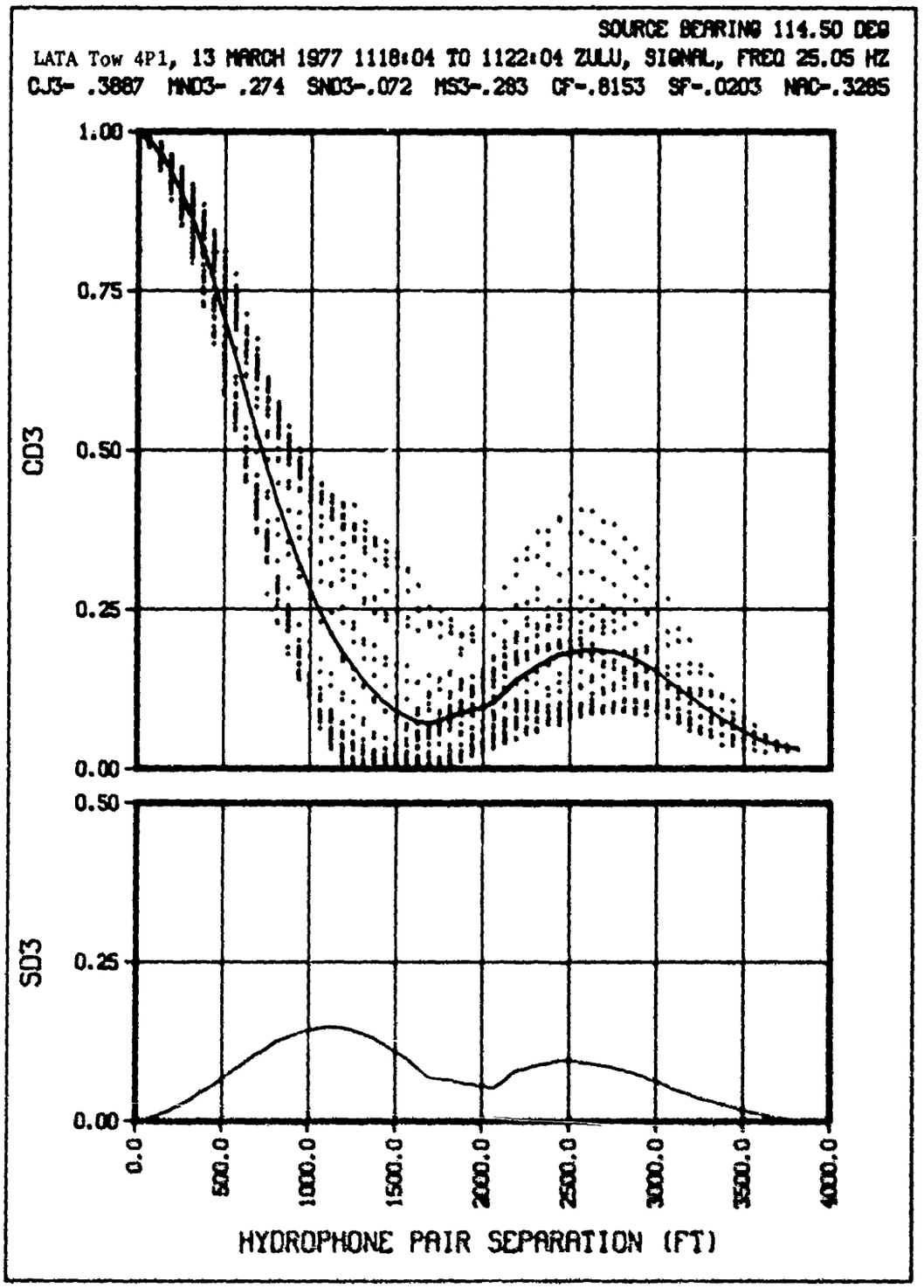

(CONFIDENTIAL)

(U) Figure 17c. Classical coherence.

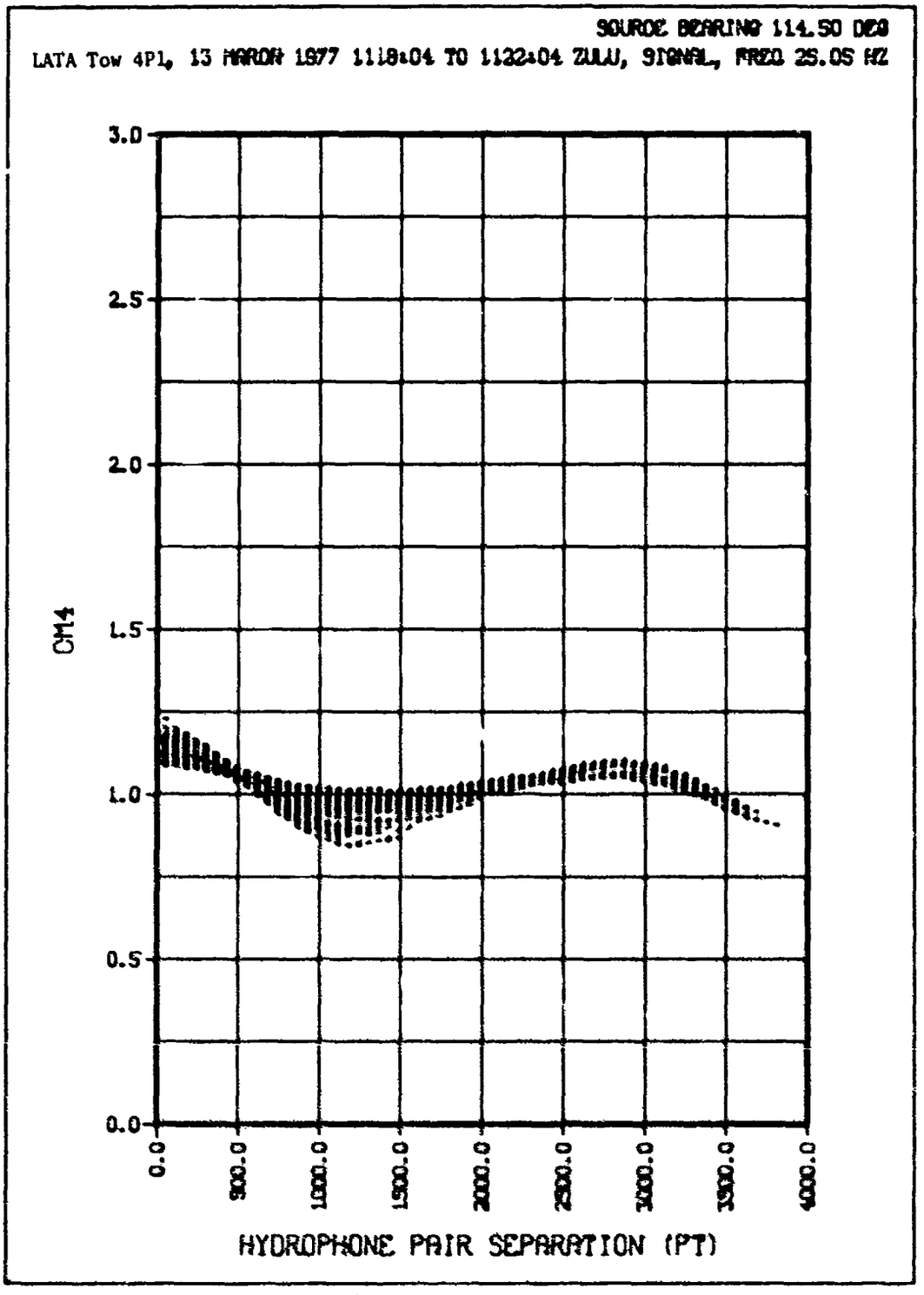

(CONFIDENTIAL)

(U) Figure 17d. Array amplitude covariance.

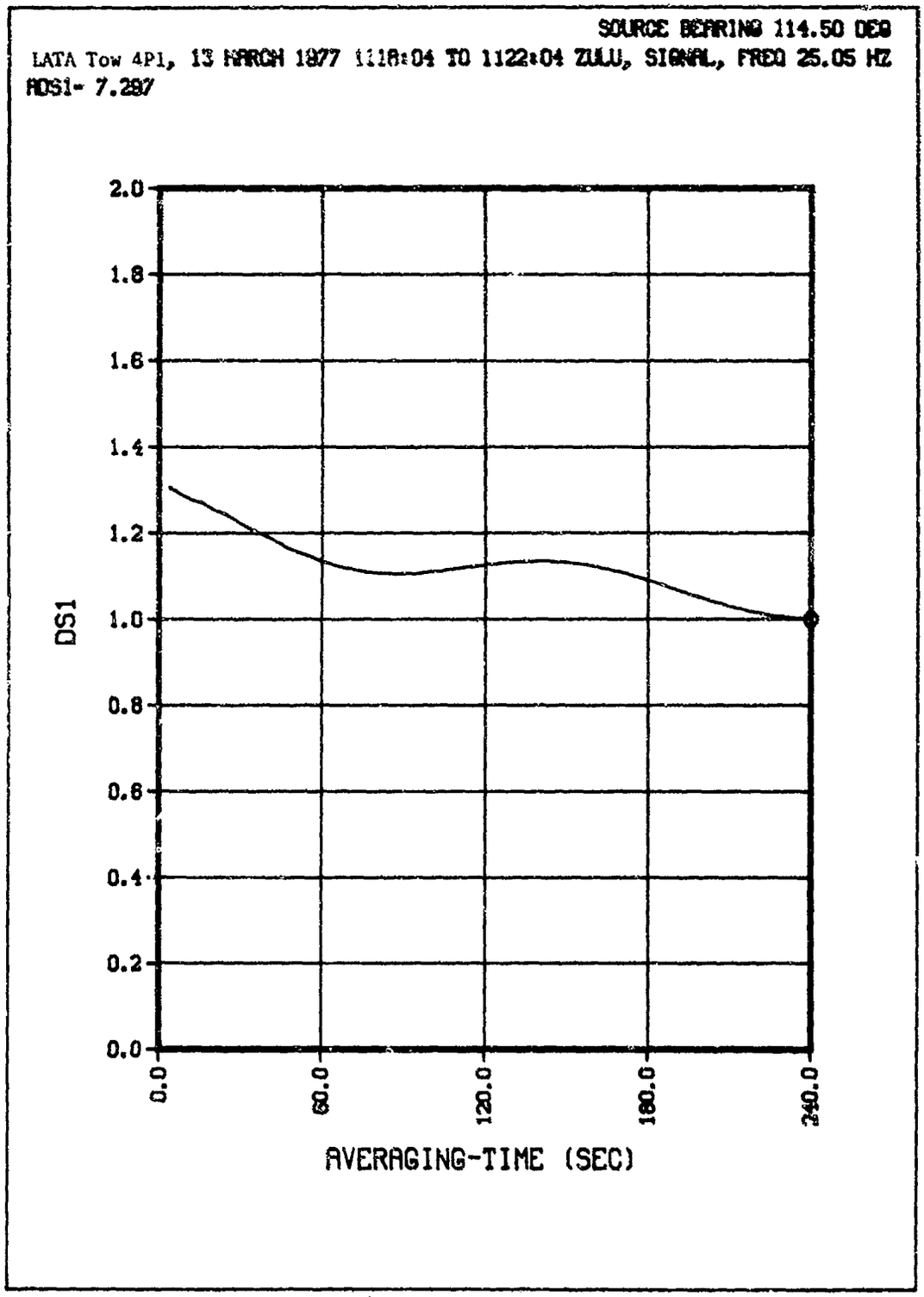

(CONFIDENTIAL)

(U) Figure 17e. Amplitude time stability.

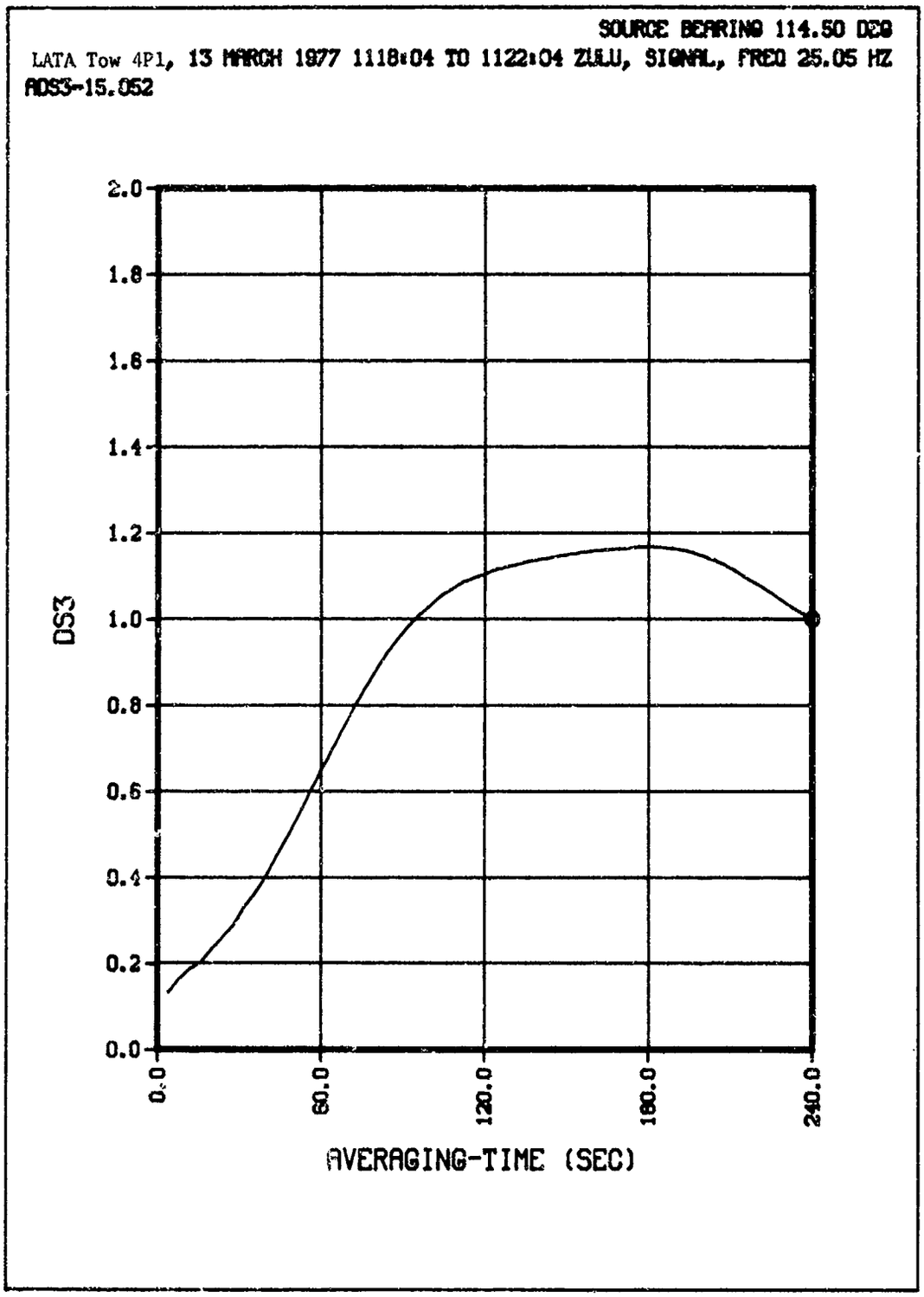

(CONFIDENTIAL)

(U) Figure 17f. Phase time stability.

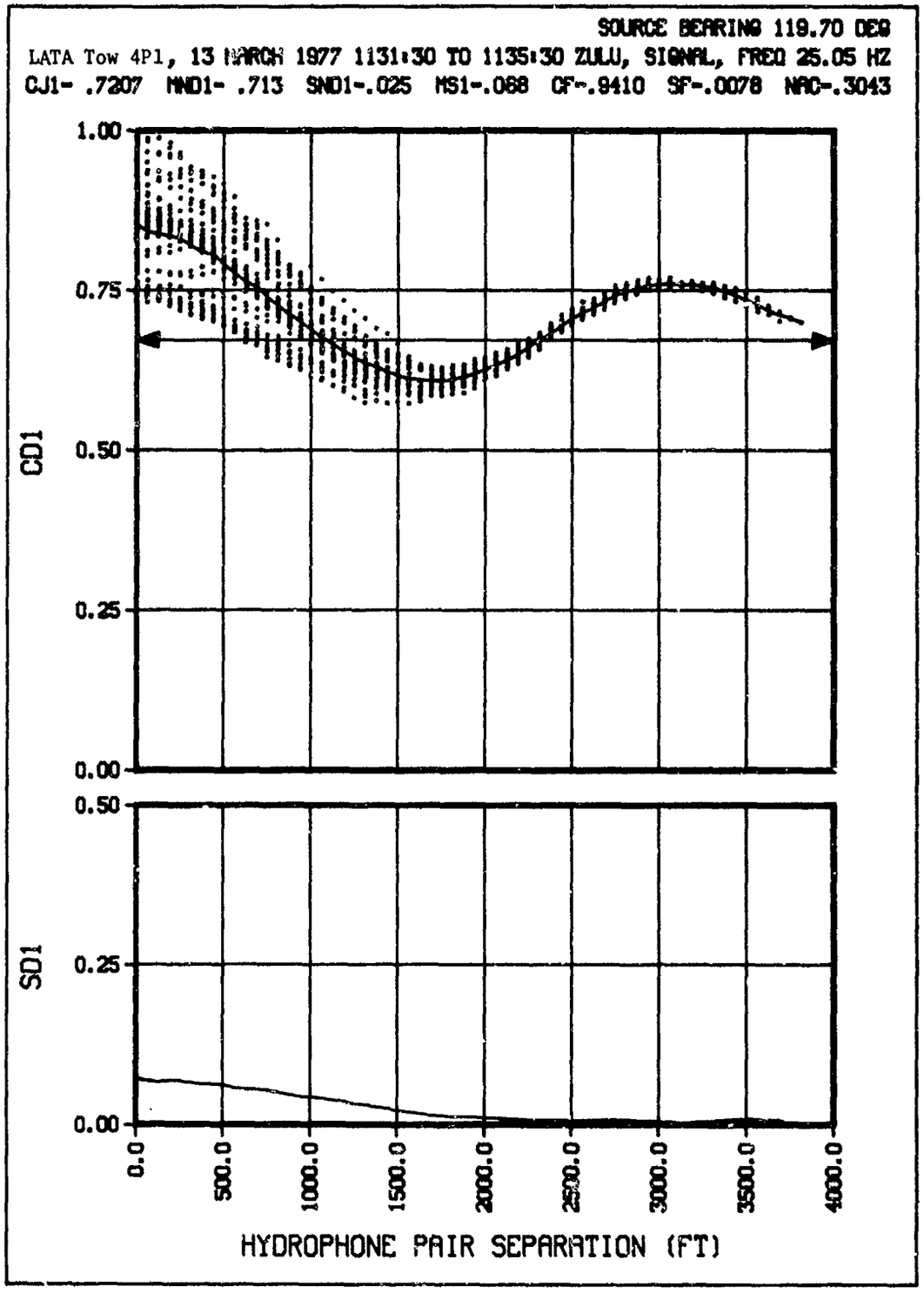

(CONFIDENTIAL)

(U) Figure 18a. Normalized amplitude covariance.

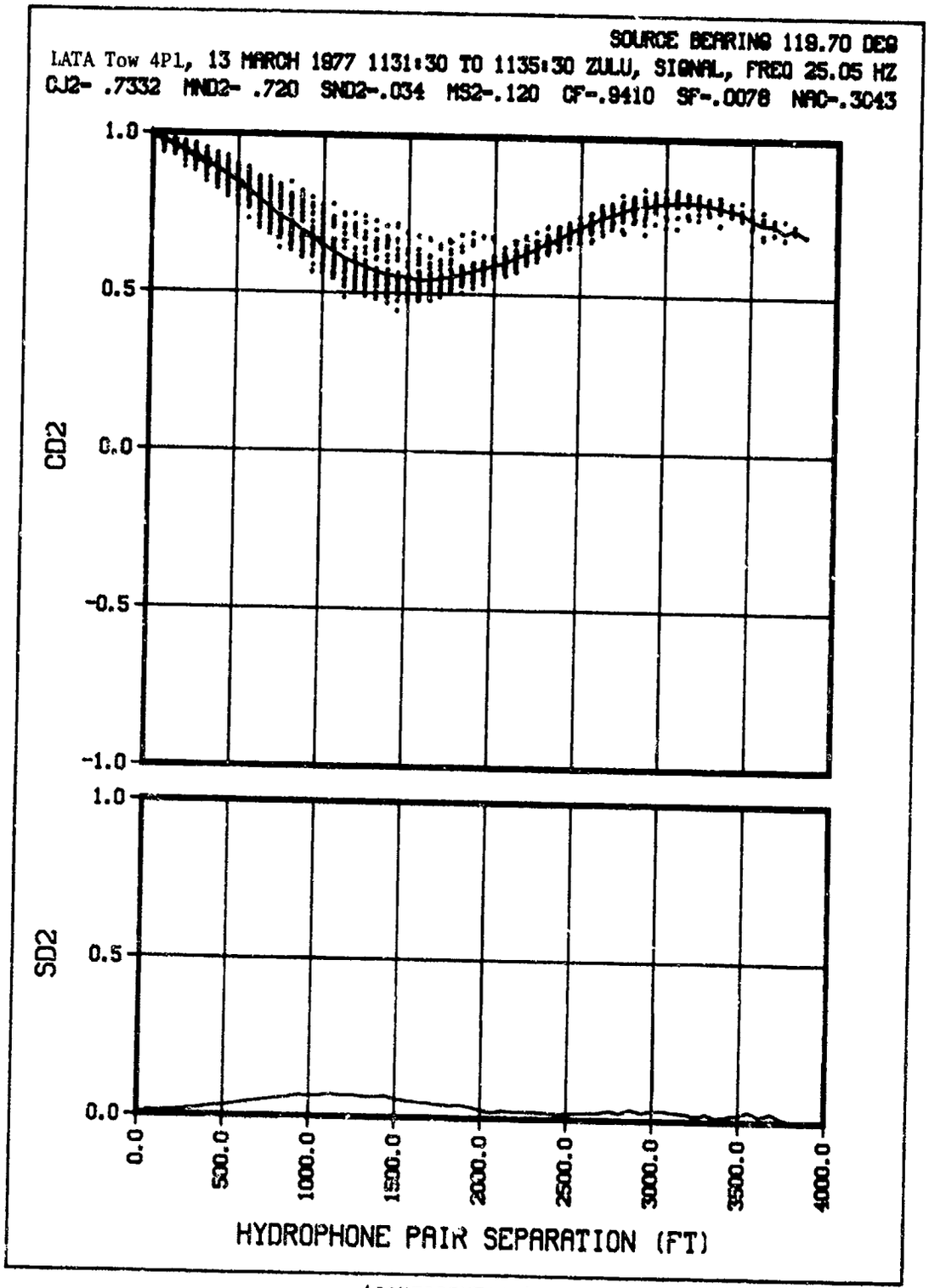

(CONFIDENTIAL)

(U) Figure 18b. Array phase coherence.

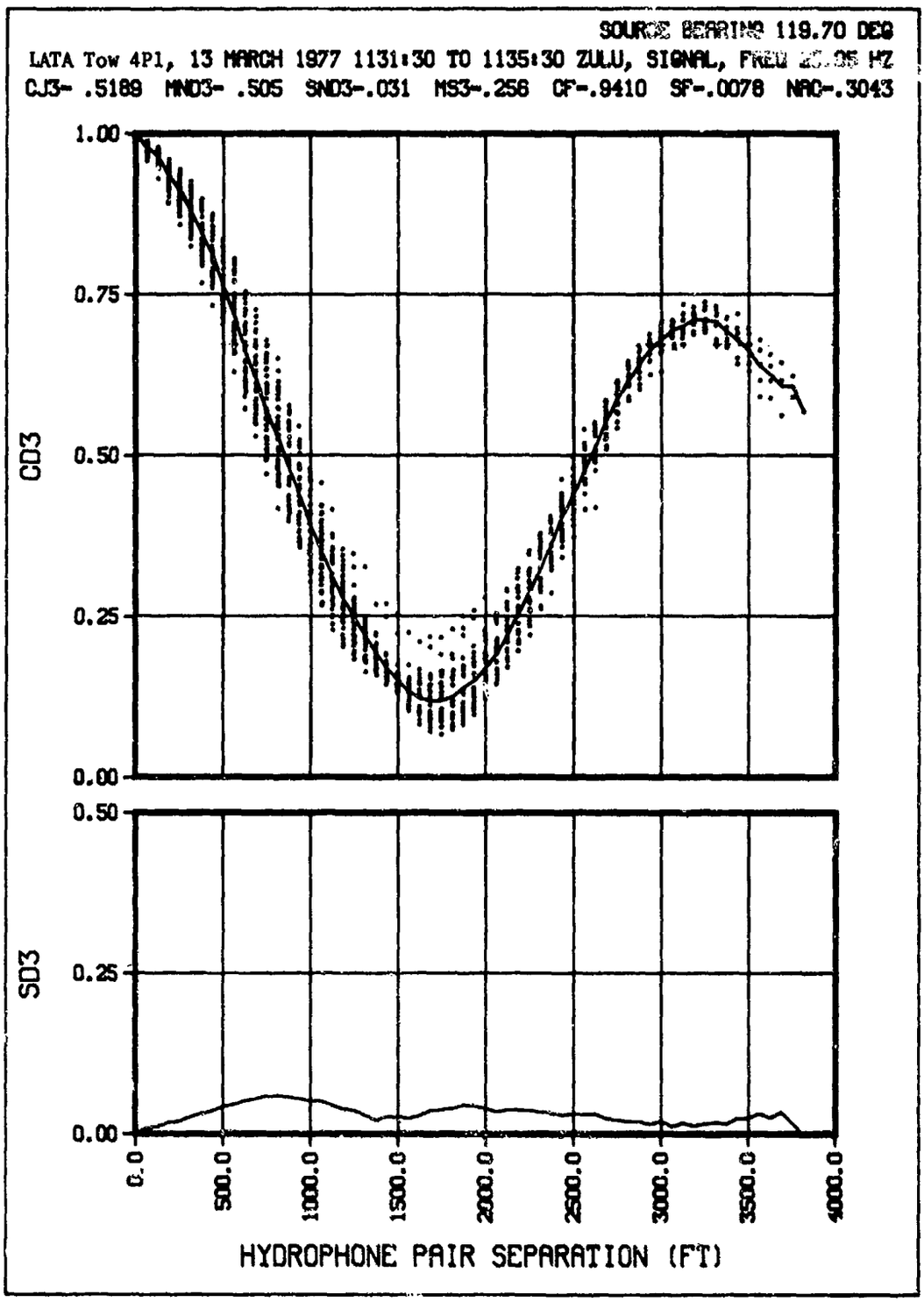

(CONFIDENTIAL)

(U) Figure 18c. Classical coherence.

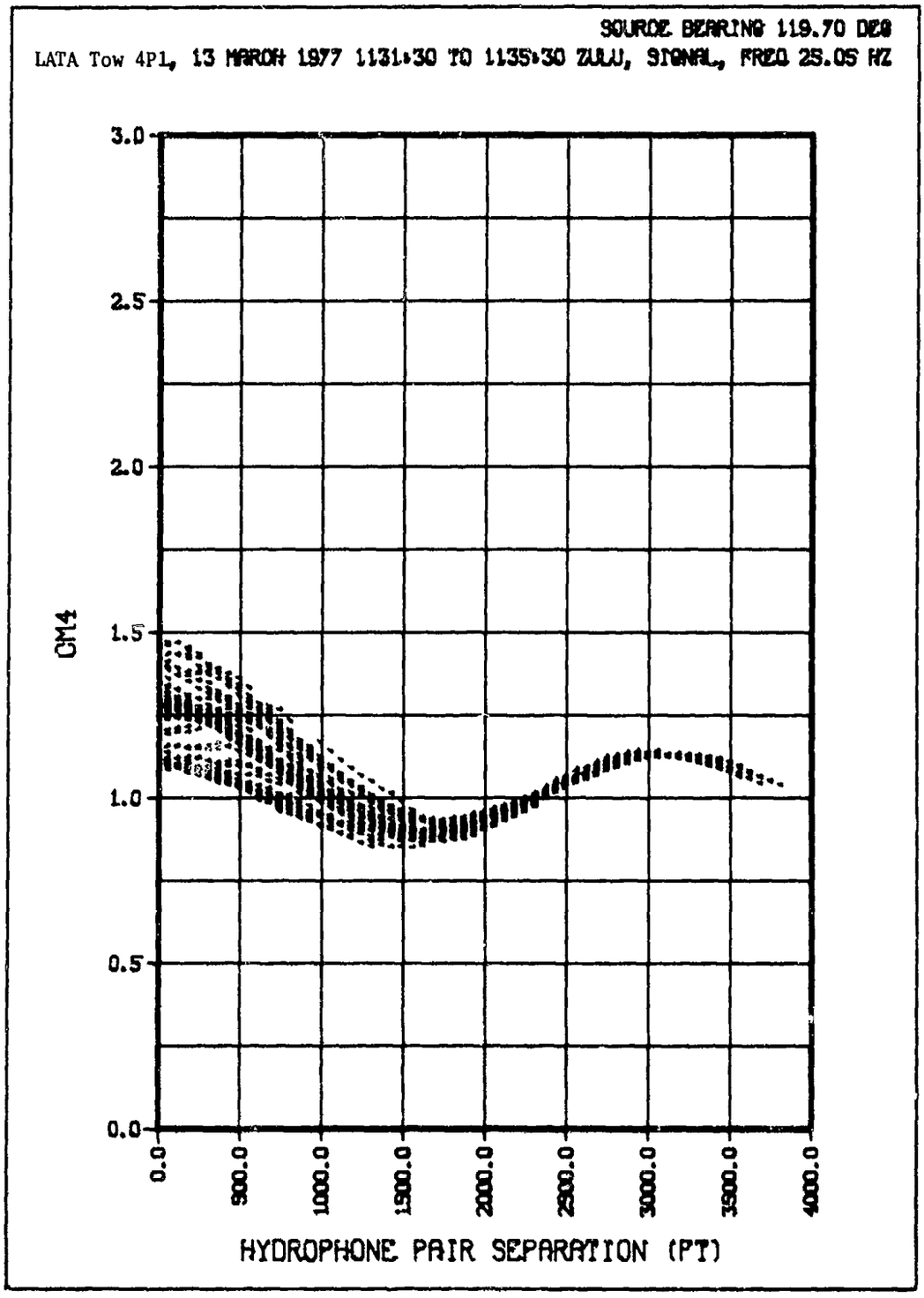

(CONFIDENTIAL)

(U) Figure 18d. Array amplitude covariance.

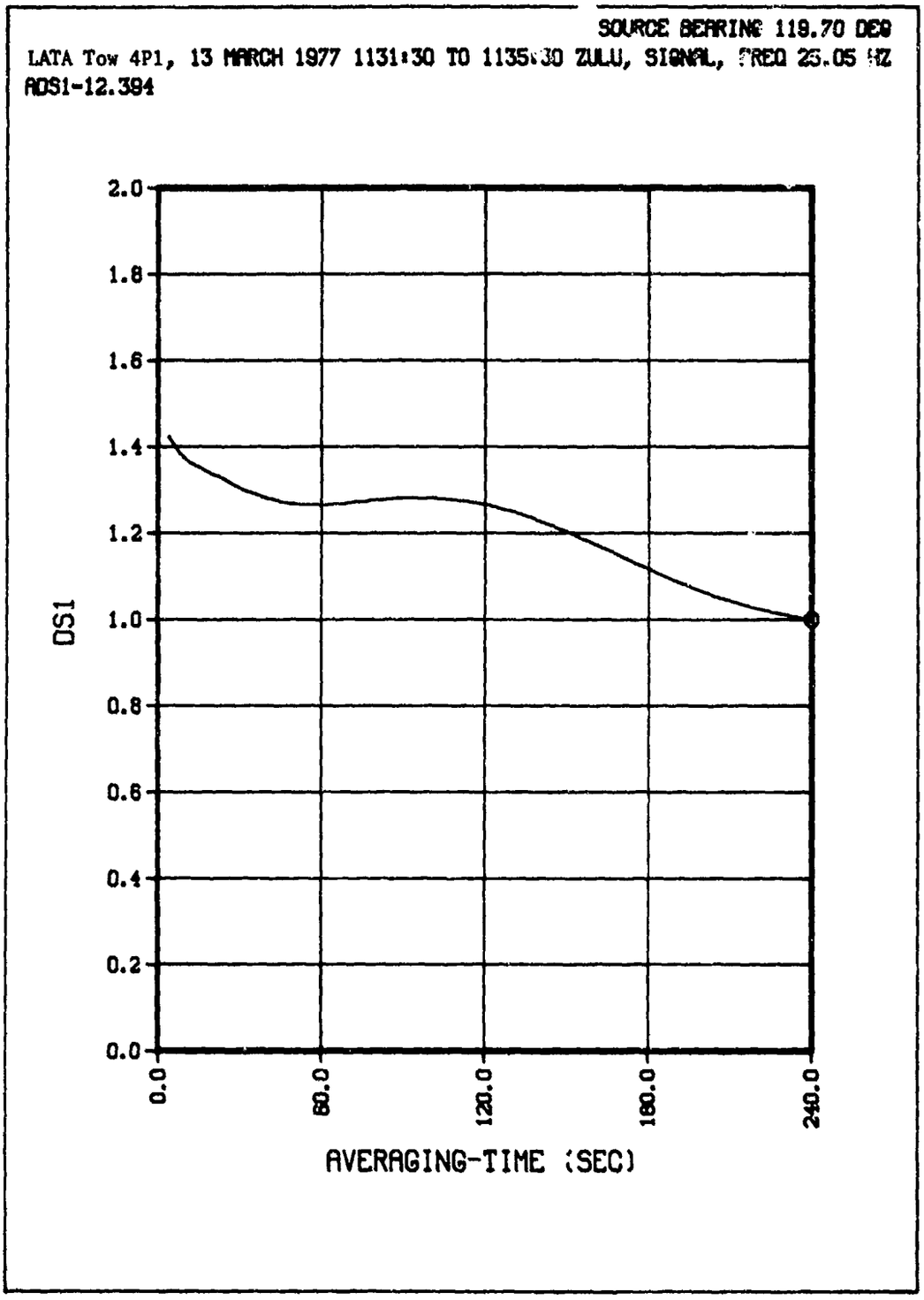

(CONFIDENTIAL)

(U) Figure 18e. Amplitude time stability.

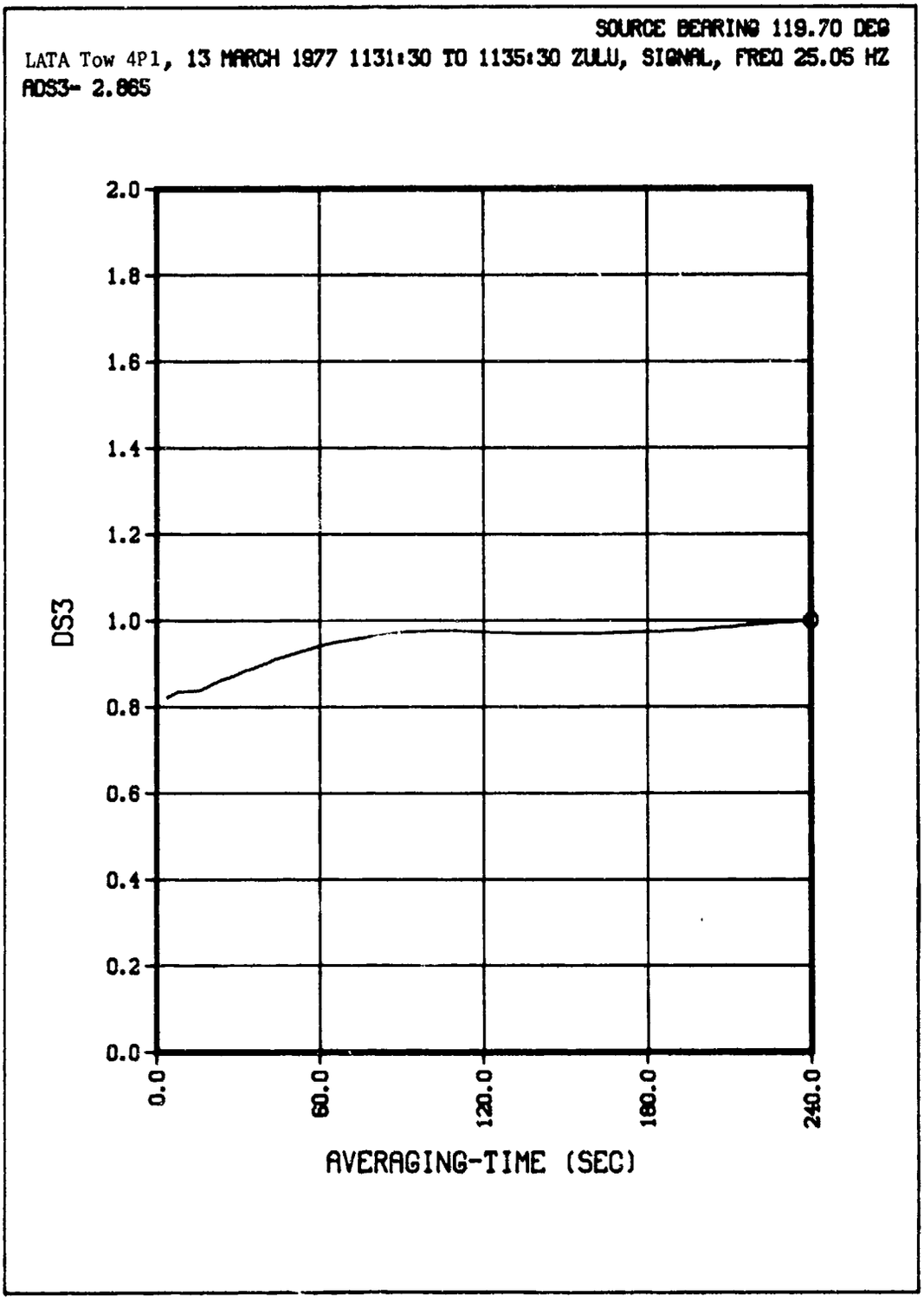

(CONFIDENTIAL)

(U) Figure 18f. Phase time stability.

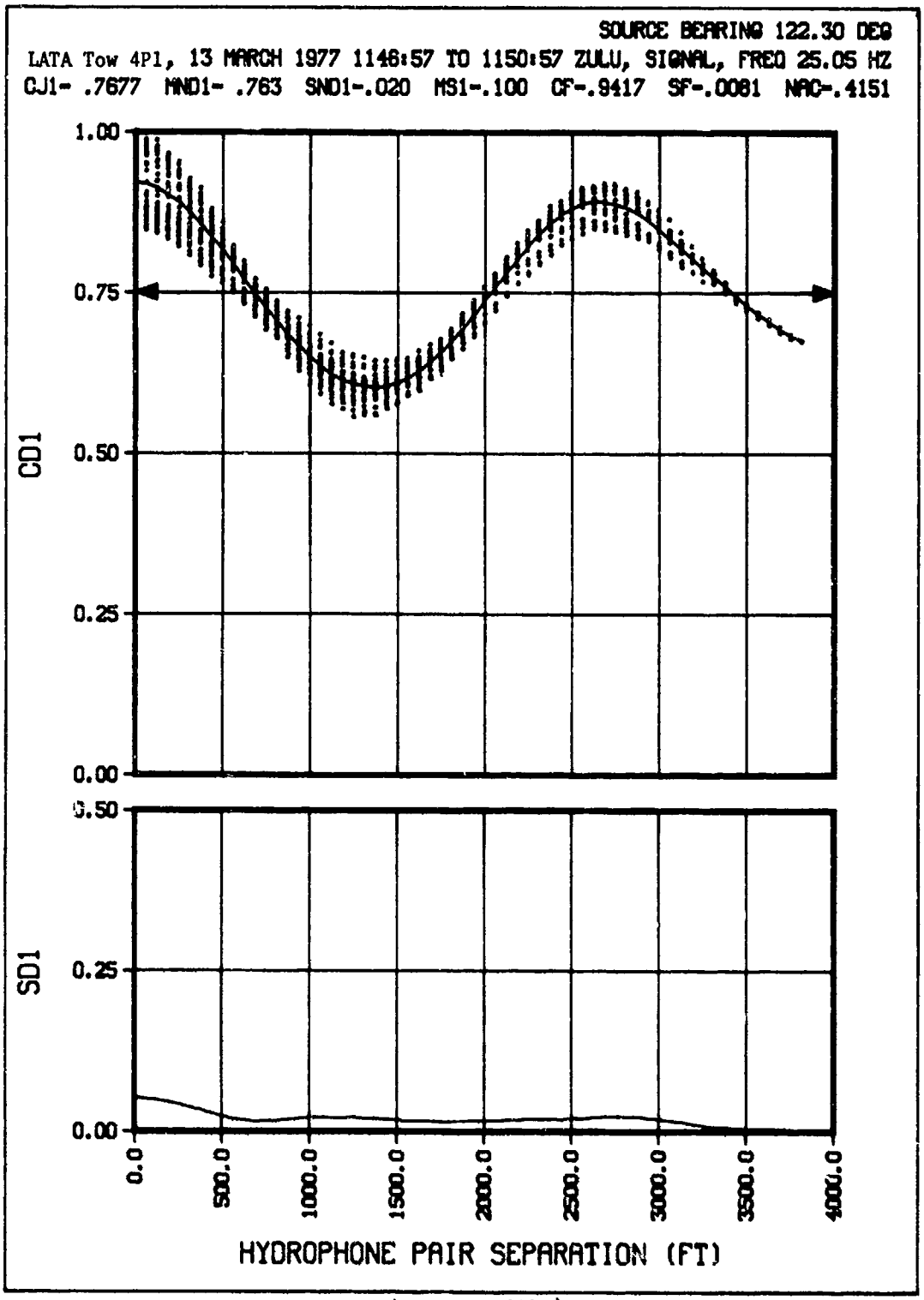

(CONFIDENTIAL)

(U) Figure 19a. Normalized amplitude covariance.

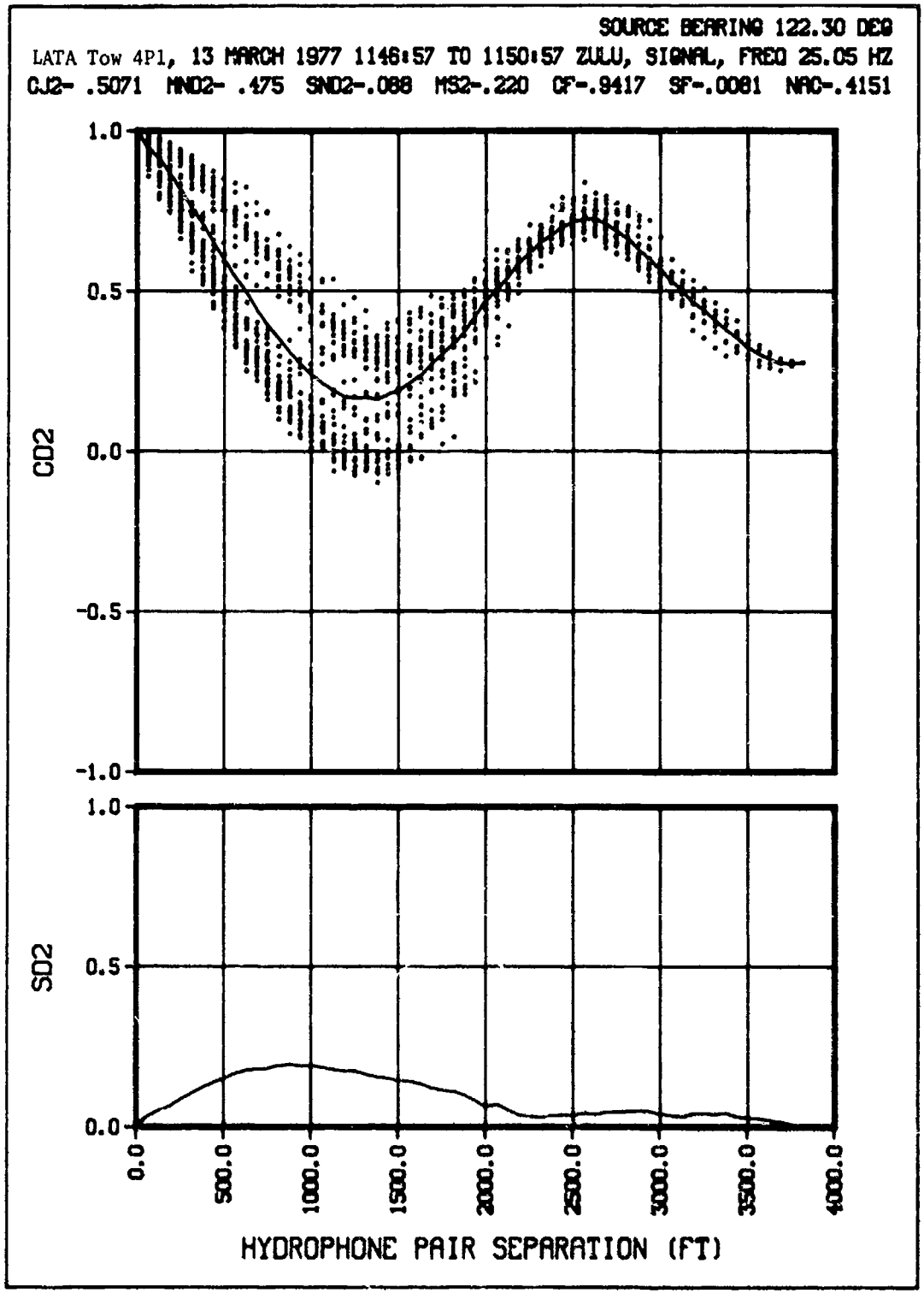

(CONFIDENTIAL)

(U) Figure 19b. Array phase coherence.

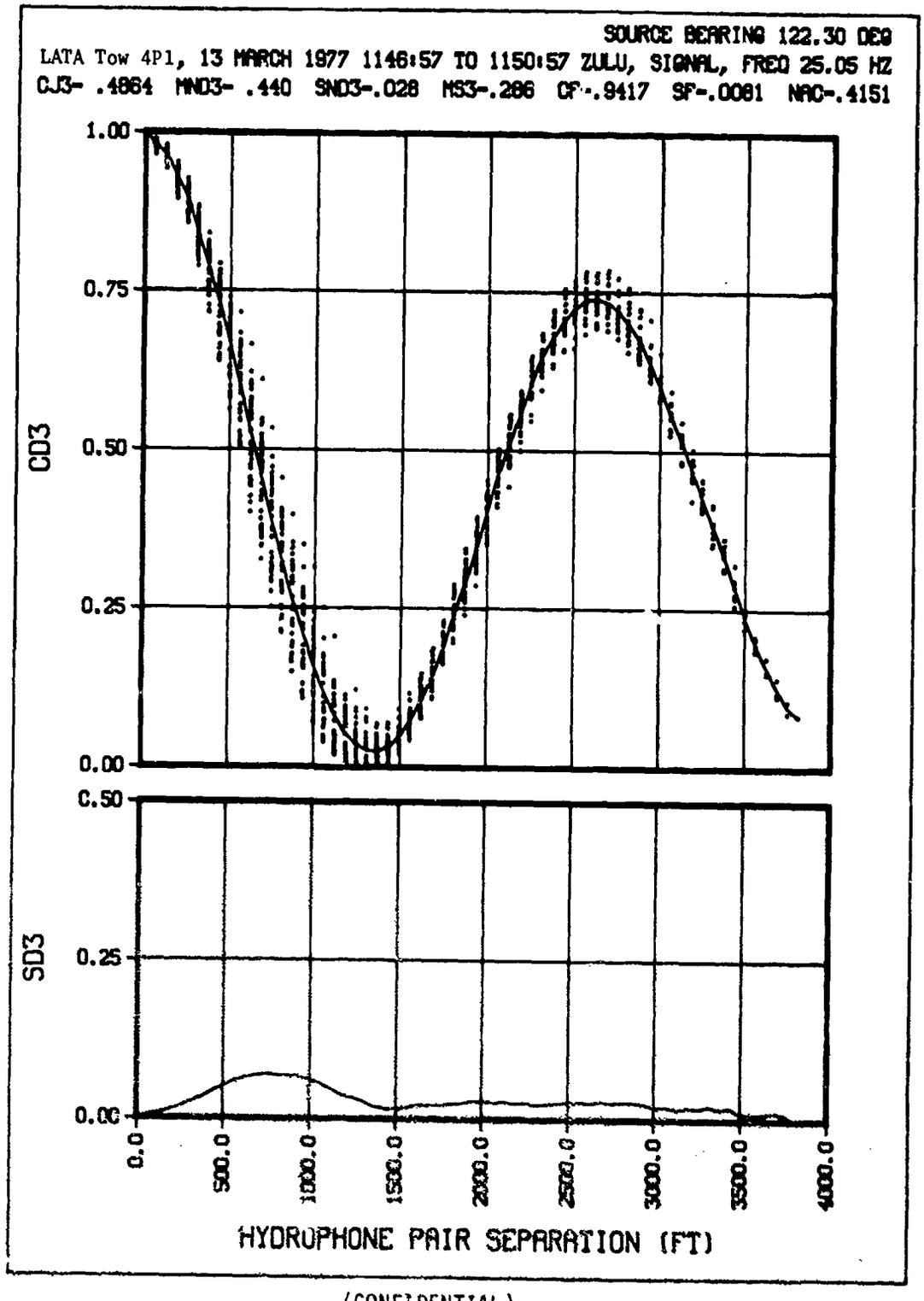

(CONFIDENTIAL)

(U) Figure 19c. Classical coherence.

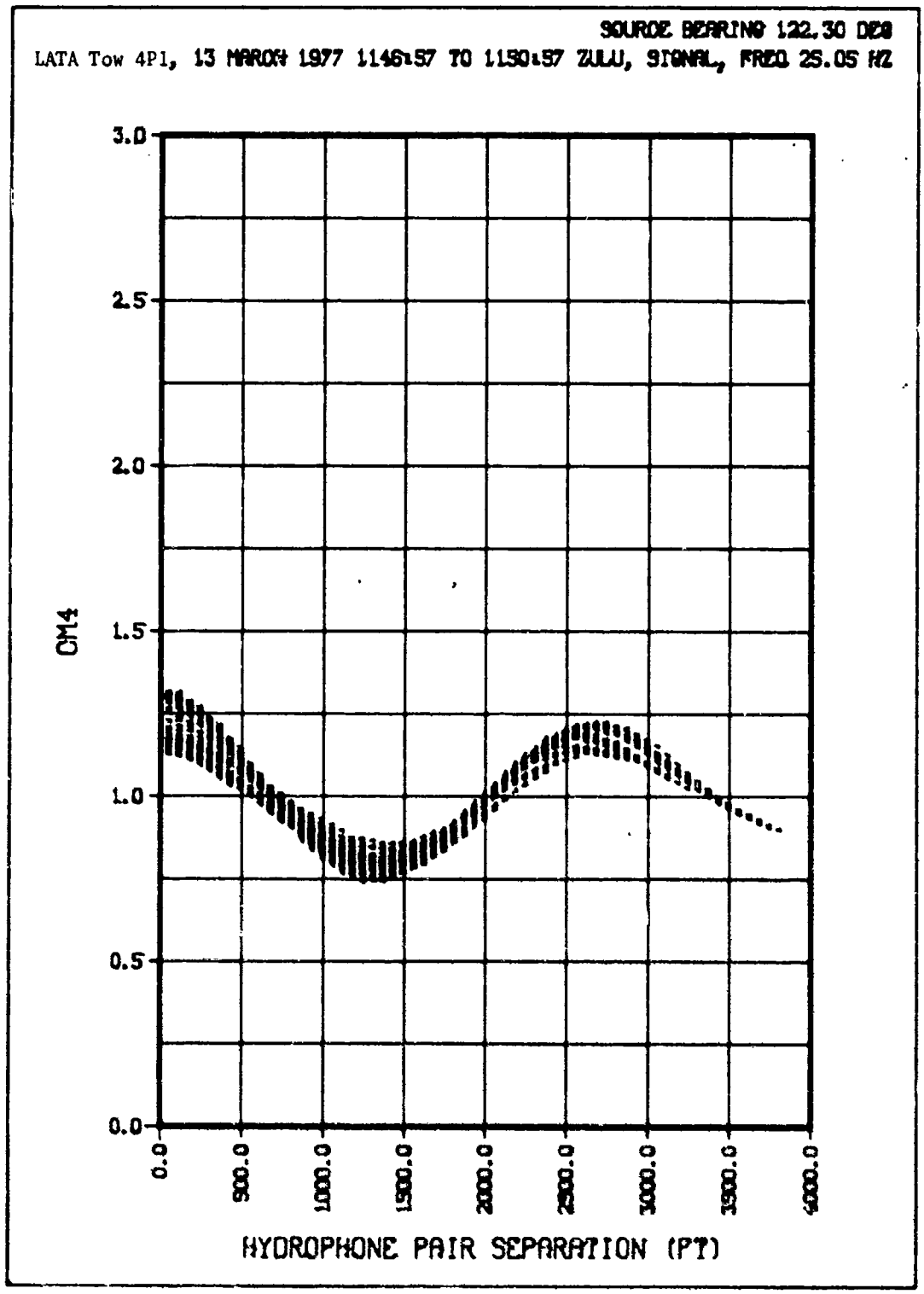

(CONFIDENTIAL)

(U) Figure 19d. Array amplitude covariance.

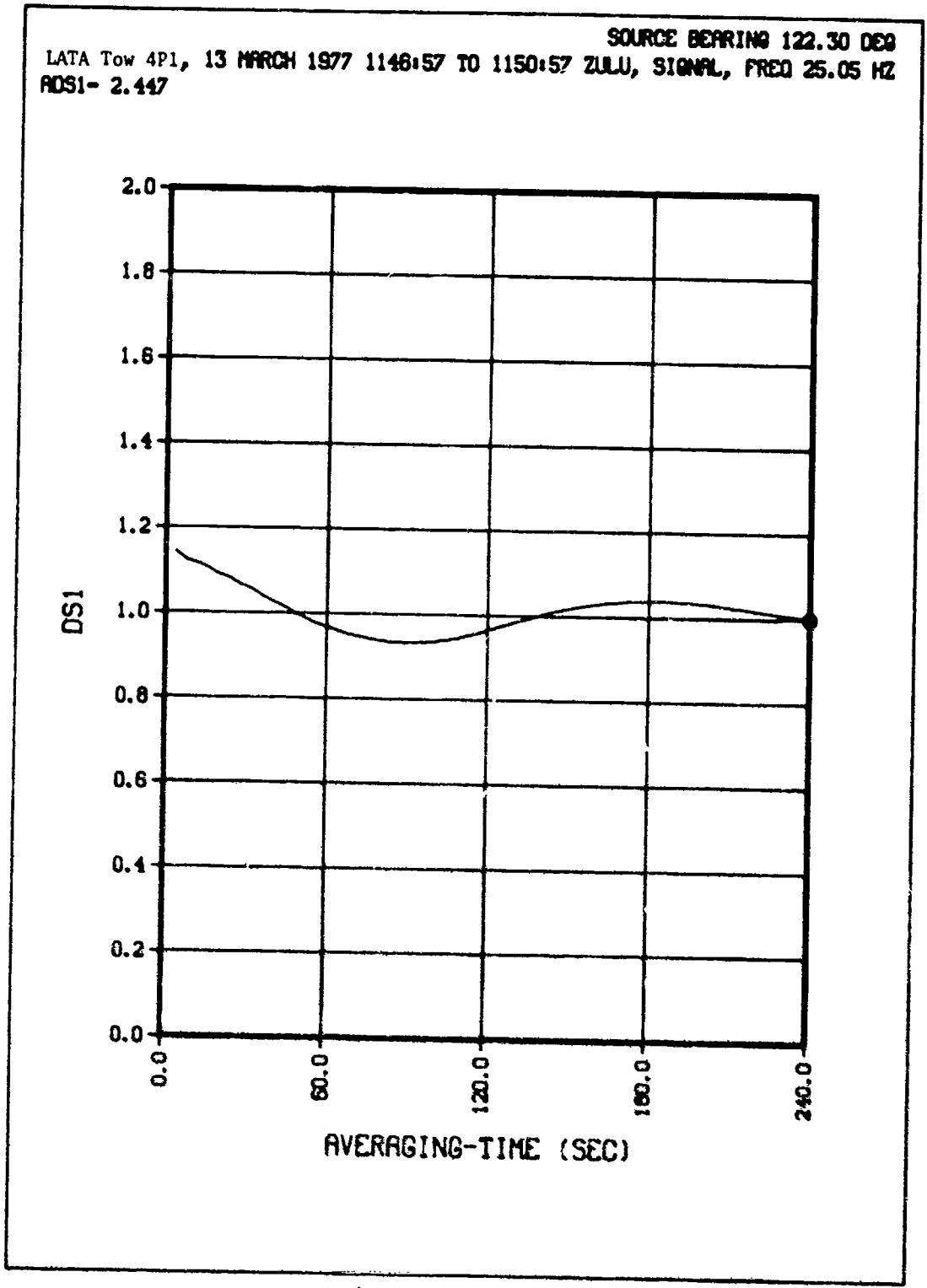

(CONFIDENTIAL)

(U) Figure 19e. Amplitude time stability.

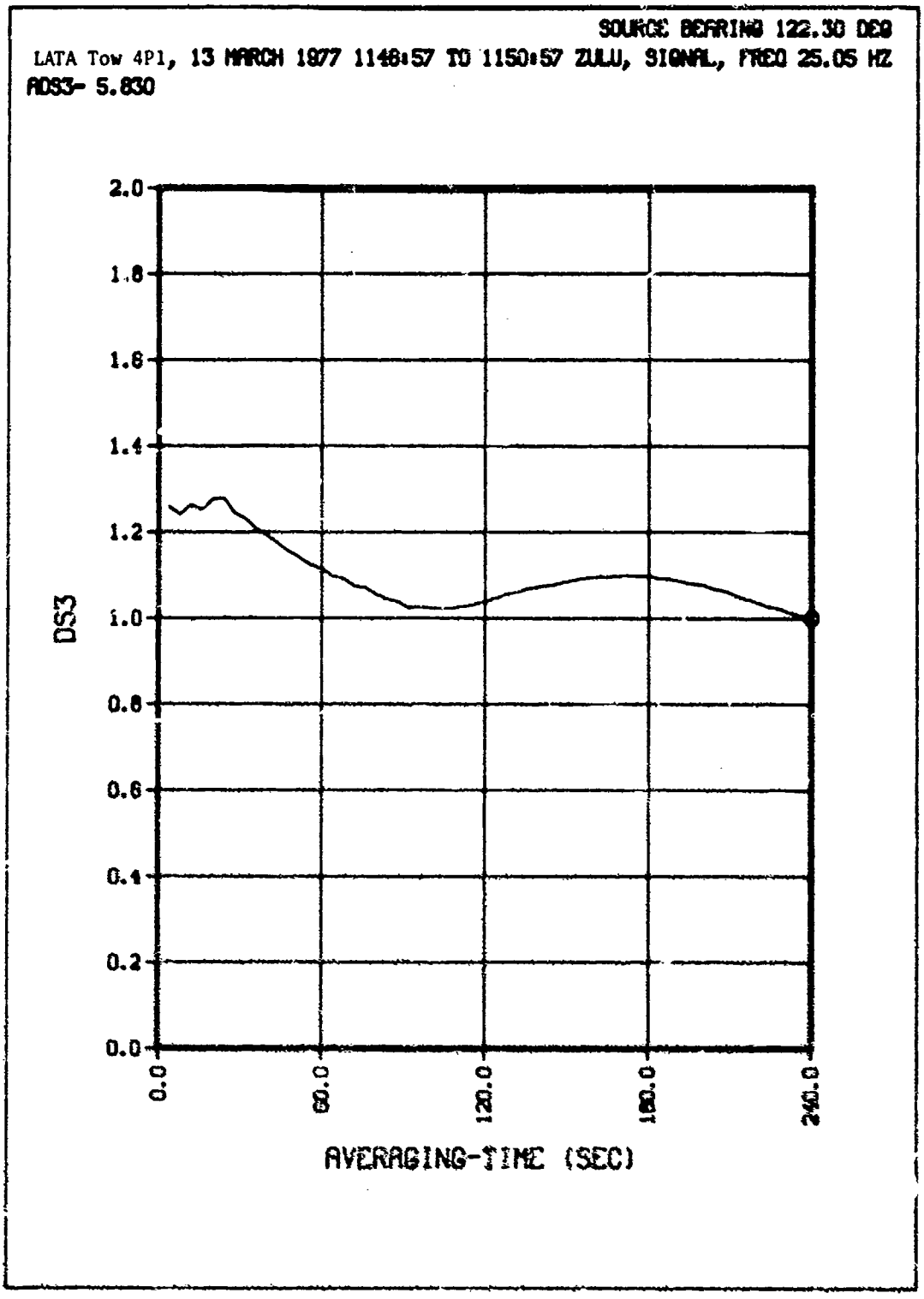

(CONFIDENTIAL)

(U) Figure 19f. Phase time stability.

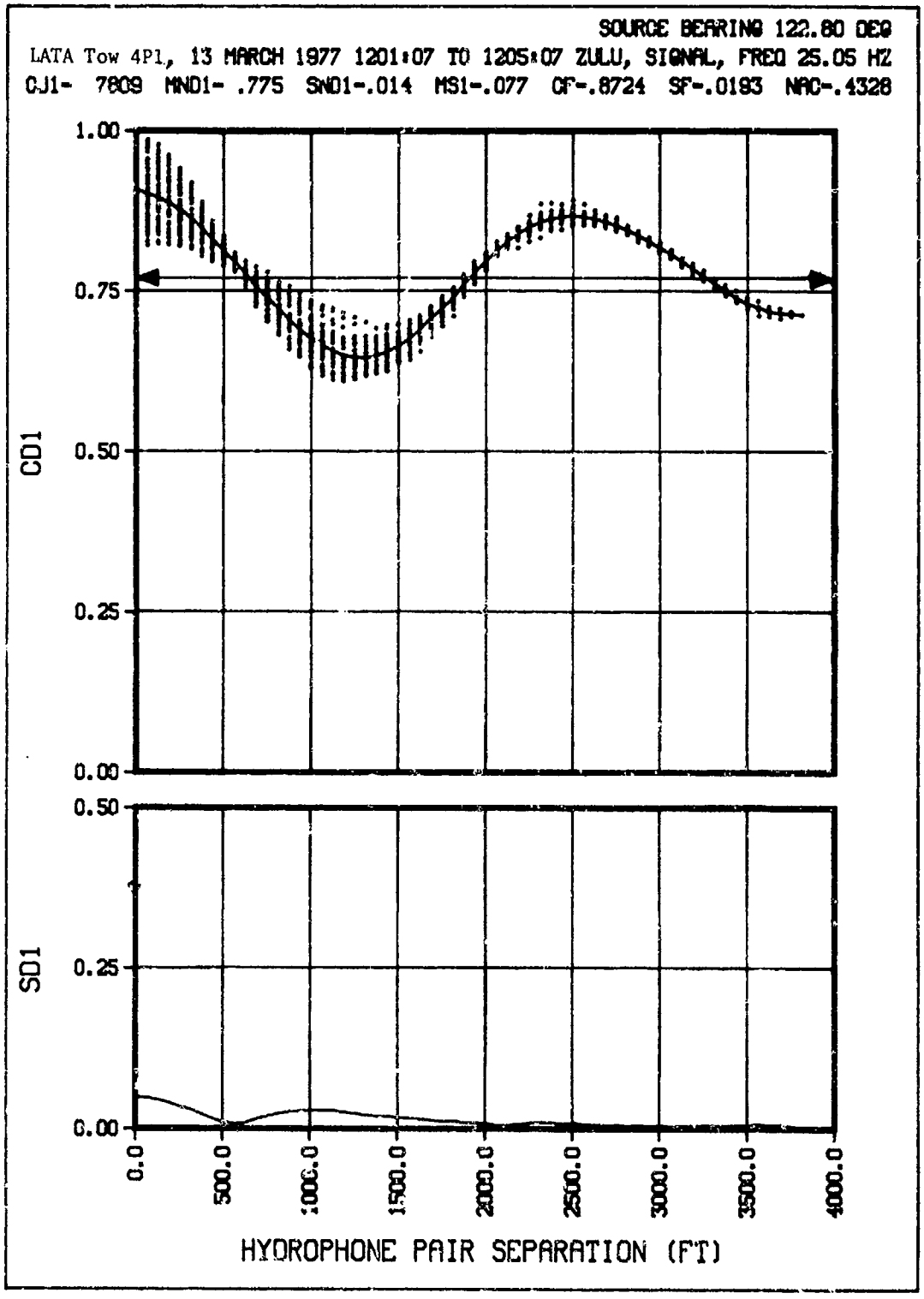

(CONFIDENTIAL)

(U) Figure 20a. Normalized amplitude covariance.

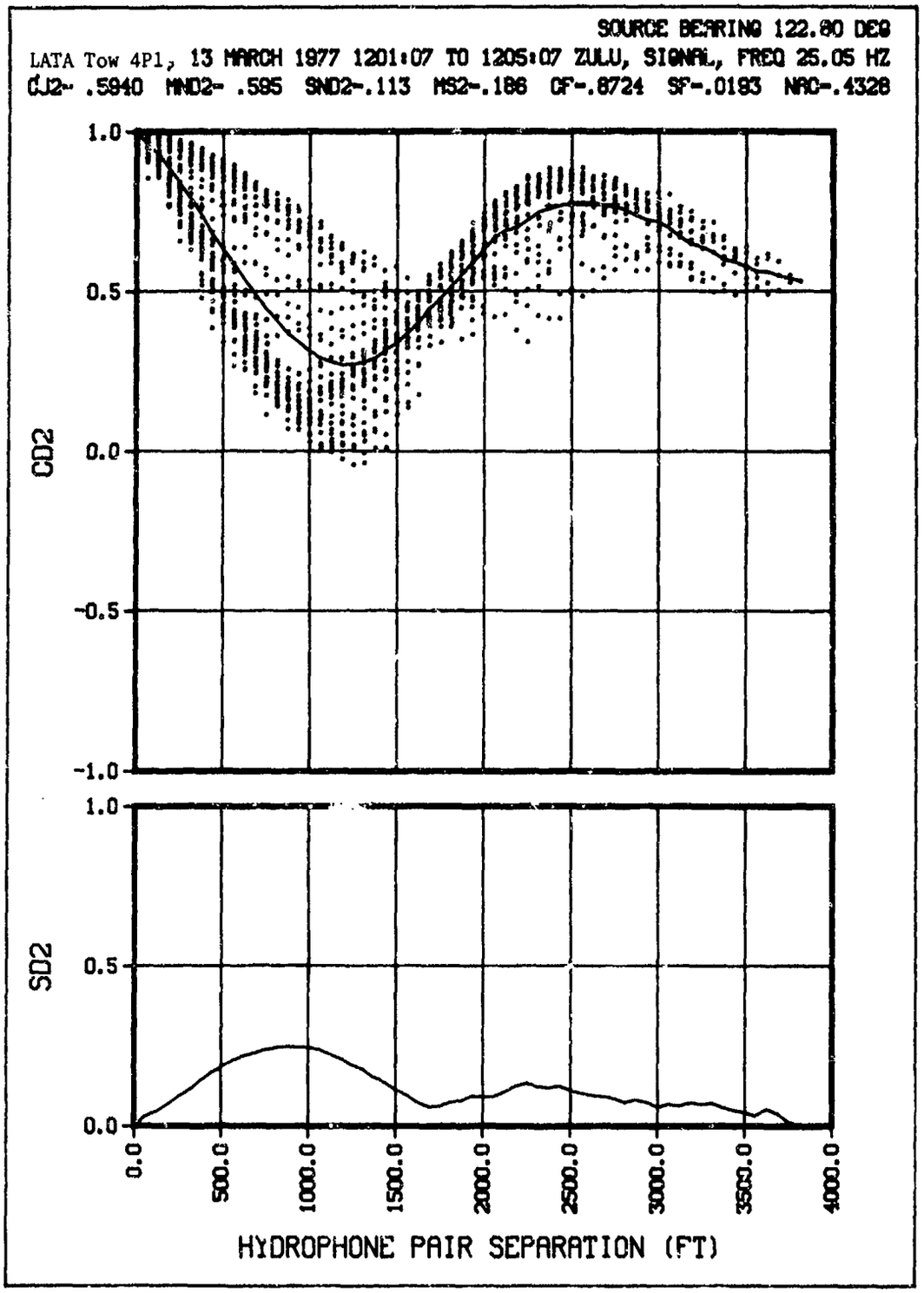

(CONFIDENTIAL)

(U) Figure 20b. Array phase coherence.

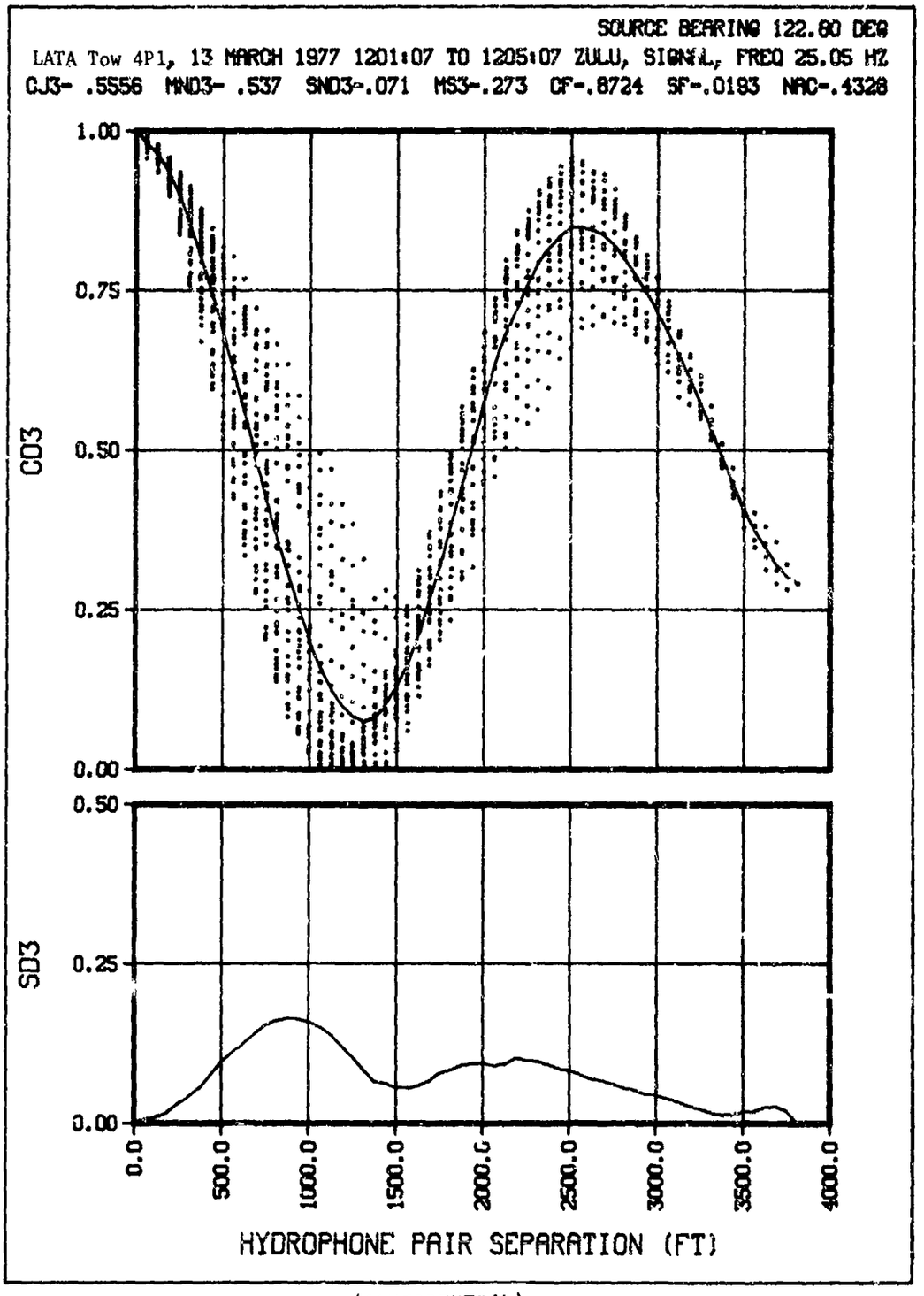

(CONFIDENTIAL)

(U) Figure 20c Classical coherence.

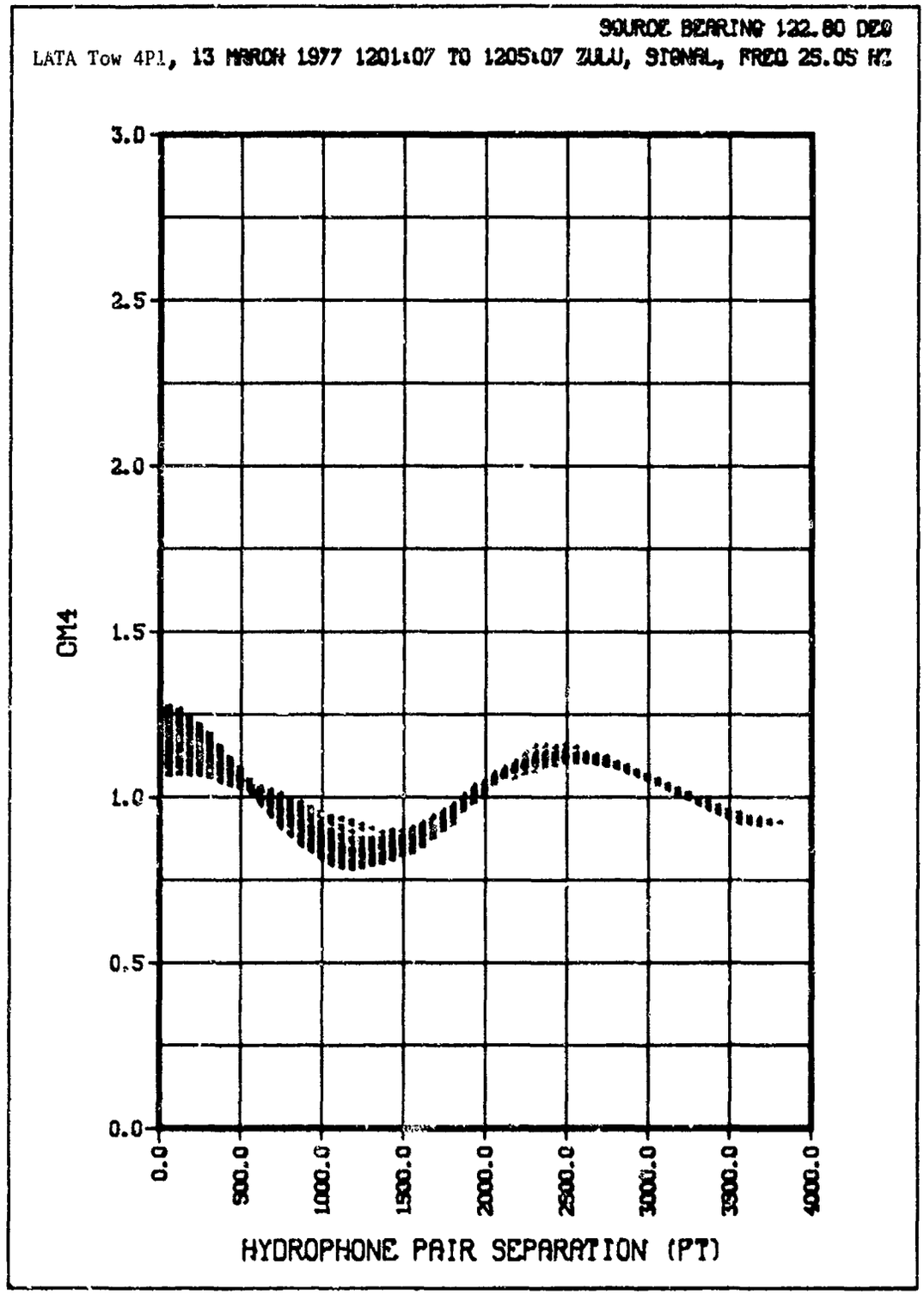

(CONFIDENTIAL)

(U) Figure 20d. Array amplitude covariance.

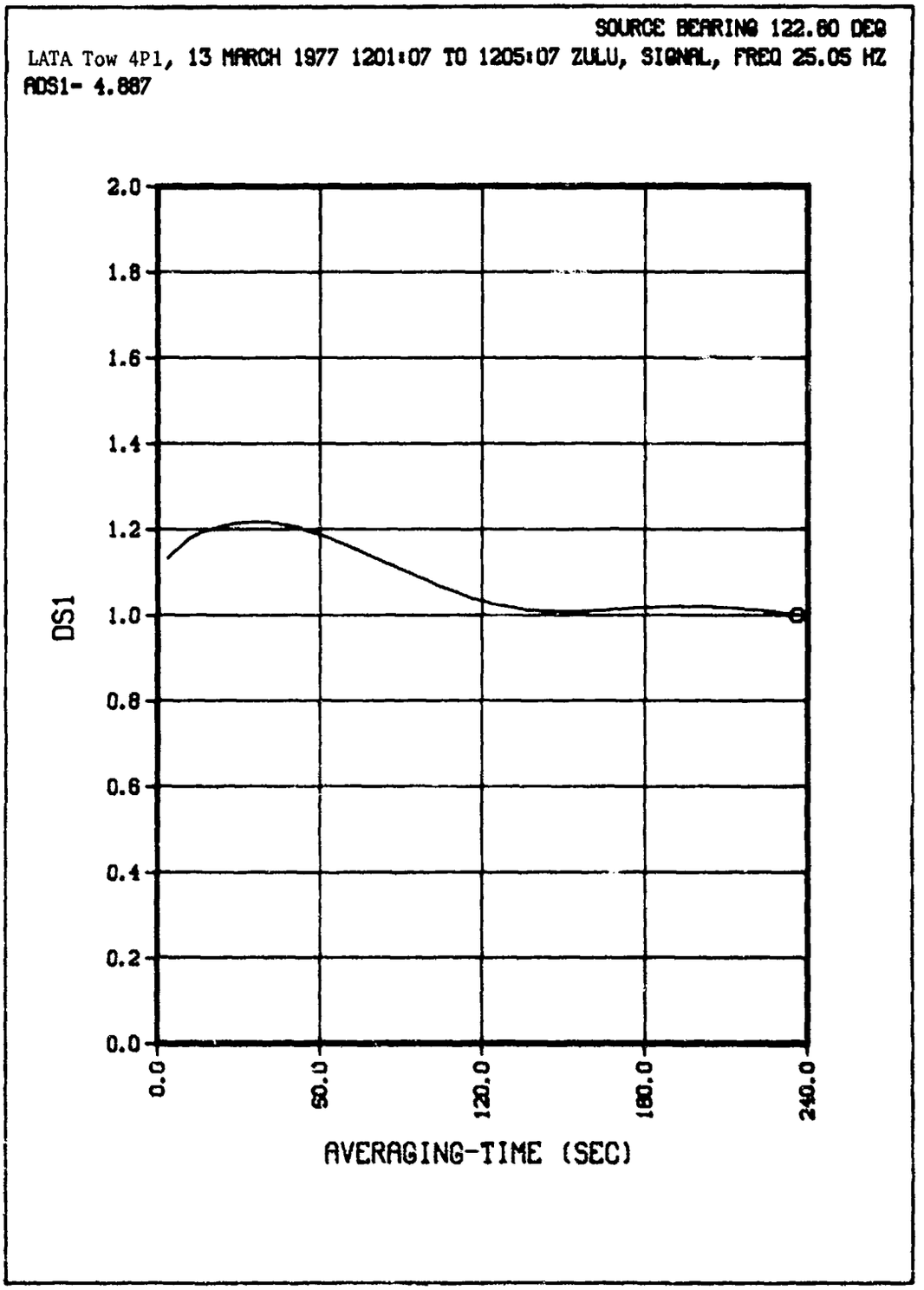

(CONFIDENTIAL)

(U) Figure 20e. Amplitude time stability.

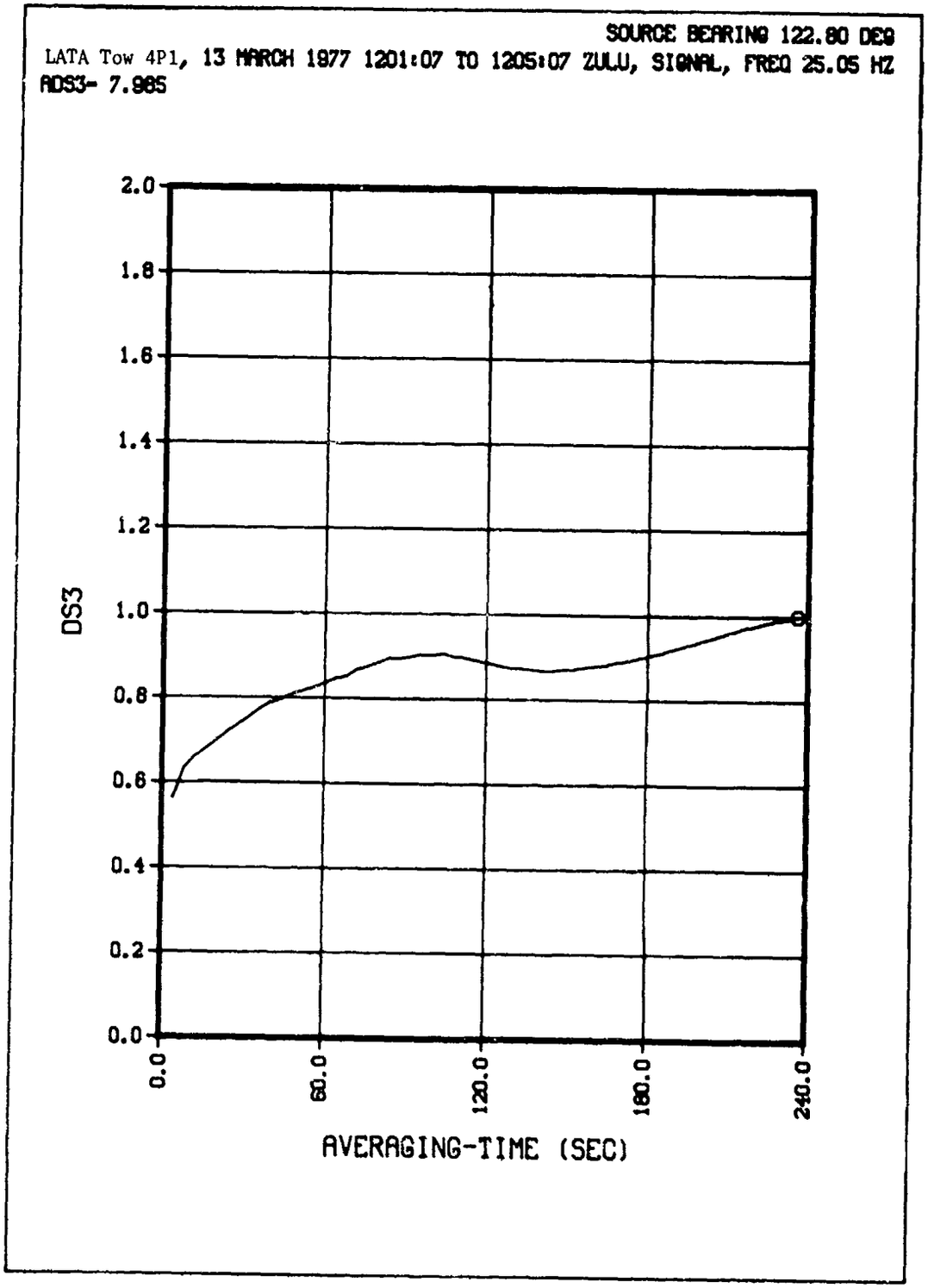

(CONFIDENTIAL)

(U) Figure 20f. Phase time stability.

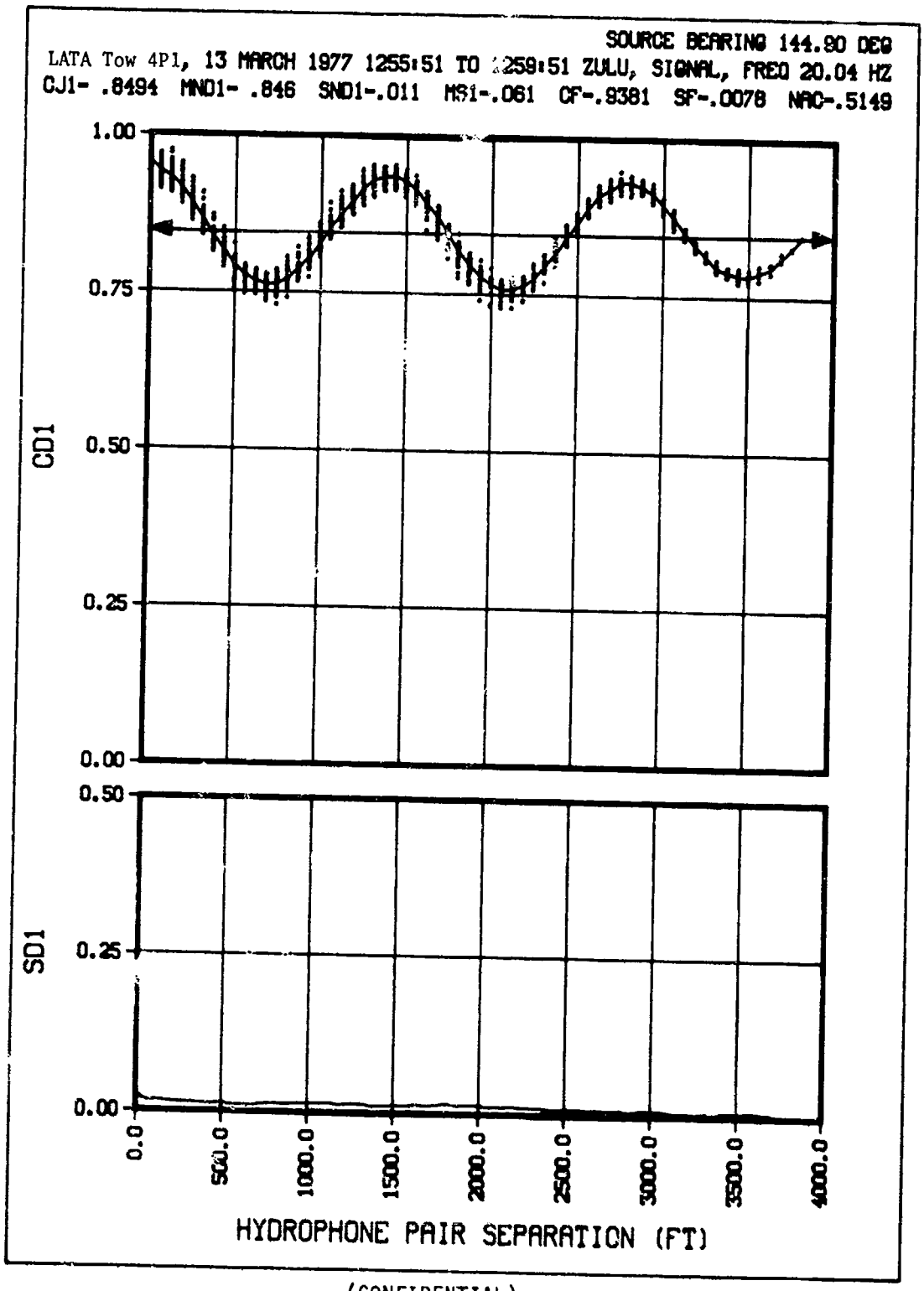

(CONFIDENTIAL)

(U) Figure 21a. Normalized amplitude covariance.

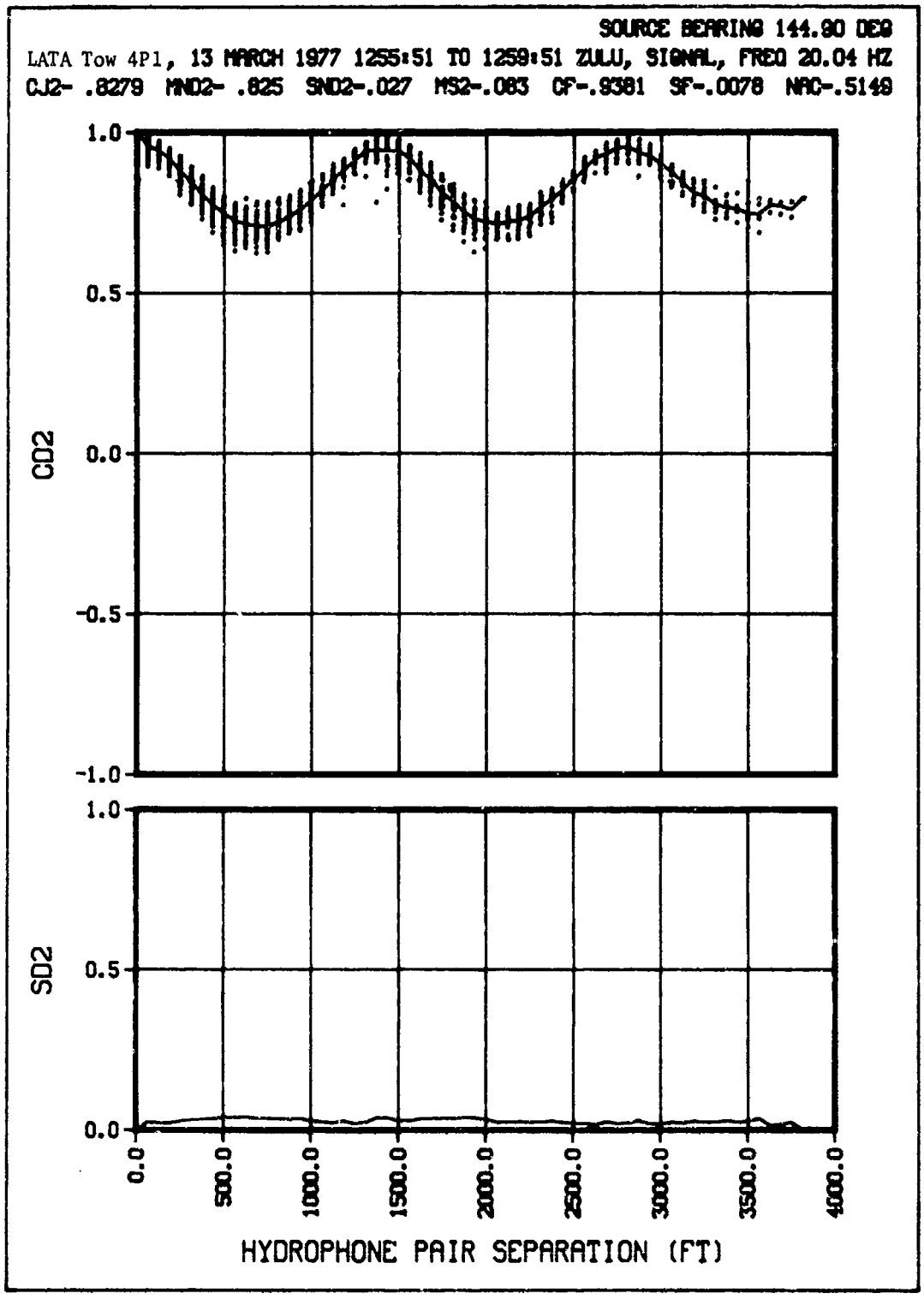

(CONFIDENTIAL)

(U) Figure 21b. Array phase coherence.

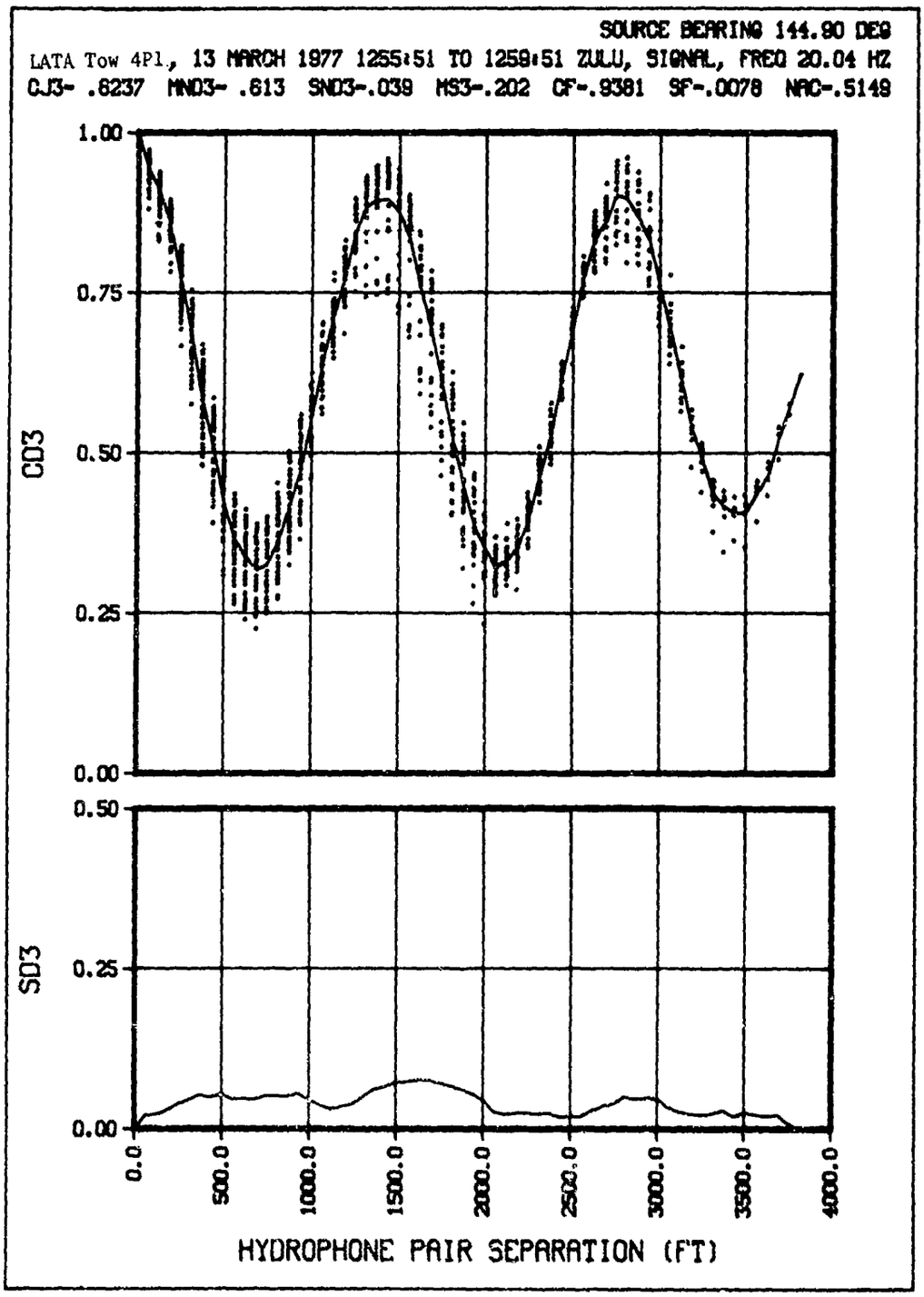

(CONFIDENTIAL)

(U) Figure 21c. Classical coherence.

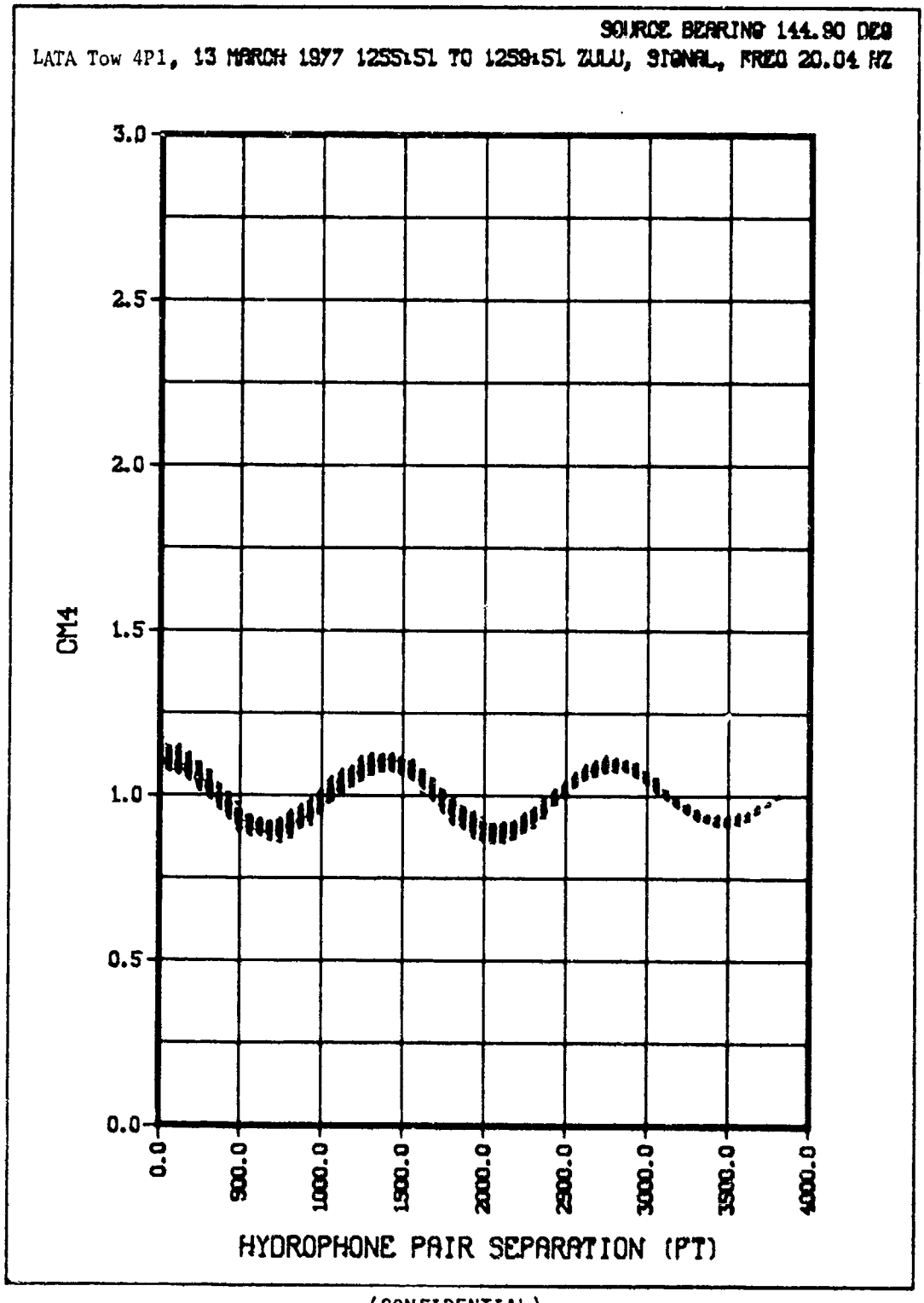

(CONFIDENTIAL)

(U) Figure 21d. Array amplitude covariance.

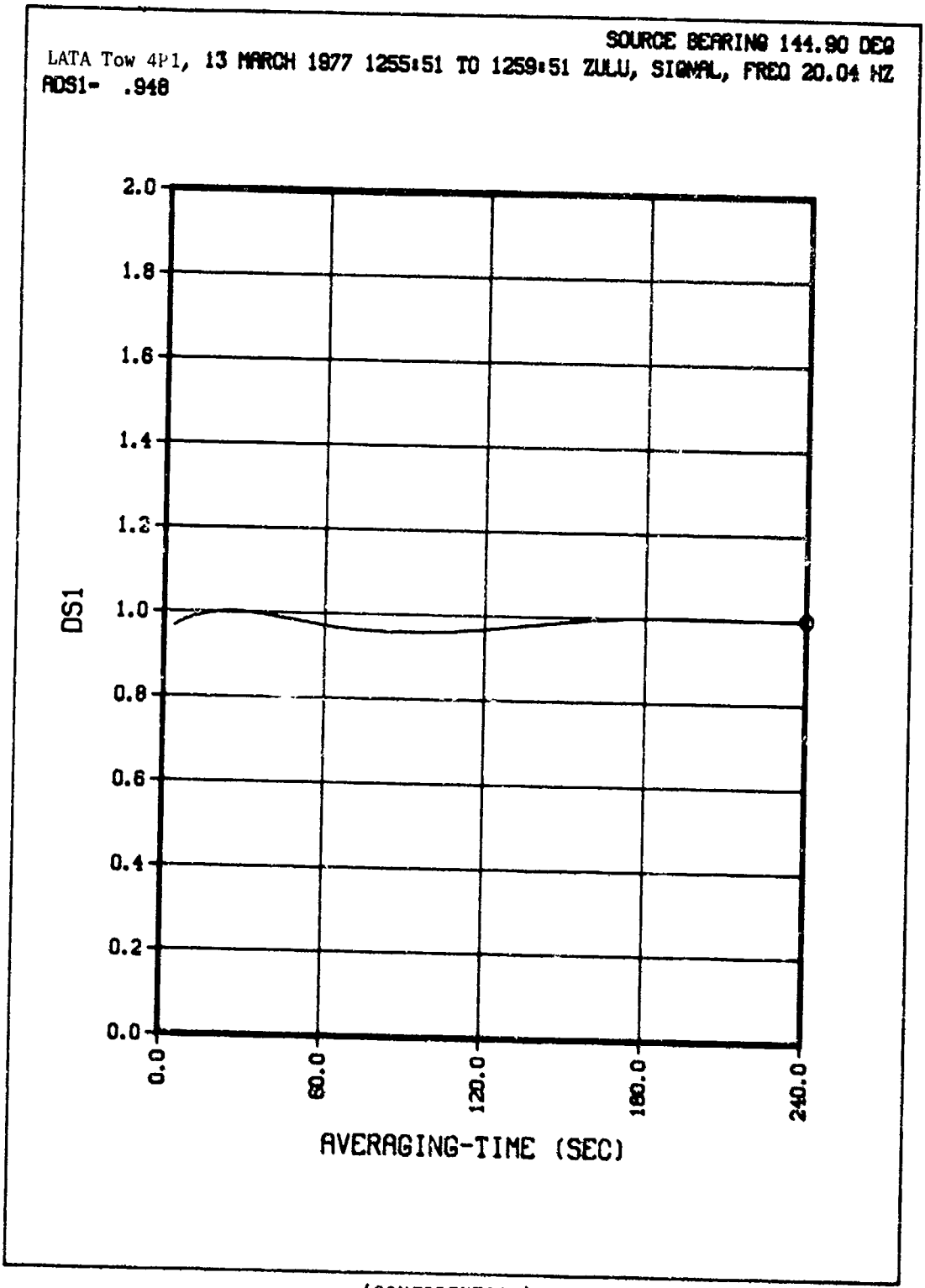

(CONFIDENTIAL)

(U) Figure 21e. Amplitude time stability.

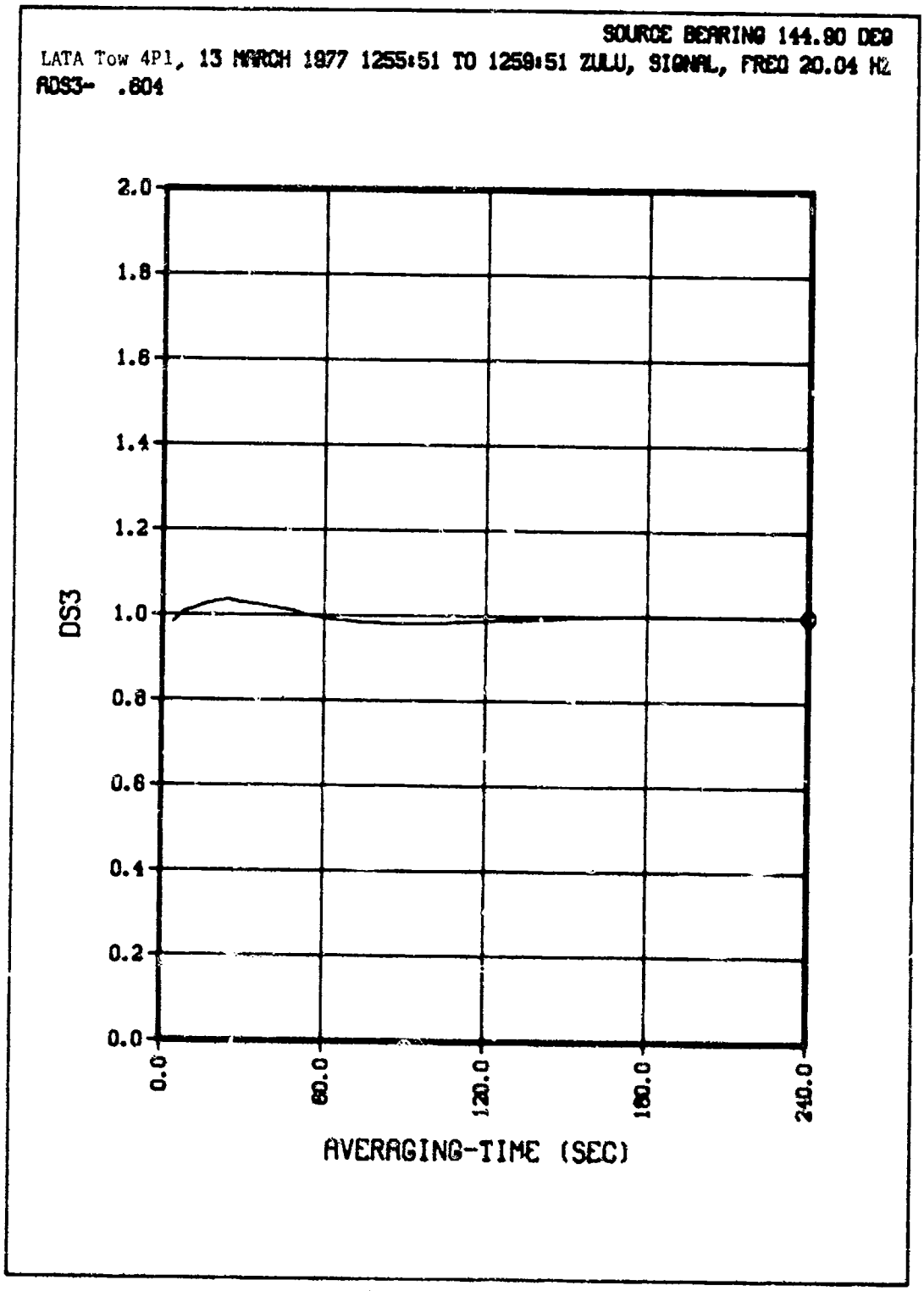

(CONFIDENTIAL)

(U) Figure 21f. Phase time stability.

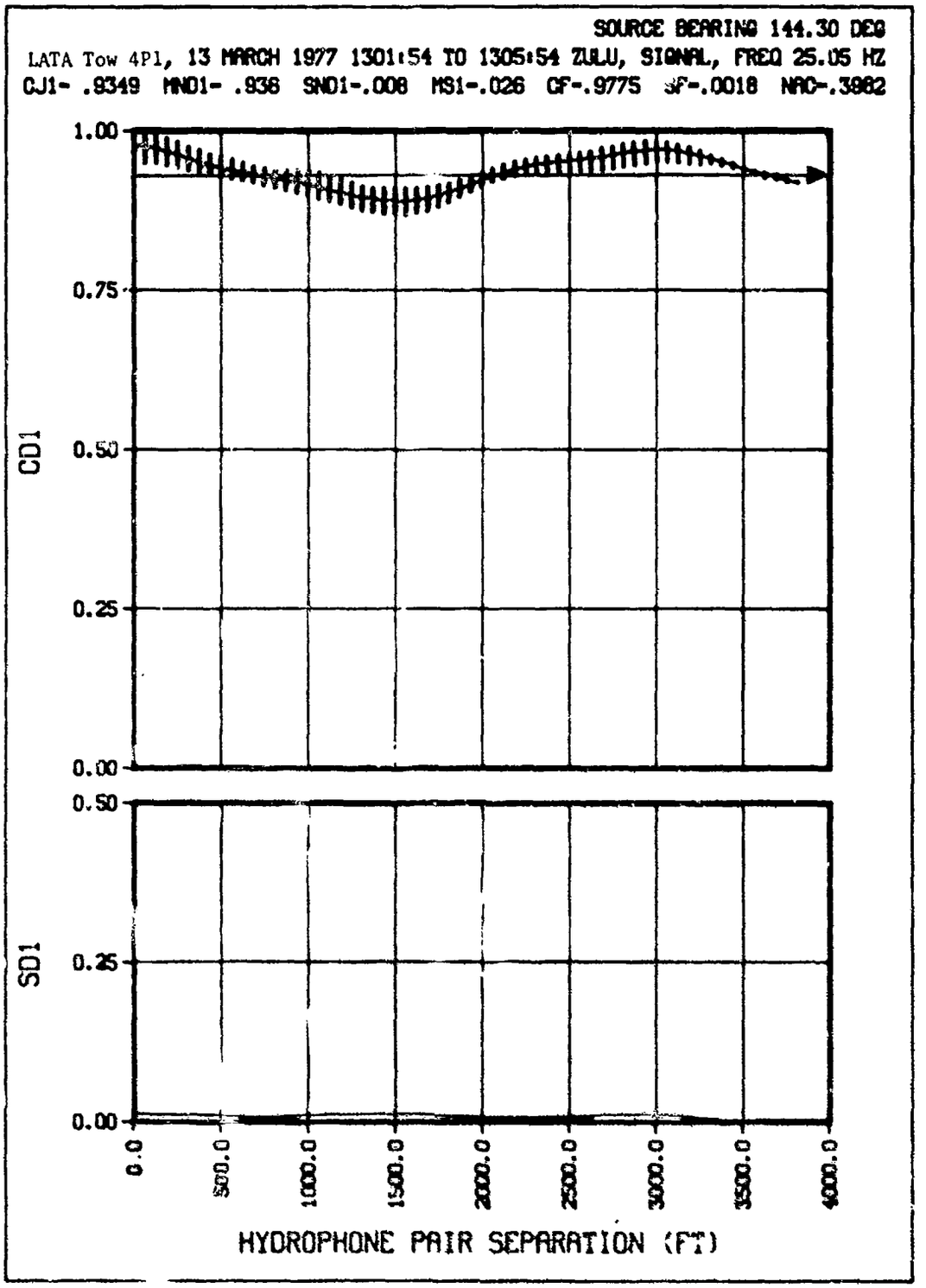

(CONFIDENTIAL)

(U) Figure 22a. Normalized amplitude covariance.

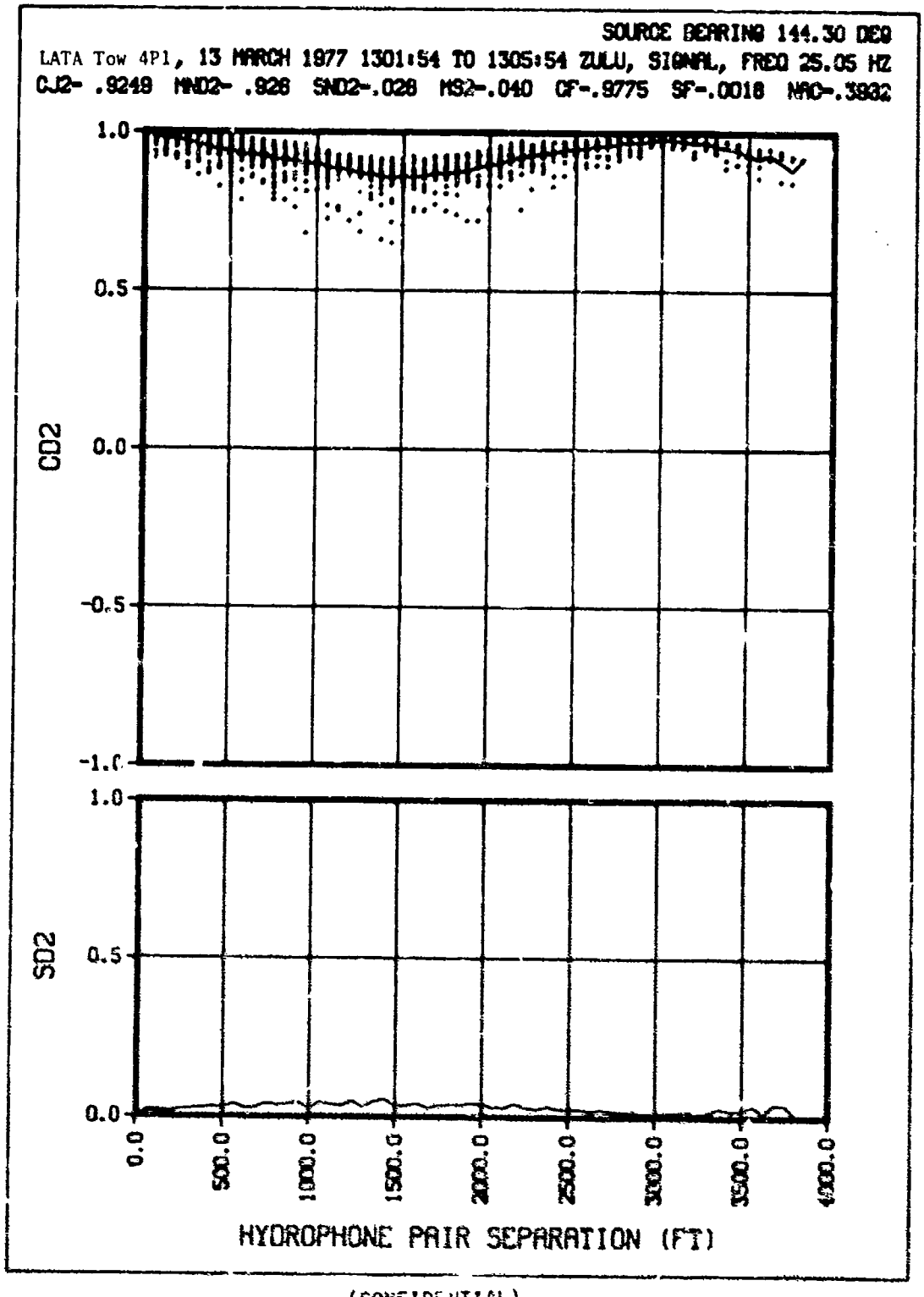

(CONFIDENTIAL)

(U) Figure 22b. Array phase coherence.

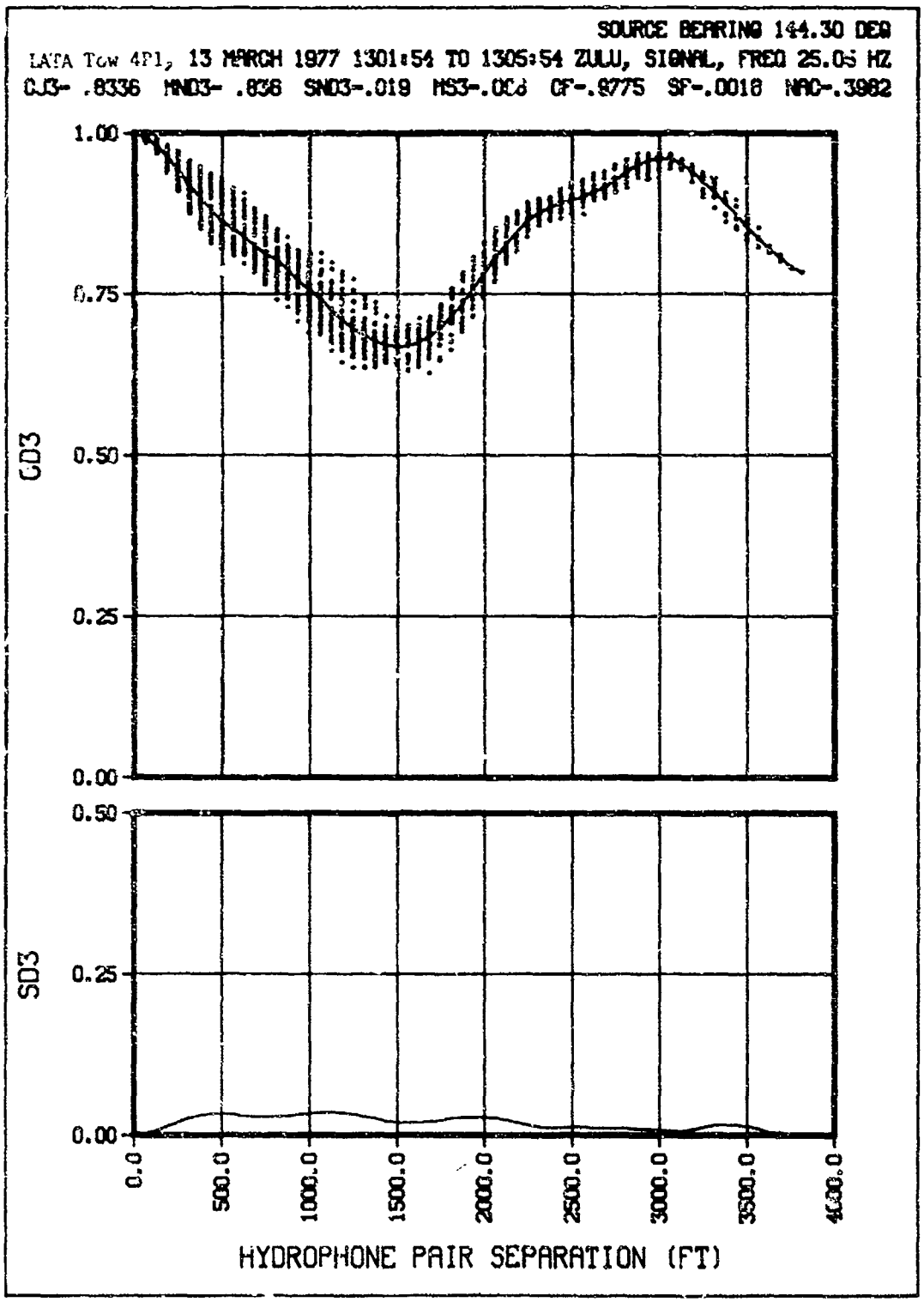

(CONFIDENTIAL)

(U) Figure 22c. Classical coherence.

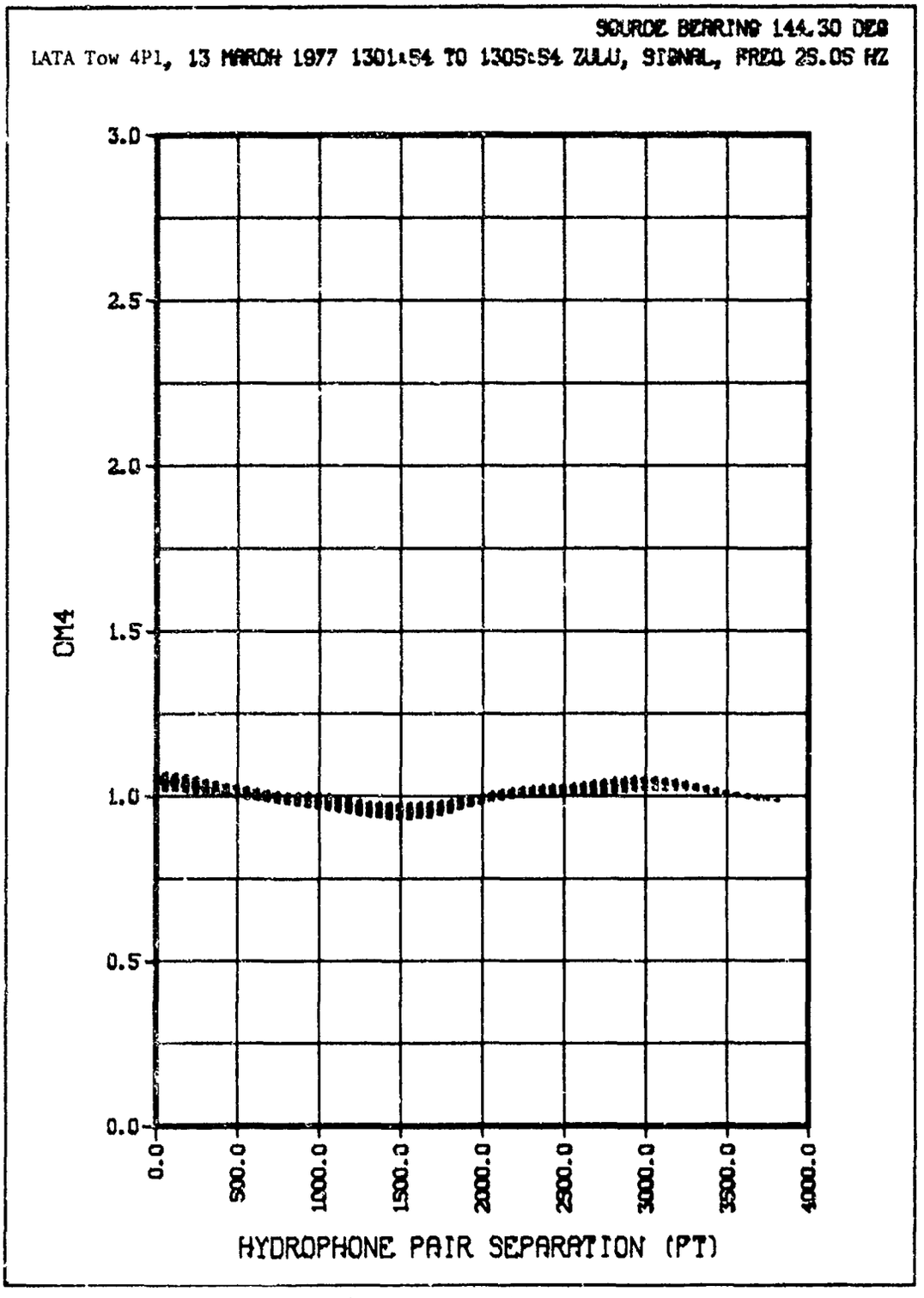

(CONFIDENTIAL)

(U) Figure 22d. Array amplitude covariance.

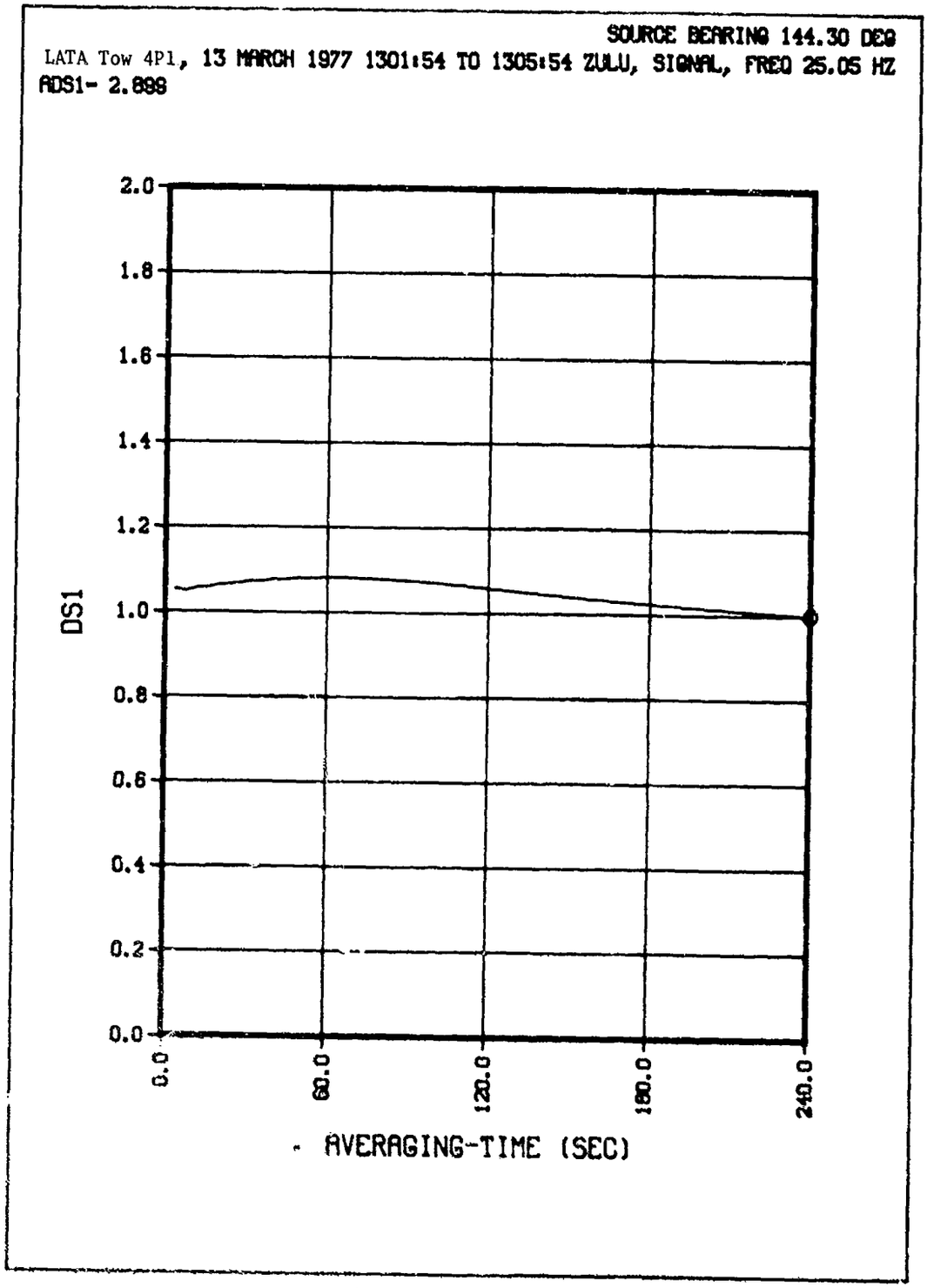

(CONFIDENTIAL)

(U) Figure 22e. Amplitude time stability.

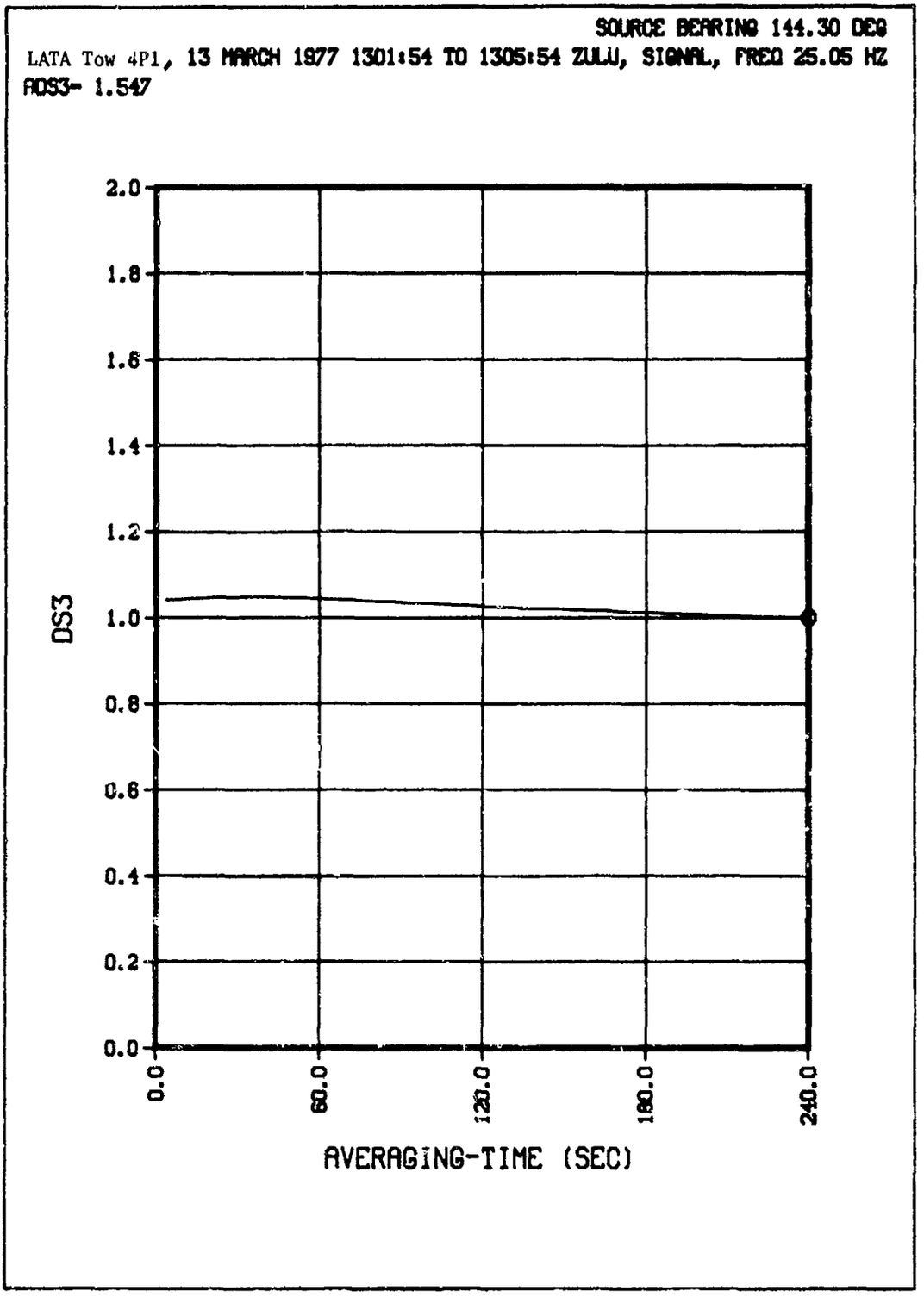

(CONFIDENTIAL)

(U) Figure 22f. Phase time stability.

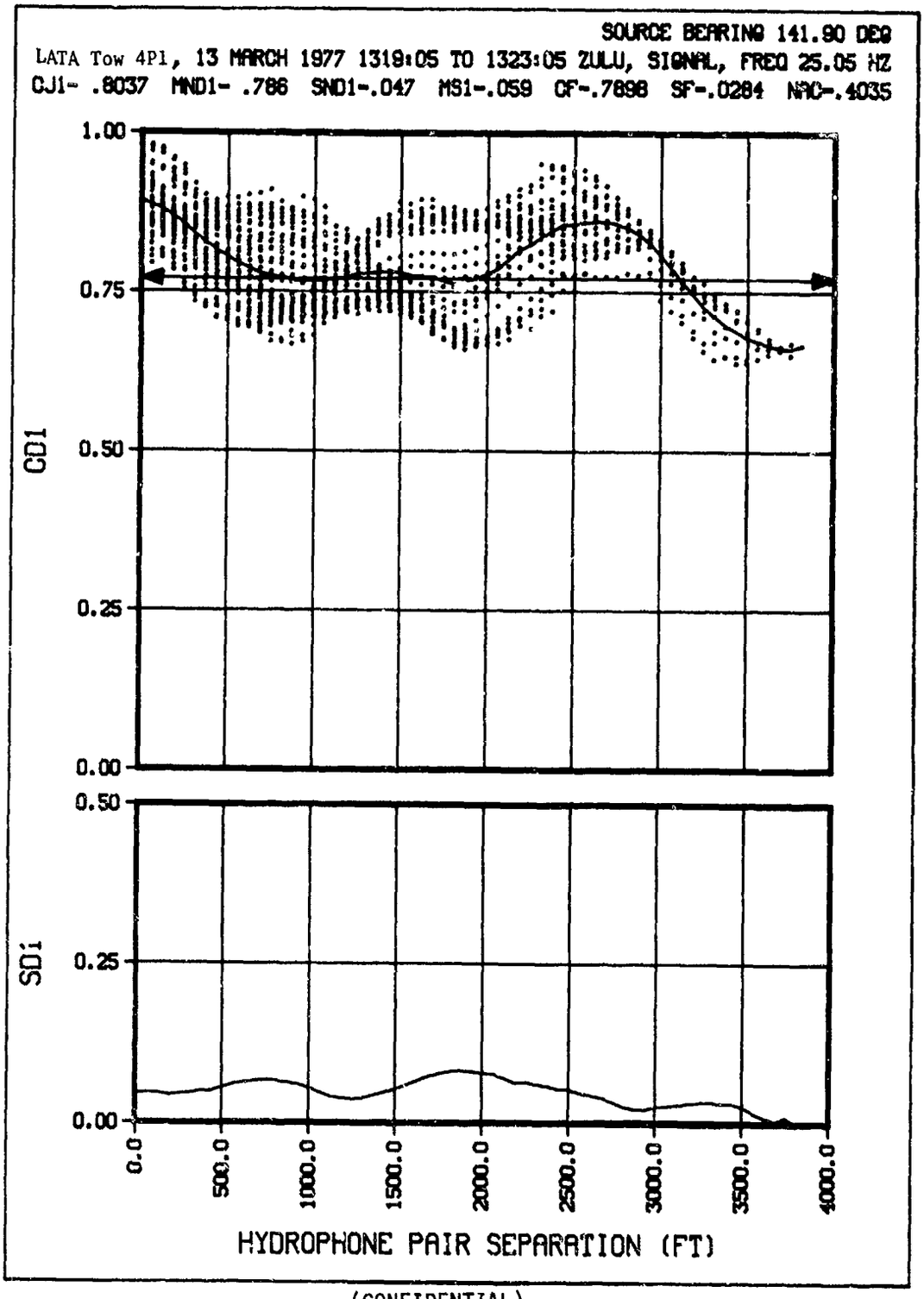

(CONFIDENTIAL)

(U) Figure 23a. Normalized amplitude covariance.

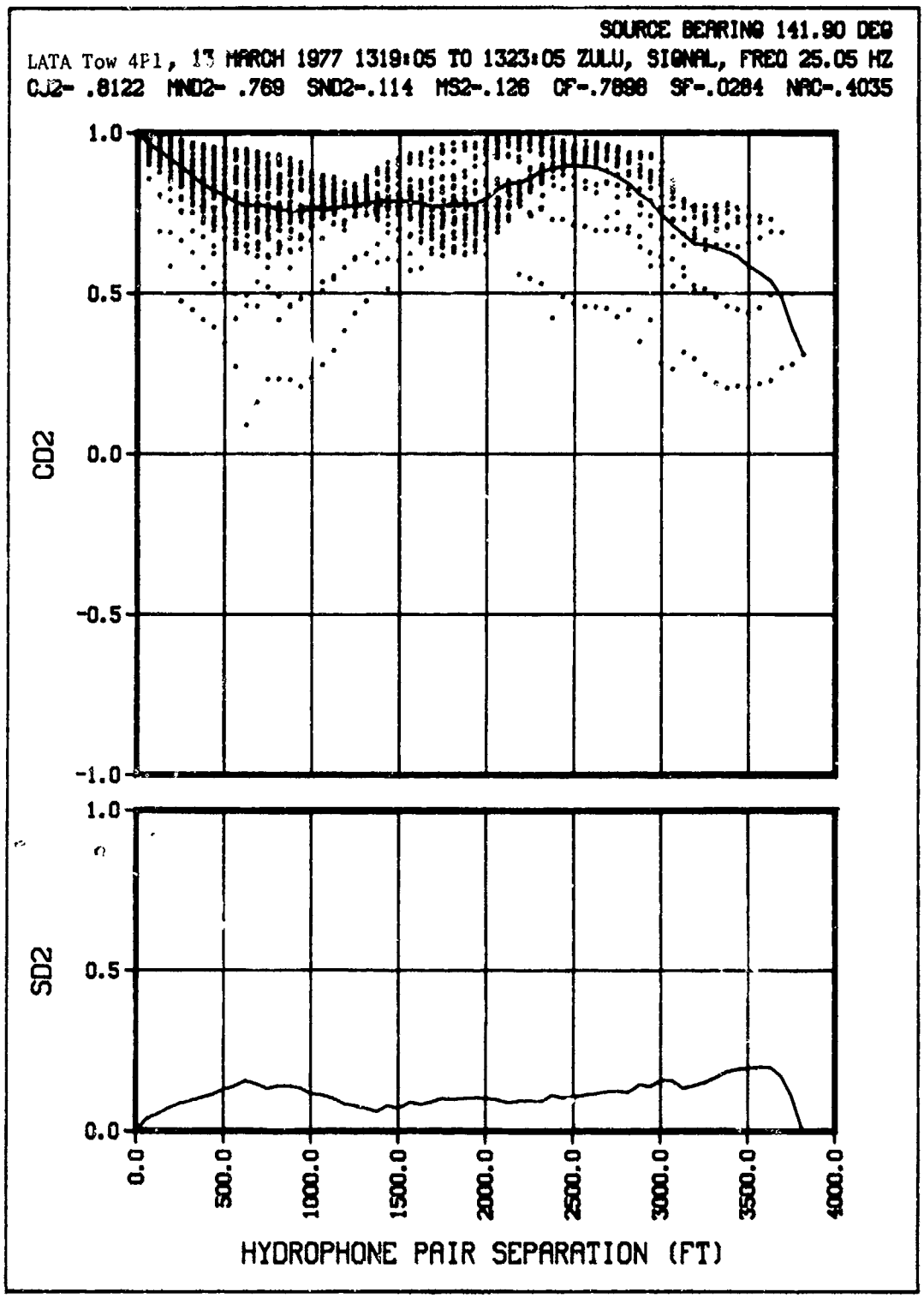

(CONFIDENTIAL)

(U) Figure 23b. Array phase coherence.

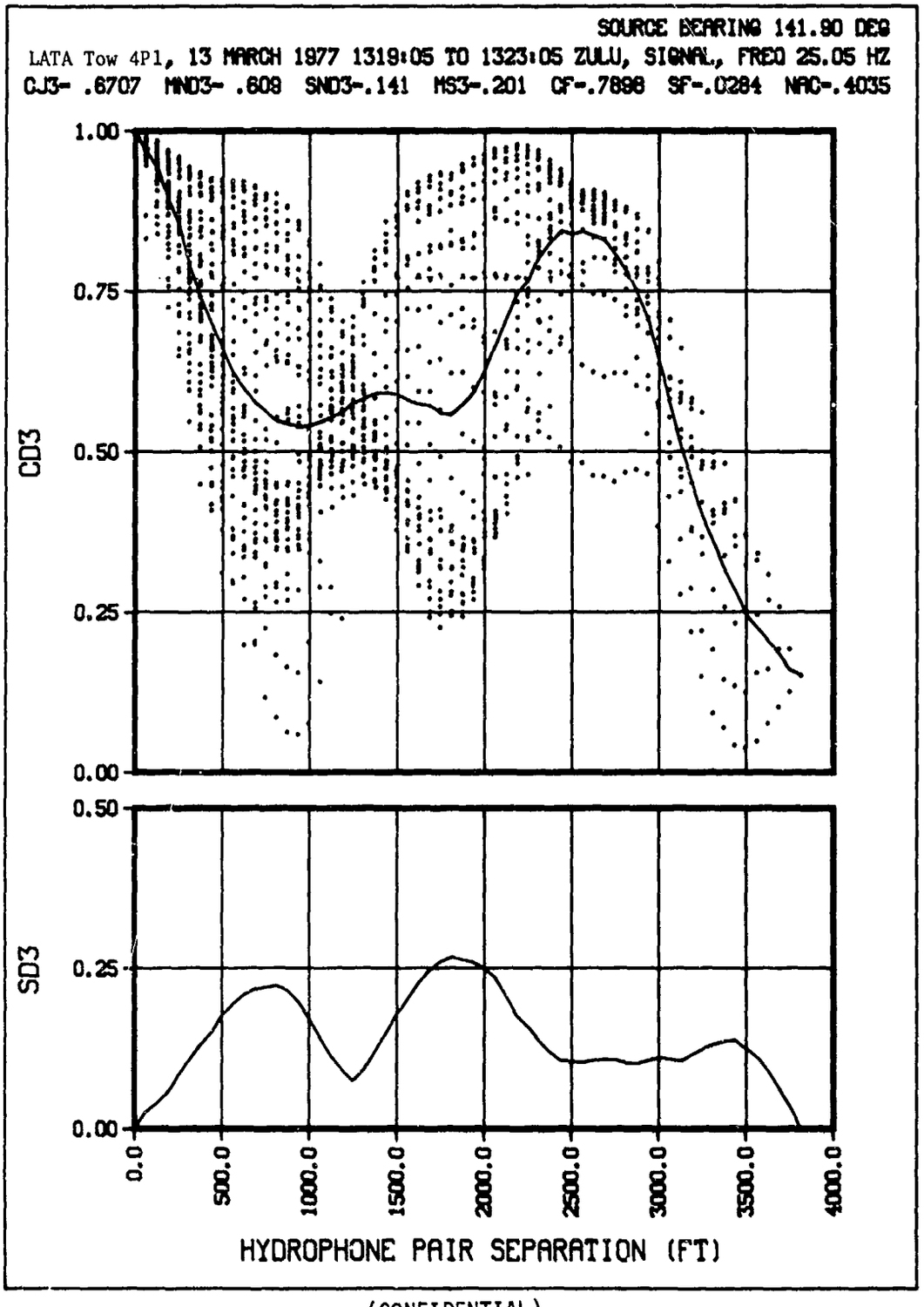

(CONFIDENTIAL)

(U) Figure 23c. Classical coherence.

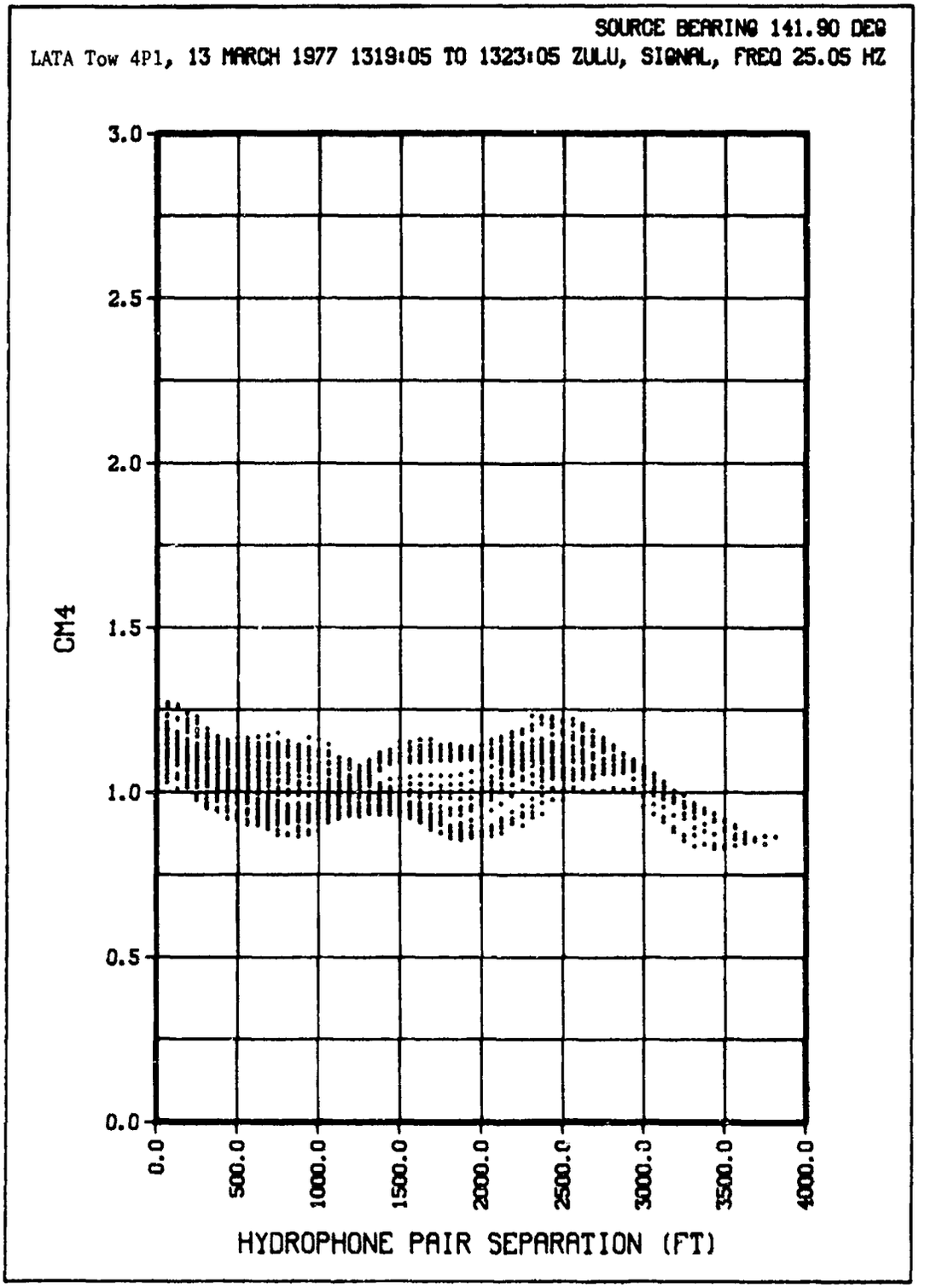

(CONFIDENTIAL)

(U) Figure 23d. Array amplitude covariance.

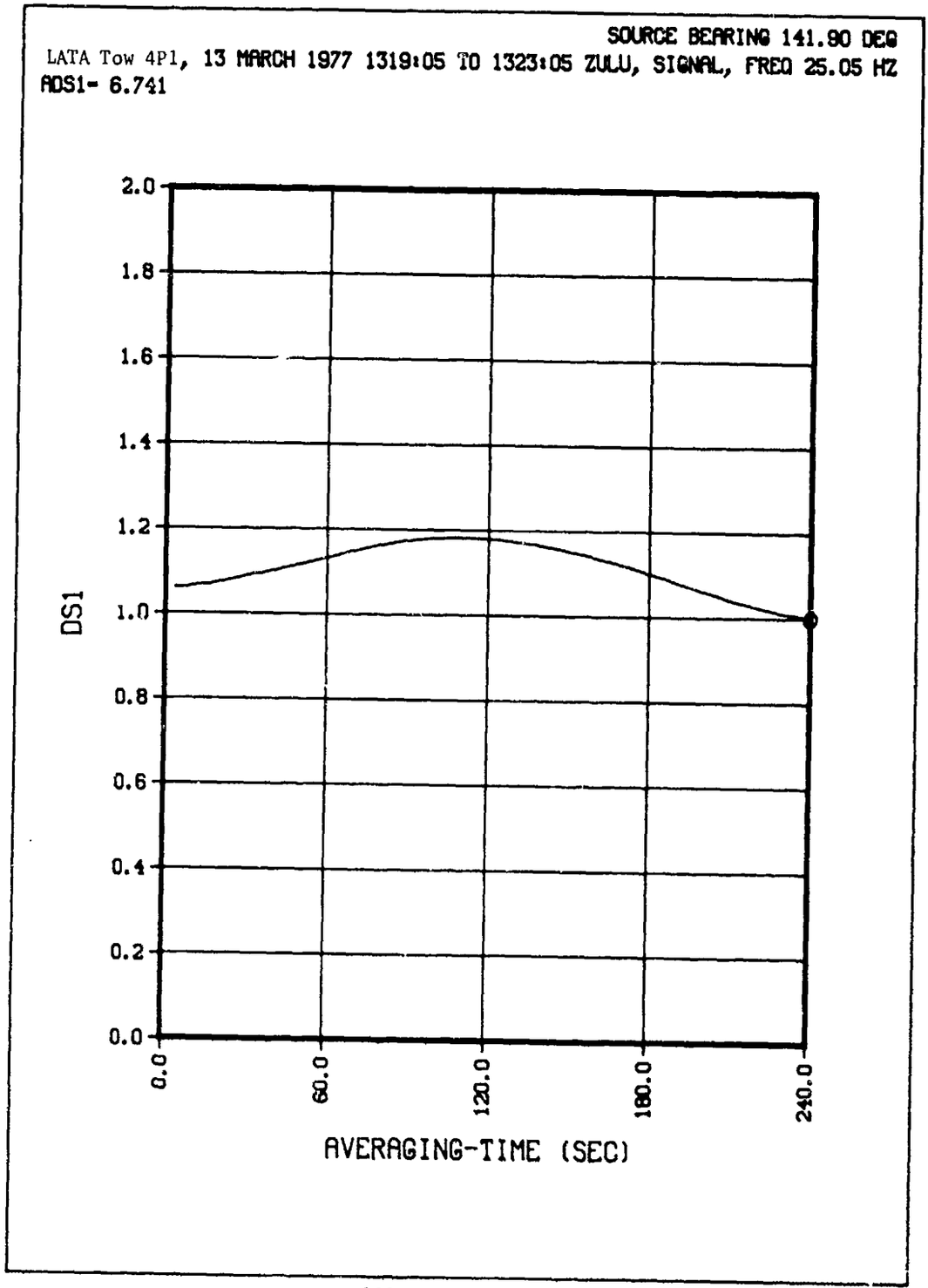

(CONFIDENTIAL)

(U) Figure 23e. Amplitude time stability.

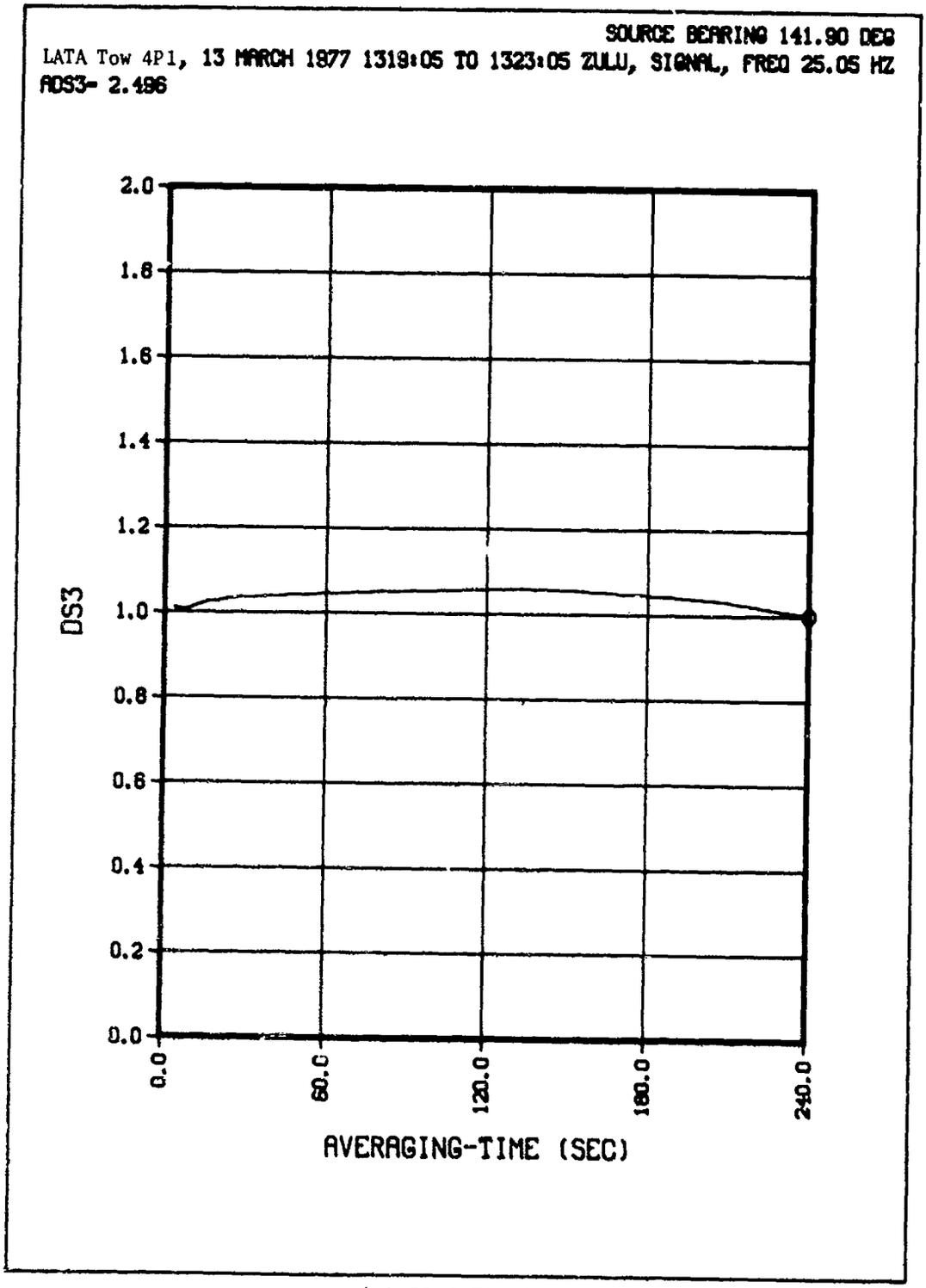

(CONFIDENTIAL)

(U) Figure 23f. Phase time stability.

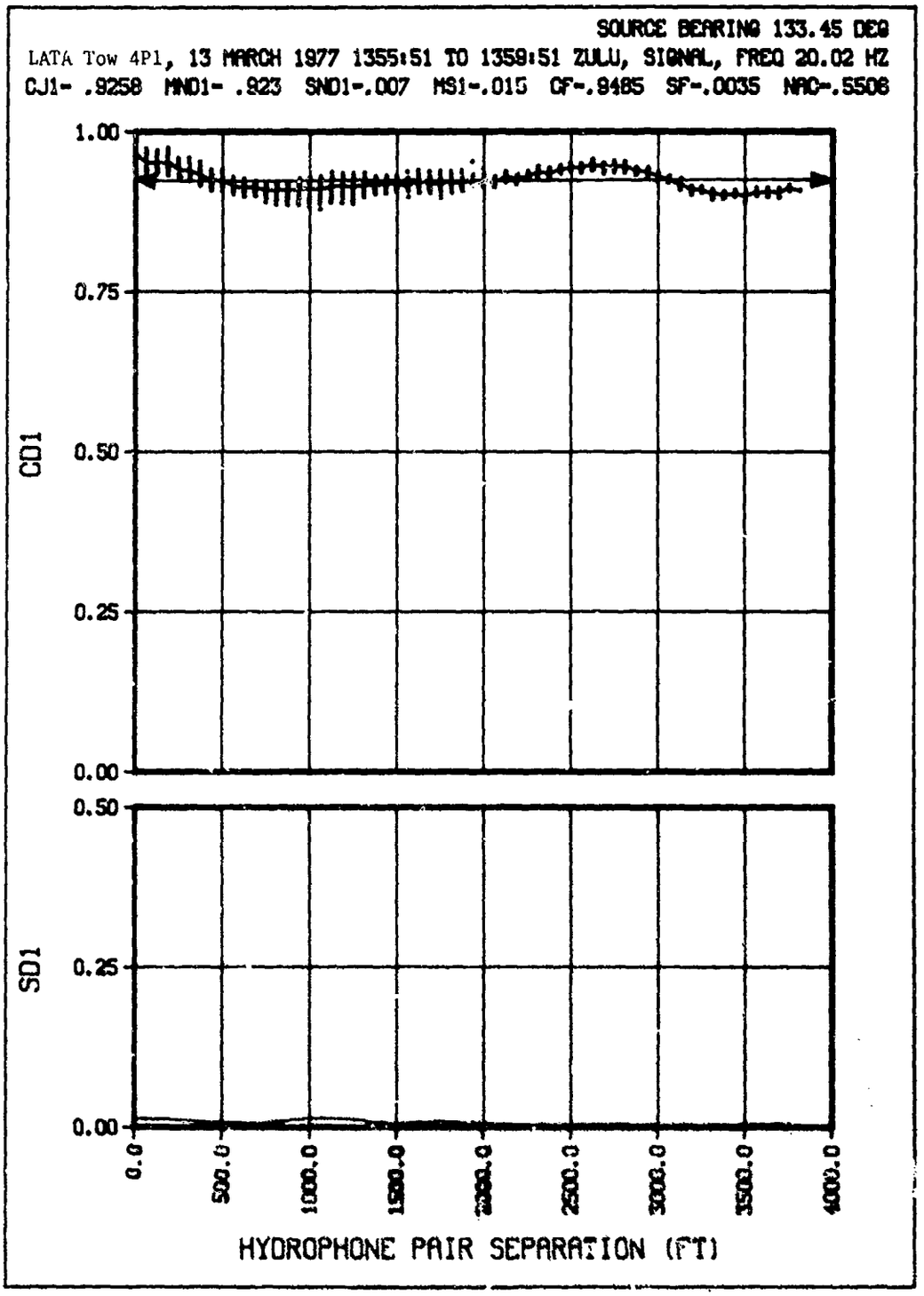

(CONFIDENTIAL)

(U) Figure 24a. Normalized amplitude covariance.

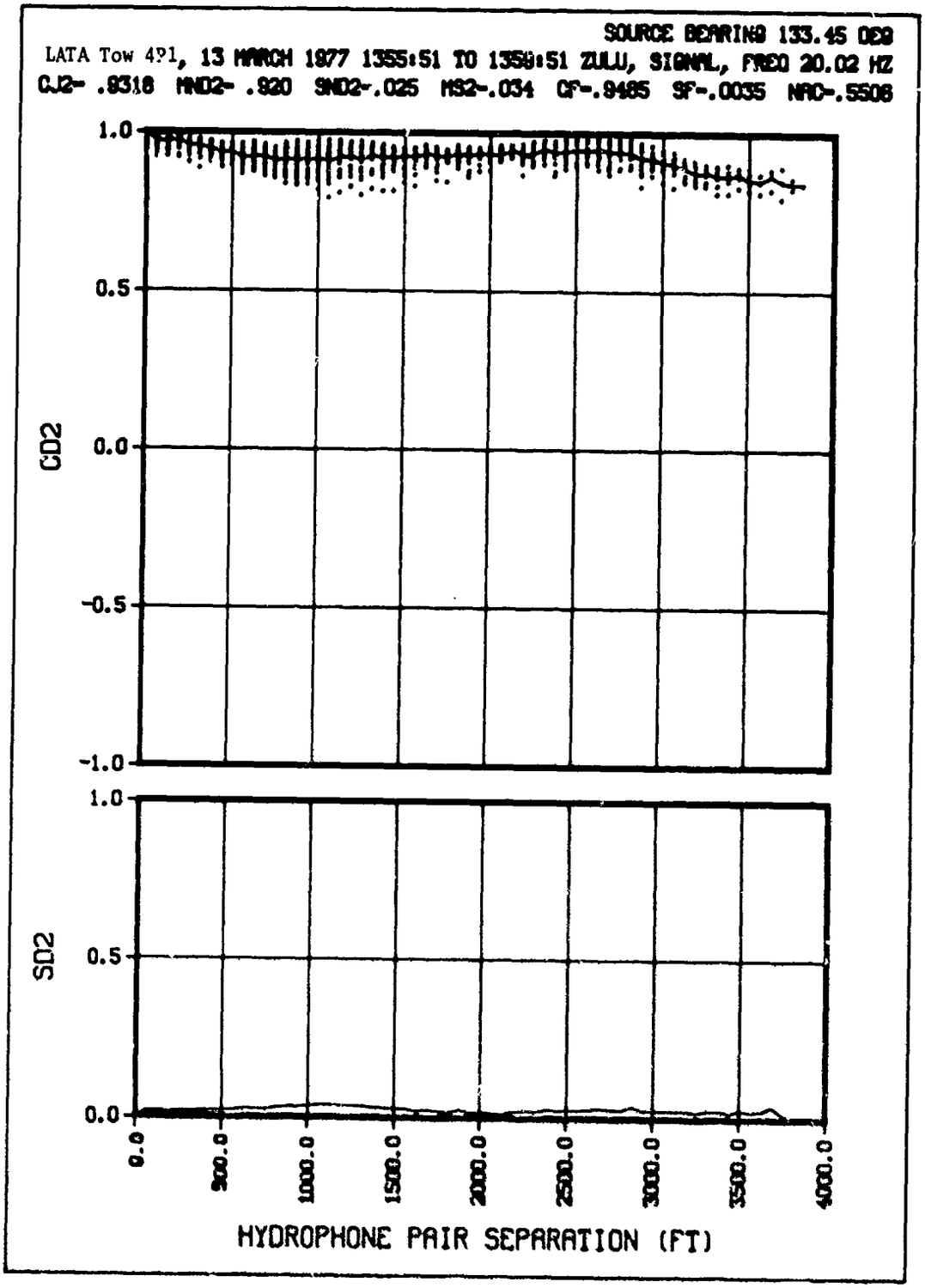

(CONFIDENTIAL)

(U) Figure 24b Array phase coherence.

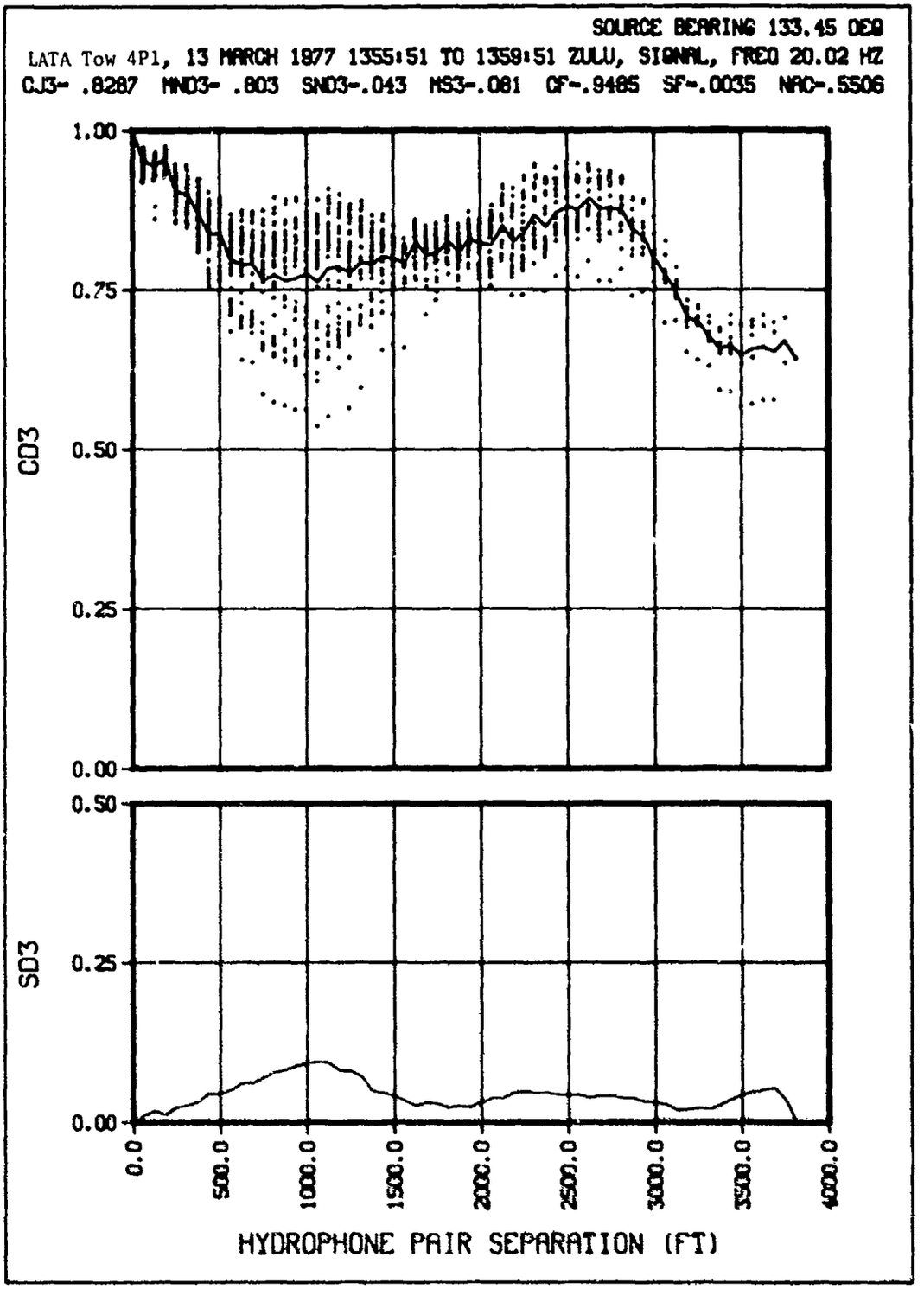

(CONFIDENTIAL)

(U) Figure 24c. Classical coherence.

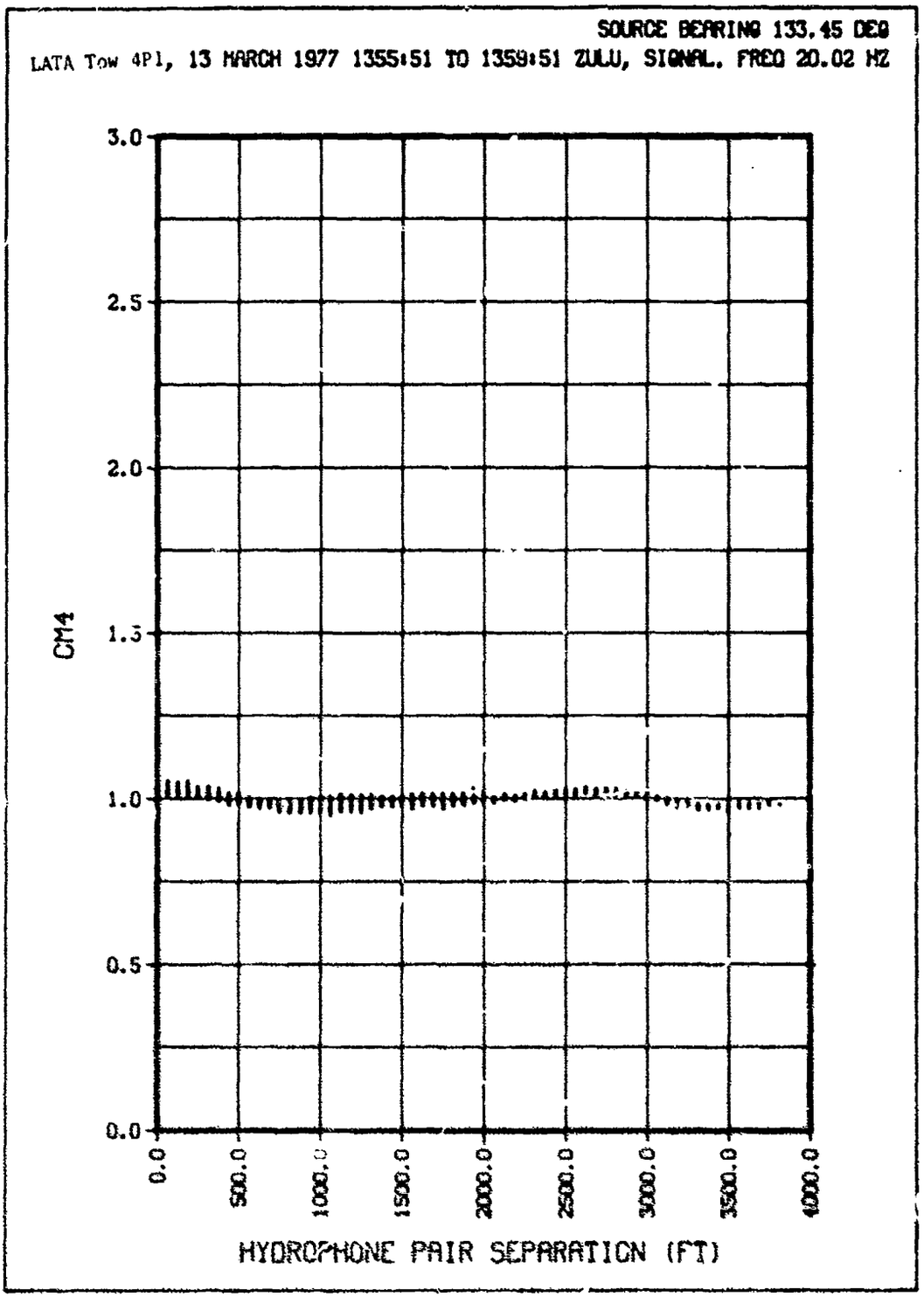

(CONFIDENTIAL)

(U) Figure 24d. Array amplitude covariance.

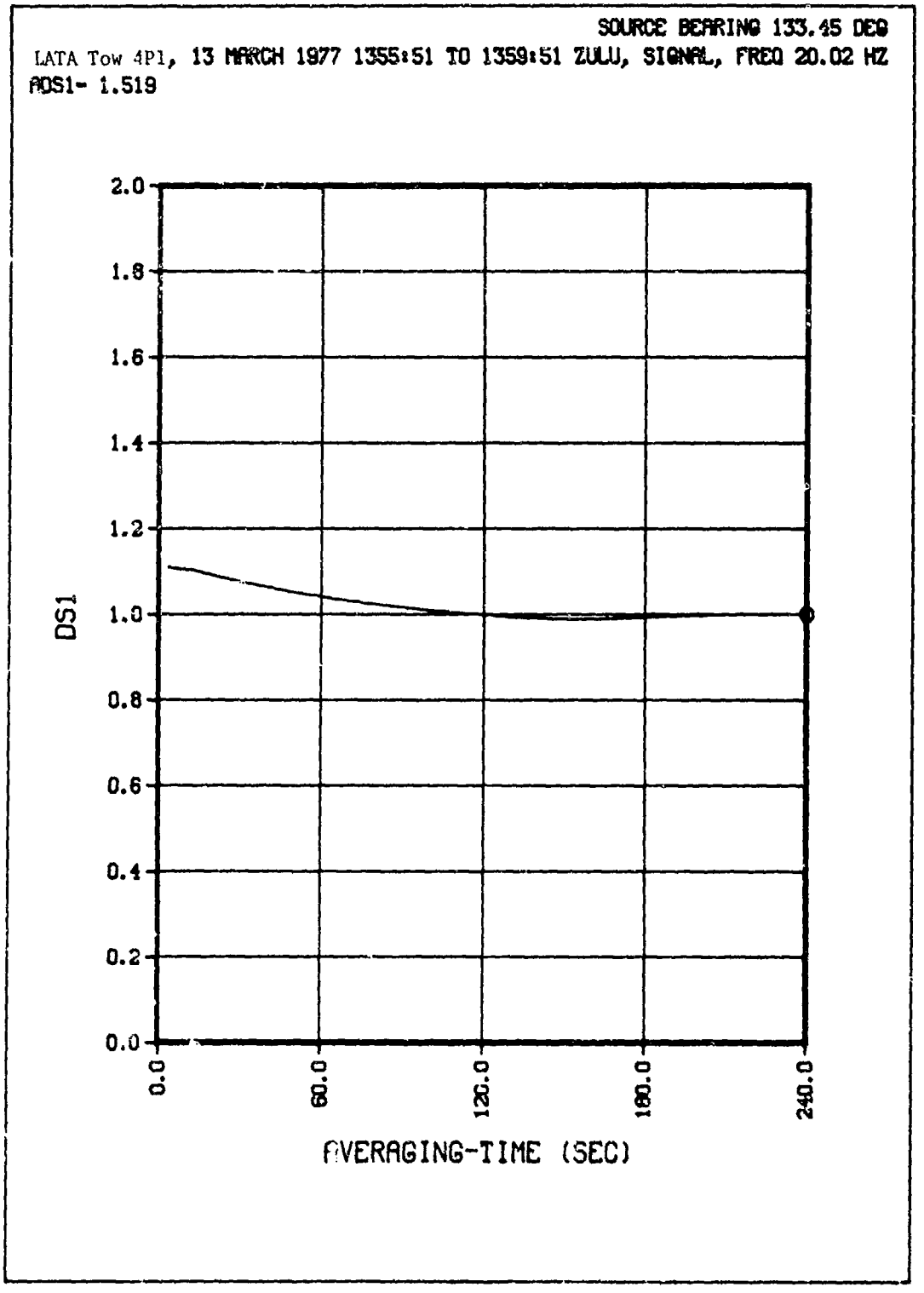

(CONFIDENTIAL)

(U) Figure 24e. Amplitude time stability.

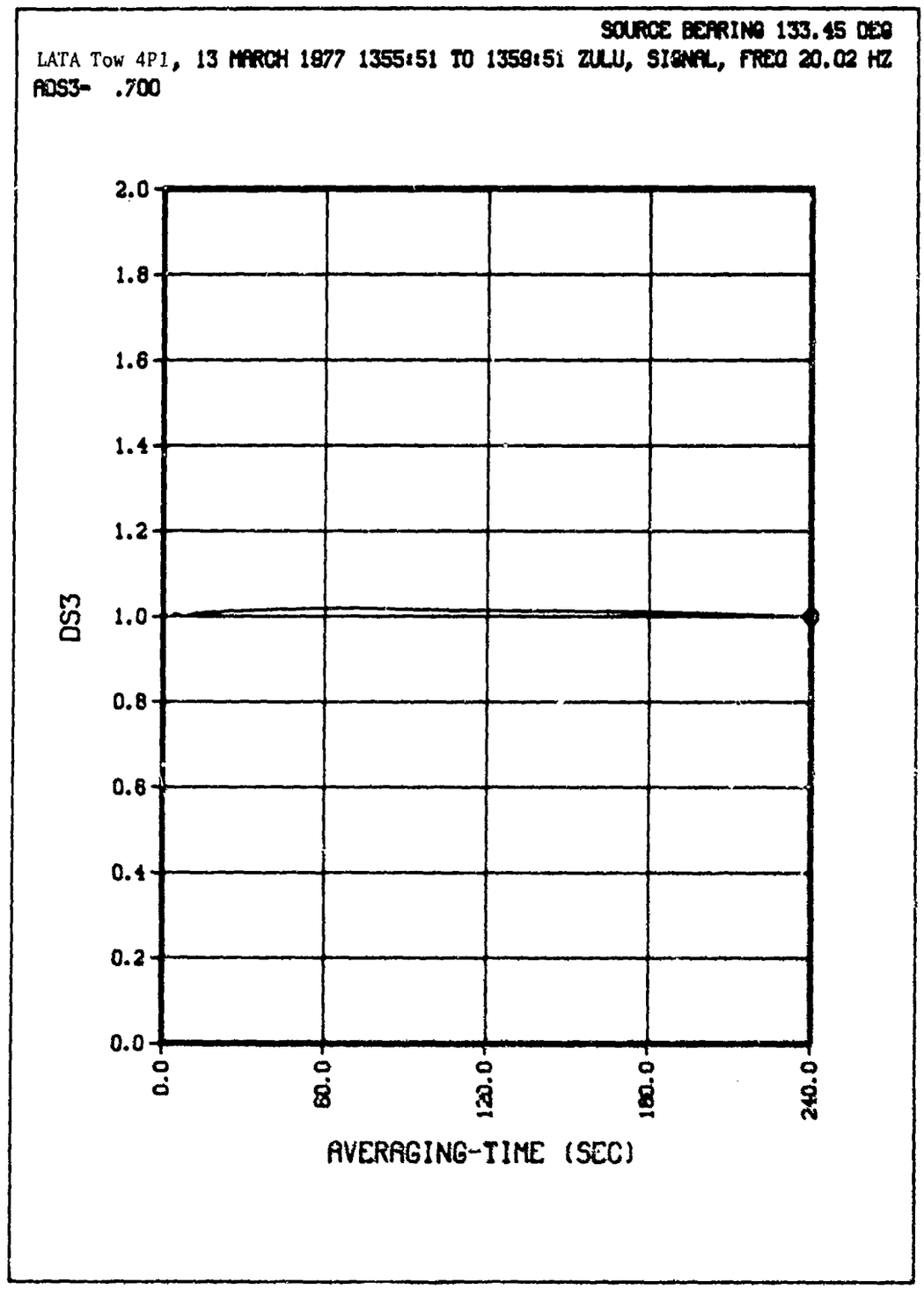

(CONFIDENTIAL)

(U) Figure 24f. Phase time stability.

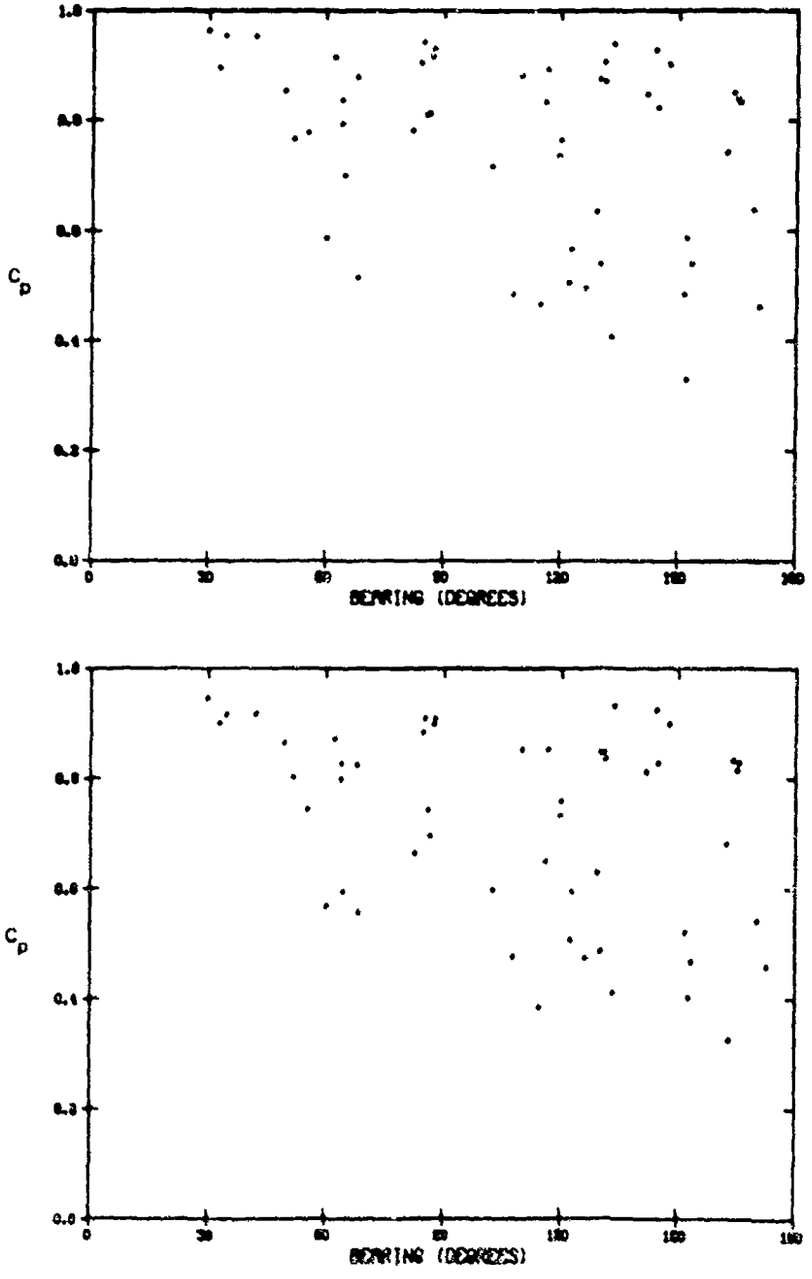

(CONFIDENTIAL)

(U) Figure 25. Comparison of C_p versus source bearing for Tow 4P1 for the LATA Subset (upper plot) and the ordinary LATA (lower plot).

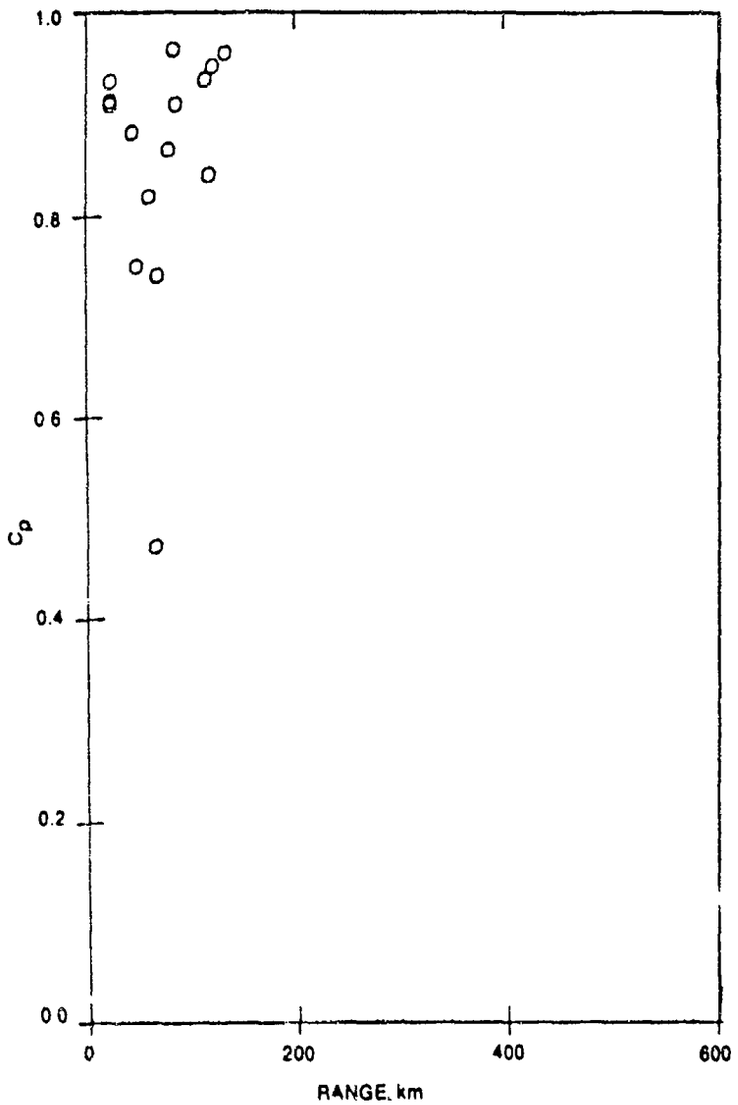

(CONFIDENTIAL)

(C) Figure 26. Phase coherence as a function of range; OAMS array; Tow 4P1, 25 Hz; 13 March 1977.

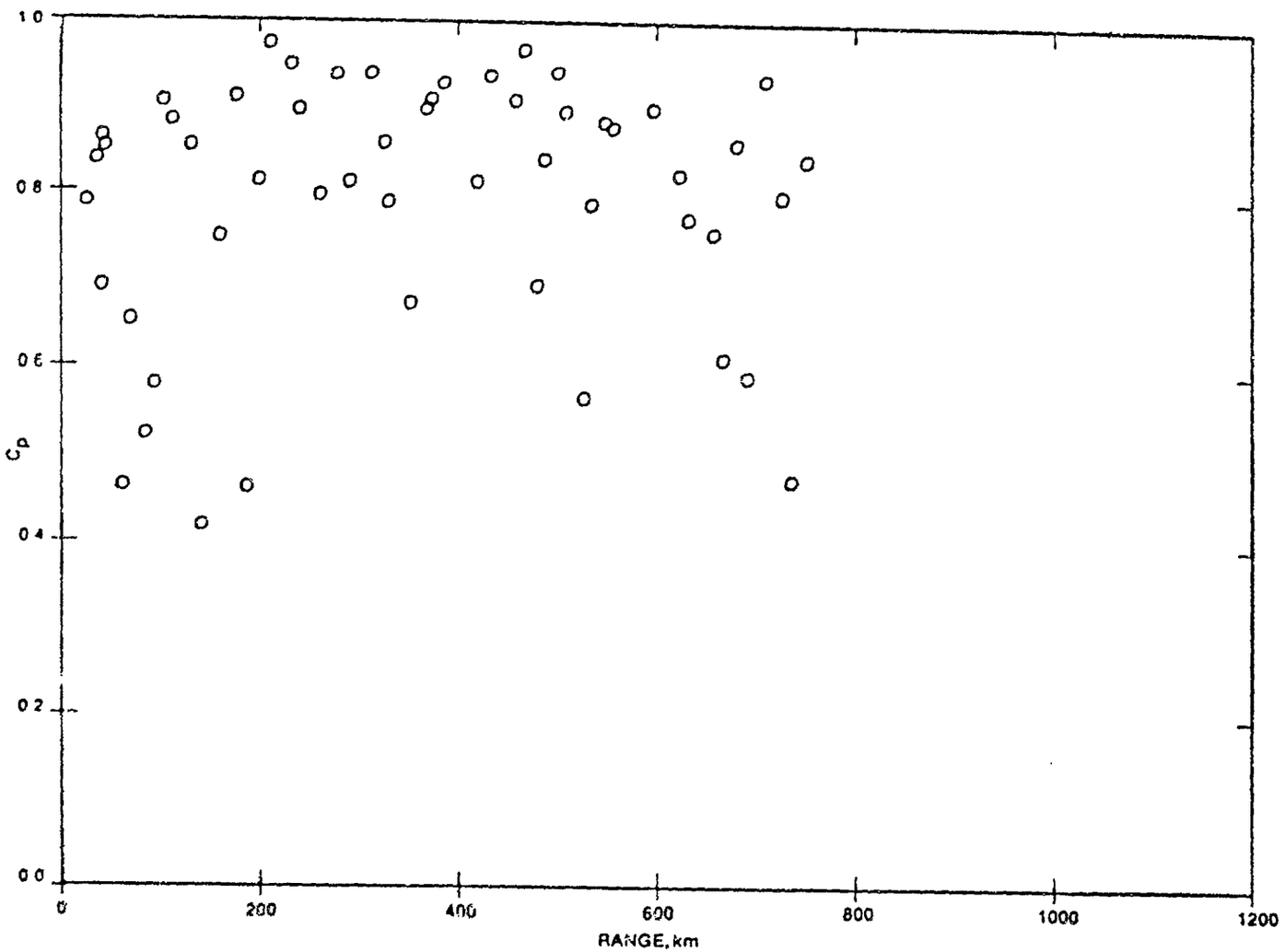

(CONFIDENTIAL)

(C) Figure 27. Phase coherence as a function of range, OAMS array; 5P1 site 5, 25 Hz, 12-14 April 1977.

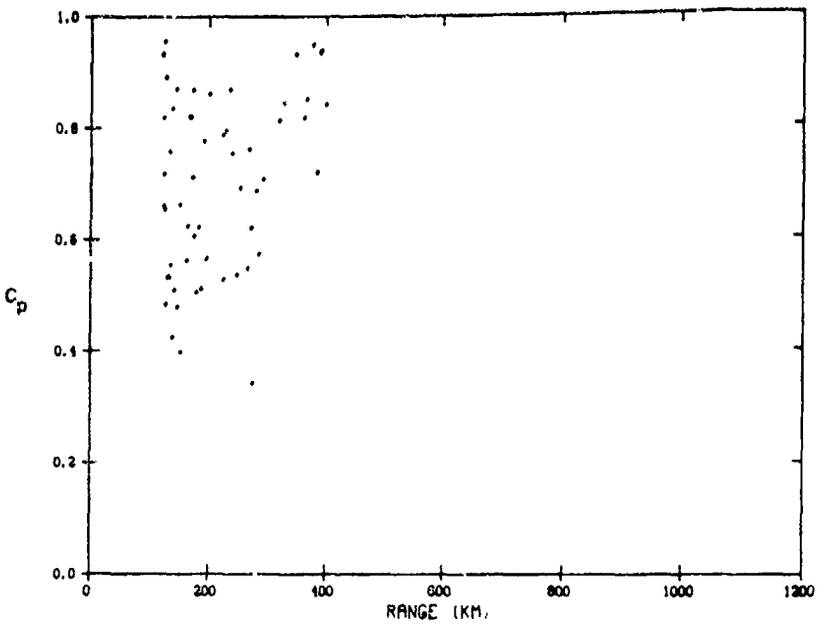

(CONFIDENTIAL)

(C) Figure 28. Phase coherence versus range. LATA; Tow 2P3A; 25 and 20 Hz.

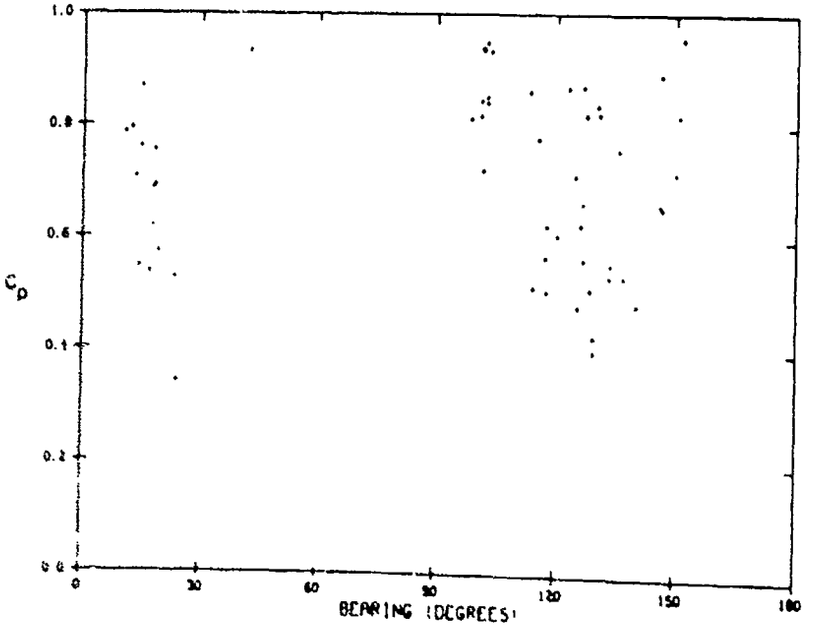

(CONFIDENTIAL)

(C) Figure 29. Phase coherence versus source bearing. LATA; Tow 2P3A; 25 and 20 Hz.

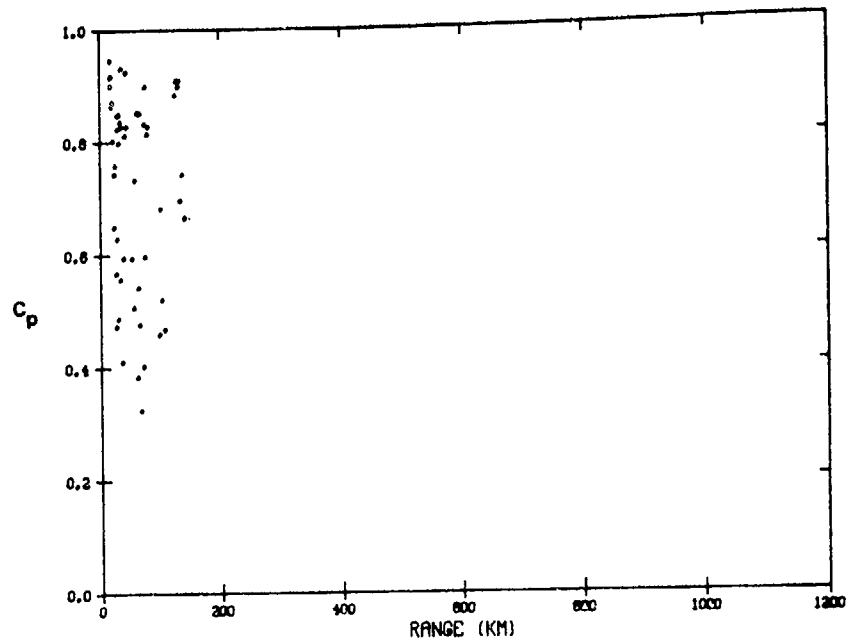

(CONFIDENTIAL)

(C) Figure 30. Phase coherence versus range. LATA; Tow 4P1; 25 and 20 Hz.

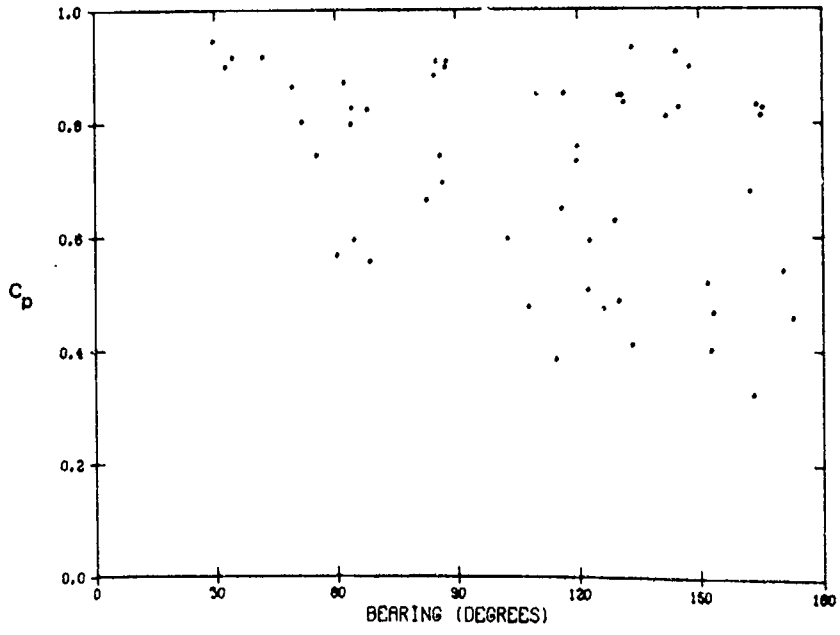

(CONFIDENTIAL)

(C) Figure 31. Phase coherence versus source bearing. LATA; Tow 4P1; 25 and 20 Hz.

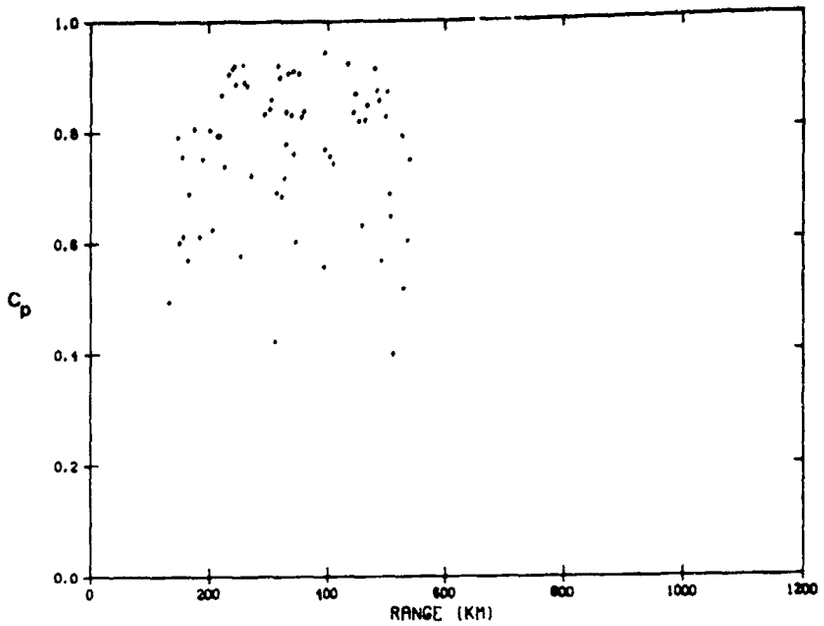

(CONFIDENTIAL)

(C) Figure 32. Phase coherence versus range. LATA; Tow 2P3; 25 and 20 Hz.

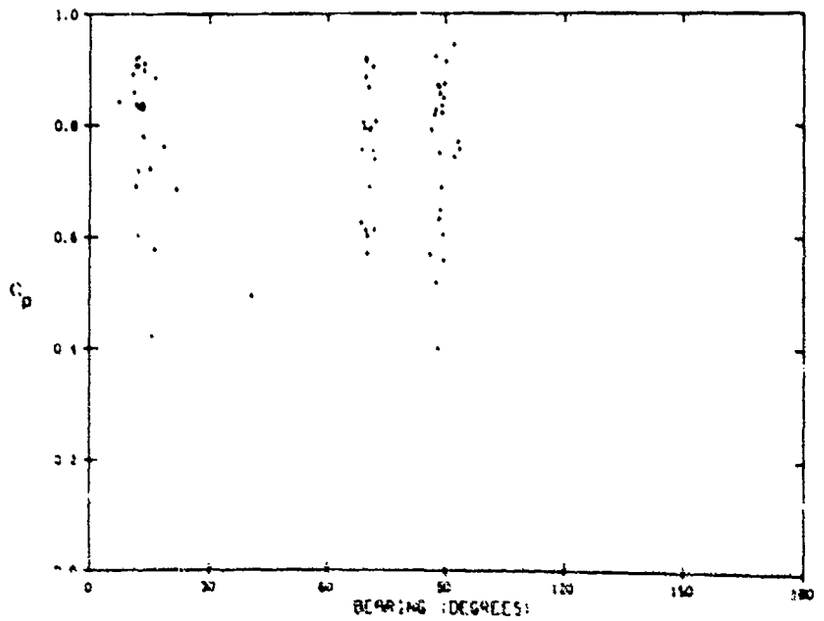

(CONFIDENTIAL)

(C) Figure 33. Phase coherence versus source bearing. LATA; Tow 2P3; 25 and 20 Hz.

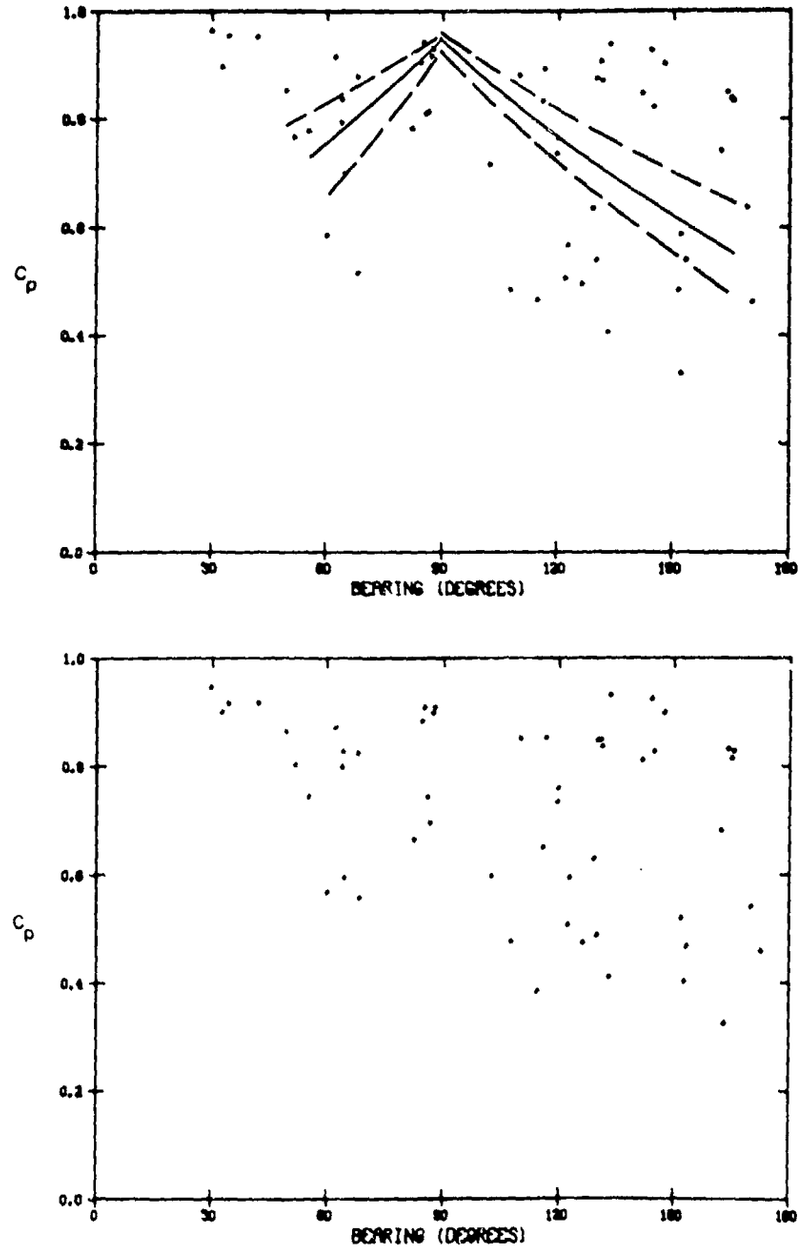

(CONFIDENTIAL)

(U) Figure 34. Comparison of C_p versus source bearing for Tow 4P1 for the LATA Subset (upper plot) and the ordinary LATA (lower plot).

DEPARTMENT OF THE NAVY
OFFICE OF NAVAL RESEARCH
875 NORTH RANDOLPH STREET
SUITE 1425
ARLINGTON VA 22203-1995

IN REPLY REFER TO:

5510/1
Ser 321OA/011/06
31 Jan 06

MEMORANDUM FOR DISTRIBUTION LIST

Subj: DECLASSIFICATION OF LONG RANGE ACOUSTIC PROPAGATION PROJECT (LRAPP) DOCUMENTS

Ref: (a) SECNAVINST 5510.36

Encl: (1) List of DECLASSIFIED LRAPP Documents

1. In accordance with reference (a), a declassification review has been conducted on a number of classified LRAPP documents.

2. The LRAPP documents listed in enclosure (1) have been downgraded to UNCLASSIFIED and have been approved for public release. These documents should be remarked as follows:

   Classification changed to UNCLASSIFIED by authority of the Chief of Naval Operations (N772) letter N772A/6U875630, 20 January 2006.

   DISTRIBUTION STATEMENT A: Approved for Public Release; Distribution is unlimited.

3. Questions may be directed to the undersigned on (703) 696-4619, DSN 426-4619.

BRIAN LINK
By direction

Subj: DECLASSIFICATION OF LONG RANGE ACOUSTIC PROPAGATION PROJECT (LRAPP) DOCUMENTS

DISTRIBUTION LIST:

NAVOCEANO (Code N121LC – Jaime Ratliff)
NRL Washington (Code 5596.3 – Mary Templeman)
PEO LMW Det San Diego (PMS 181)
DTIC-OCQ (Larry Downing)
ARL, U of Texas
Blue Sea Corporation (Dr.Roy Gaul)
ONR 32B (CAPT Paul Stewart)
ONR 321OA (Dr. Ellen Livingston)
APL, U of Washington
APL, Johns Hopkins University
ARL, Penn State University
MPL of Scripps Institution of Oceanography
WHOI
NAVSEA
NAVAIR
NUWC
SAIC

Declassified LRAPP Documents

Report Number	Personal Author	Title	Publication Source (Originator)	Pub. Date	Current Availability	Class.
ARLTR7952	Focke, K. C., et al.	CHURCH STROKE 2 CRUISE 5 PAR/ACODAC ENVIRONMENTAL ACOUSTIC MEASUREMENTS AND ANALYSIS (U)	University of Texas, Applied Research Laboratories	791029	ADC025102; NS; AU; ND	C
Unavailable	Van Wyckhouse, R. J.	SYNBAPS. VOLUME I. DATA BASE SOURCES AND DATA PREPARATION	Naval Ocean R&D Activity	791201	ADC025193	C
NORDATN63	Brunson, B. A., et al.	ENVIRONMENTAL EFFECTS ON LOW FREQUENCY TRANSMISSION LOSS IN THE GULF OF MEXICO (U)	Naval Ocean R&D Activity	800901	ADC029543; ND	C
NORDATN80C	Gereben, I. B.	ACOUSTIC SIGNAL CHARACTERISTICS MEASURED WITH THE LAMBDA III DURING CHURCH STROKE III (U)	Naval Ocean R&D Activity	800915	ADC023527; NS; AU; ND	C
NOSCTR664	Gordon, D. F.	ARRAY SIMULATION AT THE BEARING STAKE SITES	Naval Ocean Systems Center	810401	ADC025992; NS; AU; ND	C
NOSCTR703	Gordon, D. F.	NORMAL MODE ANALYSIS OF PROPAGATION LOSS AT THE BEARING STAKE SITES (U)	Naval Ocean Systems Center	810801	ADC026872; NS; AU; ND	C
NOSCTR680	Neubert, J. A.	COHERENCE VARIABILITY OF ARRAYS DURING BEARING STAKE (U)	Naval Ocean Systems Center	810801	ADC028075; NS; ND	C
HSECO735	Luehrmann, W. H.	SQUARE DEAL R/V SEISMIC EXPLORER FIELD OPERATIONS REPORT (U)	Seismic Engineering Co.	731121	AD0530744; NS; ND	C; U
MPL-C-42/76	Morris, G. B.	CHURCH ANCHOR EXPLOSIVE SOURCE (SUS) PROPAGATION MEASUREMENTS FROM R/P FLIP (U)	Marine Physical Laboratory	760701	ADC010072; AU; ND	C; U
ARLTR7637	Mitchell, S. K., et al.	SQUARE DEAL EXPLOSIVE SOURCE (SUS) PROPAGATION MEASUREMENTS. (U)	University of Texas, Applied Research Laboratories	760719	ADC014196; NS; AU; ND	C; U
NORDAR23	Fenner, D. F.	SOUND SPEED STRUCTURE OF THE NORTHEAST ATLANTIC OCEAN IN SUMMER 1973 DURING THE	Naval Ocean R&D Activity	800301	ADC029546; NS; ND	C; U
NOOTR230	Bucca, P. J.	SOUND VELOCITY CONDITIONS DURING THE CHURCH ANCHOR EXERCISE (U)	Naval Oceanographic Office	751201	NS; AU; ND	C;U
ONR SP 2-69; MC PLAN-01	Unavailable	PARKA II EXPERIMENT UTILIZING SEA SPIDER, ONR SCIENTIFIC PLAN 2-69 (U)	Maury Center for Ocean Science	690626	ADB020846; ND	U
Unavailable	Unavailable	PARKA I EXPERIMENT	Maury Center for Ocean Science	691101	AD0506209	U
USRD CR 3105	Unavailable	SEA SPIDER TRANSPONDER TRANSDUCER	Naval Research Laboratory	700505	ND	U
MC PLAN 05; ONR Scientific Plan 1-71	Unavailable	ATLANTIC TEST BED MEASUREMENT PROGRAM (U)	Maury Center for Ocean Science	701020	ND	U
ACR-170 VOL.1	Hurdle, B. G.	PROJECT NEAT- A COLLABORATIVE LONG RANGE PROPAGATION EXPERIMENT IN THE NORTHEAST ATLANTIC, PART I (U)	Naval Research Laboratory	701118	ND	U
MC-003-VOL-2	Unavailable	THE PARKA I EXPERIMENT. APPENDICES- PACIFIC ACOUSTIC RESEARCH KANEOHE-ALASKA (U)	Maury Center for Ocean Science	710101	ND	U